PREPARATION AND CHARACTERIZATION OF THERMALLY STABLE ORGANOCLAYS AND THEIR USE IN POLYMER BASED NANOCOMPOSITES

A THESIS SUBMITTED TO
THE GRADUATE SCHOOL OF NATURAL AND APPLIED SCIENCES
OF
MIDDLE EAST TECHNICAL UNIVERSITY

BY

WISSAM ABDALLAH

IN PARTIAL FULFILLMENT OF THE REQUIREMENTS
FOR
THE DEGREE OF DOCTOR OF PHILOSOPHY
IN
CHEMICAL ENGINEERING

JULY 2010

Approval of the thesis

PREPARATION AND CHARACTERIZATION OF THERMALLY STABLE ORGANOCLAYS AND THEIR USE IN POLYMER BASED NANOCOMPOSITES

submitted by **WISSAM ABDALLAH** in partial fulfillment of the requirements for the degree of **Doctor of Philosophy in Chemical Engineering Department, Middle East Technical University** by,

Prof. Dr. Canan Özgen
Dean, Graduate School of **Natural and Applied Sciences** _____

Prof. Dr. Gürkan Karakaş
Head of Department, **Chemical Engineering** _____

Prof. Dr. Ülkü Yılmazer
Supervisor, **Chemical Engineering Dept., METU** _____

Examining Committee Members:

Prof. Dr. Cevdet Kaynak
Metallurgical and Materials Engineering Dept., METU _____

Prof. Dr. Ülkü Yılmazer
Chemical Engineering Dept., METU _____

Prof. Dr. Meral Şahin
Chemistry Dept., Ankara University _____

Dr. Cevdet Öztin
Chemical Engineering Dept., METU _____

Prof. Dr. Göknur Bayram
Chemical Engineering Dept., METU _____

Date: 26. 07. 2010

I hereby declare that all information in this document has been obtained and presented in accordance with academic rules and ethical conduct. I also declare that, as required by these rules and conduct, I have fully cited and referenced all material and results that are not original to this work.

Name, Last name: Wissam ABDALLAH

Signature:

ABSTRACT

PREPARATION AND CHARACTERIZATION OF THERMALLY STABLE ORGANOCLAYS AND THEIR USE IN POLYMER BASED NANOCOMPOSITES

Abdallah, Wissam
Ph. D., Department of Chemical Engineering
Supervisor: Prof. Dr. Ülkü Yılmazer

July 2010, 255 Pages

The present study was aimed at exploring the purification and modification of montmorillonite rich Turkish bentonites by organic salts and their subsequent effects on the morphology (X-diffractometry, transmission electron microscopy, scanning electron microscopy), melt flow index, mechanical (Tensile, Impact) and especially thermal stability (thermal gravimetric analysis, differential scanning calorimetry) properties of polymer/organoclay nanocomposites with and without an elastomeric compatibilizer. The bentonite clay mined from Reşadiye (Tokat/Turkey) was purified by sedimentation, resulting in higher cation exchange capacity and thermal stability in comparison to unpurified clay, and then used in the synthesis of six thermally stable organoclays by replacing the interlayer inorganic sodium cations with two (alkyl, aryl) phosphonium and four di-(alkyl, aryl) imidazolium surfactant cations in an attempt to overcome the problem of early decomposition of alkyl ammonium organoclays usually used in polymer nanocomposites. An optimum amount of these organoclays (wt %2) was then used in the production of Polyamide 66 and Poly(ethylene terephthalate) based nanocomposites by melt blending with the help of an optimum amount of elastomeric compatibilizer (wt %5) which also acted as impact modifier. Phosphonium organoclays were used in the production of nanocomposites for both polymers, whereas imidazolium organoclays were used with PET only.

The importance of clay purification was revealed in the removal of non-clay minerals available in the raw bentonite clay as confirmed by XRF and XRD, the significant increase in cation exchange capacity and the improved thermal stability of the purified clays as proven by TGA.

The interlayer spacing of the phosphonium organoclays ranged from 1.78 to 2.52 nm indicating arrangement between pseudo-trilayers and paraffin-type chains, while the interlayer spacing of imidazolium organoclays ranged between 1.35 nm and 1.45 nm indicating a monolayer arrangement. The effects of chemical structure (chain type), counter ion and alkyl chain length on the thermal stability of the imidazolium salts were investigated. TGA analysis showed that the thermal stability of (alkyl, aryl) phosphonium and di-(alkyl, aryl) imidazolium organoclays proved to be superior to conventionally used quaternary alkyl ammonium organoclays. Not only the thermal stability of the organoclays prevented the nanocomposite from early decomposition, but these organoclays also improved the onset decomposition temperatures of PA66 and PET nanocomposites compared to the pure polymer owing to the dominant barrier effect of the silicate layers as a result of the formation of carbonaceous-silicate char.

The reinforcement of PA66 with surface modified phosphonium organoclays and PET with surface modified phosphonium and imidazolium organoclays enhanced the mechanical and thermal properties of the binary and ternary nanocomposites. The mechanical properties were in good agreement with DSC analysis for all the PA66 and PET compositions. The presence of elastomer and organoclays promoted the nucleation process in PA66 blend, binary and ternary nanocomposites. However, the presence of elastomer and organoclay retarded the nucleation in most of the PET composites.

Keywords: Polyamide 66, Poly(ethylene terephthalate), Nanocomposite, Organically modified clay, Phosphonium, Imidazolium, Thermal stability, Mechanical properties

ÖZ

ISIL KARARLILIĞI YÜKSEK ORGANOKİLLERİN HAZIRLANMASI, KARAKTERİZASYONU VE POLİMER BAZLI NANOKOMPOZİTLERDE KULLANILMASI

Abdallah, Wissam
Doktora, Kimya Mühendisliği
Tez Yöneticisi: Prof. Dr. Ülkü Yılmazer

Temmuz 2010, 255 Sayfa

Bu çalışma, montmorillonit içeriği yüksek Türk bentonitlerinin organik tuzlar ile saflaştırılması, organik tuzlarla modifikasyonu, ve sonra elastomerik uyumlaştırıcı eklenerek ya da eklenmeden elde edilmiş polimerik organokil nanokompozitlerde oluşan yapısal etkilerin, morfolojik özellikler (X-ışınları kırınımı, taramalı elektron mikroskopu, geçirgen elektron mikroskopu), erime akış indeksi, mekanik özellikler (gerilme dayanımı, darbe dayanımı) ve özellikle ısıl kararlılık (termogravimetrik analiz, taramalı diferansiyel kalorimetre) özellikleri yoluyla incelenmesini amaçlar. Reşadiye/Tokat'tan çıkarılan bentonit kili çökeltme metodu ile saflaştırılarak daha yüksek katyon değişme kapasitesi ve ısıl kararlılık elde edilmiş, nanokompozit üretiminde genellikle kullanılan alkil amonyum organokillerin düşük sıcaklıkta bozunma sorununa çözüm olması için bu çalışmada önce organik killerin ara tabaka sodyum katyonları iki adet (alkil, aril) fosfonyum ve dört adet (di-alkil, -aril) imidazolyum yüzey aktif katyonu ile değiştirilerek altı ayrı tür ısıl-kararlı organik kil elde edilimiştir. Daha sonra organik killerden optimum orandaki (% 2 ağ.) miktar ile dayanımı düzenleyici olarak davranan elastomerik uyumlaştırıcıdan yine optimum orandaki (% 5 ağ.) miktarlar harmanlanarak Poliamid 66 (PA66) ve Poli (etilen tereftalat) (PET) esaslı nanokompozitler elde edilmiştir. Fosfonyum katyonlu organik killer her iki polimer ile birlikte kullanılırken imidazoliyum katyonlu organik killer sadece PET esaslı nanokompozitlerde kullanılmıştır.

Ham bentonitte kil dışı minerallerin çıkarılması ile sağlanan saflaştırmanın önemi katyon değişme kapasitesindeki anlamlı yükseliş ile gözlenmiş, TGA analizleri ile daha yüksek ısıl kararlılığa erişildiği anlaşılmış, XRF ve XRD analizleri de sonuçları teyit etmiştir.

Fosfonyum katyonlu organik killerde 1,78-2,52 nm aralığında değişen ara tabaka genişliği psödo-üç tabakalı ve parafinik zincir tipi arasında bir düzenlemenin varlığını, imidazoliyum katyonlu organik killerde ise 1,35-1,45 nm aralığında arasında değişen ara tabaka genişliği tek tabakalı bir düzenlemeyi işaret etmektedir. Kimyasal yapı (zincir tipi), katyon partneri (anyon) ve alkil zincir uzunluğunun imidazolyum katyonlu tuzların ısıl kararlılığındaki etkileri araştırılmıştır. TGA analizleri (alkil, aril) fosfonyum ve di- (alkil, aril) imidazoliyum katyonlu organik killerin ısıl kararlılık yönünden kuaterner alkil amonyum organik killerden daha üstün olduğunu kanıtlamıştır. Çalışmadaki organik killerin yüksek ısıl kararlılığı sadece erken bozunmayı engellemekle kalmamış, ayrıca ısı karşısında karbonlu silikat kömürleşmesi sonucunda oluşan silikat tabakaları yardımıyla da sadece PET ve PA66 polimerlerine kıyasla bu polimerlerin kullanıldığı nanokompozitlerin bozunma başlangıç sıcaklıklarında da iyileşme sağlanmıştır.

PA66 polimerinin fosfonyum katyonlu organik killerle, PET polimerinin de fosfonyum ve imidazolyum katyonlu organik killer ile güçlendirilmesi sayesinde ikili ve üçlü nanokompozitlerin mekanik ve ısıl özelliklerinde gelişmeler sağlanmıştır. PA66 ve PET içeren nanokompozitlerin mekanik özellikleri DSC analiz sonuçları ile iyi bir uyum göstermektedir. Elastomerik uyumlaştırıcı ve organik killer PA66 içeren ikili ve üçlü nanokompozitlerde çekirdekleşme sürecini olumlu yönde etkilemiş, ancak PET içeren nanokompozitlerin çoğunda yavaşlamaya yol açmıştır.

Anahtar Kelimeler: Poliamid 66, Poli (etilen tereftalat), Nanokompozit, Organik kil, Fosfonyum, İmidazolyum, Isıl kararlılık, Mekanik özellikler

To the memory of my father

To my sweetest Mother

To my dearest brother Dr. Nazih

ACKNOWLEDGEMENTS

Words stay short at expressing my sincere appreciation and gratitude to my thesis supervisor, Prof. Dr. Ülkü Yılmazer for his infinite support, guidance and helpful suggestions throughout my research. It was a great honor and pleasure to work with him and benefit from his experience.

I would also like to thank Assoc. Prof. Dr. Göknur Bayram and Prof. Dr. Cevdet Kaynak, for serving as committee members, their worthy opinions and valuable suggestions.

My sincerest gratitude goes to my family for their love and belief in me, especially my sweetest mother and sincerest brother Dr. Nazih who overwhelmed me with their guidance, encouragement and support throughout my study and life. My nephew Mohamad deserves special mention for his nice cooperation and enthusiastic support.

My closest friends Dr. Faris Yılmaz and Hussein Elhatto deserve to be mentioned for their mutual support. I am also thankful to all my friends in Polymer Research Group including Dr. Işıl Işık, Dr. Mert Kılınç, Filiz Cengiz, Canan Yeniova, Ali Sinan Dike, Dr. Tijen Seyidoğlu, Seda Yılmaz, Sibel Dönmez, Fatma Işık, Saniye Yayla, Fadile Kapaklı, Ceyda İşbaşar and especially Dr. Sertan Yeşil for their cooperation and friendship. Also, Saltuk Pirgalıoğlu deserves sincere thanks for his friendship and help during my extrusion experiments.

My sincere acknowledgements go to Necmi Avcı from the Department of Metallurgical Engineering for XRD analysis and Mihrican Açıkgöz from the Department of Chemical Engineering for TGA and DSC analysis. Technical assistance of Machine Shop staff is greatly acknowledged.

Special thanks to the Scientific and Technological Research Council of Turkey (TÜBİTAK) for their financial support during my study.

TABLE OF CONTENTS

LIST OF FIGURES

FIGURES

LIST OF TABLES

TABLES

NOMENCLATURE

A_i	Area of a domain in SEM analysis, μm^2
A_0	Initial cross sectional area, mm^2
d	Interlayer spacing, Å or nm
d_{av}	Average domain size, nm
D	Distance between grips of tensile test specimen, mm
D	Extruder barrel diameter, mm
E	Young's Modulus, MPa
F	Instantaneous load, N
L	Extruder barrel length, mm
L	Total length of impact test specimen, mm
L	Overall length of tensile test specimen, mm
L_0	Initial gauge length, mm
n_i	Number of domains analyzed in SEM analysis
T	Thickness of tensile and impact test specimen, mm
T_g	Glass Transition Temperature, ºC
T_m	Melting Temperature, ºC
T_c	Crystallization Temperature, ºC
W	Width of narrow section of tensile test specimen, mm

Abbreviations

15A	Cloisite® 15A
25A	Cloisite® 25A
30B	Cloisite® 30B
AIPEA	Association Internationale pour l'Etude des Argiles
An	Analcime
ASTM	American Society for Testing and Materials
B	Sodium Tokat/Reşadiye Bentonite
B.TO-P	Bentonite modified with Tetraoctyl Phosphonium Bromide
BET	Brunauer Emmett and Teller
BTL-IM Cl	1-Butyl-3-methyl Imidazolium Chloride

BTL-IM PF6	1-Butyl-3-methyl Imidazolium Hexafluorophosphate
BZL-IM PF6	1-Benzyl-3-methyl Imidazolium Hexafluorophosphate
BZLTP-P Cl	Benzyl Triphenyl Phosphonium Chloride
C	Calcite
CEC	Cation Exchange Capacity
Cln	Clinoptilolite
D	Dolomite
DCL-IM Cl	1-Decyl-3-methyl Imidazolium Chloride
DMT	Dimethyl Terephthalate
DrTGA	Derivative Thermal Gravimetric Analysis
DSC	Differential Scanning Calorimetry
DTA	Differential Thermal Analysis
E-BA-MAH	Ethylene-Butyl Acrylate-Maleic anhydride
EG	Ethylene Glycol
E-MA-GMA	Ethylene-Methyl Acrylate-Glycidyl Methacrylate
F	Feldspar
FTIR	Fourier Transform Infrared Spectroscopy
GC-MS	Gas Chromotography-Mass Spectroscopy
GMA	Glycidyl Methacrylate
ISO	International Organization for Standardization
LS	Layered silicate
M.TO-P	Commercial montmorillonite modified with Tetraoctyl Phosphonium Bromide
MAH	Maleic Anhydride
MFI	Melt Flow Index
MMT	Montmorillonite
N-MMT	Ammonium-modified montmorillonite
OC	Opal-C
P-MMT	Phosphonium-modified montmorillonite
PA66	Polyamide 66
PB	Purified Sodium Tokat/Reşadiye Bentonite
PB.TO-P	Purified Bentonite modified with Tetraoctyl Phosphonium Bromide
PB.BZLTP-P	Purified Bentonite modified with Benzyltriphenyl Phosphonium Chloride

PB.BZL-IM	Purified Bentonite modified with 1-Benzyl-3-methyl Imidazolium Hexafluorophosphate
PB.BTL-IM	Purified Bentonite modified with 1-Butyl-3-methyl Imidazolium Hexafluorophosphate
PB.BTL-IM'	Purified Bentonite modified with 1-Butyl-3-methyl Imidazolium Chloride
PB.DCL-IM	Purified Bentonite modified with 1-Decyl-3-methyl Imidazolium Chloride
PET	Poly(Ethylene Terephthalate)
PLS	Polymer Layered Silicate
PLSNC	Polymer Layered Silicate Nanocomposite
PS	Polystyrene
PTA	Purified Terephthalic Acid
Q	Quartz
SAN	Styrene-acrylonitrile
SEM	Scanning Electron Microscopy
TEM	Transmission Electron Microscopy
TG	Thermogravimetry
TGA	Thermogravimetric Analysis
TO-P Br	Tetraoctyl Phosphonium Bromide
TOT	Tetrahedral Octahedral Tetrahedral
TPO	Thermoplastic Olefin
WAXD	Wide angle X-ray diffraction
XRD	X-Ray Diffraction

CHAPTER 1

INTRODUCTION

Nanocomposites constitute one of the most advanced areas of nanotechnology. Especially, polymer-clay nanocomposites have witnessed great upsurge in the past decade, because these materials can exhibit enhanced mechanical properties, increased optical transparency, improved gas barrier properties, superior flame retardancy, higher thermal stability, and heat distortion temperature at lower clay loadings compared to conventional polymer composites containing traditional fillers.

Polymer-clay nanocomposites are particulate-filled composites in which the reinforcement material is in the form of sheets with thickness of one to few nanometers and length of hundreds to thousands of nanometers. Layered silicates such as montmorillonite (MMT) which is a structural group of 2:1 phyllosilicates and an undergroup of smectites can be used for the synthesis of polymer-clay nanocomposites (1). Their crystal structure consists of layers made up of two silica tetrahedra fused to an edge-shared octahedral sheet of either alumina or magnesia. Stacking of the layers leads to a regular van der Waals gap between the layers called the gallery or interlayer. Isomorphic substitution within the layers results in negative charges that are counterbalanced by cations residing in the interlayer.

Pristine layered silicates usually contain hydrated sodium or potassium ions. Ion-exchange reactions with cationic surfactants, including primary, tertiary and quaternary ammonium ions, render the normally hydrophilic silicate surface organophilic, which makes intercalation of many engineering polymers possible and improve the wetting characteristics with the polymer (2) in which the surface energy of MMT decreases and the basal spacing expands (3). Additionally, the alkylammonium cations can provide functional groups that can react with the

polymer or initiate polymerization of monomers to improve the strength of the interface between the inorganic component and the polymer (2).

Organoclays are abundant, inexpensive, environmentally friendly and above all essential to develop polymer nanocomposites. All of these properties attracted researchers to surface modification of clays which creates new materials to be used in a wide spectrum of new applications (4). The earlier approaches to MMT-based organoclays adopted ammonium surfactants which usually incorporate short aliphatic chains and benzyl and sometimes hydroxyl groups. They also contain at least one long aliphatic chain (C12-C18) to cause expansion of the distance between the layers. Other MMT modifiers include alkyl amines, alkyl carbazol, poly (dimethylsiloxane), quinolinium, pyridinium, stibonium, phosphonium and imidazolium surfactants (5). The thermal stability and flammability performance of polymer nanocomposites are enormously influenced by the processing stability of both the polymer and the organic-treated layered silicate. The low thermal stability of ammonium surfactants (onset of thermal decomposition at about 200°C or below) presents a problem for melt compounding and processing (injection molding) of polymer nanocomposites into final molded products, where high processing temperatures exceeding 200°C are commonly encountered such as: Polyamides (PA6, PA66), poly(ethylene terephthalate) (PET), and polycarbonate (PC). Thermal degradation during processing can initiate/catalyze polymer degradation, in addition to causing a variety of undesirable effects during processing and in the final product (6), (7). Thus, the onset of the thermal decomposition of the organic modifier sets the ceiling temperature for polymer processing. Phosphonium salts are capable of undergoing a wider range of reactions and behave differently than their ammonium counterparts owing to the greater steric tolerance of the phosphorus atom in phosphonium salts and the participation of its low-lying d-orbitals in the processes of making and breaking chemical bonds (8).

Imidazole was found to be resistant to ring fission during thermal rearrangements of 1-alkyl- and 1-aryl-imidazoles at temperatures above 600°C, thus indicating that the imidazolium cation was more thermally stable than the alkyl ammonium cation (7).

Surface energy, basal spacing and thermal stability of these organoclays depend strongly on the chemical structure, packing density, the degree of cation exchange and the type of cation head included in the surfactant. Efforts have been made to synthesize thermally stable organoclays based on stibonium, phosphonium or imidazolium surfactants. The phosphonium surfactants incorporate mainly short alkyl chains, benzene and usually a long alkyl chain. These organoclays exhibited substantially higher thermal stability than ammonium surfactant modified organoclays. Additionally, phosphonium compounds enhance flame retardancy. (5), (8).

Smectites are the major minerals in bentonites and their quantity and quality affect directly the characteristics of a bentonite (9). In addition, bentonite contains impurities like non-clay minerals and other clay minerals. Some of these minerals that are porous materials are montmorillonite, beidellite, nontronite, saponite and hectorite and some common impurities in bentonite clay are quartz, calcite, feldspar, mica and organic matter (10). These impurities negatively affect the cation exchange capacity and thermal stability of bentonites. Also, purity is critical for reproducibly achieving maximum mechanical properties and optimum clarity in packaging applications. Impurities can lead to the degradation of thermoplastics during the melt processing stages and can also act as stress concentrators resulting in poorer impact resistance and in films they contribute to haze.

High purity smectites obtained by the purification of bentonites are used in a wide variety of areas such as, organoclay, polymeric clay, pillared clay and catalyst production. In addition, the application of bentonites in the production of selective adsorbents, bleaching earth, catalyst beds, carbonless copy paper and medication, depends on the porous structures of smectites. Therefore, the isolation of some smectite group minerals from bentonites by purification (sedimentation) is of great importance before the surface modification step (9).

A wide variety of polymers, including thermoplastics, such as styrenics, polyolefins, etc. and thermosetting materials, such as epoxy resins and phenolics have been used as starting materials under this area of research (11).

Polyamide (PA66) is an important synthetic resin and widely used in engineering plastics and fiber industries because of its excellent physical and mechanical properties. It is a flammable thermoplastic, and thus anti-flaming modification is necessary in many cases of usage (12). In recent years, the increasing interest in polyamides resulted from their high melting points to extend the boundaries of this polymer type to satisfy more stringent high temperature automobile and electronic applications. The glass transition temperature of aliphatic polyamides is rather low (40-70^{o}C) and composition does not affect T_g to any great extent. The heat deflection temperature of PA66 is about 75^{o}C, and it has a linear expansion coefficient of $8*10^{-5}$ cm/cm ^{o}C. Its high melting point (about 265^{o}C) is a function of both the strong hydrogen bonding between the chains and the crystal structure. Despite the fact that PA66 has good thermal stability, it tends to degrade when held for long periods of time at high temperatures. The adipic acid segments can cyclize, leading to chain scission, the production of cyclopentanone and derivatives and evolution of carbon dioxide and ammonia. Crosslinking occurs and the material turns into an intractable gel along with reduction of molecular weight (13).

Poly(ethylene terephthalate) (PET) is a thermoplastic polyester having poor impact resistance and high notch sensitivity. Additionally, in PET/clay nanocomposites, addition of clay sometimes imparts drawbacks to the resulting material such as brittleness. In addition, the presence of a thermally stable organoclay will also overcome the problem of melt compounding and processing at high temperatures. Also, impact modification of PET can be achieved by dispersing elastomeric polymers in the polymer matrix.

The purification of bentonites by sedimentation isolates the smectite portion and ends up in highly pure MMT with improved properties in cation exchange capacity and thermal stability. The surface modification of pure MMT with suitable phosphonium surfactants results in thermally stable organoclays which overcome the thermal degradation problem of conventional organoclays produced by alkyl ammonium surfactants when used with high melting-point polymers during compounding and processing.

The objective of the present investigation is aimed at exploring the effects of purified and organically modified Turkish layered silicates on the morphology, melt flow properties, mechanical properties and thermal stability of polymer nanocomposites. The clays were purified by sedimentation and then surface modified using two phosphonium and four imidazolium ionic liquids. The phosphonium salts used were: Tetraoctyl phosphonium bromide (TO-P Br), Benzyltriphenyl phosphonium chloride (BZLTP-P Cl). The imidazolium salts used were: 1-Benzyl-3-methyl imidazolium hexafluorophosphate (BZL-IM PF6), 1-Butyl-3-methyl imidazolium hexafluorophosphate (BTL-IM PF6), 1-Butyl-3-methyl imidazolium chloride (BTL-IM Cl) and 1-Decyl-3-methyl imidazolium chloride (DCL-IM Cl). The clay used in this study was obtained from Na^+-Bentonite rock mined from Tokat/Reşadiye (B). Polyamide 66 and PET were used as the polymer matrices for the production of the nanocomposites. Melt mixing process was performed using a co-rotating twin-screw extruder to produce the polymer nanocomposites. Polyamide 66 (PA66) and amorphous PET (PET) organoclay nanocomposites were prepared using the modified organoclays with and without the use of an elastomer which also acted as an impact modifier.

X-Ray Fluorescence (XRF) analysis was used in order to evaluate the chemical compositions of purified clays. Fourier Transform Infrared Spectroscopy (FTIR) was used to investigate the intercalation of salts on the surface of clays after modification. X-Ray Diffraction (XRD) analysis was used to investigate the morphology of the purified clays, modified organoclays, and the produced nanocomposites, and the dispersion of the clays in the polymer matrix. Transmission Electron Microscopy (TEM) analysis was performed to confirm these results. Scanning Electron Microscopy (SEM) analysis was also performed in order to analyze the dispersion of elastomeric materials in the matrix and the effects of organoclay on the phase domains. Melt flow properties were characterized by Melt Flow Index (MFI) analysis. Mechanical properties of the specimens were evaluated according to the tensile and impact test results together with the morphological characterization. Thermal Gravimetric Analysis (TGA) and Differential Scanning Calorimeter (DSC) were used to analyze the thermal stability and crystallinity of the samples respectively.

CHAPTER 2

BACKGROUND

2.1 Clays and Clay Minerals

Clays and clay mineral terms have been approached differently by geologists, mineralogists, chemists, and soil scientists. The term clay has been historically referred to the naturally occurring soil fraction of small inorganic particles having sizes less than 2 μm without regard to composition or crystallinity, and clay minerals have been referred to the specific phyllosilicates (the term for sheet silicate structures) that are the layered, hydrous, such as magnesium or aluminum silicates. AIPEA (Association Internationale pour l'Etude des Argiles) report in 1995 defined clay as a ''material composed primarily of *fine-grained* minerals which is generally *plastic* at appropriate water contents and *will harden* when dried or fired'' and clay minerals as ''phyllosilicate minerals and minerals which *impart plasticity* to clay and which harden upon drying or firing'' (14). The distinction between clay and clay mineral (Table 2.1) must always be kept in mind, as the literature used the same term for both. (15)

Table 2.1 Distinction between clay and clay mineral (15)

Clay	Clay mineral
Natural	Natural and synthetic
Fine-grained	No size criterion
Phyllosilicates as principal constituents	May include non-phyllosilicates
Plastic with some exceptions like flint clays	Plastic
Hardens on drying or firing	Hardens on drying or firing

The diversity of structures and properties of clays and clay minerals, and their wide-ranging applications, nominate them to be recognized as the materials of the 21st century. Clays are abundant, inexpensive, easily processed and environmentally friendly. Clays have been implicated in the synthesis of biomolecules and the very origins of life on earth and have also become indispensable to modern living. The increasing potential of clays to be dispersed as nanometer-size unit particles in a polymer phase, forming novel nanocomposite materials with superior thermo-mechanical properties made it of great importance for the industry.

Natural clay consists of one or more different types of clay minerals together with some impurities. The most common impurities in natural clay are quartz, calcite, feldspar, mica and organic matter while hydrated iron oxide, ferrous carbonate and pyrite are being the minor impurities. (10)

2.1.1 Structure of Clay Minerals

Clay minerals are layer-lattice silicates (phyllosilicates) formed by the hydrolysis of aluminum or magnesium silicates of alkali and alkaline earth metals. Most of them are entirely or almost entirely crystalline (10). Every clay mineral contains two types of sheets, tetrahedral and octahedral. Silica is the main component of a tetrahedral sheet, while an octahedral sheet comprises diverse elements such as Al, Mg, and Fe. A schematic representation of each is given in Figure 2.1.

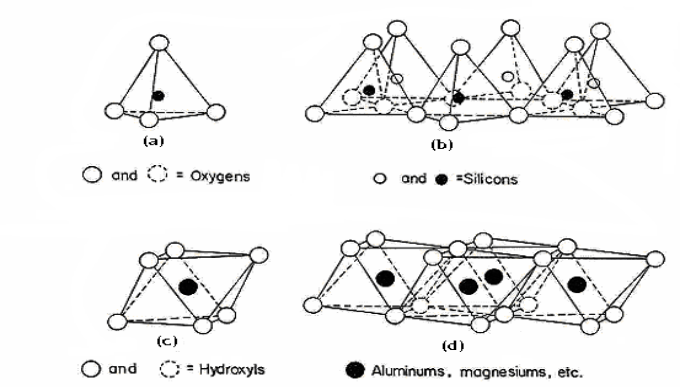

Figure 2.1 A clay tetrahedral sheet in (a) Single tetrahedral unit and (b) Sheet structure of the tetrahedral units, and a clay octahedral sheet in (c) Single octahedral unit and (d) Sheet structure of octahedral units (10)

In the tetrahedral sheets, each silicon atom is surrounded by four oxygen atoms, and the tetrahedrally coordinated cations (commonly Si^{4+} and Al^{3+}, and occasionally Fe^{3+} and Cr^{3+}) are linked to one another via covalent bonding through shared oxygens. These shared oxygens form a basal plane, and the remaining apical oxygens are shared with another layer of cations. The tetrahedral units arrange as a hexagonal network (Figure 2.1 a, b) along this basal plane.

The octahedral sheets have cations that are coordinated with six oxygens or hydroxyls, and these units are covalently linked into a sheet structure as well. In clays, tetrahedral and octahedral sheets are also covalently linked through the apical tetrahedral oxygens (Figure 2.1 c, d) (14). Because of the size limit, the cation positions are filled by such common medium sized ions as Al^{3+} ,Fe^{3+}, Fe^{2+}, Mg^{2+}, Mn^{2+} and Li^{1+} ,and less commonly by Zn^{2+}, Ni^{2+}, Cu^{2+} , Co^{2+}, and the others with similar ion size. (16)

Clay minerals are characterized by the type of layer structure, the composition of the sheets that make up the layer structure, the layer charge, and the composition of the interlayer material (14). The thickness of each structural unit depends not only on the number of sheets involved, but also on the composition of tetrahedral and octahedral sheets and the charge compensations (net negative charge on many clay lattices) as a result of unbalanced substitutions of cations in the sheets. The net compensating charge may be located either in the interlayer site as in 2:1 layer arrangements or in the additional octahedral sheet as in 2:1:1 layer arrangements (16).

Minerals are divided into two groups, silicates (or clay minerals) and non-silicates (or non-clay minerals). A schematic representation of both types is given in Figure 2.2.

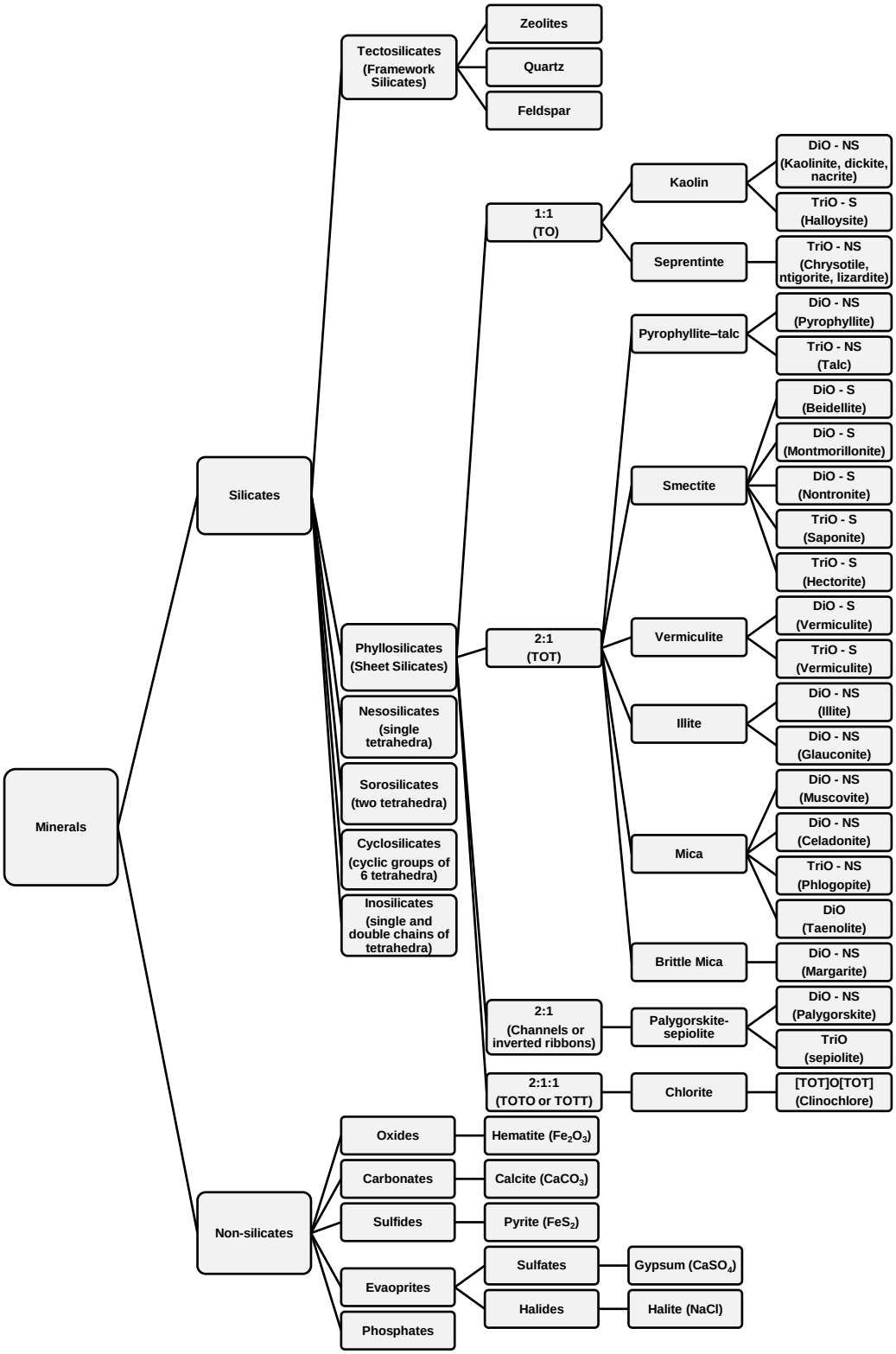

T: Tetrahedral, O: Octahedral, DiO: Dioctahedral, TriO: Trioctahedral, S: Swelling, NS: Nonswelling

Figure 2.2 Minerals groups and subgroups including examples and structures (14), (17)

Based on the combination of tetrahedral and octahedral sheets, the clay mineral structures are of three types; 1:1, 2:1, and 2:1:1.

In the 1:1 types consisting of one octahedral sheet and one tetrahedral sheet, the plane of apical oxygens of the tetrahedral sheet is superimposed on the OH plane of the octahedral sheet. The common plane of junction consists of both oxygen and unshared OH. The unshared OH occurs at the center of each six-fold ring defined by the apical tetrahedral oxygens.

In order to form 2:1 layered silicates, a natural stacking of those tetrahedral and octahedral sheets occurs in specific ratios and modes. Those sheets are arranged as 1 nm thin layers, with an octahedral sheet sandwiched between two tetrahedral silica sheets, so that their planes of apical oxygens face towards each other. These layers organize themselves to form stacks with a regular van der Waals gap between them, which is called the interlayer, gallery or basal spacing (18). The common planes between the two tetrahedral sheets and the octahedral sheet consist of sharing oxygens and unshared OH's, each unshared OH being at the center of tetrahedral apical oxygen hexagonal rings (Figure 2.3) (16). Layered silicates that are used in the preparation of polymer-layered silicate nanocomposites belong to the 2:1 phyllosilicates family and they are among the large number of inorganic layered materials (such as, mica, fluoromica, montmorillonite, vermiculite, hectorite, fluorohectorite, saponite, etc.) that have the capability of intercalation (7).

The 2:1:1 structure consists of a 2:1 layer arrangement with an additional octahedral sheet between 2:1 layers. (16)

The distance between the sheets of silicate layers can be determined by X-Ray diffraction patterns. It gives two categories of information; the first one is the basal 001 reflection that gives the distance between equivalent layers of basal oxygens or hydroxyl-oxygens and the second one is the two-dimensional hk diffraction bonds, which are independent from the basal spacing and are the same in all smectite types. (18)

The phyllosilicate 2:1 layer clays include mica, smectite, vermiculite, and chlorite. Smectite group can be further divided into montmorillonite, saponite, hectorite species, etc. Their chemical formulas are shown in Table 2.2 and chemical structures are given in Figure 2.3 (19).

Table 2.2 Chemical formula of commonly used smectite type silicates

Layered Silicate	General Formula*
Montmorillonite	$M_x(Al_{4-x}Mg_x)Si_8O_{20}(OH)_4$
Saponite	$M_xMg_6(Si_{8-x}Al_x)O_{20}(OH)_4$
Hectorite	$M_x(Mg_{6-x}Li_x)Si_8O_{20}(OH)_4$

*M = monovalent cation; x = degree of isomorphous substitution.

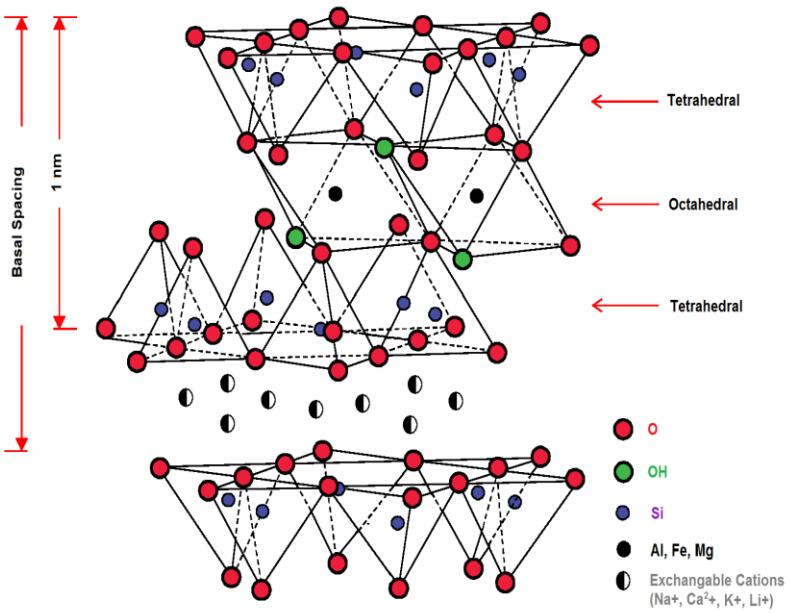

Figure 2.3 Schematic representation of the crystal structure of a 2:1 type clay mineral showing the relations between tetrahedral and octahedral layers, and interlayer spaces (reproduced from (20))

2.1.1.1.1 Montmorillonite

Smectite minerals belong to the 2:1 Tetrahedral Octahedral Tetrahedral (TOT) layer phyllosilicates with significant isomorphous substitutions taking place in the

octahedral layer, capable to raise the charge per unit cell to 0.5-1.2, while pyrophyllite-talc has no layer charge. Interlayer, hydrated cations (primarily K^+, Na^+, Ca^{2+}, and Mg^{2+}) compensate for the net negative charge aroused (14). The interlayer water constitutes an ice-like hexagonal structure (16). The charge interactions in the octahedral layer are somewhat diffuse, and thus the hydrated cations are loosely held and easily exchanged. Also, large amounts of water can be accommodated between the layers, which give rise to the swelling component that gives smectites their name. In addition, polar organic molecules are attracted by the exchangable cations and can intercalate, causing swelling. As a result of the interesting properties, smectites became among the most chemically interesting for modification and application among all clay minerals. Typical basal spacing varies from 1 to 2 nm (dehydrated state to containing multiple layers of water molecules). In dilute aqueous suspensions, Li- and Na-smectites are able to dissociate (delaminate) to such a degree, up to 4 nm, that the negatively charged silicate layers and small positively charged cations produce polyelectrolyte properties. Other exchangable cations yield smectite tactoids in dilute aqueous suspensions, which are several TOT parallel layers held together by electrostatic forces (14).

Smectite clays are characterized by certain properties:

- particles of colloidal size,
- high degree of layer stacking disorder,
- high specific surface area,
- moderate layer charge,
- large CEC that is little dependent on ambient pH,
- small pH-dependent anion exchange capacity,
- variable interlayer separation, depending on ambient humidity,
- propensity for intercalating 2 extraneous substances, including organic compounds and macromolecules, and
- ability of some members (e.g., Li^+- and Na^+-exchanged forms) to show extensive interlayer swelling in water; under optimum conditions, the layers can completely dissociate (delaminate) (15).

Montmorillonite is the most common mineral of this group; it is named for its location in Montmorillon, France (14). Among the diverse types of layered silicates,

MMT is particularly attractive as reinforcement for polymer-clay nanocomposites because it is environmentally friendly, readily available in large quantities with relatively low cost, and its intercalation chemistry is well understood. It is a naturally occurring 2:1 phyllosilicate, which has the same layered and crystal structure as talc and mica, but a different layer charge. MMT has a high surface area about 750 m^2/g, and its crystal lattice is composed of two silica tetrahedral sheets (SiO_4) and an octahedral alumina sheet ($AlO_4(OH)_4$) between the tetrahedrons.

2.1.2 Surface Properties of Clay Minerals

2.1.2.1 Cation Exchange Capacity

Montmorillonite have a distinct ability to sorb certain cations such as, Na^+, Ca^{2+}, Mg^{2+}, H^+, K^+, and NH_4^+, and to retain them in an exchangable state. These intercalated cations can be exchanged by treatment of other cations in a water solution. (21). The amount of exchangable cations that a clay mineral can adsorb at a specific pH, usually at a neutral pH of 7 is known as cation exchange capacity (CEC) (14). It is measured in milliequivalents per gram (meq/g) or more frequently per 100 g (meq/100g). Although the convention is to use this unit, it represents a charge per unit mass and, in SI units, is expressed in ‘‘coulombs per unit mass”. A CEC of 1 meq/g is 96.5 C/g in SI units (21).

Sodium MMT clay in an aqueous solution would preserve a reversible cation exchange reaction, hence to obtain a high conversion of Na^+-MMT into organoclay, an excess of intercalating organic cation $R\text{-}NH_4^+$ is used:

$$R\text{-}NH_4^+ + Na^+.MMT \leftrightarrow R\text{-}NH_4^+.MMT + Na^+$$

The reaction rate depends on the type of clay, the medium, the type of cation to be exchanged, the reaction conditions, like temperature (T), pH, concentrations and geometry of clay particles, etc (22). The CEC of MMT varies from 60 to 150 meq/100g, and its determination is a more or less arbitrary matter where no high

degree of accuracy can be claimed (21). A list of CEC values for a variety of clay minerals is provided in Table 2.3 (14).

Table 2.3 Ranges of cation exchange capacities for clay minerals

Clay Mineral	CEC (meq/100g)
Kaolinite	3-15
Chlorite	10-40
Montmorillonite	60-150
Vermiculite	100-150

2.1.2.2 Surface Area

Surface area (including porosity) is one of the most significant parameters of clays in industrial applications such as, catalysis. Different procedures of data analysis are used to derive quantitative information from experimental adsorption curves of which the Brunauer Emmett and Teller (BET) analysis is the most common (14).

The BET surface areas of non-microporous and nonswelling phyllosilicates range from a fraction to more than one hundred square meters per gram. Higher values are obtained with microporous clay minerals, such as sepiolite and palygorskite, and swelling (expanding) clay minerals (15). The specific surface area of smectites is calculated by considering them completely dissociated into single TOT layers. The ‘‘interior’’ specific surface area of the oxygen cleavage planes is then 750-800m^2/g. The exterior surface area for most natural smectites is less than 20% of this value. The interior surface area of vermiculites is around 750 m^2/g; however, the exterior area is a much smaller percentage than it is for smectites (10 m^2/g). For comparison, kaolinite has specific surface area about 10 m^2/g only (14).

2.1.3 Bentonite

Bentonite (named after Ford Benton, Wyoming) is rich in MMT (usually > 80%) with various colors (white, yellow, olive green, brown and blue) and grades. The wide spectrum of properties they offer made bentonite offer a broad variety of

applications and uses. Its origin is volcanic ash deposited in a variety of freshwater and marine basins, characterized by low energy depositional environments and temperate climatic conditions. Main uses for bentonite are in foundry sands; drilling muds, iron ore pelletizing, absorbents, as a variety of composite liners, food additive for poultry and domestic animals, in filtration, foods, cosmetics and pharmaceuticals. Bentonite is part of the most adsorbent, bleaching and catalyst clays. About 6 million tons of bentonite is produced annually (22). Bentonite is widely distributed on all continents with various mineralogical compositions. The world reserves of bentonite are given in Table 2.4.

Table 2.4 The world reserves of bentonite (23)

Continent	Reserve (Million Tons)
America	950
Europe	720
Turkey	**370**
USSR	250
Other	50
Australia	50
Other	150
Total	1870

2.1.4 Reşadiye Bentonite

The occurrences of white bentonite are Texas, Nevada, United States, Greece, Turkey, Italy, and Argentina. About 150000 tons of white bentonite is consumed annually for markets including detergents, ceramics, paper industry, cosmetics, paint, and wine clarification. Bentonite clay is very abundant in Turkey, the bentonite reserves in Turkey are given in Table 2.5 (23). The Reşadiye (Tokat) bentonite bed is one of the largest sodium bentonite reserves in Turkey with potential reserves of 200 million tons estimated by the Mineral Research and Exploration Institute of Turkey. This bentonite produces muds of high plasticity

when mixed with water. It is currently used in the preparation of drilling fluids and in iron ore pelletizing (9).

Table 2.5 Bentonite reserves in Turkey (24)

Area in Turkey	Reserve (Thousand Tons)
Ankara - Kalecik - Hançılı	19000
Ankara - Keskin - Besler	240
Artvın - Derinköy	800
Çankırı - Çerkes - Bayındır	43
Çankırı - Eldivan - KüçükHacıbey	300
Çankırı - Eldivan - BüyükHacıbey	100
Çankırı - Ilgaz - Kızılibrik	200
Çankırı - Eskipazar - Başpınar	800
Çorum - Sungurlu - Mecitözü	400
Edirne - Enez	50000
Giresun - Tirebolu	4000
Istanbul - Şile - Kızılcaköy	180
Konya - Sağlık	2400
Konya - Sille	24
Ordu - Fasta - Ünye	2564
Tokat - Reşadiye - Akdoğmuş - Kaşpınar	**200000**
Trabzon - Araklı - Arsin - Yolüstü	60

2.1.5 Purification of Bentonite

Bentonites have a broad scope of application domains before and after processing (9). Clay minerals are found associated with other minerals (clay or non-clay) and/or amorphous materials, except for some vermiculites and micas. In many applications, the bentonite clays are used as mined from the deposit without separation or enrichment of the clay minerals. However, the increasing applications of clay minerals in the manufacture of advanced materials raised the need for enrichment by purification (15). Since smectites are the major minerals in bentonites, the isolation of some smectite group minerals from bentonites is of great

importance. Some of these minerals that are porous materials are montmorillonite, beidellite, nontronite, saponite and hectorite (9).

2.1.5.1 Associated (Non-clay) Minerals

A clay deposit usually contains non-clay constituents (minerals) as impurities which do not impart plasticity to clay (15), such as quartz, sand, silt, feldspar, mica, chlorite, opal, volcanic dust, fossil fragments, heavy minerals, sulfates, sulfides, carbonate minerals, zeolites, and many other rock and mineral particles ranging in size from colloidal to pebbles (22). They are referred to as associated minerals since they are closely associated with the phyllosilicate component of clay, and hence interfere with its identification.

The presence of associated minerals in natural clay deposits also reduces the commercial value of the resource, as their quality and characteristics depend largely on the quality and quantity of the smectite, which is a micro-mesoporous material. For these reasons, much effort has been expended in purifying raw clays and in synthesizing ‘pure’ clay minerals. High purity smectites obtained by the purification of bentonites are used in a wide variety of areas such as carbonless copy paper, selective adsorbent, medication, membrane, organoclay, polymeric clay, pillared clay and catalyst production (9), (15).

2.1.6 Organic Modification of Bentonite

There are many mechanisms for modification of clay surfaces such as adsorption, ion exchange with inorganic and organic cations, binding of inorganic and organic anions, grafting of organic compounds, reaction with acids, pillaring by different types of poly (hydroxo metal) cations, intraparticle and interparticle polymerization, dehydroxylation and calcination, delamination and reaggregation of smectites, lyophilisation, ultrasound, and plasma. Modified clays are also used in other applications such as adsorbents of organic pollutants in soil, water and air; rheology control agents, paints, cosmetics, refractory varnish, thixotropic fluids, etc (4).

The hydrophilic structure of MMT and other layered silicates presents a problem of incompatibility to mix and disperse with organic hydrophobic polymers. The electrostatic forces holding the clay platelets tightly also cause another problem. In order to overcome these problems, the layered silicates should be organically modified. One way of modifying clay surface to make it more compatible with a polymer is through ion exchange. Since the inorganic cations on the clay surface are not strongly bound, they can be replaced by other organic cations, which are tailored to the polymer in which the clay would be incorporated. For example one side of the molecule can have a quaternary ammonium ion with the other side of the molecule having a long chain alcohol group (25). This process of ion exchange (Figure 2.4) would help render the hydrophilic surface hydrophobic (polymer compatible) by matching the clay surface polarity with the polarity of the polymer (26) and also to separate the clay platelets so that they can be more easily intercalated and then subsequently exfoliated into the polymer (25). In addition, the organic cations may provide various functional groups that can react with the polymer chain to increase adhesion between the inorganic filler and the organic polymer matrix (27).

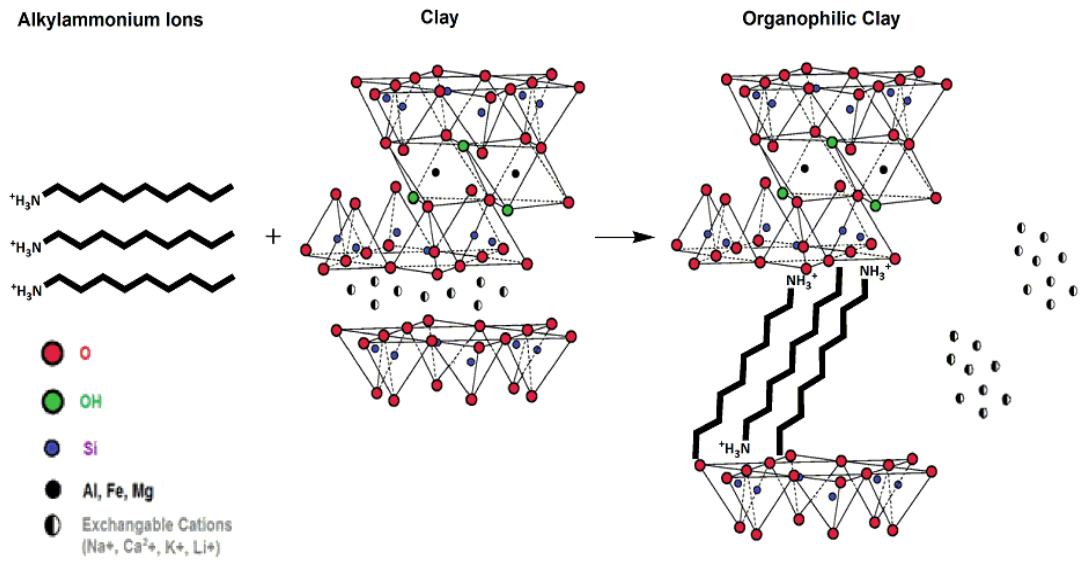

Figure 2.4 Cation exchange process between alkylammonium ions and exchangable cations of layered silicate (modified from (20) & (27))

Depending on the charge density of the clay and the onium ion surfactant, different arrangements of the onium ions as monolayer, lateral bilayer, pseudo-trimolecular layer, and inclined paraffin structure are possible (Figure 2.5) (26).

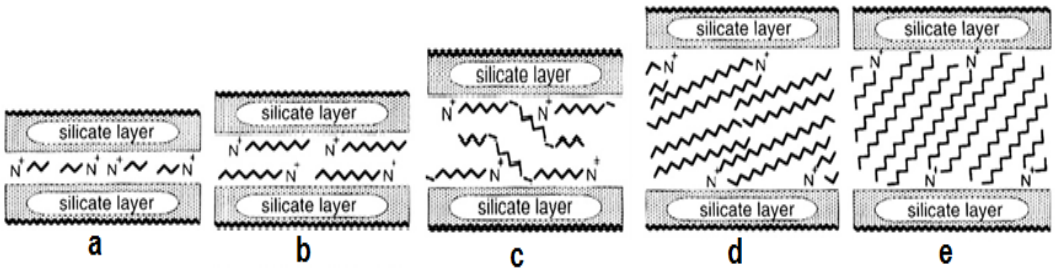

Figure 2.5 Orientations of alkylammonium ions in the galleries of layered silicates: (a) monolayer, (b) bilayers, (c) pseudo-trimolecular layers, and (d, e) paraffin-type arrangements of alkylammonium ions with different tilting angles of the alkyl chains (28)

2.2 Composites

The term composite is used to describe macroscopic combinations of two or more phases, which are insoluble in each other, to give a new material with unique combination of properties (29). The main phase is generally continuous, and termed as the *binder* or *matrix*, and surrounds other embedded discontinuous phase(s), often called the *dispersed* or *reinforcement* phase(s) (30).

Composite materials can be classified according to the matrix (carbon, ceramic, glass, metal, and polymer) or reinforcement (particulate, fibrous). A good understanding of composites can be explained by the reinforcement of plastics with fibers.

In general, the fibers enhance the mechanical properties of the composite by carrying about 70 to 90% of the load present on it. They also provide stiffness, strength, thermal stability, and other structural properties in the composites. They can provide electrical conductivity or insulation, depending on the type of fiber used.

A matrix material plays significant roles in the manufacturing of a satisfactory composite structure. The matrix material binds the fibers together and transfers the load to the fibers, provides rigidity and shape to the structure, isolates the fibers so that individual fibers can act separately and thus stops or slows the propagation of a crack, provides a good surface finish quality and aids in the production of net-shape or near-net-shape parts, provides protection to reinforcing fibers against chemical attack and mechanical damage (wear). (31)

The properties of composites, mainly physical and mechanical, are dependent on the properties, geometry, and concentration of the constituents. In addition, the anticipated mechanical loads, the operating environment for the composite, etc., must all be taken into account. The volume content of the reinforcements should not increase a value, after which the matrix amount will not be enough to keep them separate and thus become tangled (30). Depending on the matrix material selected, performance characteristics such as ductility, impact strength, etc. are also influenced. The failure mode is strongly affected by the type of matrix material used in the composite as well as its compatibility with the reinforcement (31). The matrix-reinforcement interphase where material parameters, such as the concentration of an element, crystal structure, atomic chemistry, elastic modulus, density, coefficient of thermal expansion, etc. differ from one another has great effect on the performance of the composite as well (32). Wettability, surface roughness and interfacial bonding are the main important factors affecting the matrix and reinforcement interface (29).

2.2.1 Polymer Composites

Polymer composites have become more common and are widely used in various industries because of the various advantages they provide. They are low-density cheap materials, easy to process; offer good mechanical properties, generally wet reinforcements well, and provide good adhesion. Above all, they can be processed at low temperatures, where many organic reinforcements can be used.

The terms *thermoset* and *thermoplastic* are often used to identify a special property of many polymeric matrices. The reinforcements used with polymers are mainly

organic and inorganic additives having certain geometries, such as fibers, flakes, spheres and particulates (33). A thermoplastic matrix has polymer chains that are not crosslinked although the chains can be in contact. A thermoplastic can be remolded to a new shape when it is heated to approximately the same temperature at which it was formed. A thermoset matrix has highly cross-linked polymer chains and cannot be remolded after it has been processed. Thermoset matrices are sometimes used at higher temperatures for composite applications (30).

2.3 Nanocomposites

Nanocomposites are a combination of two or more phases containing different compositions or structures, where at least one of the phases is in the nanoscale regime. These materials exhibit behavior different from conventional composite materials with microscale structure, due to the small size of the structural unit and the high surface-to-volume ratio. (34)

Nanocomposites are classified into three main classes, depending on the shape of the nanofiller, i.e., the number of dimensions of the dispersed particles in the nanometer range.

(a) *Nanoparticulate composites* composed of embedded isodimensional particles with three dimensions in the order of nanometers, such as spherical silica nanoparticles, semiconductor nanoclusters.
(b) *Nanofilamentary composites* composed of a matrix with embedded (generally aligned) nanoscale diameter filaments. In this type, two dimensions are in the nanometer scale and the third one is larger, forming an elongated structure such as, carbon nanotubes or cellulose whiskers which are extensively studied as reinforcing nanofillers yielding materials with exceptional properties.
(c) *Nanolayered composites* composed of alternating layers or sheets in which only one dimension is in the nanometer range. In this case, the filler is in the form of sheets (i.e., silicates) one to a few nanometers thick and hundreds to thousands nanometers long. Polymer-layered crystal nanocomposites belong to this group. These materials are almost exclusively obtained by the

intercalation of the polymer (or a monomer subsequently polymerized) inside the galleries of layered host crystals. (19), (35)

Nanolayered composites based on layered silicates have been more widely investigated; probably because of the abundance of the starting clay materials and the variety of advantages they offer (19).

2.3.1 Polymer-Layered Silicate Nanocomposites

Depending on the nature of the components and processing conditions, layered silicates filled into a polymer matrix, produce either conventional composite or nanocomposite. Figure 2.6 shows the types of nanocomposites structures. If the polymer cannot intercalate into the galleries of clay minerals, conventional microcomposite is obtained with properties similar to that of polymer composites reinforced by microparticles. Intercalated nanocomposite (i) is produced when a monolayer of extended polymer chains is inserted into the gallery of clay minerals resulting in a well ordered multilayer morphology, stacking alternately polymer layers and clay platelets and a repeating distance of a few nanometers. Exfoliated or delaminated nanocomposite (ii) forms when the clay platelets are completely and uniformly dispersed in a continuous polymer matrix. However, it should be noted that in most cases the cluster nanocomposite (iii) is common in polymer nanocomposites (36).

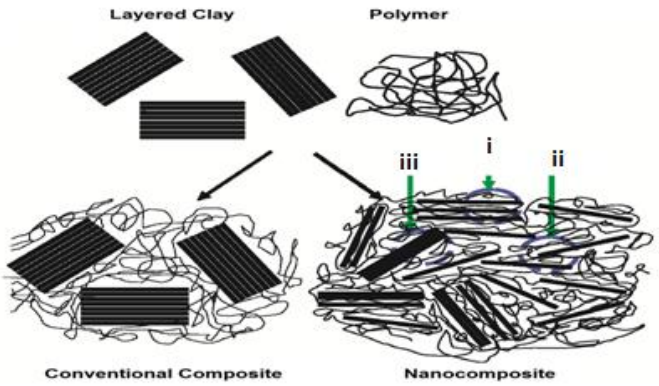

Figure 2.6 Schemes of polymer/clay composites, including conventional composite and nanocomposite with intercalated (i), exfoliated (ii) or cluster (iii) structure (36)

The attractive characteristics of polymer-layered silicate nanocomposites already suggest a variety of possible industrial applications: automotive (gas tanks, bumpers, interior and exterior panels), construction (building sections and structural panels), aerospace (flame retardant panels and high performance components), food packaging, textiles, etc. It is for this reason that many companies have taken a strong interest and have invested in developing nanoclays and polymer nanocomposites. The first commercial product of clay-based polymer nanocomposites was the timing-belt cover made from PA6 nanocomposites by Toyota Motors in the early 1990s. This timing-belt cover exhibited good rigidity, excellent thermal stability and no wrap. It also saved weight by up to 25%. Later, General Motors and partners Basell, Southern Clay Products and Blackhawk Automotive Plastics announced external automotive body parts (step-assist) made from thermoplastic, olefin layered silicate nanocomposites. A thermoplastic olefin (TPO) nanocomposite with as little as 2.5% layered silicate is as stiff as and much lighter than parts with 10 times the amount of conventional talc filler. Thus, the weight savings can reach 20%, depending on the part and the material that is being replaced by the TPO nanocomposite. (37)

2.3.2 Nanocomposite Preparation

Polymer-layered silicate nanocomposites can be prepared by various methods including; in-situ polymerization, solution intercalation, melt intercalation and sol-gel.

2.3.2.1 In-Situ Polymerization Method

In in-situ polymerization method, a liquid monomer (or a monomer solution) is inserted between the galleries of the layered silicates and then polymerized within the gallery via an initiator such as, heat, radiation, pre-intercalated initiators or catalysts (36). The swelling step depends on the polarity of the monomer molecules, the surface treatment of the organoclay, and the swelling temperature. The high surface energy of the clay attracts polar monomer molecules so that they diffuse between the clay layers and intercalate. Then, polymerization reaction starts

by the attraction between the monomer and the curing agent. Finally, the delamination of organic molecules within the clay layers occurs (Figure 2.7). The polymerization initiator for thermosets, such as epoxies or unsaturated polyesters, can be a curing agent or peroxide, respectively. For thermoplastics, the polymerization can be initiated either by the addition of a curing agent or by an increase of temperature. In-situ polymerization is the first method used to synthesize polymer-layered silicate nanocomposites based on polyamide 6 (21).

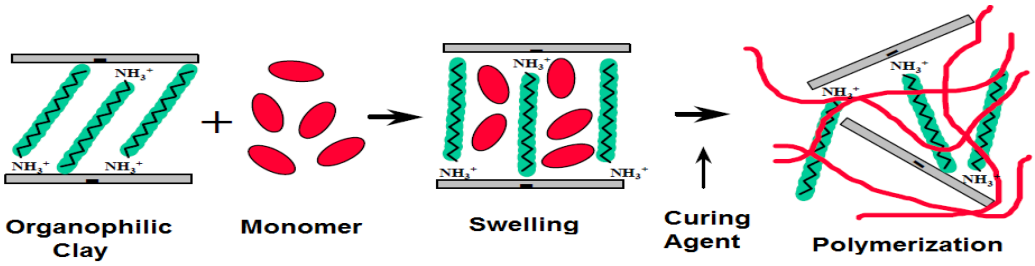

Figure 2.7 In-Situ polymerization method (21)

2.3.2.2 Solution Intercalation Method

In solution method, layered clays are separated into single platelets due to the weak van der Waals forces that hold the clay platelets together using a solvent in which the polymer is soluble. Then, the polymer, dissolved in the solvent, is added to the clay suspension and intercalates between the clay layers. The solvent is finally removed from the clay-polymer complex through evaporation (Figure 2.8). The decrease in conformational entropy of the intercalated polymer chains is compensated by the entropy gained by desorption of solvent molecules. This entropy is the main driving force for polymer intercalation from solution (21), (36).

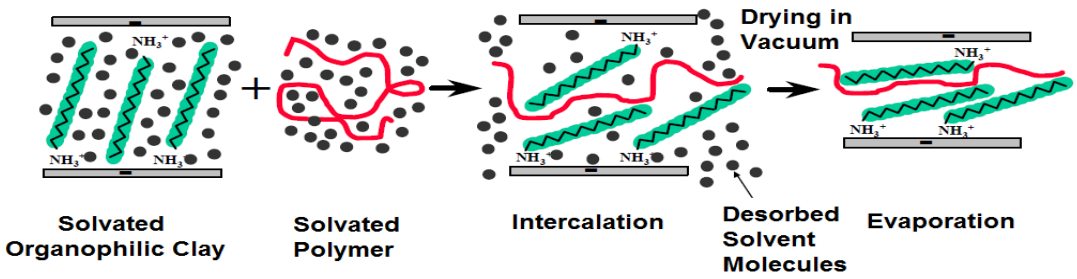

Figure 2.8 Solution intercalation method (21)

2.3.2.3 Melt Intercalation Method

First reported by Vaia et al. in 1993 (38), melt intercalation process involves heating a polymer and layered silicate mixture above the glass transition temperature under static or flow conditions in the absence of solvent. The polymer chains spread from the molten mass and invade the silicate galleries, to form either intercalated or delaminated hybrids according to the degree of penetration (Figure 2.9). Polymer-compatible modified layered silicates are usually employed to promote intercalation.

A gain in entropy, due to the greater conformational energy of the aliphatic chains of the alkylammonium cations due to the increase in the size of the galleries caused by insertion of the polymer, is suggested to be the driving force for a spontaneous melt intercalation process (39).

The melt intercalation process has become popular because of its great potential for application in industry. Indeed, polymer-clay nanocomposites have been successfully produced by extrusion of a wide range of thermoplastics, from strongly polar polyamide, to weakly polar PET to non-polar polystyrene. Polyolefins, which represent the biggest volume of polymers produced, have so far only been successfully intercalated to a limited extent (21). Direct polymer melt intercalation is also known as the most attractive way because of its low cost, high productivity and compatibility with current polymer processing techniques (40).

In addition to absence of solvent in melt intercalation process, it differs from other preparation methods in the strong shear forces acting on the system, which affect the dispersion of clay platelets. Besides, matrix viscosity and the mean residence time also affect the degree of the dispersion. (41)

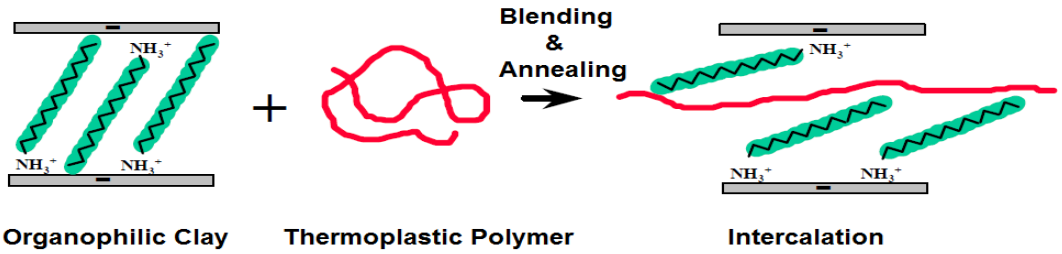

Figure 2.9 Melt intercalation method (21)

2.4 Polymer Matrices

Two polymer matrices, Polyamide 66 (PA66) and amorphous Poly(ethylene terephthalate) (PET) were used throughout this study.

2.4.1 Polyamide 66 (PA66)

Polyamides, with linear synthetic aliphatic class named as nylons (42), are considered as the first high performance engineering plastics owing to their excellent balance of properties; such as, high thermal stability, flame retardancy, resistance to oils and solvents, fatigue resistance, abrasion resistance, low coefficient of friction, toughness, ductility and mechanical strength, electrical, and chemical resistances (due to their crystalline structure) (43). Although introduced in the 1930's, these materials have retained their vitality, with new types of polyamides being developed especially for automotive and electrical applications (13), (44).

Polyamides are divided into two classes according to regularity of the amide linkages along the polymer chain i.e., the number of carbon atoms in the monomer chains. Amino acid polymers are designated by a single number, as Polyamide 6 (PA6) for polycaprolactam. Polyamides from diamines and dibasic acids are designated by two numbers, the first representing the diamine, as polyamide 66 (PA66) for the polymer of hexamethylenediamine and adipic acid by stepwise polymerization (42). The synthesis reaction of PA66 is given in Figure 2.10.

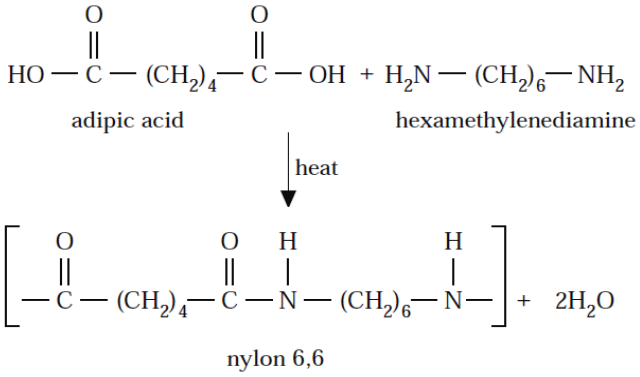

Figure 2.10 Synthesis reactions of polyamide 66 (45)

Polyamide 66 is an important resin which is widely used in engineering plastics and fiber industries. It is flammable and thus anti-flaming modification is necessary in many cases of usage (12). The possible production of PA66-organoclay nanocomposites with better flammability properties is of great importance too.

2.4.1.1 Properties of Polyamide 66

2.4.1.1.1 Physical Properties

Crystallinity: The semicrystalline structure of polyamides and their high melting point are mainly owed to the high degree of stability offered by hydrogen bonding between the carbonyl and NH groups in adjacent sections of the polyamide chains. This hydrogen bonding exists due to the presence of the polar amide groups. The crystal structure of PA66 is composed of triclinic α and β forms with one chemical per unit cell (46). Figure 2.11 shows the unit cell for polyamide 66. The average crystal size in polyamides is usually a function of the mechanical and thermal history of the polymer. When the chains in polyamide 66 are aligned together, the regular spatial alignment of amide groups allows hydrogen bonding to be developed and give rise to a crystalline structure in that region. Polyamide 66 is a polar semicrystalline polymer consisting of ordered crystalline regions and more amorphous regions having much lower concentration of hydrogen bonding. The good balance of properties in polyamide 66 are virtue to this structure in which the crystalline regions contribute to the stiffness, strength, chemical resistance, creep resistance, temperature stability, and electrical properties; and the amorphous areas contribute to the impact resistance and high elongation at break (44).

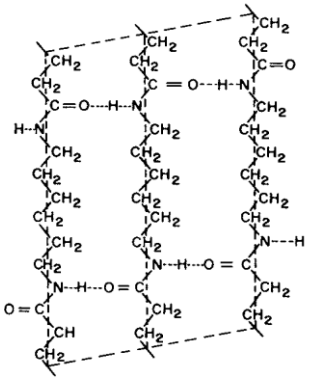

Figure 2.11 Chain conformations of Polyamide 66 (13)

Thermal Properties: The strong hydrogen bonding between the chains, which depends on the density of amide groups and the crystal structure, imparts thermal stability to polyamide 66 such as, a high melting point of about 265°C which permits retaining of significant stiffness above the glass transition temperature (T_g) and almost up to the melting point. The majority of the hydrogen bonding rapidly breaks down at that temperature, giving a low viscosity, water-like melt. The influence of structure on the melting point is further complicated by factors that affect the ease of crystallization. The glass transition temperature of aliphatic polyamides is rather low (40-70°C) and composition does not affect T_g to any great extent. The heat deflection temperature of PA66 is about 75°C and it has a linear expansion coefficient of $8*10^{-5}$ cm/cm °C. (43)

Moisture Absorption: Moisture absorption is determined by both the degree of crystallinity and the density of amide groups of the polyamides. Polyamides are highly sensitive to moisture. Polar water molecules coordinate around the polar amide groups of polyamides, mainly in the amorphous regions during absorption process. Upon moisture absorption the polymer hydrogen bonding is interrupted, by lowering its T_g, tensile strength (making it more flexible) and increasing the impact strength and the polymer is plasticized (13).

Electrical Properties: The combination of mechanical, thermal, chemical, and electrical properties of polyamides opened the path for their wide uses in electrical applications. They are reasonably good insulators at low temperatures and humidity and are generally suitable for low frequency, moderate voltage applications (44).

Flammability: Most polyamides are self-extinguishing within a certain time-scale. They achieve this performance by means of giving off burning drips (44).

2.4.1.1.2 Mechanical Properties

The semicrystalline structure of nylons imparts high strength (tensile, flexural, and compressive) and modulus (stiffness) as a result of increasing density of amide groups and thus crystallinity in the crystalline region, and good toughness (impact strength) due mainly to the amorphous region. Nylons containing aromatic

monomers tend to have increased stiffness and strength by virtue of the greater rigidity of the chains. Thus, reinforcing these polymers with aromatic chains should impart better properties in this sense. The molecular weight, moisture content, temperature, and the presence of additives affect the properties of PA66. The impact strength increases with molecular weight without affecting the tensile strength (13).

PA66 is notch-sensitive and the unnotched impact strength is dramatically reduced when a notch or flaw is introduced into the material. This notch sensitivity can be reduced by incorporating impact modifiers. The increased ductility of the material that accompanies impact modification does, however, reduce stiffness and strength. Moisture conditioning of moldings is often used to increase impact strength and flexibility before such operations as snap fitting or assembling cable ties, which can be avoided in some cases by using impact-modified resins (44).

Properties such as stiffness and strength can be considerably increased by adding a reinforcing agent to the polymer, particularly glass or carbon fiber, which forces the material to fail in a brittle rather than ductile fashion. Mechanical properties can also be modified by the inclusion of plasticizers, which have a similar effect to that of water in breaking down hydrogen bonding in the amorphous region and increasing ductility, flexibility, and impact strength. Nylons have good resistance to dynamic fatigue, i.e., the application of cyclic loads, abrasion resistance and low coefficient of friction (43).

2.4.1.1.3 Chemical Properties

Thermo-chemical Degradation: The presence of adipic acid is the main cause for thermal degradation in PA66 in the melt when held for long periods of time or at high temperatures. Adipic acid segment can cyclize, leading to chain division and the production of cyclopentanone and derivatives and evolution of carbon dioxide and ammonia. As well as reduction of molecular weight, cross-linking also occurs, and the material eventually sets into an inflexible gel. When the residence time is short or the shot size is small, the only problem is the loss of molecular weight during injection molding, particularly at high temperatures over 300°C (13).

Oxidation - Ultraviolet Aging: Polyamides are vulnerable to oxidation which includes the initial formation of a free radical on the carbon alpha to the NH group. The free radical reacts to form a peroxy radical with subsequent chain reactions leading to chain scission and yellowing. Discoloration or loss of molecular weight can be avoided by minimizing the exposure of hot nylon to air. Oxidation of polyamides also occurs when their parts are exposed to high temperature in air. This process can be minimized by using material containing stabilizer additives. Nylon parts exposed to sunlight and UV rays undergo a similar free-radical aging process and can be reduced with appropriately stabilized materials (13).

Effect of Chemical Solvents: Polyamides have superior resistance to many chemicals depending on their natures. The site of attack may be in the molecule: the end groups, the amide nitrogen, the amide carbonyl, or the hydrocarbon portion depending on the nature of reaction (46). They are resistant to aqueous salts, alkalis and nonpolar solvents such as hydrocarbons. Resistance weakens in the presence of strong acids, alcohols and phenols which are most effective at disrupting the hydrogen bonding and which can sometimes dissolve the nylon (44).

2.4.2 Poly(ethylene terephthalate), (PET)

Polyesters have hydrocarbon backbones which contain ester linkages in long chains. Poly(ethylene terephthalate), or PET, is a linear semicrystalline thermoplastic typical member of the polyester family composed of repeated units of (-CH_2CH_2-OOC-C_6H_4-COO-) containing a phenyl group (C_6H_4). PET was first synthesized in 1946 and was commercially introduced in 1953 as a semicrystalline textile fiber. PET is considered as one of the most multifunctional engineering plastics because of its low cost, high strength, rigidity, and toughness; low creep at elevated temperatures; excellent dimensional stability; low coefficient of friction; good chemical resistance of grease, oil, and solvent; minimal moisture absorption; good thermal resistance and excellent electrical properties. PET and its composites are widely used in packaging, construction, automobile, household, electrical and textile industries (47), (48). Considerable efforts have been devoted to improve various physical, mechanical and barrier properties of PET through mixing it with nanoclays to produce layered clay-incorporated PET composites (49).

PET is a polycondensation polymer which can be synthesized by direct esterification of purified terephthalic acid (PTA) and ethylene glycol (EG), or transesterification of dimethyl terephthalate (DMT) with ethylene glycol (EG) (47). PET synthesis from DMT is shown in Figure 2.12.

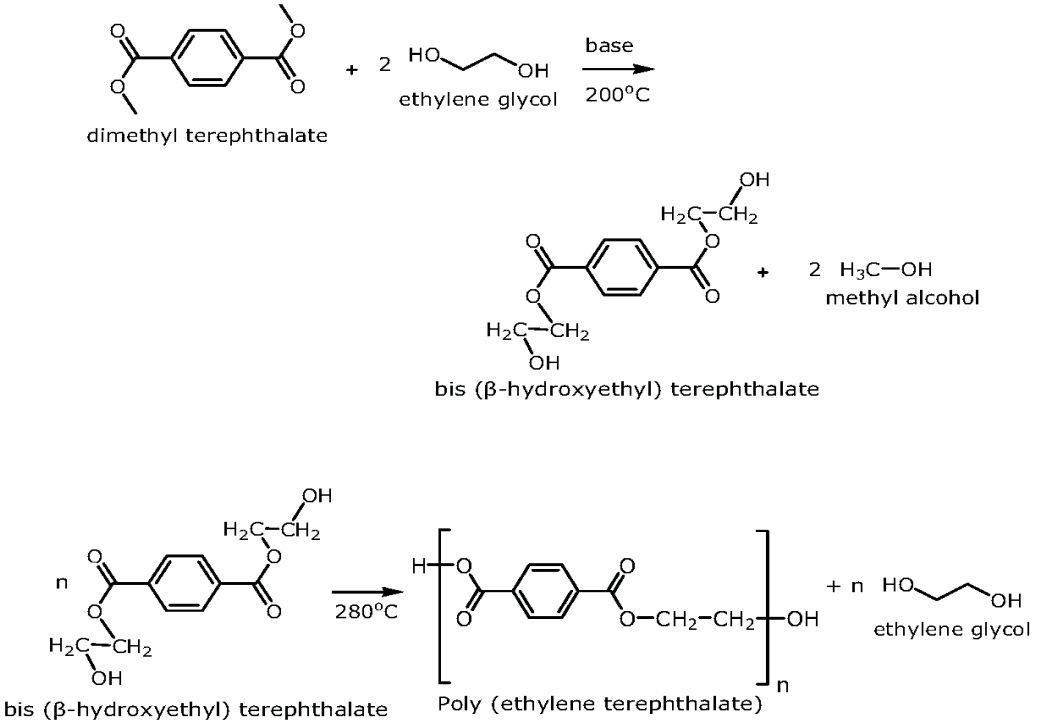

Figure 2.12 Synthesis reactions of poly(ethylene terephthalate) (45)

2.4.2.1 Properties of Poly(ethylene terephthalate)

2.4.2.1.1 Physical Properties

Crystallinity: PET is a crystallizable polymer. Its degree of crystallization mainly depends on the manufacture process, molecular weight, catalyst system and co-monomer kind and content. This polymer can be produced in glassy or amorphous transparent solid forms by rapid quenching of the melt below the glass transition temperature. Amorphous PET is prepared by rapidly cooling the molten resin from a melt temperature of 260°C to temperature below the glass transition of 73°C. On the other hand, slow cooling of the molten resin will produce a crystalline polymer. Amorphous resin tends to soften and stick at elevated temperatures of drying,

forming clumps and adhering to the walls of the drying unit. The low mechanical properties, high gas permeation rates, and low dimensional stability of amorphous PET decrease its commercial significance. The properties of a polymer depend on its structural arrangement and are closely related to the internal morphology structure of the polymer (47).

The crystallization rate of PET is very important in processing. Crystallinity has a great effect on the product clarity and processability. However, if the size of the crystallite is small enough to minimize light scattering, clarity can be achieved inspite of the crystallinity of the polymer. The full crystal structure of PET forms triclinic crystals with one polymer chain per unit cell. PET does not crystallize well in the un-oriented state even in a hot mold unless nucleating agents and/or plasticizers are added. Commercial PET molding-grade polymers are nearly always filled (13).

Thermal Properties: The thermo-chemical data depend on the degree of crystallinity in PET. The melting point of highly annealed PET can have values higher than 260-265°C. The glass transition temperature depends on the method of measurement and the state of this polymer (44).

Moisture Absorption: The hygroscopic property of PET, natural ability to absorb water from its surroundings, is one drawback of its usage. When wet PET is heated, the water hydrolyzes the PET, decreasing its resilience (elasticity). Thus, the removal of moisture from PET, by desiccants, ovens or dryers, before processing is crucial to obtain good properties of the product. Typically residual moisture levels in the resin must be less than 5 ppm (parts of water per million parts of resin, by weight) before processing (17).

Mechanical Properties: The molecular orientation of chains in PET, achieved by stretching during processing, enhances its mechanical properties in the orientation direction. The enhanced properties of oriented PET molecules can be diminished or lost and change to random state during cooling process. To avoid that, and maintain orientation, the oriented molecules are frozen during the stretching process. Un-oriented PET has average tensile strength at yield of 50-55 MPa

compared to up to 165 MPa when PET has an orientated structure. The main properties attributed to the molecular orientation of PET are excellent gloss and clarity, toughness and impact resistance, low permeability to CO_2, good processability, good dimensional ability and high heat resistance (50). Because of the slow crystallization rate, PET injection molded parts, for example automotive, electronic, and furniture parts, have poor mechanical properties. To promote crystallization in injection molded parts, the mould temperature can be increased to 140°C and the resin is modified using nucleating agents. Generally, commercial PET resins used in engineering applications are filled with 20-50% of fiberglass to increase strength, stiffness (51).

2.4.2.1.2 Chemical Properties

PET has ester groups in the polyester chain which are polar, having both a negative and a positive charge (Figure 2.13). The positive charge of the carboxyl carbon atom and the negative charge of the carboxyl oxygen atom in different ester groups are attracted to each other. This allows the ester groups of nearby chains to line up with each other in crystal form. This is the cause of PET's high glass transition and melting temperature (52).

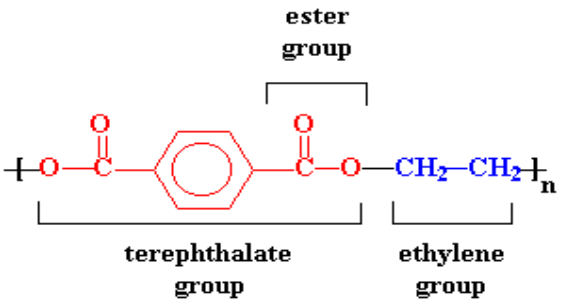

Figure 2.13 Hydrocarbon backbone of PET (52)

Degradation: PET can experience various degradation processes such as hydrolytic degradation in the presence of moisture, thermal degradation under the influence of heat alone, oxidative degradation upon heating in the presence of atmospheric oxygen, photo-oxidative degradation under the influence of light and oxygen, radiochemical degradation under the influence of ionizing radiation, and chemical degradation in the presence of various reagents. In hydrolytic

degradation, the chemical reaction of PET with water at elevated temperatures leads to a reduction in molecular weight and the formation of carboxyl and hydroxyl end groups. The amount of hydrolytic degradation in the melt is larger when the material has previously been dried in an air atmosphere rather than in a vacuum or inert environment. Thermal-oxidative degradation of PET causes a more severe reduction of molecular weight and increase in the formation of gaseous products than purely thermal degradation. When PET is melted in the presence of air, degradation increases rapidly with increasing temperature. The rate of degradation increases in the following order as a result of melting and drying conditions: vacuum drying-nitrogen melting, air drying-nitrogen melting, vacuum drying-air melting, and air drying-air melting (highest degradation). In this study, vacuum drying was applied on PET prior to melt compounding; however PET was melted in air rather than in a nitrogen environment. The degradation processes of PET can be minimized by physical means such as drying temperature and time, processing temperatures, residence time in the melt, melt and drying environments, and moisture content. Chemical factors involve controlling molecular weight or intrinsic viscosity and polymerization conditions (47).

2.5 Compatibilizing Agents

The presence of an organoclay as a reinforcing agent for polymeric materials increases the stiffness in the polymer-clay composite system. In general, the Young's modulus and tensile strength increase, but ductility and fracture toughness decrease (53). Elastomeric materials with low Young's modulus and mechanical properties are used to increase the number of functional groups that can interact with the organoclay surface. In order to end up with polymer composites having balanced toughness and stiffness, an optimum combination of organoclay acting as a reinforcing and stiffening agent, and elastomeric phase (toughening agent and compatibilizer) can be incorporated together or alone depending on the final aimed product.

Maleic anhydride containing elastomers can generally be incorporated into the polymer matrix as a compatibilizer as well as an impact modifier since the interfacial

interaction between polymer, organoclay and impact modifier results in finer dispersion of elastomeric domains and increase in toughness (54). Maleated elastomers are known to improve the toughness properties of PA66 (53). Also glycidyl methacrylate (GMA) containing elastomers are popular to bond with polyolefins, polyesters due to the GMA reactivity with acid, amine and hydroxyl groups (55), (56), (57). In the present study, Lotader® 2210 resin (a random terpolymer of ethylene, butyl acrylate and maleic anhydride (E-BA-MAH)) and Lotader® AX8900 resin (a random terpolymer of ethylene, methyl acrylate and glycidyl methacrylate (E-MA-GMA)) were used with PA66 and PET respectively.

2.6 Polymer Processing Methods

Processing involves the conversion of the solid polymer into the desirable size and shape. There are a number of methods to shape the polymer, including extrusion and injection molding.

2.6.1 Extrusion

Extrusion is one of the most widely used ways of fabricating plastic products. It is a processing technique for converting thermoplastic materials in powdered or granular form into a continuous melt, which is shaped into items by forcing it through a die (45). Different materials can be formed through an extrusion process, such as metals, ceramics, clays, foodstuffs, and plastics either in the molten or solid state. The most common plastics being extruded are thermoplastics, with some thermosets extruded at temperatures lower than the curing temperature. Extruders in the polymer industry come in many different designs, where the main distinction is their mode of operation: either continuous (single screw, multiple screws) having a rotating member or discontinuous having a reciprocating member (58).

Among multiple screw extruders the most commonly used type is the twin screw type. Twin screw extruders offer some advantages such as; good mixing, good heat transfer rate and large melting capacity. For this type, different screw configurations are possible; intermeshing and non-intermeshing. While non-intermeshing twin

screws are offered only with counter-rotation, intermeshing screws can be employed in a co-rotating or counter-rotating pattern. In co-rotating pattern, the screws rotate in the same direction. This type of extruder support high contact with the extruder barrel, which improves the efficiency of the thermal heating, and provides better mixing compared to other processes. The path also ensures that most of the resin will be subjected to the same amount of shear as it passes between the screws and the barrel (59).

2.6.2 Injection Molding

Injection molding is a process used for producing plastic parts with required shapes and dimensions (60). In this process, usually a thermoplastic material is forced by a ram through a heating chamber and then to a nozzle or die and finally into a closed mold where the material takes up the required form (61). The thermoplastic must be cooled under pressure below T_g and T_m before the opening of the mold followed by part ejection (62).

The main processing parameters of injection molding process are the cycle time, temperature and pressure. The molding cycle consists of three main steps; filling, packing and cooling. The pressure rises slowly during the filling cycle and the shrinkage is offset by the maintenance of high pressures at the packing stage, and the pressure in the mold relaxes during the cooling stage. The total cycle time that is controlled by the cooling stage is dependent on the thickness of the molded piece, since the heat transfer through the poorly conductive polymer is the resistance to cooling. Cooling time typically changes in the range of 10 to 100 seconds (63). In the case of heat sensitive materials, especially during the processing of thermosets, the residence time in the barrel should be minimized. Usually, a fast cycle time and mold temperature with the lowest possible value is preferred for economic reasons. However, too low mold temperature may end up with inadequate surface finish and crystallization which affects performance of the article negatively. Moreover, the injection speed and pressure should be determined according to the types of the materials and the nature of the mold. High injection speed is generally preferred to avoid the formation of premature freezing due to crystallization, especially when the parts are complicated (64).

Jetting, short shot and thermal degradation are some problems of injection molding process. Jetting occurs if the flow progress inside the cavity is not uniform. A short shot mainly occurs when flow rates decrease due to insufficient process pressures. It is an incomplete part caused by premature solidification inside the cavity (65). Thermal degradation problem usually appears when significant temperature rises of the melt may arise from high viscosity and fast flow as the melt proceeds towards the cavity (63).

2.7 Previous Studies

2.7.1 Studies on Surface Modification of Layered Silicates

Clays and clay minerals can be surface modified by many processes such as adsorption, ion exchange with inorganic cations and organic cations, binding of inorganic and organic anions (mainly at the edges), grafting of organic compounds, reaction with acids, pillaring by different types of poly(hydroxo metal) cations, intraparticle and interparticle polymerization, dehydroxylation and calcination, delamination and reaggregation of smectites, and lyophilisation, ultrasound, and plasma (4). Ion exchange with alkylammonium ions is well-known and the desirable method to prepare organoclays. Other clay surfactants, like phosphonium or imidazolium salts, have been used in order to enhance the thermal stability of organoclays and overcome the problem presented by ammonium surfactants (8).

Clay Purification Studies

Lee and Kim (66) purified smectite sample containing quartz, and some heavy minerals as impurities. Fractions of smectite with size less than 2 μm were obtained by wet sedimentation in which smectites were dispersed in distilled water and left to stand several hours to allow settling of quartz sand and heavy minerals.

Onal et al. (9) isolated a smectite from the Reşadiye (Turkey/Tokat) bentonite by precipitating the bentonite in water for various time intervals. The original bentonite, its fractions and the high purity smectite product were analyzed by XRD, and a

chemical analysis was done by absorption spectrophotometer. XRD patterns showed that bentonite contained clay minerals such as sodium rich smectite, sodium-calcium smectite and illite. In addition, the bentonite had clinoptilolite (Cln), analcime (An), feldspar (F), calcite (C), dolomite (D), quartz (Q) and opal-C (OC) as non-clay minerals. Final fraction obtained from water-bentonite suspension after one and a half month contained trace amount of Opal-C and was almost pure sodium smectite. They found the structural formula of the smectite by chemical analysis and stated that it was very similar to sodium-rich mineral montmorillonite. They concluded that settlement of bentonite suspension for various time intervals was successful in isolating the sodium-smectite similar to sodium-montmorillonite.

Lee and Lee (13) purified Ca-montmorillonite-rich clay from bentonite of Korean origin, and it was treated with many cationic organo-surfactants. The exchanged weight contents of the organo-surfactants increased with the increase in their molecular weight. For the same main chain carbon number of the surfactants, the exchanged contents in mole of the primary types were higher than those of the tertiary types.

Yilmaz and Yapar (67) purified Tokat/Reşadiye Turkish bentonite to use it in surface modification. Coarse-fraction impurities such as iron oxides and silica were removed by subjecting the bentonite dispersions to repeated sedimentation. The layer at the bottom was removed and upper portions were exposed to sedimentation until no gritty layer remained.

Gracia-Lopez et al. (68) used MMT and low cost bentonite in polyamide 6 nanocomposites formation to see the effect of bentonite usage which is cheaper than the MMT. They purified the bentonite firstly dispersing in water, then eliminating supernatant organic phases, wet shieving, milling with steatite balls and then treatment with high shear dispersion in a machine. Their low cost bentonite exhibited similar microscopic and macroscopic results to the MMT.

Song et al. (69) worked on the beneficiation of Ca-montmorillonite fines from ores by dispersion-sedimentation process using sodium phosphates as the dispersant. Several parameters in the dispersing step, such as type and dosage of dispersant,

solid concentration, and slurry stirring time were tested to understand their effects on beneficiation. It was shown that the beneficiation process was very effective in upgrading montmorillonite, producing a high-grade montmorillonite concentrate. Simultaneously, the Ca-montmorillonite was transformed to Na-montmorillonite. Sodium pyrophosphate was found as the best phosphate dispersant for achieving good beneficiation of montmorillonite from the ore, which might be due to the fact that pyrophosphate ions adsorbed on montmorillonite surfaces lead to a smaller swelling capacity of the mineral particles than other phosphate ions.

Tyagi et al. (70) upgraded montmorillonite rich Indian bentonite from Barmer district by sedimentation to remove impurities like grit before use. Ten fractions were analyzed and the purity of the clays increased after each sedimentation treatment.
Patel et al. (71) purified montmorillonite rich Indian bentonite clay by sedimentation technique according to Stokes' law. The purified bentonite was rich in montmorillonite with Na^{+} and Ca^{+2} as exchangable cations. The purified bentonite contained minor amount of kaolinite (1-2% w/w).

Tabak et al. (72) synthesized organobentonites from different origins (Wyoming and Reşadiye) with cetylpyridinium chloride by ion exchange and compared them. It was concluded from the XRD, thermal analysis, FTIR and surface area measurements data that the amount of organic cation penetrated into the interlamellar space of Na-bentonite (Wyoming) was higher than that of Na-bentonite (Reşadiye). The difference in the basal spacing was 0.65 Å and a higher mass loss by 13.32% of organobentonite (Wyoming) in the temperature range 200-550°C compared to that of organobentonite (Reşadiye) were in conformity with the CEC values of organobentonites.

Nakaş et al. (73) worked on the purification and surface modification of Reşadiye Turkish sodium montmorillonite. The highly pure bentonite (90%) was purified further before surface modification in order to increase the efficiency of the intercalation. The main principle of purification procedure was Stokes' Law according to which the non-clay minerals, that have higher weight than the clay minerals, settle down by leaving the clay minerals in suspension. So the purification was accomplished by using the difference between the settlement rates of the clay

and water. Separation of clay minerals from non-clay minerals such as mica was enough for purification of this clay, since it did not contain other types of minerals, such as kaolinite or even Ca-montmorillonite.

Thermal Stability Studies with Ammonium Organoclays

Xie et al. (74) investigated the thermal stability of MMT modified by long carbon-chain alkyl quaternary ammonium ions and found that the onset decomposition temperature of the resultant organically modified layered silicates was approximately 180°C.

Zheng and Wilkie (75) interestingly reported that methyl tallow bis-2-hydroxyethyl ammonium modified clay and dimethyl dihydrogenated tallow alkyl ammonium modified clay showed very good thermal stability, with 10% degradation (10% mass loss) occurring around 390°C.

Xie et al. (76) reported that the thermal decomposition of organic substances between silicate layers was mainly in the range of 200-500°C. They also showed that the Na^+-MMT exhibited no weight loss in this range of temperature; in contrast, the organic MMTs (modified with dimethyldioctadecyl ammonium or trimethyloctadecyl ammonium) exhibited significant weight loss. The MMT modified with dimethyldioctadecyl ammonium exhibited larger weight loss in the range of 200-350°C than MMT modified by trimethyloctadecyl ammonium. This indicated that the former contained more organic matter than the latter, which accounted for the larger interlayer distance of MMT modified with dimethyldioctadecyl ammonium. In addition, the thermal stability of ammonium salts is not suitable for processing at temperatures above 200°C.

Thermal Stability Studies with Phosphonium and Imidazolium Organoclays

Singh et al. (77) prepared high-temperature polymer inorganic nanocomposites using organically modified layered silicates with phosphonium surfactants (i.e.: tetra-phenyl phosphonium with thermal stability in the range of 190-200°C). The

heat resistance and thermal stability of the nanocomposite systems were enhanced from ranges of 100-150°C to over 250°C.

Gilman, et al. (6) prepared polymer/layered silicate nanocomposites from thermally stable trialkylimidazolium-treated montmorillonite. Several trialkylimidazolium salt derivatives were prepared with propyl, butyl, decyl, and hexadecyl alkyl chains attached to the imidazolium through one of the nitrogens, and then used to prepare the corresponding treated layered silicates. They reported that the use of 1-alkyl-2,3-dimethylimidazolium salts to replace the sodium in natural MMT gives organophilic MMT with a 100°C improvement in thermal stability (in N_2) as compared to the alkylammonium-treated MMT. The use of 1,2-dimethyl-3-hexadecylimidazolium- treated MMT gave an exfoliated PA-6 nanocomposite, and depending on processing conditions, either a partially exfoliated or an intercalated polystyrene nanocomposite was obtained. The XRD data showed that the longer the alkyl chain length is, the higher the interlayer distance and thermal stability of Na^+-MMT become.

Xie et al. (8) studied the thermal stability of quaternary phosphonium modified montmorillonite. The non-oxidative thermal degradation chemistry of alkyl and aryl quaternary phosphonium-modified montmorillonite (P-MMT) was examined using TGA, combined with pyrolysis/GC-MS. The onset decomposition temperature via TGA of these P-MMTs ranged from 190 to 230°C. Overall, the interlayer environment of the montmorillonite had a more severe effect on stability of the phosphonium surfactant than previously reported for ammonium-modified montmorillonite (N-MMT). Nonetheless, the overall thermal stability of P-MMT was higher than that of N-MMT. These observations indicated that, in addition to their conventional purpose as stabilizers, phosphonium salts offer unique opportunities for melt processing polymer layered silicate nanocomposites.

Hartwig et al. (78) investigated the thermal decomposition and the flammability behavior of epoxy resin layered silicate nanocomposites based on ammonium salt and phosphonium salt modified organoclays. The thermal stability and clay distribution were better in the phosphonium organobentonite even though the filler was not homogeneously distributed in both materials.

Awad et al. (7) investigated the thermal degradation of alkyl-imidazolium salts and their application in nanocomposites. These organically-modified clays were characterized by X-ray diffraction (XRD) and thermogravimetry coupled with Fourier transform infrared spectroscopy (TGA-FTIR) and compared to the conventional quaternary alkyl ammonium montmorillonite. Results indicated that the counter ion has an effect on the thermal stability of the imidazolium salts, and that imidazolium salts with PF_6^-, $N(SO_2CF_3)_2^-$ and BF_4^- anions are thermally more stable than the halide salts. A relationship was observed between the chain length of the alkyl group and the thermo-oxidative stability; as the chain length increased from propyl, butyl, decyl, hexadecyl, octadecyl to eicosyl, the stability decreased. The results also showed that the imidazolium-treated montmorillonite had greater thermal stability compared to the imidazolium halide. Analysis of the decomposition products by FTIR provided an insight about the decomposition products which were water, carbon dioxide and hydrocarbons.

Chu et al. (79) prepared Styrene-acrylonitrile (SAN) layered silicate nanocomposites by melt compounding. These nanocomposites exhibited improved thermal stability and reduced flammability. Four different organic treatments were used on the clay surface to study the effects of organic treatment on clay dispersion: dimethyl, bis(hydrogenated tallow) ammonium (DMHTA), methyl tallow bis-2-hydroxyethyl ammonium (MTBHA), triphenyl n-hexadecyl phosphonium (TPHDP), and 1,2-dimethyl-3-n-hexadecyl imidazolium (DMHDI). The MTBHA organic treatment also provided lower flammability as measured by micro-cone calorimeter, and improved thermal stability as measured by TGA.

Chua et al. (80) produced thermally stable organically modified clays based on 1,3-didecyl-2-methylimidazolium (IM2C10) and 1-hexadecyl-2,3-dimethyl-imidazolium (IMC16) and used these to prepare poly(ethylene naphthalate) (PEN)/montmorillonite (MMT) nanocomposites via a melt intercalation process. Examination by X-ray diffraction and transmission electron microscopy indicated that an intercalated nanocomposite was formed with IMC16-MMT, while unmodified MMT (Na-MMT) and IM2C10-MMT were generally incompatible with PEN. Thermogravimetric analysis revealed that the peak derivative weight loss temperature of the intercalated PEN/IMC16-MMT was more than 10°C higher

compared to neat PEN, PEN/Na-MMT, or PEN/IM2C10-MMT. Dynamic mechanical analysis also showed that a more significant improvement of the storage modulus was achieved in the better dispersed PEN/IMC16-MMT.

Ding et al. (81) investigated the possibility of organic modification of montmorillonite (MMT) in hydrocarbon solvents by employing ionic liquid-type surfactant. The ionic liquid-type surfactant, 1-methyl-3-tetradecylimidazolium chloride, was used in effective ion exchange reaction with Na-MMT in xylene, resulting in organically modified MMT with sufficiently enlarged interlayer spacings. A polypropylene/MMT nanocomposite was prepared by directly dissolving polypropylene in the MMT modification system and found to possess an excellent thermal stability.

Kadar et al. (82) studied the surface characteristics of layered silicates to obtain more information about the effects of interfacial interactions on exfoliation and composite properties. The surface tension of sodium montmorillonite and organophilic clays was determined by inverse gas chromatography, and decrease in surface tension in MMT after modification was observed. Increase in interlayer gallery was high in the case of Nanofil 948 which had two long alkyl chains compared to others. Increased gallery distance and decreased surface energy should lead to easier exfoliation. They pointed out that, the amount of surfactant located in the galleries and the orientation of the molecules should significantly influence the structure and properties of layered silicate/polymer nanocomposites.

Kim et al. (83) used pyridinium, imidazolium and phosphonium based ionic liquids to modify pristine Na-MMT clay in order to use it in PP based nanocomposites. TGA results revealed that thermal stability of trialkyl imidazolium decreases as the length of the alkyl group attached to the nitrogen increases. This analysis further proved that the thermal stability of the commercial clays was lower than that of their samples. Visual observation of PP nanocomposite films produced by melt mixing revealed very little clay dispersion and the presence of agglomerates in samples containing IL-l (l-ethyl-3-methylimidazolium bromide), IL-2 (1-hexyl-3-methylimidazolium chloride) and IL-3 (N-ethyl pyridinium tetrafluoroborate); by contrast, samples containing MMTs, modified with ionic liquids IL-4 (Trihexyl tetradecyl phosphonium decanoate) and IL-5 (Trihexyl tetradecyl phosphonium

tetrafluoroborate), having much longer, hydrophobic carbon chains, were much more efficient in promoting dispersion in the polypropylene matrix. The highest thermal stability was obtained with ionic liquid IL-3 (higher than that of commercial organoclays), whereas the highest extent of intercalation was obtained with ionic liquid IL-2 (still lower than that of commercial organoclays).

Langat et al. (84) synthesized imidazolium salts and studied their application in epoxy montmorillonite nanocomposites. He modified sodium montmorillonite with the following modifiers: 1-Hexadecyl-2-methylimidazolium chloride (HDMIM CL) and 1-Hexadecyl-3-(10-hydroxydecyl)-2-methylimidazolium chloride (HDHDMIM CL) and analyzed the composites by XRD and TEM. The clay interlayer spacing increased with the long alkyl chain of the imidazolium salt on the clay surface. Thermal stability of imidazolium functionalized clay (HDMIM-MMT and HDHDMIM-MMT) was found to be far superior to that of ammonium modified clay reported earlier in the literature.

Schartel et al. (85) investigated phosphonium-modified layered silicate epoxy resin nanocomposites with respect to their thermal, thermo-mechanical, and flammability properties. Different drying methods of the modified montmorillonite resulted in different particle morphology, influencing the distribution of silicate layers in the epoxy resins and thus producing nanocomposites of different qualities. With increasing BET of the silicate particles, the delamination and distribution of the composites increased and the systems became more similar to exfoliated systems. The systems showed enhanced mechanical moduli and worsened charpy toughness. The silicate functioned as inert filler, induced limited additional residue formation of the polymer matrix, resulted in a small effect on the effective heat of combustion of the volatile decomposition products, and showed a pronounced barrier effect. The well-distributed phosphonium-modified systems showed properties superior to the ammonium system.

Byrne et al. (86) modified a natural and a synthetic layered silicate (LS) with trihexyltetradecyl phosphonium tetrafluoroborate (an ionic liquid) via a cationic exchange reaction. The exchange reaction and loading of modifier were investigated using a combination of wide angle X-ray diffraction (WAXD),

inductively coupled plasma-optical emission spectroscopy and thermogravimetric analysis. The thermal stability of the modified LS was enhanced by up to 150°C, when compared to conventional quaternary ammonium cations, making melt mixing of such modified nanoclays possible with PET.

Costache et al. (87) prepared nanocomposites of polystyrene (PS), acrylonitrile-butadiene-styrene copolymer (ABS) and high impact polystyrene (HIPS) with two new homologous benzimidazolium surfactants used as organic modifications for the clays. The morphology of the polymer/clay hybrids was evaluated by powder X-ray diffraction and transmission electron microscopy, showing good overall dispersion of the clay. Unlike imidazolium, substitution at the 2-position of benzimidazolium was not required in order to achieve high thermal stability for the modified clays, but it seemed to allow a better entry of the polymer into the clay intergallery space and, therefore, better dispersion. The organically-modified clays had enhanced thermal stability compared to the conventional ammonium-based organo-clays and were comparable with the imidazolium-treated clays, showing promise for utilization with higher melting polymers. The thermal stability of the polymer/clay nanocomposites was enhanced, as evaluated by thermogravimetric analysis. From cone calorimetric measurements, the peak heat release rate of the nanocomposites was observed to decrease by about the same amount as seen for other organically-modified, commercially available clays.

Hedley et al. (88) analyzed the thermal stability of seven organically modified montmorillonites by quaternary phosphonium and ammonium surfactants using differential thermal analysis, differential scanning calorimetry, and thermogravimetry conjunct with X-ray diffractometry. The samples modified with tetrabutylphosphonium (TBP), and butyltriphenylphosphonium (BTPP) ions had an appreciably higher thermal stability than the octadecyltrimethylammonium (ODTMA)-modified clays. In the case of TBP and BTPP modified montmorillonites, the onset temperature of decomposition was close to 300°C. Samples modified with hexadecyltributylphosphonium (HDTBP) ions had a lower onset temperature of decomposition of 225°C. ODTMA modified organoclays at different concentrations exhibited lower onset decomposition temperatures ranging from 158 to 222°C, in which the highest surfactant concentration exhibited the lowest values. The basal

spacing of the TBP- and BTPP-modified clays was 1.7-1.8 nm, indicating a monolayer arrangement of quaternary phosphonium ions in the interlayer space, while the value of 2.5 nm for HDTBP-montmorillonite indicated a more open structure. The ODTMA-modified samples had basal spacings ranging from 1.9 to 2.1 nm, indicative of a bilayer to pseudo-trilayer arrangement. It was indicated that the thermal properties of organoclays are apparently related to the nature of the surfactants and their arrangement in the interlayer space of montmorillonite.

Hrcahova et al. (89) noted that imidazolium cation significantly decreased resistance of montmorillonite toward mechanical destruction. Extensive grinding led to complete breakdown of the layered structure of IM-MMT after 2 hrs and Ca-MMT after 3 hrs treatment in a laboratory vibration mill. Grinding caused distortion of the layers and facilitated dehydroxylation of montmorillonite. Stability of the OH and Si-O-(Si, Al) bonds in IM-MMT was lower than in Ca-MMT.

Lateif and Detellier (90) intercalated imidazolium ionic liquids into the interlamellar spaces of the clay mineral kaolinite. The intercalation procedure was successfully accomplished via a melt reaction strategy using the dimethylsulfoxide-kaolinite intercalate (DMSO-K) as a precursor. Increase of the basal spacing from 1.1 nm in DMSO-K to 1.3-1.7 nm in the nanohybrid materials was observed, indicating that imidazolium derivatives were oriented in a way such that the imidazole ring is parallel or slightly tilted by an angle of 10-25°, with respect to the kaolinite internal surfaces. The number of moles of organic material loaded in the nanohybrids was obtained from several independent measurements. The intercalation of the imidazolium salts increased the thermal stability of the resulting material by more than 150°C with respect to DMSO-K. After heating under air at 300°C for two hours, XRD showed that the intercalate was kept with only a slight decrease of the intercalation ratio. The original kaolinite structure was recovered after heating the intercalate at 350°C for an additional two hours. This observed high thermal stability was promising for the use of these nanohybrid materials as precursor for the synthesis of new nanocomposites by incorporation of polymer in kaolinite at high temperature.

Mittal (91) studied the gas permeation and mechanical properties of polypropylene nanocomposites with thermally-stable imidazolium modified clay. He modified Na^+-MMT with 1-decyl-2-methyl-3-octadecylimidazolium bromide and dimethyldioctadecylammonium and analyzed the composites using XRD, TGA, and TEM. The oxygen permeation properties improved markedly with a decrease of nearly 50% at 4 vol. % of filler fraction, significantly better than ammonium composites. The improvement in the overall composite properties seemed to be a combined result of better thermal stability and interfacial interactions. The thermal stability of the composites was observed to improve significantly with increasing filler volume fraction.

Monemian et al. (92) synthesized PET/organically modified montmorillonite (OMMT) nanocomposites by applying interlayer in-situ polymerization. 1-Decyl-2-methyl-3-dodecyl imidazolium salt was synthesized and used as a thermally stable organomodifier for Na^+-MMT. Application of such an OMMT prevented its degradation process as previously experienced at high temperatures. XRD analysis demonstrated that the ion exchange reaction increased the d-spacing of pristine MMT. Also, the in-situ polymerization process increased the gallery spacing of the OMMT by the diffusion of polymeric chains to the OMMT interlayers. The TEM images showed that the nanocomposite containing 3 wt % OMMT had better state of dispersion compared to that contained 4 wt % OMMT. These observations were confirmed by atomic force microscopy (AFM) and XRD. TGA thermograms of all synthesized nanocomposite samples showed an unexpected lag in the weight loss at high temperatures, which could be related to higher thermal stability of the imidazolium salt as an organomodifier in comparison with alkyl ammonium one as reported previously in the literature. On the other hand, the sample with 3 wt % OMMT had greater maximum degradation temperature than that of 4 wt % OMMT due to its better barrier effect which correlated with its better state of dispersion. DSC results in the nonisothermal mode that were investigated using Jeziorny's equation confirmed significantly the enhanced heterogeneous nucleation rate and tridimensional crystallites growth in nanocomposite samples.

Patel et al. (71) intercalated quaternary phosphonium salts into montmorillonite rich bentonite of Indian origin, by ion exchange reaction. The phosphonium cations

significantly influenced the particle size distribution. With longer alkyl chain, finer particles were formed. The finer particle size distribution was observed for the intercalated MMT with longer chain phosphonium ions, because the alkyl chains prevented silicate platelets from aggregation. The phenyl group substituted phosphonium MMT showed the highest thermal stability of 350-400°C (5% decomposition) and potential usage of these materials for melt processing of polymer/layered silicates nanocomposites.

Abate et al. (93) organically modified montmorillonite with imidazolium surfactants (MMT) at various alkyl chain lengths. C12, C16 and C18 were used to prepare the corresponding PS/MMT/C12, PS/MMT/C16 and PS/MMT/C18 nanocomposites by in-situ polymerization. XRD and TEM analyses indicated the formation of both intercalated and exfoliated structures. The results showed that nanocomposites were more thermally stable than polystyrene, and suggested an increasing degree of exfoliation as a function of alkyl chain length of surfactant, associated with enhanced thermal stability.

Calderon et al. (5) modified sodium montmorillonite (MMT) with several organic phosphonium salts. Organoclays with water soluble surfactants were prepared by the traditional cation exchange reaction. The effects of chemical composition and molecular weight of the salts on the thermal stability and basal spacing were evaluated. The phosphonium montmorillonites exhibited higher thermal stability than conventional ammonium organoclays. The basal spacing was generally larger for the phosphonium montmorillonites.

Lakshmi et al. (94) synthesized epoxy/clay nanocomposites using hexadecylammonium clay and hexadecylphosphonium clay respectively. The montmorillonite clay was modified with quaternary ammonium salt and with triphenylphosphonium salt which were intercalated into the interlayer region of MMT-Clay. The X-ray diffraction results confirmed the dispersion of MMT-Clay in the epoxy networks at the nanoscale. The ammonium clay-modified systems displayed appreciable mechanical and glass-transition temperature properties, while the phosphonium clay-modified system exhibited highest thermal resistance properties compared to unmodified epoxy systems.

Makhoukhi et al. (95) studied the intercalation of diphosphonium salts bis(triphenylphosphonium methylene) benzene-dichloride and bis(tributylphosphonium methylene) benzene-dichloride into bentonite through the ion-exchange of purified bentonite with a solution of diphosphonium salt. Experimental results demonstrated that the purified bentonite had a basal spacing of 13.2 Å while the modified bentonites showed a greater basal spacing of about 18 Å and had a higher thermal stability (300-400°C) than that of bentonite.

Modesti et al. (96) worked on several kinds of organically modified layered silicates in order to understand the influence of the surfactant nature on the intercalation/exfoliation mechanism. Acrylonitrile-butadiene-styrene/organoclay nanocomposites were also produced using an intercalation-adsorption technique from polymer in solution. They showed that only imidazolium-treated montmorillonite was stable at the processing temperature of 200°C, used for hot-pressing, whereas alkyl-ammonium modified clays showed significant degradation. DMA and TGA showed that the nanocomposites based on imidazolium-modified clay out-performed the nanocomposites based on quaternary-ammonium-modified clays in terms of mechanical properties and thermal stability.

Stoeffler et al. (97) used alkyl phosphonium, alkyl pyridinium and dialkyl imidazolium surfactants as intercalating agents for the preparation of highly thermally stable organophilic montmorillonites. In order to investigate the influence of the thermal decomposition of the intercalating agent during processing, the various organoclays were incorporated into a polyethylene terephthalate matrix. The color of the nanocomposites was significantly affected by the thermal decomposition of the intercalating agent. In the case of the alkyl pyridinium modified clay, the degradation of the intercalating agent during processing was found to alter the clay dispersion. Finally, the crystallization was analyzed by DSC analysis and polarized optical microscopy (POM). It was demonstrated that the kinetics of nucleation and growth were not only affected by the dispersion state of the clay, but also depended on the clay/polymer interface properties, and therefore on the nature of the intercalating agent.

Avalos et al. (98) intercalated an aliphatic and an aromatic phosphonium salt by Na-montmorillonite. Tri-phenyl vinylbenzyl phosphonium chloride and tetraoctyl phosphonium bromide salts were used as intercalant agents for Na-montmorillonite. An easier and more effective intercalation took place with the tetraoctyl phosphonium salt giving rise to a higher concentration of intercalant with a sensible increase in the interlayer spacing. This phosphonium salt modified montmorillonite was thermally more stable than the aromatic one and easier to exfoliate during the compounding process.

Bottino et al. (99) modified montmorillonite using imidazolium or standard alkylammonium surfactants in order to produce polystyrene/montmorillonite nanocomposites via in-situ bulk polymerization. The samples that presented higher degree of exfoliation showed a shorter induction period and degraded more quickly than the less exfoliated one.

2.7.2 Studies on PA66/Organoclay Nanocomposites

Effects of elastomer and clay

Karayannididis et al. (100) investigated rubber toughening of glass fiber reinforced PA66 with functionalized block copolymer poly[styrene-b-(ethylene-co-butylene)-b-styrene (SEBS-g-MA). Blending was performed in a single screw extruder. Incorporation of SEBS-g-MA in PA66 matrix increased the resistance to crack propagation and hence toughness. Toughening was influenced by the size of cavitation and the extent of reaction.

Liu et al. (101) prepared Polyamide 66/clay nanocomposites via melt compounding method by using a new kind of organophilic clay obtained through co-intercalation of epoxy resin and quaternary ammonium into Na-montmorillonite. The clay was dispersed homogeneously in the polyamide 66 matrix as a result of the interaction between the epoxy groups confined in the layers and PA66 chains. Tensile strength and heat distortion temperature increased dramatically, as well as Izod impact strength. Water absorption was reduced by 40 % upon incorporation of 10 wt % co-intercalation clay into the polymer matrix. The presence of silicate layers increased

the crystallization rate and had strong hetero-phase nucleation effect on PA66 matrix.

Nair et al. (102) showed that toughening in layered silicate clay composites can be enhanced by better dispersion of the clay, by exfoliation of the clay layers and by a stronger clay/matrix interface at low clay loading levels. At high clay loading levels, where the toughness was low, composites with a multiscale distribution of reinforcing elements (mixture of exfoliated and particulate clays) exhibited maximum toughening, significantly higher than the fracture initiation toughness.

Tanaka et al. (103) predicted the binding energy for PA66/clay nanocomposites by molecular modeling and showed that the binding energy between a clay platelet and PA66 decreased as the volume of the adsorbed quaternary ammonium salt increased. It was the opposite for the binding energy of PA66 and quaternary ammonium salt. The substitution of polar groups like -OH and -COOH for hydrogens on ammonium ions seemed to increase the binding energies with the nylon.

Han et al. (104) prepared organophilic montmorillonites, co-treated by octadecylammonium and amino-undecanoic acid, and used them to prepare nylon 66/montmorillonite nanocomposites via melt compounding in a twin screw extruder. WAXD and TEM characterization indicated that a disordered or delaminated structure was derived and the montmorillonite platelets were dispersed in nanoscale in the nylon 66 matrix. The nanocomposites with co-treated montmorillonite displayed comparatively higher strength and modulus compared to pure nylon 66.

Liu et al. (105) found using in-situ X-ray diffraction that the crystalline phase transition temperature was lower for PA66 nanocomposites prepared by melt compounding in a co-rotating twin-screw extruder and it was attributed to γ crystalline phase induced by the silicate layers. Crystal structure of PA66 matrix was changed upon addition of silicate layers and its phase transition behavior was affected.

Qin et al. (12) compared the flammability and thermal stability of PA66/MMT microcomposite with PA66/OMMT nanocomposite obtained by melt compounding. Addition of MMT decreased the heat release rate of PA66 matrix (i.e., Peak HRR decreased from 802 to 209 kW/m^2 with 10 wt % OMMT). The reason of PA66 matrix ignition that was accelerated with MMT addition was related to the catalytic decomposition effect of MMT in isothermal oxidation experiments. The silicate layers were found to have a barrier effect that retarded flammability, and nanocomposites were more thermally stable compared to microcomposites.

Tomova et al. (106) indicated that end group configuration was important for the interfacial adhesion and morphology formation in binary polyamide/elastomer blends and in ternary PA6/PA66/maleated elastomer blends obtained by melt mixing in a Brabender single screw extruder. The domain size of elastomeric phase was found to be 1 μm for PA6, whereas it was 4-7 μm for PA66. It was attributed to difunctionality of PA66 that enabled it to react twice per chain with the maleated elastomer.

Effects of clay modification

Yu et al. (107) prepared Nylon-66 nanocomposites by melt-compounding nylon-66 with an alkyl ammonium surfactant pretreated montmorillonite. They showed that the clay was exfoliated but not randomly dispersed in PA66 matrix but oriented along the injection molding direction in the specimen. The decomposition of the surfactant on the MMT occurred from 200 to 500°C. They proposed that MMT with more thermally stable surfactants has to be produced to increase the onset decomposition temperatures of alkyl ammonium pretreated MMT when polymers with high melt-compounding temperatures are used. The influence of the spatial distribution of the organic MMT on crystallization of nylon-66 was also investigated.

Zhang et al. (108) and Kang et al. (109) investigated the effect of organoclay on the crystallinity of PA66 nanocomposites produced by melt blending and concluded that size of the spherulites decreases upon addition of the organoclay since clay has a nucleation effect on the polymer matrix.

Chavarria et al. (110) compared PA6 nanocomposites with PA66 nanocomposites prepared by melt processing in a twin-screw extruder and stated that PA6 nanocomposites have superior mechanical properties, lower average particle length, thickness and aspect ratio that was indicative of a better exfoliated structure in comparison with PA66 nanocomposites.

Lu et al. (111) studied the influence of thermal processing on the perfection of crystals in PA66 and PA66 nanocomposites which were melt mixed and extruded in a co-rotating twin-screw extruder. Nanoclay seemed to have two overwhelming effects on PA66 crystallization. One of them was the nucleation effect that increased the crystallization rate, and the second one was the constrained motion of the chains hindering refinement of crystal structures.

Mehrabzadeh et al. (112) prepared PA66/clay, HDPE/clay and HDPE/PA66/clay nanocomposites by melt mixing in a twin-screw co-rotating extruder. They revealed that compatibility of the clay modifier with the polymer matrix, mixing and kneading elements and higher residence times in twin-screw extrusion aid intercalation or exfoliation. Clay seemed to have no effect on crystallinity apart from acting as a nucleating agent.

Shen et al. (113) investigated the mechanical properties of PA66/organoclay nanocomposites prepared by melt compounding in a Brabender twin-screw extruder in terms of nanoindentation technique. Hardness, elastic modulus, storage modulus and creep were gradually improved with increasing clay concentration up to 5 wt %.

Yu et al. (114) prepared PA66 nanocomposites by melt compounding with an organically modified montmorillonite whose ammonium surfactant was about 14 wt %, which was a much lower value than the 35-46 wt % surfactant contents in commercial organic montmorillonite powders. They observed exfoliation of the organoclay by TEM analysis and enhanced mechanical values. Increases in the tensile strength and Young’s modulus led to decreases in ductility and fracture toughness.

Dasari et al. (115) showed that the microstructure of ternary PA66/SEBS-g-MA/organoclay nanocomposites and their mechanical properties were seriously affected by the mixing sequence. It was demonstrated that location of the organoclay greatly influenced the impact strength. Mixing PA66 with the organoclay first and blending with SEBS-g-MA in the next step gave the best impact strength results since most of the organoclays were found to be in the polymer matrix.

Vlasveld et al. (116) made a comparison between the temperature dependence of modulus, yield stress and ductility of nanocomposites based on high and low molecular weight PA6 and PA66 produced via melt blending. It was reported that high processing temperatures do not seem to encounter a problem for PA66 nanocomposite production for which modulus and yield stress were found to be slightly higher. Molecular weight of the polymer was concluded to be chosen according to the required mechanical properties and processing conditions.

Nylon 66 nanocomposites with different smectite clay loadings were prepared by conventional melt compounding process by Chen et al. (117). The fracture toughness decreased with increasing clay content, which is a direct result of reduced plastic zone size at the crack tip region. The fracture mechanisms were studied using double-notched four-point-bending technique. A constraining effect from nanoclay fillers on plastic deformation of matrix was revealed by TEM. Micron-sized and submicron voids could be observed around the clay platelets. The voids coalesced and formed premature cracks that promote crack propagation, thus reducing toughness.

Dasari et al. (53) found out that addition of clay does not accelerate the crystallization process although SEBS-g-MA compatibilizer acts as a nucleating agent. When the organoclay was situated in SEBS-g-MA phase, cavitation ability of the elastomer was retarded despite the increases in flexural strength. Extruding the polymer matrix containing elastomer more than once also had a negative effect on the toughness of the nanocomposites. The mechanical test results were supported by TEM, SEM, X-ray and elastomeric domain size analysis.

Gonzáles et al. (118) modified PA66 nanocomposites with PA6 by melt mixing to obtain exfoliated nanocomposites. PA6 had a mediating role in dispersing the clay platelets. High yield stress and elastic modulus results were associated with exfoliation of the organoclay. Ductility decreased as the amount of the organoclay content increased.

Gyoo et al. (119) used epoxy-modified organoclay to observe its effects on morphology, thermal and mechanical properties of PA66/clay nanocomposites obtained by melt compounding using a Brabender mixer. According to the evaluated results, the epoxy resin amount was determined be kept at an optimum value, since excess epoxy resin caused a strong interaction between the hydroxyl end groups of the modifier on the silicate surface and diffusion of PA66 into silicate layers was limited. Tensile strength, Young's modulus, storage modulus and the crystallization rate increased after introduction of the organoclay into the polymer matrix.

Hedicke et al. (120) compared the crystallization behavior of PA6 and PA66 nanocomposites. Compounding was carried out in a twin-screw extruder. Organoclay was not fully dispersed in PA66 matrix whose crystal structure change was not affected by the presence of the organoclay in contrast to PA6 nanocomposites in which the organoclay exhibited fully exfoliated behavior.

Farahani et al. (121) prepared PA66/SEBS-g-M alloys and their nanocomposites by melt compounding using a twin screw extruder. Rubber toughened samples exhibited significantly more impact strength and elongation at break compared to pure polyamide. A general type organoclay (Nanolin DK4) at 4% and 8% was used with rubber toughened samples to increase their modulus and tensile strength. Results showed that nanoclay could significantly increase modulus and tensile strength of rubber modified Polyamide 66 without considerable effects on impact strength. WAXD and SEM results showed that the Polyamide 66 nanocomposites were better exfoliated in presence of SEBS-g-MA. The shear viscosity of PA66 nonlinearly decreased with incorporation of SEBS-g-MA and organoclay into it.

Mert et al. (1) prepared binary and ternary polyamide 66 nanocomposites containing 2 wt % organoclay, polyamide 66 blend containing 5 wt % impact modifier, and ternary polyamide 66 nanocomposites containing 2 wt % organoclay and 5 wt % impact modifier by melt compounding method. Partial exfoliation and improved mechanical properties were observed for Cloisite® 15A and Cloisite® 25A ternary nanocomposites. On the other hand, the organoclay was intercalated in the form of tactoids in Cloisite® 30B nanocomposites. Components of the nanocomposites containing Cloisite 15A and Cloisite 25A were compounded by different addition orders. Mixing sequence of the components affected both the dispersion of the organoclay and the mechanical properties drastically. SEM analyses revealed that homogeneous dispersion of the organoclay results in a decrease in the domain sizes and promotes the improvements in the toughness of the materials. Melt viscosity was also found to have a profound effect on the dispersion of the organoclay according to MFI and XRD results. Crystallinity of the nanocomposites did not change significantly. It is only the type of the constituents and their addition order what dramatically influenced the nanocomposite properties.

Araujo et al. (122) prepared Polyamide 66/Brazilian clay nanocomposites via direct melt intercalation. The Brazilian montmorillonite sample was organically modified with esthearildimethylammonium chloride, quaternary ammonium salt. The nanocomposites exhibited a partially exfoliated structure, heat deflection temperature values which were higher than those of pure PA66, and good thermal stability.

2.7.3 Studies on PET/Organoclay Nanocomposites

The literature contains enormous amount of studies about PET/clay nanocomposites. In this study, focus was placed on the thermal stability of PET/clay nanocomposites using thermally stable organoclays. The elastomeric phase incorporation in the polymer matrix is also crucial and thus mentioned too. Previous studies on this subject are summarized in the following sections.

PET with Elastomers

Xanthos et al. (123) showed that the compatibilization reaction of PET and ethylene-acrylic ester-GMA terpolymer occurred between epoxy group of the terpolymer with carboxyl group of PET.

Kalfoglou et al. (124) reported that the addition of GMA grafted polyolefins is useful for the reactive compatibilization of blends of polyolefins with PET. A polyolefin-polyester graft copolymer was generated in-situ by a reaction involving the grafted epoxy moieties and the carboxyl/hydroxyl polyester end groups.

Loyens et al. (125) confirmed that a very effective compatibilization of PET/elastomer blends is obtained in the presence of glycidyl methacrylate functional groups. In another study (56), they evaluated various modifiers with and without functional groups for ultimate mechanical properties of rubber modified semicrystalline PET. The most toughening route for PET was provided by dispersing a preblend of ethylene-co-propylene rubber (EPR) and a low amount of ethylene-glycidyl methacrylate copolymers (E-GMA) with highly increased impact strength and reasonable elongation at break.

Chapleau et al. (57) showed that the addition of the modifiers containing GMA to PET resulted in a decrease of the tensile modulus and tensile strength, whereas the elongation at break and toughness were generally increased.

PET/Clay Nanocomposites

Davis et al. (126) studied PET/Montmorillonite nanocomposites compounded via melt-blending in a co-rotating mini twin-screw extruder. They found that nanocomposites produced with N,N-dimethyl- N,N-dioctadecylammonium treated montmorillonite (DMDODA-MMT), which has a decomposition temperature of 250°C, were black, brittle, and tarlike resulting from DMDODA degradation under the processing conditions. Nanocomposites compounded with 1,2-dimethyl-3-*N*-hexadecyl imidazolium treated MMT, which has a decomposition temperature of 350°C, showed high levels of dispersion and delamination. Alternative mixing

conditions, longer residence times, and higher screw speeds resulted in lower quality nanocomposites.

Costache et al. (127) prepared PET/clay nanocomposites by melt blending with montmorillonite, hectorite and magadiite clays modified with quinolinium and lauryl thermally stable surfactants. All organoclays exhibited significant thermal stability, the mass loss at 300°C being less than 2%, except for magadiite. Moreover, up to 320°C, their thermal behavior was comparable to imidazolium-based clay. (e.g. MMT exchanged with 1-(11-hydroxy-undecyl)-2,3-dimethyl-3H-imidazol-1-ium), but above this temperature the imidazolium clay outperformed the respective quinolinium and lauryl clays. All nanocomposites showed about the same value for the peak heat release rate.

Wang et al. (128) prepared PET/montmorillonite (MMT) nanocomposites via melt-blending, and its dispersion morphology at nanoscale was confirmed by XRD and TEM. The crystallization rate of PET nanocomposite increased significantly. Also, they showed that 1 wt% MMT content was optimum. At this composition, the thermal degradation onset temperature and the heat distortion temperature of PET were increased by 12 and 35°C, respectively, and the tensile strength of the PET was increased by 25% with slight increase of the notched impact strength.

Alyamac et al. (129) worked on the impact modification PET/organoclay/E-MA-GMA ternary nanocomposites with different organoclay percentages and sequences. The impact strength results were improved as a result. DSC analysis showed that the crystallization temperature decreased by the addition of the clay, since clay acted as a nucleating agent and decreased the crystallization temperature of pure PET.

Bandyopadhyay et al. (130) prepared PET/clay nanocomposites with two different weight percentages of montmorillonite (MMT) by melt-extrusion technique. The TGA analyses showed that although the degradation started earlier in nanocomposites due to the Hoffman degradation of the surfactant present in the organoclay, the average stability (indicated by the derivative curves) increased in nanocomposites. In air atmosphere, nanocomposite samples showed higher stability than nitrogen atmosphere, which may be due to the different type of char

formation mechanism under oxidative environment which actually slowed down the oxygen diffusion, thus hindering the oxidation procedure under thermo-oxidative conditions. This observation indicated improved flame retardancy property of the nanocomposite.

Bizzaria et al. (131) prepared recycled PET/organoclay nanocomposites by melt intercalation process with several amounts (1, 3, and 5 wt %) of clay modified with quaternary ammonium salt. Although the mechanical properties of the nanocomposites exhibited improvements (modulus and yield strength), the thermal analysis did not show significant changes in the thermal properties from those of recycled PET.

Chang et al. (132) prepared PET/organoclay nanocomposites from two different phosphonium salts: dodecyltriphenylphosphonium montmorillonite (C12PPh-MMT) and dodecyltriphenylphosphonium-mica (C12PPh-Mica). Transmission electron microscopy micrographs showed that some of the clay layers were dispersed homogeneously within the polymer matrix at the nanoscale, although some clay particles were agglomerated. It was also found that the addition of only a small amount of organoclay (1–5 wt %) was enough to improve the thermal stability and mechanical properties of the PET hybrid fibers. Even polymers with low organoclay contents were found to exhibit much higher strength and modulus values than pure PET.

Kim et al. (133) prepared PET/organosilicate nanocomposites using the melt intercalation method at 280^{o}C for 10 min. Organosilicate was prepared with a new synthesized salt 2.3-dimethyl-3H-imidazolium bromide and compared to commercial organoclays Cloisite 15A and 30B. The use of the new organosilicate yielded almost exfoliated and thermally stable PET nanocomposite, whereas the PET nanocomposites prepared by use of commercial organoclays showed only an intercalated morphology with earlier thermal decomposition. Particularly, the use of the new organosilicate showed an enhanced tensile modulus, without sacrifice of the tensile strength and elongation at break, while the use of commercial organoclays only exhibited a trade-off between those mechanical properties.

Kracalik et al. (134) prepared thermally stable recycled PET-organoclay nanocomposites from modification of Na-MMT with 1,2-dimethyl-3-octadecyl-1Himidazol-3-ium chloride in addition to a treatment with [3-(glycidyloxy)propyl]trimethoxysilane. In comparison to the organoclays modified with quaternary ammonium compounds, the prepared clays showed substantial suppression of matrix degradation during melt mixing. The improved rheological characteristics, mechanical properties and thermal stability were dependent on the higher degree of delamination in the nanocomposites filled with imidazole organoclays.

Monemian et al. (92) synthesized thermally stable PET/organically modified montmorillonite (OMMT) nanocomposites by applying interlayer in-situ polymerization. 1-Decyl-2-methyl-3-dodecyl imidazolium salt was synthesized and used as an organic modifier for Na^{+}-MMT. Application of such an OMMT prevented its degradation process as previously experienced at high temperatures. XRD analysis demonstrated that the ion exchange reaction increased the d-spacing of pristine MMT. Also, the in-situ polymerization process increased the gallery spacing of the OMMT by the diffusion of polymeric chains to the OMMT interlayers. TGA thermograms of all synthesized nanocomposite samples showed an unexpected lag in the weight loss at high temperatures, which could be related to higher thermal stability of the imidazolium salt as an organomodifier in comparison to alkyl ammonium one as reported previously in the literature. On the other hand, the sample with 3 wt % OMMT had greater maximum degradation temperature than that of 4 wt % OMMT, due to its better barrier effect which correlates with its better state of dispersion. DSC results in the nonisothermal mode that were investigated using Jeziorny's equation confirmed the enhanced heterogeneous nucleation rate and tridimensional crystallite growth in nanocomposite samples.

Yuan et al. (135) studied the effects of thermal stability of surfactants with amino and imido groups on thermal properties of PET/clay composites. The imidosilane surfactant was synthesized successfully from the imide reaction between amino silane and phthalic anhydride. TGA showed that imidosilane decomposition behaviors had two major stages according to the degradation of different functional groups. After melt extrusion, the decomposition of amino functional groups in amino

surfactants decreased the thermal stability of organoclay and accelerated the degradation behavior of PET composites. Because of the enhanced thermal stability of imidosilane surfactants, PET/imidopalygorskite composites exhibited enhanced thermal stability, good dispersion and low thermal expansion.

Xu et al. (136) used organoclays with various contents of hydroxyl groups and absorbed ammonium to prepare PET/clay nanocomposites via melt extrusion. The composites, based on clay with larger amount of hydroxyl groups on the edge of clay platelets, experienced much more degradation, because the hydroxyl groups acted as Bronsted acidic sites to accelerate polymer degradation. Furthermore, organoclays with different amounts of absorbed ammonium led to different extents of polymer degradation, depending upon the acidic sites produced by the Hofmann elimination reaction of ammonium. In addition, the composite with better clay dispersion state, which had an increasing amount of clay surface and ammonium exposed to the PET matrix, experienced polymer degradation more seriously.

Guan et al. (137) investigated the crystallization behavior of PET/clay nanocomposites prepared via in-situ polycondensation in terms of DSC, polarizing optical microscopy (POM), and SEM observation. Crystalline morphologies were observed through POM and SEM. The nonisothermal and isothermal crystallization rates of different samples were determined by comparison based on DSC data. Secondary nucleation analysis was also performed based on bulk crystallization data derived from DSC analysis. The nucleating abilities of MMT depended on the dispersion state of clay in matrix and the surface modification status during in-situ synthesis.

Calcagno et al. (138) prepared PET nanocomposites using montmorillonite with different organic modifiers (Cloisite 15A, 30B and 10A). Nanocomposites of intercalated and exfoliated morphologies were obtained. The clay nucleated the PET crystallization process, and the nucleating effect was higher when Cloisite 10A was used. This study allowed the evaluation of the characteristics of the organic modifiers' influence on the intercalation and exfoliation processes in PET. When apolar modifiers were present, tactoids were obtained. However, when polar modifiers were present, PET nanocomposites were intercalated and exfoliated.

2.8 Choice of Materials

Phosphonium Salts: The enhancement of thermal stability of phosphonium modified clay means that it could be useful for polymers, which must be processed at temperatures above that at which the ammonium clays undergo degradation. The above results raised the focus on using different structures of phosphonium surfactants with different chain groups (aryl and alkyl) attached to the phosphonium cation;

1. PH1 Surfactant (TO-P Br): Four long octyl chain groups attached to the phosphonium cation with bromide counter ion.
2. PH2 Surfactant (BZLTP-P): One benzyl and 3 phenyl groups attached to the phosphonium cation with chloride counter ion.

Imidazolium Salts: Imidazolium organoclays exhibited a 100°C improvement in thermal stability as compared to the ammonium-treated ones. One of the most interesting findings in this area was the enhancement in the thermal stability of imidazolium compounds after being intercalated into montmorillonite (6). Awad et al., 2004 investigated the thermal degradation of alkyl-imidazolium salts and their application in nanocomposites. These organically-modified clays were characterized by (XRD), TDMS and thermogravimetry coupled with Fourier transform infrared spectroscopy (TGA-FTIR), and compared to the conventional quaternary alkyl ammonium montmorillonite. The results also showed that the imidazolium-treated montmorillonites have greater thermal stability compared to the imidazolium halide. (7). Some of their results indicated the following:

1. The imidazolium cation is more thermally stable than the alkyl ammonium cation. Imidazole is resistant to ring fission during thermal rearrangements of 1-alkyl- and 1-aryl-imidazoles at temperatures above 600°C.
2. The counter ion has an effect on the thermal stability of the imidazolium salts, and that imidazolium salts with PF_6^-, $N(SO_2CF_3)_2^-$ and BF_4^- anions are thermally more stable than the halide salts.

3. A relationship was observed between the chain length of the alkyl group and the thermo-oxidative stability; as the chain length increased from propyl, butyl, decyl, hexadecyl, octadecyl to eicosyl, the stability decreased.
4. The atmosphere has an effect on the thermal stability of certain imidazolium salts, namely the hexafluorophosphate. Both the onset decomposition temperature and the peak decomposition temperature were markedly decreased if the sample was run under ambient conditions compared to that under N_2 atmosphere. In addition, a relationship was observed between the chain length of the alkyl group attached to the nitrogen atom and the oxidative decomposition of the imidazolium salts, indicating that the thermal stability decreases as the organic content of the molecule increases. In our study N_2 gas was used.

In addition to the indications of all imidazolium salt studies which confirm the higher thermal stability of imidazolium salts in comparison to the ammonium ones, the above results placed the focus on using different structures of di-imidazolium surfactants with different chain groups (aryl and alkyl) attached to the first nitrogen atom with different counter ions;

1. IM1 Surfactant (BZL-IM PF6): The chain group attached to the first nitrogen atom is aromatic with hexafluorophosphate counter ion.
2. IM2 Surfactant (BTL-IM PF6): The chain group attached to the first nitrogen atom is short aliphatic with hexafluorophosphate counter ion.
3. IM3 Surfactant (BTL-IM Cl): The chain group attached to the first nitrogen atom is short aliphatic with chloride counter ion.
4. IM4 Surfactant (DCL-IM Cl): The chain group attached to the first nitrogen atom is long aliphatic with chloride counter ion.

In the present study, the organoclays produced from the first two surfactants were compared according to the chemical structure of the cations (aryl and alkyl). The second and the third surfactants were compared according to their thermal stability by comparing the anions attached and their subsequent effect on organoclays produced. The third and fourth surfactants were compared according to the chain length attached to the first nitrogen atom.

CHAPTER 3

EXPERIMENTAL

3.1 Materials

3.1.1 Bentonites

The sodium montmorillonite rich bentonite clay (KAR-BEN) used in this study was mined from Reşadiye/Tokat region in Turkey and supplied by Karakaya Bentonit (Turkey). The raw bentonite clay (B) with elemental composition of $[Al_{1.47}Fe_{0.29}Mg_{0.23}][Al_{0.076}Si_{3.29}]O_{10}(OH)_2$ contained 90% Montmorillonite. The CEC of the Reşadiye bentonite as received has been given by the researchers Onal et al. (9), Tabak et al. (72) and Nakaş et al. (73) by methylene blue procedure as 65 meq/100 g, 76 meq/100 g and 50 meq/100 g, respectively. It was also determined using the same procedure as 67.5 meq/100 g clay. The Montmorillonite PGW 105 (M) used for comparison purpose only was supplied by Desi Kimya A. Ş., Istanbul, Turkey, the distributor of Nanocor. The properties of the types of sodium clays are given below in Table 3.1 as determined in this thesis.

Table 3.1 Properties of sodium clays

Property	KAR-BEN (B)	Purified KAR-BEN (PB)	PGW 105 (M)
Color	Yellowish Green	White	White
CEC (meq/100g) ± 10%	67.5	95.0	145.0
Maximum Moisture (%)	10.0	-	12.0

The drying conditions of the clays is known to play a crucial effect on the process results, since the clays are hydrophilic and the moisture can cause significant decrease in the thermal stability of the clays and as a result decrease the synergistic properties between the polymer and clay. Thus, all clays and tetraoctyl phosphonium bromide (TO-P Br) modified organoclays were dried at 80^{o}C and 120^{o}C. For the rest of the study, purified clays and organoclays were dried at 120^{o}C before extrusion with the polymers used throughout this study. A summary of the drying conditions of the clays used for this part is given in Table 3.2.

Table 3.2 Drying conditions of the clays

Material	Drying Temperature (^{o}C)	Drying Time (hr)
Bentonite Clays (B)	80 and 120	12
Purified Bentonite Clays (PB)	80 and 120	12
Montmorillonite (M)	80 and 120	12
B.TO-P	80 and 120	12
PB.TO-P	80 and 120	12
M.TO-P	80 and 120	12

3.1.1.1 Clay Purification

Purification of the bentonite clay before surface modification is necessary in order to obtain highly pure clays by removing non-clay and other clay minerals. This step increases the intercalation between the polymer and clay in addition to the significant improvement in the thermal stability of the clay. The purification procedure was accomplished via the separation of the clay minerals from other minerals by sedimentation.

Stokes' Law defines the main principle of the sedimentation process. According to Stokes' Law, particles with a diameter of 2 μm settle 1 cm in 45 min at 20^{o}C. Since the non-clay minerals have higher weight and thus higher settlement rates than the clay minerals, the purification was accomplished by using the difference between the settlement rates of the two. The non-clay and other clay minerals will settle

down 10 cm during each period of 500 min (~8.5 hours) while leaving the clay minerals in suspension. The whole procedure is summarized in Figure 3.1 (73).

The steps of the purification procedure used were as follows:

1. 50 g of dried Na-montmorillonite clay sample (80^{o}C for 12-15 hrs) and a small quantity of Sodium Pyrophosphate (in order to avoid agglomeration of bentonite-water mixture) were put into a 5 L flask.
2. Distilled water was added into the flask in small portions while mixing with a stirrer and the temperature of the mixture was kept at 40^{o}C for 2 hrs.
3. After filling the flask with distilled water, the suspension stayed for 9 hrs for sedimentation.
4. The upper 25 cm of the solution was siphoned and centrifuged at 6000 rpm for 10 min.
5. The clay minerals collected at the end of centrifugation (around 25 wt% of starting amount) were dried in an oven at 120^{o}C for 12 hours.

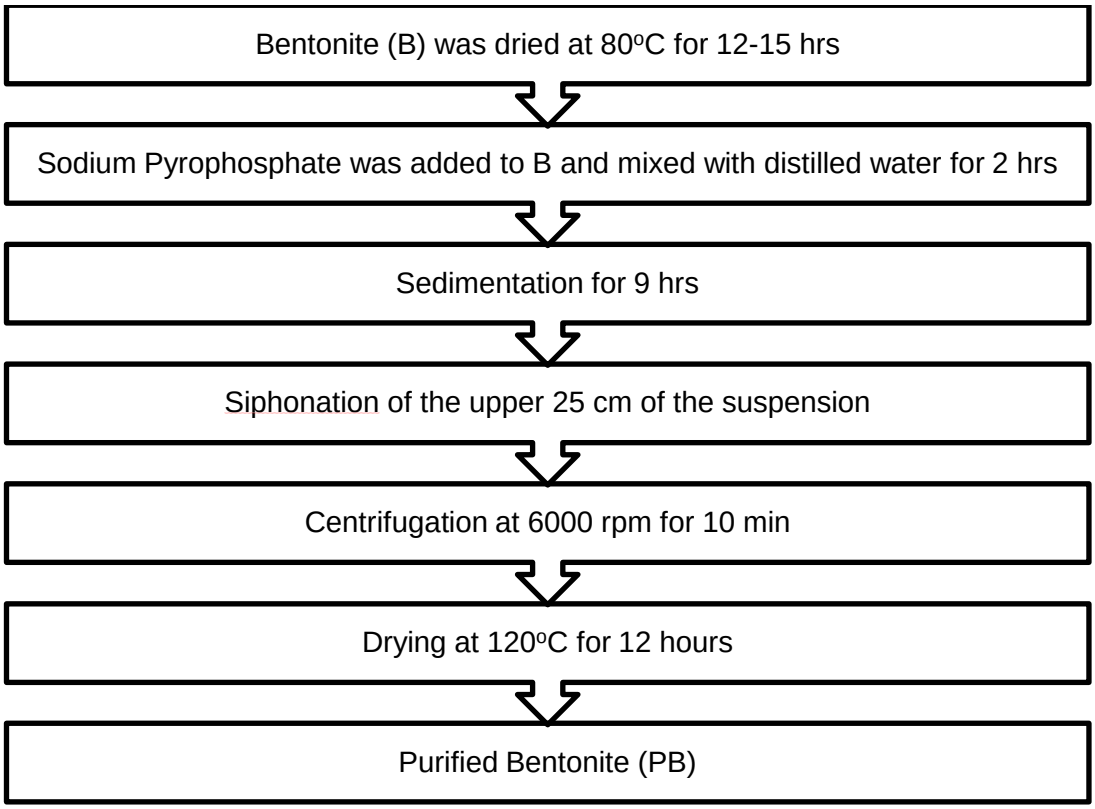

Figure 3.1 Purification flowchart of the layered silicate

3.1.1.2 Cation Exchange Capacity (CEC)

The CEC of the bentonite clays as received and as purified were determined as 67.5 meq/100g clay and 95 meq/100g clay respectively in accordance with the procedure in ASTM Test Method C 324. The steps of the analysis were as follows:

1. 2.00 g of dry clay were placed in the 600-ml beaker.
2. 300 ml of distilled water were added to the beaker and stirred with the mixer until the clay was uniformly dispersed.
3. The pH of the slurry was determined and sufficient amount of sulfuric acid was added to bring the pH within the range of 2.5 to 3.8. Stirring was continued while the pH was adjusted and also for 10 to 15 min after the last addition of acid.
4. The pH of the slurry was tested again; additional acid was added if necessary to restore the pH to the 2.5 to 3.8 range.
5. With the slurry still under the mixer, the burette was filled with the methylene blue solution; 5 ml of the solution was added to the slurry, and stirred for 1 to 2 min.
6. A drop of the slurry was removed, using the dropper or the glass stirring rod, and placed on the edge of the filter paper.
7. The appearance of the drop on the filter paper was observed. The end point was determined by the formation of a light blue halo around the drop. Addition of the methylene blue solution to the slurry in 1.0-ml increments was continued with 1 to 2 min of stirring after each addition. Then testing was performed until the end point was reached.
8. After the end point was reached, stirring was continued for 2 min and the test was repeated.

3.1.1.3 Clay Modification Agents

Phosphonium and imidazolium clay modifiers were purchased from Sigma-Aldrich Company. Their names, structures and properties are given below as defined by producer in Table 3.3.

Table 3.3 Chemical structures of the surfactants

Surfactant	Cation	Anion
Tetraoctyl phosphonium Bromide TO-P Br (MW: 563.76 g/mol)	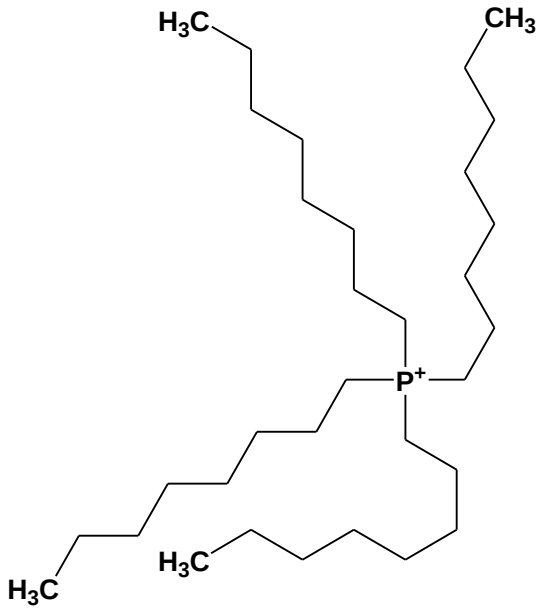	Br^-
Benzyltriphenyl phosphonium chloride BZLTP-P Cl (MW: 388.87 g/mol)	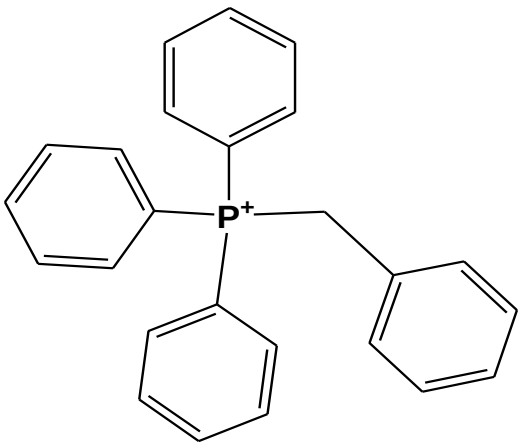	Cl^-

Table 3.3 Chemical structures of the surfactants (Cont'd)

Surfactant	Cation	Anion
1-Benzyl-3-methyl imidazolium hexafluorophosphate purum, ≥97.0% BZL-IM PF6 (MW: 318.20 g/mol)	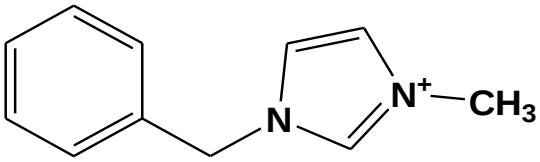	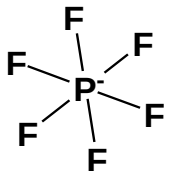
1-Butyl-3-methyl imidazolium hexafluorophosphate purum, ≥97.0% BTL-IM PF6 (MW: 284.18 g/mol)	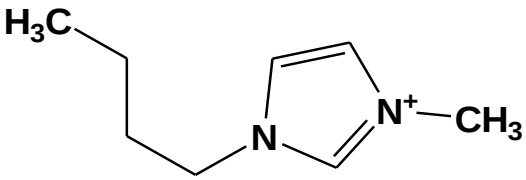	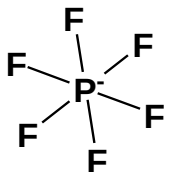
1-Butyl-3-methyl imidazolium chloride purum, ≥98.0% BTL-IM Cl (MW: 174.67 g/mol)	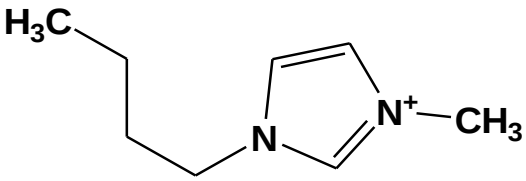	Cl^-
1-Decyl-3-methyl imidazolium chloride 96.0% DCL-IM Cl (MW: 258.83 g/mol)		Cl^-

3.1.1.4 Preparation of Phosphonium Organoclays

To prepare phosphonium treated purified bentonites (PB); the purified bentonites were initially dried in vacuum at 120^{o}C for 12 hrs. The amounts of the surfactants added to all clays were 1.1 * the CEC. 10 grams of clay were put into 1 l of distilled water at room temperature, in a glass beaker equipped with a mechanical stirring bar. After 24 hrs, mixing was stopped and the system was heated till it reached 80^{o}C. 400 ml of ethyl alcohol solution containing the salt at 1.1 * the CEC were poured into the clay dispersion. At 80^{o}C, mixing was continued for 2 hours, and then the organoclay was filtered and washed with hot water (80°C) using coarse Whatman filter paper. Washing was repeated for at least three times, and no halide traces were detected with silver nitrate. After washing, the organoclay was dried overnight at room temperature followed by drying at 120°C for 24 hrs under vacuum. Then, it was ground in a mortar (<106μm) and dried again under the same conditions and stored in a dessicator. Tetraoctyl phosphonium organoclays were greasy due to the insolubility of the salt itself, and thus they couldn't be sieved to sizes less than 150 μm. A trial was done using Tetraoctyl phosphonium bromide salt to check the effect of using excess surfactant on clays by adding 1.7 * the CEC.

3.1.1.5 Preparation of Imidazolium Organoclays

Imidazolium treated organoclays were prepared by a cation-exchange reaction between the purified bentonites and excess of the imidazolium salt (1.1 the exchange capacity of the host). 10 grams of purified bentonite (PB) was dispersed in 1 L deionized water and then added to a mixture of dissolved imidazolium salt in 50:50 mixture of ethyl alcohol and deionized water. The mixture was heated till 60°C and stirred for 5 hrs. The imidazolium exchanged montmorillonite was collected by filtration under vacuum and washed by mixing again with a mixture of hot ethyl alcohol and deionized water (more than 6 times) to remove all the residual anions. The final product was dried overnight at room temperature and then under vacuum at 120°C for 24 hrs. Then, it was ground in a mortar (<106μm) and dried again under the same conditions and stored in a dessicator (4).

3.1.2 Polymer Matrix

Two polymer matrices, Polyamide 66 (PA66) and amorphous Poly(ethylene terephthalate) (PET) were used throughout this study.

3.1.2.1 Polyamide 66 (PA66)

Polyamide 66 (PA66) with trade name Bergamid A65 was purchased from PolyOne Company, Istanbul-Turkey. PA66 was supplied in pellet form in 25 kg polyethylene bags. Properties of PA66 as given by the supplier are listed in Table 3.4.

Table 3.4 Properties of PA66 matrix

Properties	Standards	Unit	Test Conditions	Values	
Physical				d.a.m	Cond.
Water Absorption	ISO 62	%	23°C	8.5	-
Density	ISO 1183	g/cm^3	23°C	1.13	-
Moisture Absorption	ISO 62	%	23°C (50% R.H.)	2.8	-
Mechanical				d.a.m	Cond.
Tensile Strength	ISO 527-1/2	MPa	23°C,50 mm/min	80	60
Tensile Strain at Yield	ISO 527-1/2	%	23°C,50 mm/min	4.5	25
Tensile Strain at Break	ISO 527-1/2	%	23°C,50 mm/min	22	>50
Tensile Modulus	ISO 527-1/2	MPa	23°C,1 mm/min	3200	1600
Flexural Strength	ISO 178	MPa	23°C	140	70
Charpy Notched Impact Strength	ISO 179/1eA	kJ/m^2	23°C	6	25
			-30°C	4	-
Izod Notched Impact Strength	ISO 180/1A	kJ/m^2	23°C	6	-
			-30°C	6	-

Table 3.4 Properties of PA66 matrix (Cont'd)

Properties	Standards	Unit	Test Conditions	Values	
Thermal				d.a.m	Cond.
Melting Temperature	ISO 3146	°C	10 K/min	261	-
Heat Deflection Temperature	ISO 75-1/2	°C	0.45 MPa	220	-
			1.8 MPa	80	-
Coefficient of Linear Expansion	DIN 53752	E-4/K	normal	0.85	-
			perpendicular	0.82	-
Flammability				d.a.m	Cond.
Flammability	UL 94	-	0.8 mm	V-2	-
		-	1.6 mm	V-2	-

d.a.m: Dry as molded Cond.: Conditioned according to ISO 1110

3.1.2.2 Poly(ethylene terephthalate) (PET)

Poly(ethylene terephthalate) was purchased from ADVANSA Company, Adana, Turkey. The pellets were in amorphous form and, thus were transparent. Typical properties of PET obtained from the producer are listed in Table 3.5.

Table 3.5 Properties of PET matrix

Properties	Unit	Standards	Value
Relative Density	g/cm^3	20°C	~1.25
Melting Temperature	°C		255
Glass Transition Temperature	°C		78
Decomposition Temperature	°C		>350
Intrinsic viscosity	dl/g	23°C	0.57

Following injection molding, both matrices were immediately stored in polyethylene bags and kept in dessicator for 24 hours prior to testing, since they are very sensitive to moisture uptake that significantly influences the properties of the materials and is one of the major drawbacks of their use.

3.1.3 Impact Modifiers

3.1.3.1 Impact Modifier Used for PA66

Lotader® 2210 resin (a random terpolymer of ethylene, butyl acrylate and maleic anhydride (E-BA-MAH)) was purchased in pellet form from Arkema Inc., France and used as an impact modifier and also as a compatibilizer for Polyamide 66. This elastomer contains MAH group which can react with the amine ends of PA66 (55). The chemical structure and properties of E-BA-MAH are given in Figures 3.2 and Table 3.6, respectively.

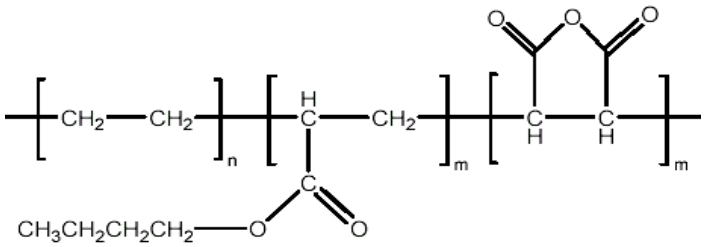

Figure 3.2 Chemical structure of E-BA-MAH

Table 3.6 Properties of E-BA-MAH

Properties	Unit	Method	Values
Ester Content	%	FTIR	6
MAH Content	%	FTIR	2.6
Melt Index	g/10 min	ISO 1133	3
Vicat Point	°C	ISO 306	80
Melting Point	°C	DSC	107
Decomposition Temperature	°C	TGA	>300
Tensile Strength	MPa	ISO 527	12
Young's Modulus	GPa	ISO 527	-
Elongation at Break	%	ISO 527	600
Density	g/cm^3	ISO 1183	0.94
Hardness	Shore D	ISO 868	46

3.1.3.2 Impact Modifier Used for PET

Lotader® AX8900 resin (a random terpolymer of ethylene, methyl acrylate and glycidyl methacrylate (E-MA-GMA)) was purchased in pellet form from Arkema Inc., France and used as an impact modifier for Poly(ethylene terephthalate). The epoxy functionality of GMA can react with the carboxyl and hydroxyl end groups of PET in the melt phase to form a graft copolymer (55). For this reason, E-MA-GMA may also be called as a functionalized polymer used as a compatibilizer. The chemical structure of and properties of Lotader® AX900 are given in Figure 3.3 and Table 3.7, respectively.

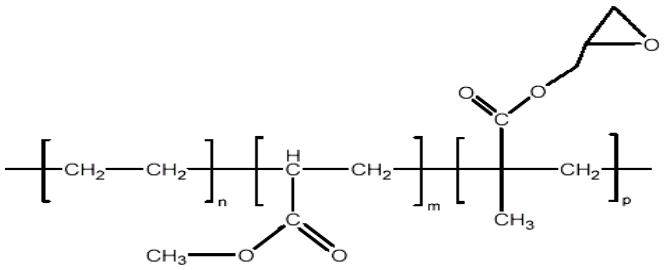

Figure 3.3 Chemical structure of E-MA-GMA

Table 3.7 Properties of E-MA-GMA

Properties	Unit	Method	Values
Ester Content	%	FTIR	25
GMA Content	%	FTIR	8
Melt Index	g/10 min	ISO 1133	6
Vicat Point	°C	ISO 306	< 40
Melting Point	°C	DSC	60
Decomposition Temperature	°C	TGA	>300
Tensile Strength	MPa	ISO 527	4
Young's Modulus	GPa	ISO 527	0.008
Elongation at Break	%	ISO 527	1100
Density	g/cm^3	ISO 1183	0.94
Hardness	Shore D	ISO 868	64

3.2 Nanocomposite Preparation

3.2.1 Melt Blending

Polymer based nanocomposites were prepared in air atmosphere by melt compounding using a co-rotating, intermeshing Thermoprism TSE 16 TC twin screw extruder with an L/D ratio of 24 (L = 384 mm, D = 16 mm). Maximum torque and screw speed that can be achieved during compounding are 12 Nm and 500 rpm, respectively. Figure 3.4 shows the extruder used in this study. In addition to ternary polymer/organoclay/elastomer nanocomposites, polymer/organoclay and polymer/elastomer blends were also prepared for comparison purposes.

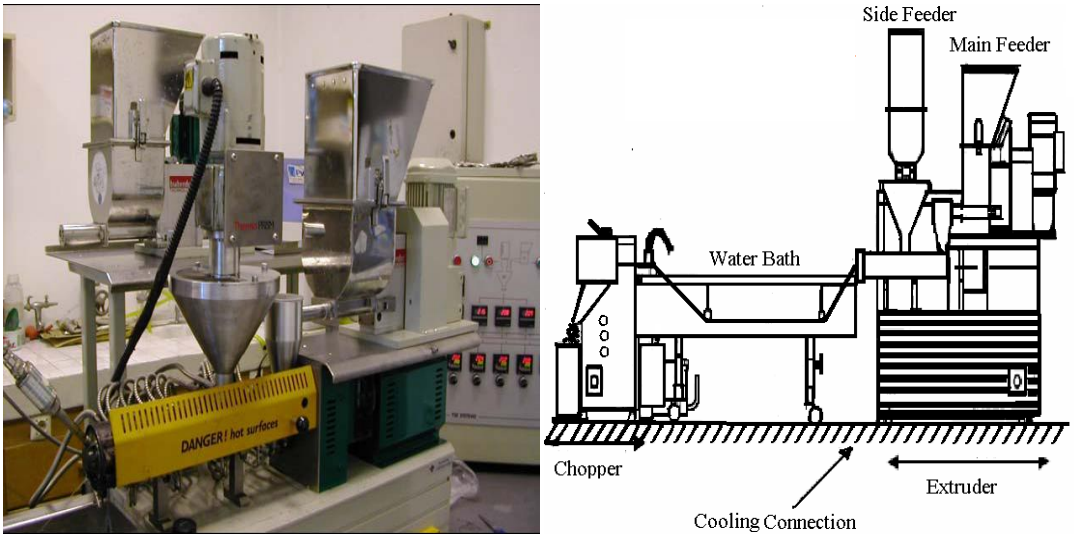

Figure 3.4 Thermoprism TSE 16 TC twin screw extruder

3.2.1.1 Melt Blending of PA66

During the experiments, the feed rate, screw speed and the temperature profiles were kept constant for PA66 at 25 g/min, 200 rpm and 260-275-275-275-280˚C from the main hopper to the die respectively. A summary of these parameters is given in Table 3.8.

Table 3.8 Melt blending parameters for PA66 Sets

Material	PA66 Sets
Extruder Hopper (^{o}C)	260
Extruder Mixing Zone I (^{o}C)	275
Extruder Mixing Zone II (^{o}C)	275
Extruder Mixing Zone III (^{o}C)	275
Extruder Die (^{o}C)	280
Screw Speed (rpm)	200
Feed rate (g/min)	~25

Extrusion parameters are crucial in order to obtain good intercalation. The effects of extrusion passes on the intercalation of the PA66 into the clays were investigated. Four sets of PA66/PB.TO-P/E-BA-MAH nanocomposites were prepared and analyzed, two of which were extruded once and the rest twice. Extrusion twice with simultaneous injection molding was found to be the most feasible procedure in order to obtain better products, and thus, the nanocomposites and blends prepared afterwards were extruded twice to increase the effect of shear intensity on the organoclay dispersion and to achieve the desired compositions.

After the first extrusion step, the extrudate was cooled in a cooling bath and pelletized using a chopper. The pellets of PA66 containing compounds obtained at the end of the process were stored in polyethylene bags and were all dried at 100°C under vacuum for 12 hours before the next extrusion step or injection molding. Drying was performed in vacuum for 24 hours at 120°C for the organoclays and for 12 hours at 40°C for the elastomers, since elimination of physiabsorbed water is required before processing, in order to obtain materials with improved properties. Drying step was repeated before each processing step, since the presence of even small traces of moisture can cause significant hydrolytic degradation of the materials. Table 3.9 shows the drying conditions of the materials used to produce PA66 based products.

Table 3.9 Drying conditions for PA66 sets

Material	Drying Temperature (^{o}C)	Drying Time (hr)
Before 1st run extrusion		
PA66	100	12
Modified Purified Clays	120	24
Elastomers	40	12
Before 2nd run extrusion		
PA66	100	12
PA66/Elastomer	100	12
PA66/Organoclay	100	12
PA66/Organoclay/Elastomer	100	12
Before injection molding		
PA66	100	12
PA66/Elastomer	100	12
PA66/Organoclay	100	12
PA66/Organoclay/Elastomer	100	12

3.2.1.2 Melt Blending of PET

The feed rate, screw speed and the temperature profiles were kept constant during the experiments of PET. A summary of these parameters is given in Table 3.10.

Table 3.10 Melt blending parameters for PET sets

Material	PET Sets
Extruder Hopper (^{o}C)	200
Extruder Mixing Zone I (^{o}C)	275
Extruder Mixing Zone II (^{o}C)	275
Extruder Mixing Zone III (^{o}C)	275
Extruder Die (^{o}C)	280
Screw Speed (rpm)	350
Feed rate (g/min)	~25

Pure PET, PET/elastomer blend, binary and ternary PET nanocomposites were extruded twice to increase the effect of shear intensity on the organoclay dispersion. After the first extrusion step, the extrudate was cooled in a cooling bath and pelletized in a chopper. The pellets of PET containing compounds obtained at the end of the process were stored in polyethylene bags and were all dried at 110°C under vacuum for 15 hours before the next extrusion step or injection molding. Drying was performed under vacuum for 24 hours at 120°C for the organoclays and for 12 hours at 40°C for the elastomers. Drying step was repeated before each processing step since the presence of even small traces of moisture can cause significant hydrolytic degradation of the materials. Table 3.11 shows the drying conditions of the materials used to produce PET sets.

Table 3.11 Drying conditions for PET sets

Material	Drying Temperature (^{o}C)	Drying Time (hr)
Before 1st run extrusion		
PET	110	15
Modified Purified Clays	120	24
Elastomers	40	12
Before 2nd run extrusion		
PET	110	15
PET/Elastomer	110	15
PET/Organoclay	110	15
PET/Organoclay/Elastomer	110	15
Before injection molding		
PET	110	15
PET/Elastomer	110	15
PET/Organoclay	110	15
PET/Organoclay/Elastomer	110	15

3.2.2 Injection Molding

The specimens were injection molded by a DSM Xplore laboratory scale micro injection molding equipment. The photograph of this equipment is given in Figure 3.5. It consists of a mold on the left hand side and a pressure cylinder on the right hand side, where a nozzle is connected to the mold. The maximum pressure that this machine can reach is 16 bars. In each molding operation, two specimens were obtained, one of which had the shape of a dogbone, whereas the other one is the sample of the impact test with rectangular shape.

Figure 3.5 DSM Xplore injection molding machine

3.2.2.1 Injection Molding of PA66 Sets

PA66 specimens were injection molded in two ways (pelletized and simultaneous) depending on the procedure used for production of nanocomposites. During the molding process, the barrel temperature was adjusted to 275°C and the mold temperature was set to 60°C.

In the pelletized way (abbreviated as P), the pellets were dried after the first or second extrusion and put into the barrel using a spoon. After waiting for three minutes for the material to melt, the melt was injected into the mold with a pressure of 15 bars.

The simultaneous way (abbreviated as S) is continuous injection molding while the nanocomposites are being extruded. In this step, the barrel head was attached to the die and filled up, and directly put in the injection molding machine for molding at a pressure of 15 bars. This method was used only for PA66 nanocomposites.

Pressure profile of the molding cycle is one of the critical parameters affecting the alignment of the polymer chains, crystallinity and filling of the mold cavities to prevent short shots. The total cycle time can be calculated using $t_{cycle} = t_{closing} + t_{injection\ (filling)} + t_{cooling\ (holding)} + t_{ejection}$. The closing and ejection times can last from a fraction of a second to a few seconds, depending on the size of the mold and machine. Here it was 2 seconds and 1 second, respectively. The injection (filling) time was 5 seconds at 10 bars and it was increased to 15 bars in another 5 seconds during the packing cycle to offset shrinkage. The pressure was relaxed during the cooling (holding) time (12 seconds), which dominates the process. Total molding cycle time of the specimen took 25 seconds for the pelletized way and 60 seconds for the simultaneous one. The injection molding parameters were given in Table 3.12. All injected molded samples were kept for 24 hrs under vacuum in a dessicator prior to analysis.

Table 3.12 Injection molding parameters for PA66 sets

Material	PA66 (Pelletized)	PA66 (Simultaneous)
Nozzle Temperature (^oC)	275	275
Mold Temperature (^oC)	60	60
Waiting Time in Barrel (min)	3	0.1
Closing Time (s)	2	2
Injection (filling) Time (s),	5+5	5+5
Injection (filling) Pressure (bar)	10 to 15	10 to 15
Cooling (holding) Time (s),	12	12
Cooling (holding) Pressure (bar)	15	15
Ejection Time (s)	1	1
Injection Speed	Fast	Fast

3.2.2.2 Injection molding of PET Sets

PET pellets were dried after the second extrusion and put into the barrel using a spoon (pelletized way). After waiting four minutes for the material to melt in the barrel, the melt was injected into the mold with a pressure of 6 bars. The closing and ejection times, can last from a fraction of a second to a few seconds, depending on the size of the mold and machine. Here, it was 2 seconds and 1 second respectively. The injection (filling) time was 5 seconds at 6 bars and it was increased to 8 bars in another 5 seconds during the packing cycle to offset shrinkage. The pressure was relaxed during the cooling (holding) time (60 seconds), which dominates the process. Total molding cycle time of the specimen took 73 seconds. During the molding process, the barrel temperature was adjusted to 275°C and the mold temperature was set to 21°C. The injection molding parameters are given in Table 3.13. All injected molded samples were dried for 24 hrs under vacuum in a dessicator prior to analysis.

Table 3.13 Injection molding parameters for PET sets

Material	PET (Pelletized)
Nozzle Temperature (^{o}C)	275
Mold Temperature (^{o}C)	21
Waiting Time in Barrel (min)	4
Closing Time (s)	2
Injection (filling) Time (s),	5+5
Injection (filling) Pressure (bar)	6 to 8
Cooling (holding) Time (s),	60
Cooling (holding) Pressure (bar)	8
Ejection Time (s)	1
Injection Speed	Fast

3.3 Experimental Procedure

3.3.1.1 Experimental Procedure of PA66 Sets

Calderon, et al., 2008 used TO-P Cl salt (in order to modify Sodium MMT (Na^+ Cloisite) supplied by Southern Clay Product company. The idea behind using the same salt (with different anion) again was to investigate the usage of Turkish bentonite (with and without purification). Thus, TO-P Br was taken as the reference for the investigations regarding bentonite purification, salt percentage used in modification and nanocomposite production by different extrusion passes and molding methods.

PA66 ternary nanocomposites with 1% PB.TO-P organoclay were prepared using different procedures in order to investigate the effects of extrusion passes (1 or 2) and injection method (pelletized or simultaneous) on the intercalation of the polymer and clays. These were extruded according to four procedures in order to re-evaluate the most convenient way to have better intercalation of the polymers in the clays. In all the processes, the polymer, clay and elastomer were mixed together and fed through the feeder. It is more favorable to mix all of the components simultaneously, since the same shear intensity is applied on all of them and the interactions that can take place between the components are not minimized (59). These processes were:

1. PA66/PB.TO-P/E-BA-MAH (1-S): Extrusion once and simultaneous injection molding.
2. PA66/PB.TO-P/E-BA-MAH (1-P): Extrusion once, pelletizing, drying at 100°C for 24 hrs and injection molding.
3. PA66/PB.TO-P/E-BA-MAH (2-P): Extrusion, pelletizing, drying for 24 hrs, extrusion again, pelletizing, drying for 24 hrs, and injection molding.
4. PA66/PB.TO-P/E-BA-MAH (2-S): Extrusion, pelletizing, drying for 24 hrs, extrusion again and simultaneous injection molding.

where 1 and 2 in the brackets stand for extrusion times, while P and S stands for pelletized and simultaneous injection molding, respectively.

After the analysis of the above processes with 1% PB.TO-P organoclay, the best way was found to extrude twice which increases the effect of shear intensity on the organoclay dispersion and then simultaneous injection molding. The names of PA66 sets produced with 2% organoclays do not contain (2-S) for brevity purposes, but they were extruded twice. Only the ternary sets of PA66/PB.TO-P(1%)/E-BA-MAH are named with brackets according to processing times and method. Table 3.14 shows the composition of PA66 sets produced.

Table 3.14 Composition of PA66 samples

		Concentration (wt %)		
No.	Composition	Polymer	Elastomer	Organoclay
	Polymer			
1	PA66 (Extruded Twice)	100	---	---
	Polymer/Elastomer Blend			
2	PA66/E-BA-MAH	95	5	---
	Polymer/Organoclay Binary Nanocomposites			
3	PA66/PB.TO-P	98	---	2
4	PA66/PB.BZLTP-P	98	---	2
	Polymer/Organoclay/Elastomer Ternary Nanocomposites			
5	PA66/PB.TO-P/E-BA-MAH (1-S)	94	5	1
6	PA66/PB.TO-P/E-BA-MAH (1-P)	94	5	1
7	PA66/PB.TO-P/E-BA-MAH (2-P)	94	5	1
8	PA66/PB.TO-P/E-BA-MAH (2-S)	94	5	1
9	PA66/PB.TO-P/E-BA-MAH	93	5	2
10	PA66/PB.BZLTP-P/E-BA-MAH	93	5	2

3.3.1.2 Experimental Procedure of PET Sets

PET, organoclay (%2) and elastomer (%5) were mixed together and fed to the extruder barrel directly at an approximate feed rate of 25 g/min. The product was cooled using a water bath, pelletized and then dried for 24 hrs at 110°C before they were extruded again, cooled, pelletized, dried and then injection molded. Table 3.15 shows the composition of PET sets produced. The abbreviation (E3) in composition number 22 stands for three extrusion times.

Table 3.15 Composition of PET samples

		Concentration (wt %)		
No.	Composition	Polymer	Elastomer	Organoclay
	Polymer			
11	PET (Extruded Twice)	100	---	---
	Polymer/Elastomer Blend			
12	PET/E-MA-GMA	95	5	---
	Polymer/Organoclay Binary Nanocomposites			
13	PET/PB.TO-P	98	---	2
14	PET/PB.BZLTP-P	98	---	2
15	PET/PB.BZL-IM	98	---	2
16	PET/PB.BTL-IM	98	---	2
17	PET/PB.BTL-IM’	98	---	2
18	PET/PB.DCL-IM	98	---	2
	Polymer/Organoclay/Elastomer Ternary Nanocomposites			
19	PET/PB.TO-P/E-MA-GMA	93	5	2
20	PET/PB.BZLTP-P/E-MA-GMA	93	5	2
21	PET/PB.BZL-IM/E-MA-GMA	93	5	2
22	PET/PB.BZL-IM/E-MA-GMA (E3)	93	5	2
23	PET/PB.BTL-IM/E-MA-GMA	93	5	2
24	PET/PB.BTL-IM’/E-MA-GMA	93	5	2
25	PET/PB.DCL-IM/E-MA-GMA	93	5	2

A general experimental procedure for the whole research is summarized and given in Figure 3.6.

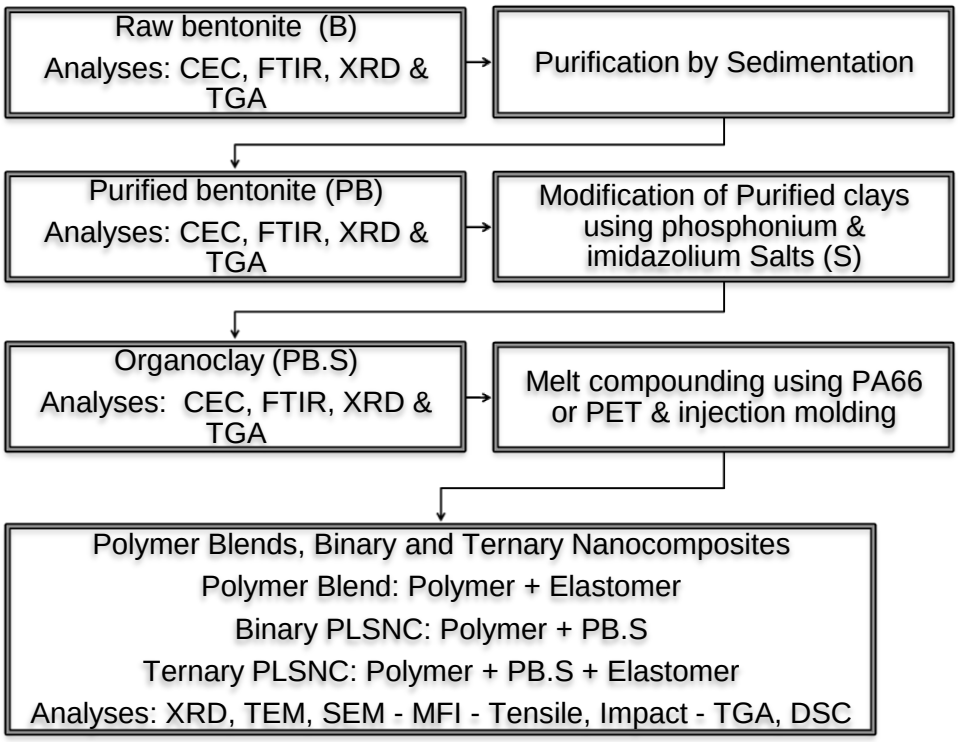

Figure 3.6 Flowchart of the experimental procedure

3.4 Characterization Experiments

In order to determine the properties of the newly developed materials and the applications for which they can be used, some analyses (morphology, rheology, mechanical and thermal) were conducted. XRF analysis was conducted in order to analyze the changes in chemical composition of clays after purification. FTIR technique was used to investigate the intercalation between the clays and surfactants used. Morphology of the nanocomposites was investigated by XRD, TEM and SEM analyses. Increases in the basal spacings of the organoclays were calculated from XRD patterns. TEM analyses were performed for observations at higher magnifications to observe the degree of organoclay dispersion in the polymer. The dispersion of elastomeric phase in the polymer matrix was observed by SEM. MFI tests were carried out to investigate the flow characteristics. Mechanical behavior of the nanocomposites was evaluated by measuring impact

strength and tensile properties (tensile strength, Young's modulus, elongation at break). The thermal stability of the nanocomposites was studied by TGA analysis. Melting and crystallization behavior of the nanocomposites were studied by DSC.

3.4.1 Chemical Analyses

3.4.1.1 X-Ray Fluorescence Analysis (XRF)

The chemical analyses of bentonite samples were carried out using a Rigaku ZSX Primus II model XRF instrument at METU central laboratory. Sample pellets were positioned in front of a Si (Li) detector and irradiated with X-rays originating from an Rh target. The X-ray tube power was a 4kW, the voltage was 50 kV and the current was 5 mA. The spectra were obtained and analyzed using SQX software.

3.4.1.2 Fourier Transform Infrared Spectroscopy Analysis (FTIR)

FTIR analysis was carried out using IR Prestige-21 Shimadzu equipment in the range of 4000 - 500 cm^{-1}. The samples were first dried to remove excess moisture and then 0.0015 mg of sample was ground with 0.1985 mg of spectral grade KBr until a homogeneous powder was obtained. The mixtures were then pressed into disc-pellets and then analyzed.

3.4.2 Morphology Analyses

3.4.2.1 X-Ray Diffraction (XRD)

RIGAKU D/MAX 2200/PC X-Ray diffractometer, that generates a voltage of 40kV and current 40 mA from monochromatic Cu Kα radiation source (λ = 1.5418), available in the Metallurgical and Materials Engineering Department, METU was used to analyze the organoclays and nanocomposites. The diffraction angle 2θ was scanned from 1˚ to 10˚ for the polymers (dog bone shaped tensile bars) and from 1˚ to 40˚ for clays at a scanning rate of 2˚ per minute and a step size of 0.02˚. In order to calculate the distance between the silicate layers, Bragg's law was used.

3.4.2.2 Scanning Electron Microscopy (SEM)

In order to examine the failure mechanism and elastomer dispersion, the impact-fracture surface of the nanocomposites were scanned by a low voltage Scanning Electron Microscope (JEOL JSM-6400) at METU central laboratory. Nanocomposites containing elastomers were etched with boiling Xylene for 6 hours to extract the elastomeric phases. SEM photographs of the impact-fractured surfaces were taken at x250 and x4000 magnifications.

3.4.2.3 Transmission Electron Microscopy (TEM)

For TEM analysis ultra sections of 70 nm in thickness were cryogenically cut with a diamond polymer knife at a temperature of -100˚C for polymer/organoclay binary and polymer/organoclay/elastomer ternary nanocomposites. These samples were examined by a Tecnai™ G2 F30 Transmission Electron Microscope at an acceleration rate of 120 kV at UNAM Institute of Materials Science and Nanotechnology in Bilkent University. All samples were trimmed parallel to the molding direction.

3.4.3 Melt Flow Index Analysis

3.4.3.1 Melt Flow Index (MFI) Measurements

Melt flow index measurements were carried out using an Omega Melt Flow Indexer. This method is based on determining the melt index, defined as the mass flow rate of polymer through a specified capillary. Mass flow rate is expressed as grams per 10 min. Since melt flow index values are inversely related to the melt viscosity, changes in viscosity values were evaluated for each formulation. For each sample at least five measurements were done to get accurate results. Conditions of temperature and load were selected as 275°C and 0.325 kg for PA66 (ISO 1333), and 260°C and 2.16 kg for PET (ASTM D1238-79), respectively, which are in accordance with material specifications.

3.4.4 Mechanical Tests

For most applications, mechanical properties of the materials are the most important of all physical and chemical properties. In this study, the relationship between the material's response and deformation to an applied load or force are determined by tensile and impact tests.

3.4.4.1 Tensile Tests

Tensile tests were performed by using Shimadzu Universal Testing Machine AG-IS (100kN) according to ISO 527. During the test, the specimen was placed in the grips of the testing machine, taking care that it was properly aligned, and the grips were tightened evenly and firmly enough to prevent the slippage of the specimen. Tensile strength (MPa), Young's modulus (GPa) and percent elongation at break (%) were determined from the stress-strain curves. These properties were evaluated on five specimens. Tensile test specimen and its dimensions are given in Figure 3.7 and Table 3.16, respectively. The crosshead speed was applied as 3 mm/min, based on the gauge length of 30 mm and strain rate of 0.1 min^{-1}. The test temperature was 23 $\pm$ 2°C for all samples.

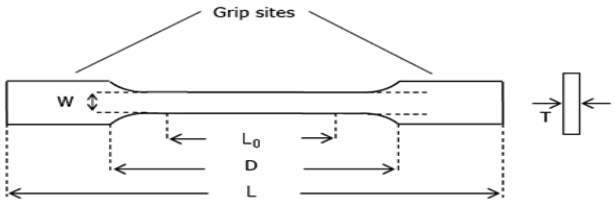

Figure 3.7 Tensile test specimen

Table 3.16 Dimensions of the tensile test specimens

Definition	Dimensions (mm)
L-Overall length	75.0
D-Distance between grips	50.0
L_0-Gauge length	30.0
W- Narrow section width	4.0
T-Thickness	2.1

3.4.4.2 Impact Tests

Charpy impact strength of one sided notched specimens with the dimensions of 80x10x4 mm was measured by pendulum Ceast Resil Impactor according to ISO 179. All tests were performed at room temperature and the results are the averages of five tests carried out for all compositions.

3.4.5 Thermal Analyses

TGA and DSC were used for the thermal analysis of organoclays, and PA66 and PET based nanocomposites.

3.4.5.1 Thermal Gravimetric Analysis (TGA)

TGA analysis was performed by a Shimadzu DTG-60H thermal analyzer under ultrahigh purity nitrogen atmosphere. The scanning rates used were 10^{o}C/min, 15^{o}C/min and 15^{o}C/min for the salts, clays and nanocomposites, respectively. The maximum temperatures analyzed were 1000^{o}C, 800^{o}C and 600^{o}C for the same materials.

3.4.5.2 Differential Scanning Calorimetry (DSC)

DSC measurements were carried out under nitrogen atmosphere by using DSC-60 Shimadzu differential scanning calorimeter, in order to evaluate the possible changes in melting temperature (T_m) and glass transition temperature (T_g) for each composition due to the presence of impact modifiers and organoclays in the polymer used. Indium was used as a calibration standard. Samples of about 6.5 mg were cut from dry tensile bars and were placed in the DSC aluminum pans. They were heated from 25 to 300°C at a heating rate of 10°C/min. Percent crystallinity was calculated using the heat of fusion of the specimen. The heat of fusion for 100 % crystalline PA66 was taken as 206 J/g (114), and for 100 % crystalline PET it was taken as 135.98 J/g (139).

CHAPTER 4

RESULTS AND DISCUSSION

4.1 Chemical Analyses

4.1.1 X-Ray Fluorescence Analysis

XRF analysis was done on both purified and unpurified bentonites, and the chemical compositions are given in Table 4.1.

Table 4.1 Major oxides as determined using XRF analysis (wt %)

Oxide	B	PB
SiO_2	66.30	68.60
Al_2O_3	19.50	19.60
Fe_2O_3	3.84	4.17
CaO	3.56	0.80
Na_2O	2.88	2.87
MgO	2.14	2.28
K_2O	1.05	0.54
TiO_2	0.32	0.64
P_2O_5	0.16	0.39
SO_3	0.11	-
SrO	0.12	0.05
MnO	0.11	0.03

The chemical composition of the raw bentonite as given by the supplier is: 61.28% SiO_2, 17.79% Al_2O_3, 3.01% Fe_2O_3, 4.54% CaO, 2.70% Na_2O, 2.10% MgO, and 1.24% K_2O. The most abundant oxides are SiO_2 and Al_2O_3, whereas Fe_2O_3, CaO, Na_2O, MgO, K_2O and TiO_2 are present only in small quantities. P_2O_5, SO_3, SrO and MnO oxides are present in negligible amounts. After purification, the weight percent of SiO_2 increased, the CaO percent decreased significantly and the SO_3, SrO and MnO oxides were minimized.

4.1.2 FTIR Analysis

4.1.2.1 FTIR Results of Clays and Organoclays

Infrared (IR) spectroscopy has been used for decades to investigate the structure, bonding and chemical properties of clay minerals. In 2003, Madejova et al. (140) mentioned that in the studies of clay minerals the absorption bands due to structural OH and Si-O groups play frequently an important role in the differentiation of clay minerals from each other. The assignments for FTIR bands of bentonite clays are given in Figure 4.1.

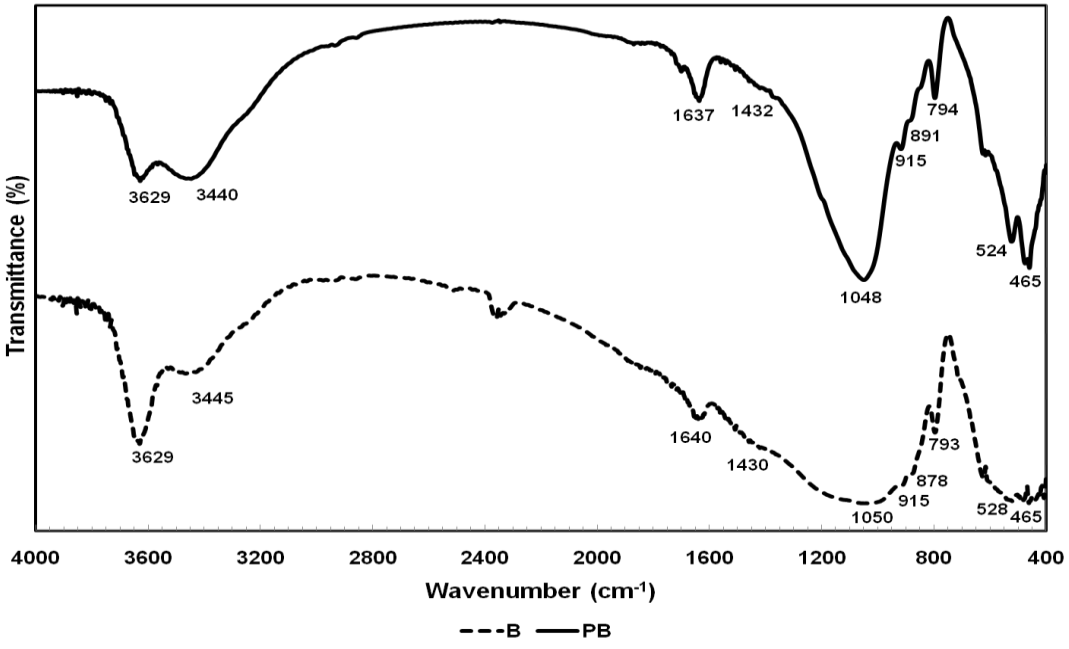

Figure 4.1 FTIR band assignments for bentonite (B) and purified bentonite (PB)

The characterized vibrations of various hydroxyl groups associated with octahedral cations, silicates and water present in the clay are listed in Table 4.2.

Table 4.2 FTIR spectral data for bentonite clays

Band Assignment	B (cm^{-1})	PB (cm^{-1})
υ(X–O–H), X = Al, Mg	3629	3629
υ(H–O–H)	3445	3440
δ(H–O–H)	1640	1637
υ(Si–O)	1430	1432
υ(Si–O)	1050	1048
δ(Al–Al–OH)	915	915
δ(Al–Fe–OH)	878	891
υ(Si–O) of SiO_2 impurity	793	794
δ(Al–O–Si)	528	524
δ(Si–O–Si)	465	465

υ: Stretching δ: Bending

The bands of bentonite and purified bentonite exhibited close values of the peaks. The bands between 3400-3700 cm^{-1} of the bentonite clays (B and PB) are indication of montmorillonite. The band at 3629 cm^{-1} refers to OH stretching region, which is assigned to hydroxyl groups coordinated to octahedral cations (-OH stretching mode of Al-OH of montmorillonite structure). The bands at 3445/3440 and 1640/1637 cm^{-1} of B/PB are respectively the stretching and bending vibrations for the hydroxyl groups of physisorbed free water molecules present in the clay. The shoulders 1430/1432 and 1050/1048 cm^{-1} of B/PB show Si-O stretching vibration. The bands at 915 cm^{-1} stands for Al-Al-OH bending. The bands at 878/891 cm^{-1} of B/PB indicate a moderate Fe^{3+} content expressed by Al-Fe-OH bending. The bands at 793/794 cm^{-1} of B/PB stand for Si-O stretching of the silicate (silica phase [SiO_2] impurity). The bands at 528/524 and 465/465 cm^{-1} of B/PB are due to Al-Si-O and Si-O-Si bending vibrations. The assignments for FTIR bands of phosphonium and imidazolium modified clays in Figure 4.2 are listed in Tables 4.3 and 4.4, respectively.

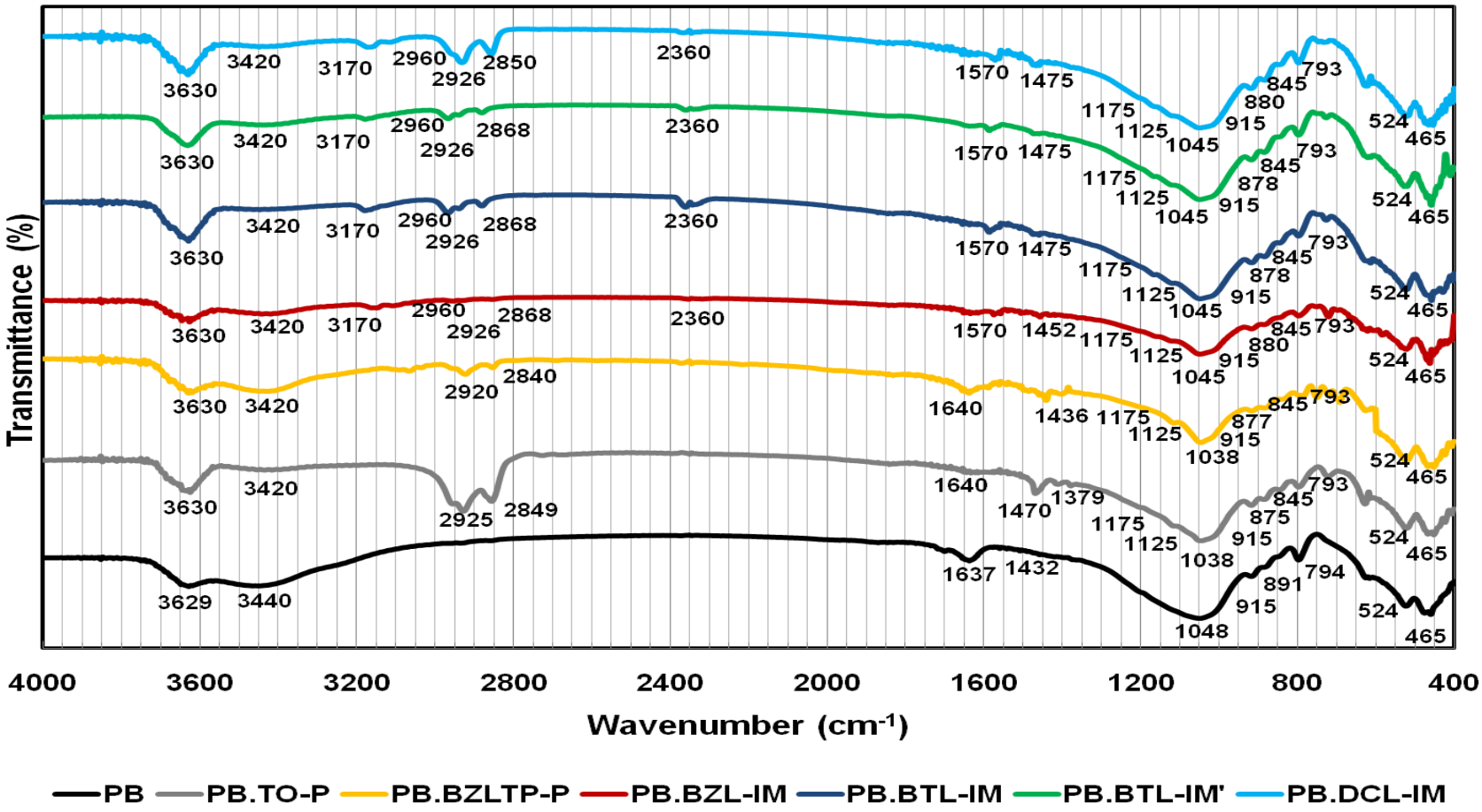

Figure 4.2 FTIR spectra for purified bentonite (PB) and modified organoclays

Table 4.3 FTIR spectral data of phosphonium organoclays

Band Assignment	PB.TO-P (cm^{-1})	PB.BZLTP-P (cm^{-1})
υ(X–O–H), X = Al, Mg	3630	3630
υ(H–O–H)	3420	3420
Asymmetric C-H in $(CH_2)_n$	2925	2920
Symmetric C-H in $(CH_2)_n$	2849	2840
δ(H–O–H)	1640	
υ(C=C) in the phenyl group		1640
υ(C–C) in aliphatic chain $(CH_2)_n$	1470	-
δ(C–C) in phenyl group	-	1436
υ(C–C) in aliphatic chain $(CH_2)_n$	1379	-
υ(Si–O)	1175	1175
υ(Si–O)	1125	1125
υ(Si–O)	1038	1038
δ(Al–Al–OH)	915	915
δ(Al-Fe–OH)	875	877
δ(Al–Mg–OH)	845	845
υ(Si–O) of SiO_2 impurity	793	793
δ(Al–O–Si)	524	524
δ(Si–O–Si)	465	465

υ: Stretching δ: Bending

The C-H stretching vibrations for methyl and methylene are the most characteristic in terms of recognizing the compound as an organic compound containing at least one aliphatic fragment or center. The bending vibrations help to tell more about the basic structure. For example, a strong methylene/methyl band (around 1470 cm^{-1}) and a weak methyl band (around 1380 cm^{-1}), plus a band at 725 cm^{-1} (methylene rocking vibration) is indicative of a long-chain linear aliphatic structure (141).

In the FTIR spectra of phosphonium organoclays (Fig. 4.2), the band at 3630 cm^{-1} in PB.TO-P (aliphatic) and in PB.BZLTP-P (aromatic) refer to OH stretching region,

which is assigned to hydroxyl groups coordinated to octahedral cations (-OH stretching mode of Al-OH of montmorillonite structure). The bands at 3420 cm^{-1} in both phosphonium organoclays are due to the stretching vibration of the hydroxyl groups of physisorbed free water molecules present in the clay.

The peaks at 2925 and 2849 cm^{-1} are ascribed to the asymmetric and symmetric vibration of methyl groups $(CH_2)_n$ of the aliphatic chain in the PB.TO-P organoclay. PB.TO-P shows a weak intensity of the OH bending vibration at 1640 cm^{-1} due to adsorbed water. In addition to this, there is also the H-C-H stretching vibration band at 1470 cm^{-1} in IR spectrum of PB.TO-P organoclay. The strong methylene/methyl band at 1470 cm^{-1} (stretching of aliphatic C–C bonds in a long chain) and the weak methyl band at 1379 cm^{-1} (characteristic of methyl groups) are characteristics of the aliphatic phosphonium organoclay PB.TO-P.

The phenyl ring attached to the phosphonium atom displayed an unusually sharp vibration band at 1436 cm^{-1} as shown in the infrared spectrum of PB.BZLTP-P. The main peaks of the aromatic phosphonium organoclay PB.BZLTP-P at 1640 cm^{-1} (stretching vibrations of aromatic C=C bonds in the phenyl group), and 1436 cm^{-1} (bending of C–C bonds) are present in the spectrum of the aromatic PB.BZLTP-P. IR absorption bands at 1125 cm^{-1} (out of plane stretching vibration of the Si–O bond), and at 1038 cm^{-1} (in-plane Si–O stretching vibration in layered silicates) confirm the presence of Bronsted acid sites.

The assignments for FTIR bands of imidazolium modified clays are listed in Table 4.4.

Table 4.4 FTIR spectral data of imidazolium organoclays

Band Assignment	PB.BZL-IM (cm^{-1})	PB.BTL-IM (cm^{-1})	PB.BTL-IM' (cm^{-1})	PB.DCL-IM (cm^{-1})
υ(X–O–H), X = Al, Mg	3630	3630	3630	3630
υ(H–O–H)	3420	3420	3420	3420
υ(N–H)	3170	3170	3170	3170

Table 4.4 FTIR spectral data of imidazolium organoclays (Cont'd)

Asymmetric υ(C-H)	2960	2960	2960	2960
Asymmetric υ(C-H)	2926	2926	2926	2920
Symmetric υ(C-H)	2868	2868	2868	2850
C-O	2360	2360	2360	2360
δ(H–O–H)	1570	1570	1570	1570
υ(Si–O)	1452	1475	1475	1475
υ(Si–O)	1175	1175	1175	1175
υ(Si–O)	1125	1125	1125	1125
υ(Si–O)	1045	1045	1045	1045
δ(Al–Al–OH)	915	915	915	915
δ(Al-Fe–OH)	880	878	878	880
δ(Al–Mg–OH)	845	845	845	845
υ(Si–O) of SiO_2 impurity	793	793	793	793
δ(Al–O–Si)	524	524	524	524
δ(Si–O–Si)	465	465	465	465

υ: Stretching δ: Bending

In the FTIR spectra of imidazolium organoclays (Fig. 4.2), the imidazole exhibits typical broad hydrogen N–H bonding expressed by stretching absorption in the 3100-3300 cm^{-1} region. This stretching can be clearly seen at the band 3170 cm^{-1}. The peaks in the range of 2920 and 2960 cm^{-1} are ascribed to the asymmetric C-H vibration of methyl groups $(CH_2)_n$. Peaks in the 2850 and 2868 cm^{-1} range describe the symmetric C-H vibration of methyl groups. Peaks at 2360 cm^{-1} are identified to correspond to the undissociated molecular CO_2. Water vapor has an infrared spectrum which covers large parts of the FTIR wavenumber window as given by the broad band characteristic of hydrogen bonded OH stretching vibration in the 3400-3700 cm^{-1} region, and the usual Si-O and H-O-H bending vibration bands in the 1400-1600 cm^{-1} region.

The intercalation of phosphonium and imidazolium salts in the purified bentonite layers is clarified considering the observations of FTIR analysis which exhibited new peaks for the cations intercalated between the silicate layers. However, the IR

absorption bands in the low frequency region of the purified bentonite and the phosphonium and imidazolium organoclays exhibited comparable peaks indicating that the clay mineral has not changed upon exchange of the interlayer sodium ions by the quaternary phosphonium and imidazolium ions.

4.2 Morphology Analyses

4.2.1 X-Ray Diffraction

XRD is a useful technique to analyze the dispersion state of an organoclay in the polymer matrix and the interlayer spacing of the silicate layers. The patterns obtained from the analysis are used for the characterization of the structure of nanocomposites by using the 2θ peak, which is used for the calculation of the distance between the silicate layers by Bragg's law. The intercalation of polymer chains between the silicate layers results in an increase in the interlayer spacing. For those intercalated structures, the characteristic peak tends to shift to a lower angle due to the expansion of the basal spacing (142). Although the layer spacing increases, there still exists an attractive force between the layers to stack them in an ordered structure. Change in intensity and the shape of the basal reflections is the evidence that specifies the intercalation of polymer chains (19).

On the contrary, no peak can be observed in the XRD pattern of exfoliated polymer nanocomposites owing to fully dispersed clay platelets in the matrix (143). The absence of a diffraction peak may indicate an exfoliated or delaminated structure; however, it should not be used as the only evidence for the formation of an exfoliated structure. Due to the low concentration of the organoclay, X-ray beams may hit to a non-uniformly dispersed region of the sample and Bragg's reflection may be eliminated demonstrating exfoliation or it may remain unchanged as in conventional structures. The features of the local microstructures from TEM give useful detail to the overall picture that is drawn from the XRD results (144). Thus, XRD and TEM analyses are regarded complementary to each other for the material characterization of polymer/clay nanocomposites. In addition to the exfoliated and

intercalated structures, intermediate structures may also be observed that display both of these two morphologies.

One of the most important reasons that results in exfoliated structures is the interaction between the clay surface and the polymer. Also, increasing viscosity and other shear elements like screw configuration and screw speed cause delamination of the layers. As a consequence, the clay platelets may be dispersed uniformly in the polymer matrix rather than be agglomerated as tactoids.

The orientations of organic chains in clay minerals were initially deduced by Lagaly and Weiss in 1969. Depending on the layer charge (or interlayer cation density or packing density of the alkyl-onium ions) of the clay mineral and the chain length of the organic ion, different arrangements of organic molecules between the layers can be formed. As illustrated in Figure 2.5, the organic ions may lie flat on the silicate surface as a monolayer or bilayer, or depending on the packing density and the chain length an inclined paraffin-type structure, with the chains radiating away from the silicate surface can be formed. In the pseudo-trimolecular layers, some chain ends are shifted above one another, so that the spacing is determined by the thickness of the three alkyl chains (15), (28).

Torok et al. in 1999 indicated that, using computer simulations, the interlayer distances generated by monolayer and bilayers of alkyl chains would be 1.42 and 1.77 nm, respectively. Murray et al. in 2000 reported slightly different interlayer distances of 1.32, 1.8, and 2.27 nm for mono, bi and pseudo-trilayers, respectively (145). Following the procedure employed by Torok, the distance for a pseudo-trilayer would be 2.34 nm (5).

4.2.1.1 X-Ray Diffraction Results of Clays and Organoclays

The XRD diffraction patterns of the clays, raw bentonite (B), purified bentonite (PB), commercial montmorillonite (M), modified bentonites with salt S (B.S, PB.S and M.S), polymer blends and polymer binary and ternary nanocomposites used in this study were obtained. The basal spacing values of clays and organoclays are shown in Table 4.5.

Table 4.5 XRD results of clays and organoclays

Composition	1st Peak		2nd Peak	
	2 θ (˚)	d_{001} (nm)	2 θ (˚)	d_{002} (nm)
Clays				
B	7.42	1.19	19.86	0.45
PB	8.00	1.11	19.86	0.45
M	7.12	1.24	19.86	0.45
B.TO-P	3.56	2.48	7.42	1.19
PB.TO-P	3.50	2.52	6.78	1.30
M.TO-P	3.37	2.62	6.82	1.30
PB.TO-P 1.7	3.50	2.52	6.78	1.30
PB.BZLTP-P	4.96	1.78	9.38	0.94
PB.BZL-IM	6.16	1.43	18.50	0.48
PB.BTL-IM	6.60	1.34	13.28	0.67
PB.BTL-IM'	6.60	1.34	13.28	0.67
PB.DCL-IM	6.08	1.45	9.44	0.94

4.2.1.1.1 Effects of Clay Purification

X-Ray diffraction analyses of the raw natural bentonite (B), purified bentonite (PB) and commercial montmorillonite (M) are shown in Figures 4.3-4.5. XRD analyses of the B, PB and M are compared in Figure 4.6.

The analysis by XRD of the B confirmed the major presence of montmorillonite, with reflections relative to the planes (001) and (002) (M_{001} and M_{002}). Qualitative mineral analysis of the clay samples was used to determine the other minerals present. The unpurified bentonite clay (B) contained analcime (An), calcite (C), clinoptilolite (Cln), dolomite (D), feldspar (F), quartz (Q), Illite (I), opal-C (OC) and α-cristobalite (α-Cr) as non-clay minerals. These results were also compared to earlier studies and confirmed (9), (72), (146). After purification, these minerals did not exist except for negligible amounts of quartz (Q) and α-cristobalite (α-Cr). The interlayer distance of

bentonite (B) 1.19 nm ($2\theta = 7.42^{o}$) did not change significantly after purification. (PB) had an interlayer spacing of 1.11 nm ($2\theta = 8.00^{o}$), and this can be attributed to the elimination of some of the monomolecular water layer between the montmorillonite layers (9). After purification, the bentonite crystalline structure was similar to that of M supplied by Nanocor Company with 1.24 nm interlayer spacing ($2\theta = 7.12^{o}$) indicating the success of purification process.

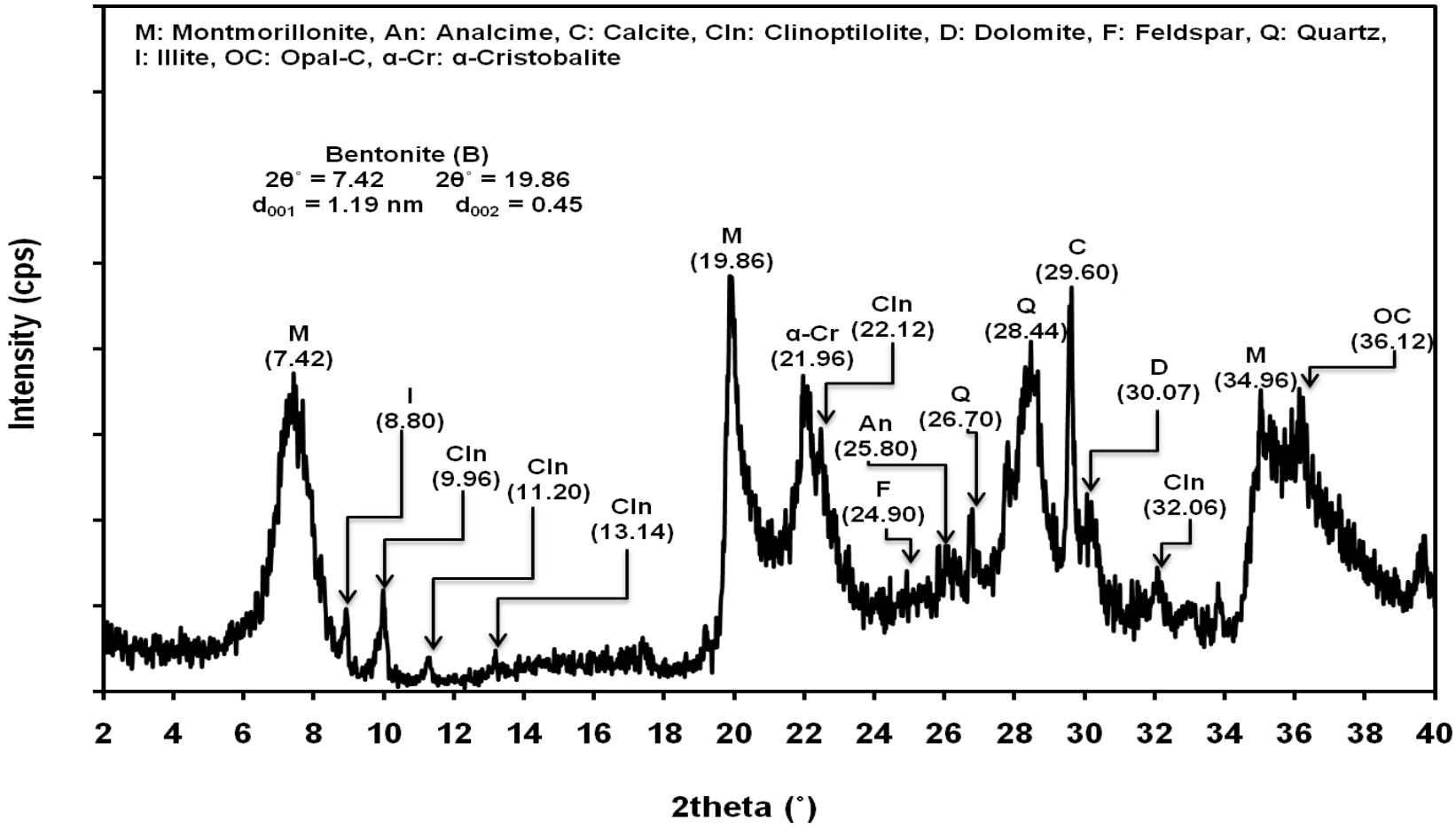

Figure 4.3 XRD pattern of raw bentonite (B)

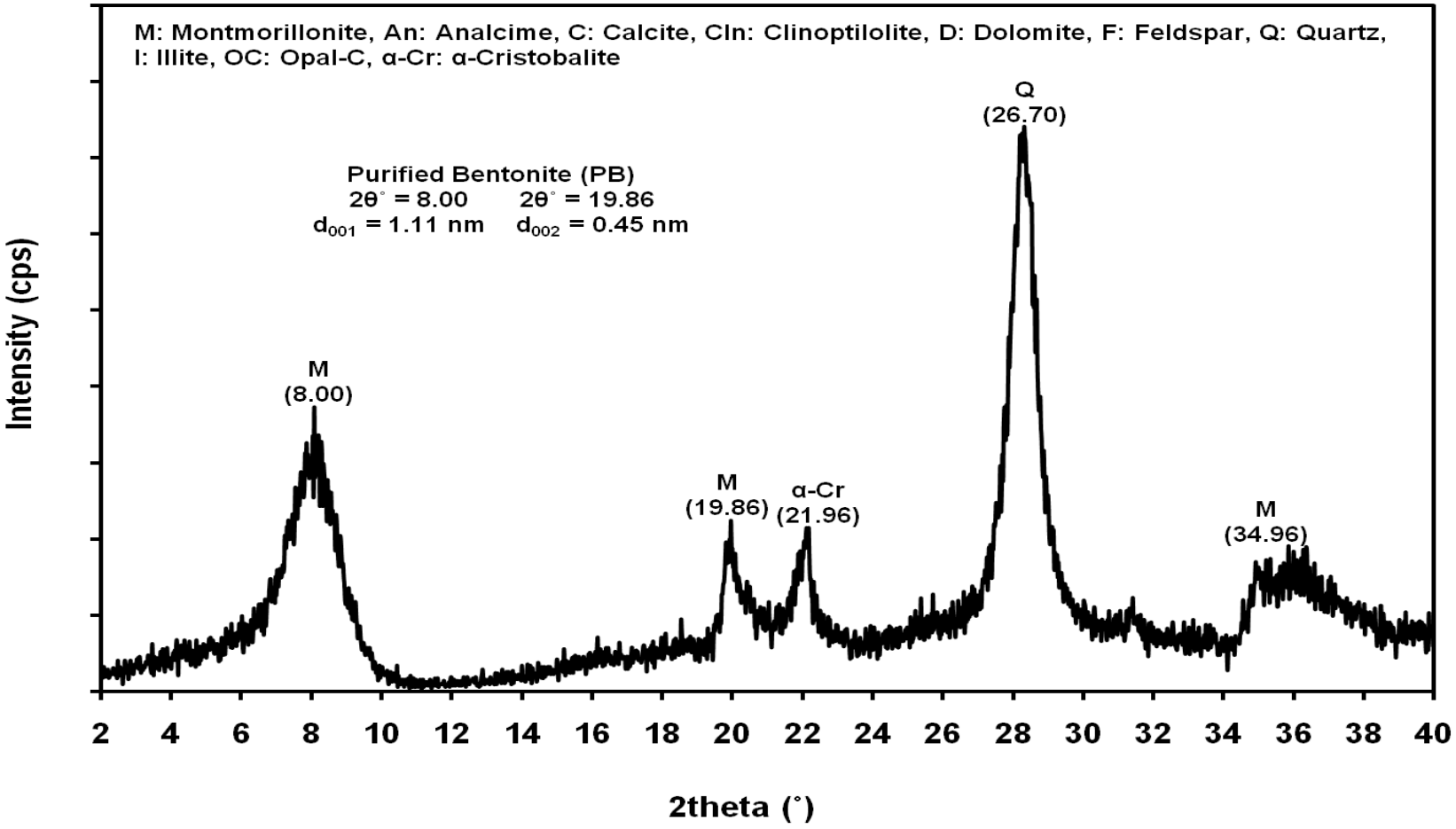

Figure 4.4 XRD pattern of purified bentonite (PB)

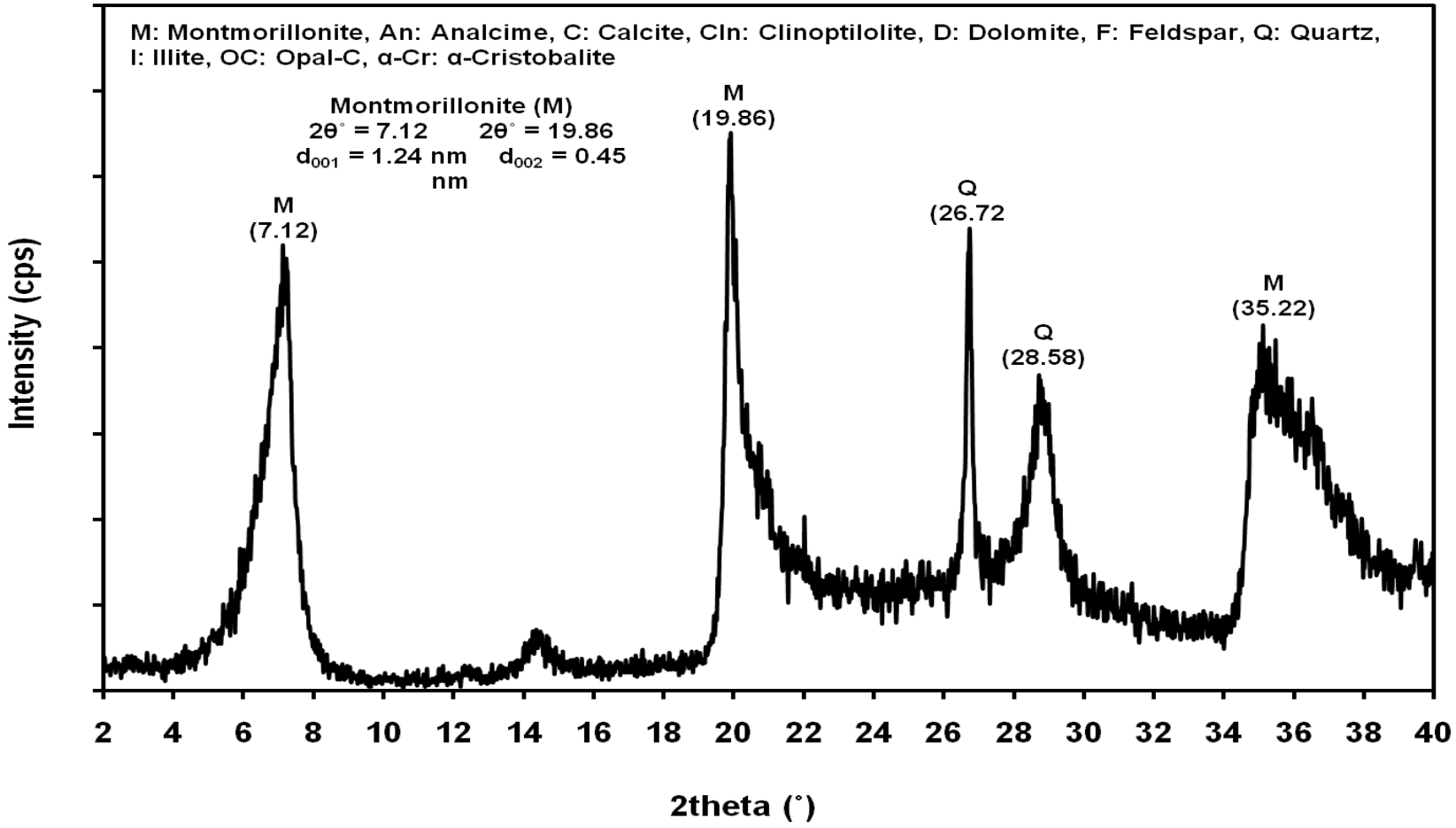

Figure 4.5 XRD pattern of commercial montmorillonite (M)

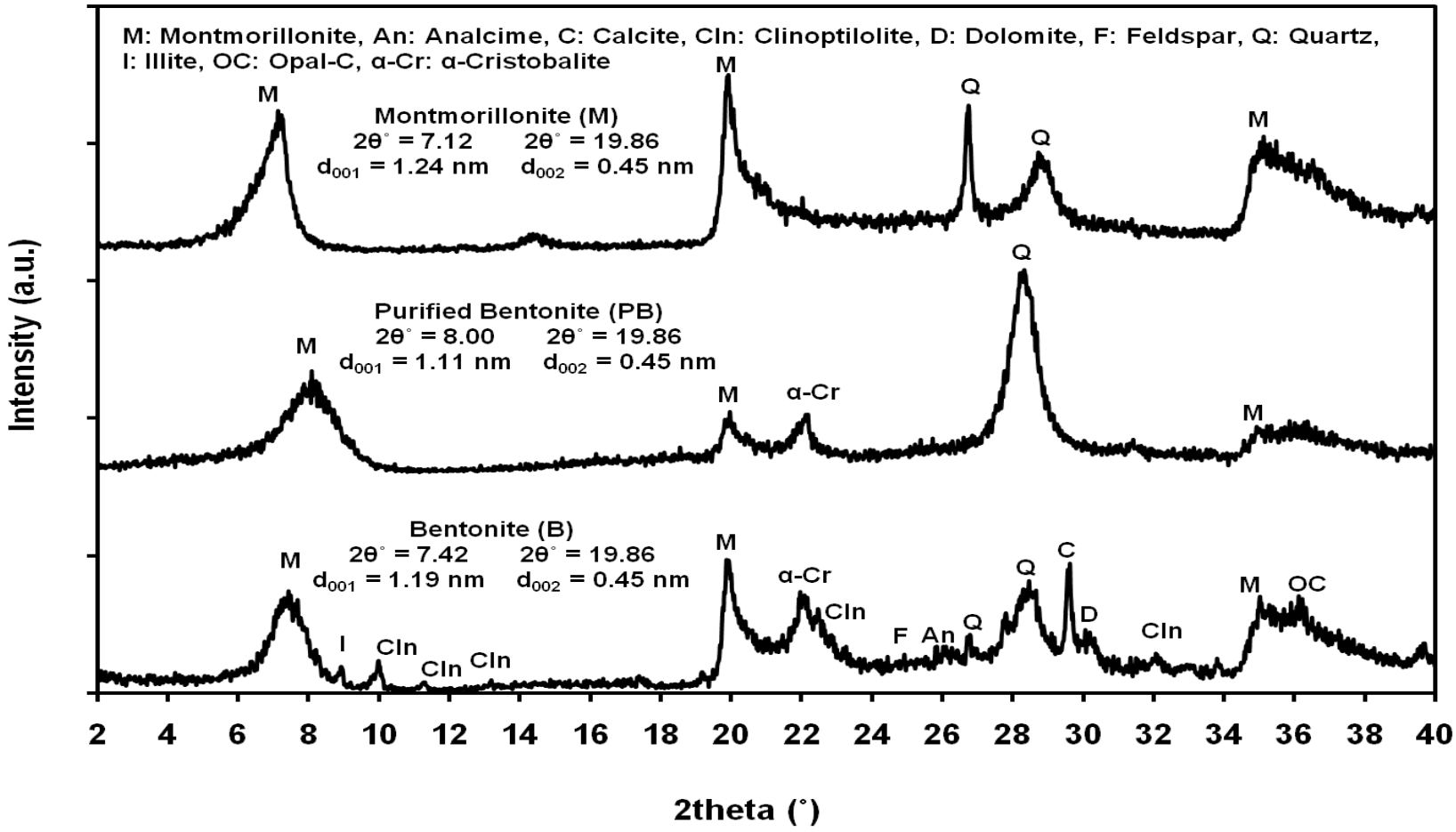

Figure 4.6 XRD patterns of bentonite (B), purified bentonite (PB) and commercial montmorillonite (M)

4.2.1.1.2 Effects of Clay Modification

Tetraoctyl phosphonium salt (TO-P Br) was used as the clay modifier, and the X-Ray diffractograms of both raw bentonite B and commercial montmorillonite M were compared. The X-Ray diffractograms of both B and M clays, unmodified and modified, are presented in Figures 4.7 and 4.8, respectively. B.TO-P and M.TO-P designate clays B and M modified with TO-P Br salt. The X-ray patterns of B.TO-P clay revealed a shift in the position of (001) planes (2θ changed from 7.42^{o} to 3.56^{o}), meaning a relatively large increase in the basal distance of these planes from 1.19 nm to 2.48 nm (109% increase). This increase confirms the occurrence of salt molecule intercalation between the bentonite clay layers. The XRD patterns of M.TO-P revealed a shift in the position of (001) planes (2θ changed from 7.12^{o} to 3.37^{o}), meaning an increase in the basal distance of these planes from 1.24 nm to 2.62 nm (111% increase) and also confirming the occurrence of salt molecule intercalation between M clay layers.

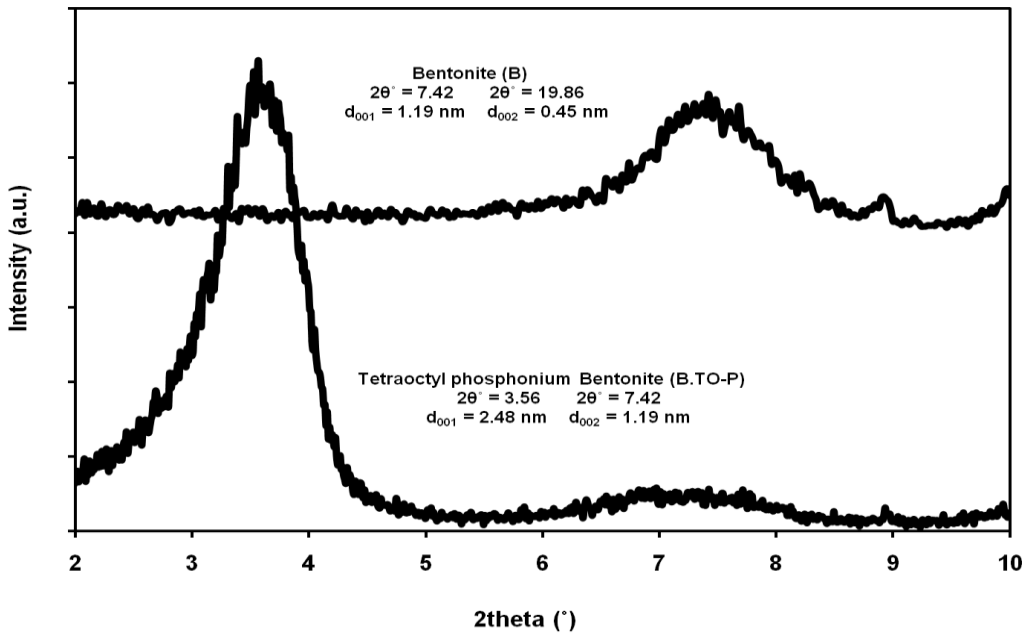

Figure 4.7 XRD patterns of unmodified bentonite (B) and TO-P Br modified bentonite (B.TO-P)

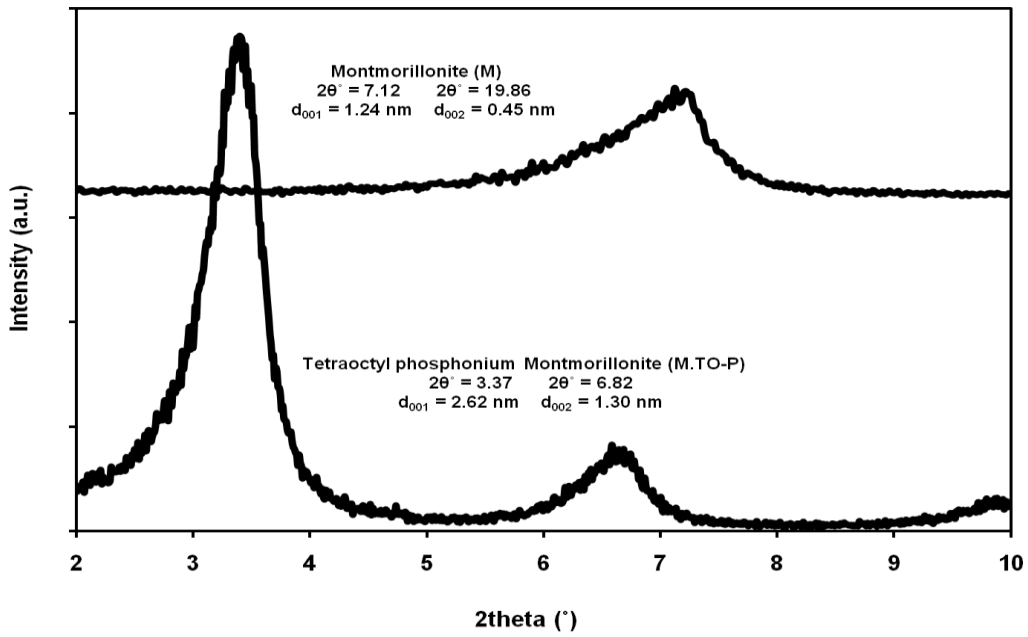

Figure 4.8 XRD patterns of montmorillonite (M) and TO-P Br modified montmorillonite (M.TO-P)

After purification, the XRD patterns of the modified PB clay given in Figure 4.9 revealed a shift in the position of (001) planes (2θ changed from 8.00^{o} to 3.50^{o}), indicating also an increase in the basal distance of these planes, from 1.11 nm to 2.52 nm, corresponding to an increase of 127% and confirming the occurrence of salt molecule intercalation between the purified bentonite clay layers. No significant difference was noticed between B and PB before and after modification with the TO-P Br salt regarding the d-spacing of the layers, but the significance of purification is revealed by removal of the non-clay minerals. From the XRD of Figure 4.9, it is observed that the peaks from α-cristobalite (α-Cr) and also from (002) planes of montmorillonite corresponding to interlayer spacings of 1.11 nm (d001 for unmodified clay-MMT), were not changed with the treatment. This observation highlights that the unique effect of salt in sample structure is the intercalation of (001) planes of montmorillonite due to an incomplete ion exchange, with some residual sodium-MMT remaining in the material (122). In the present study, Reşadiye bentonites were purified and used for further modifications and preparations of binary and ternary polymer nanocomposites.

4.2.1.1.2.1 Effects of the Amount of Salt Used for Modification

The effects of using extra amount of salt during the modification of the clays were studied using the same salt TO-P Br. Purified bentonite was modified with TO-P Br salt at 1.7 times the CEC of the clay (PB.TO-P1.7) and with 1.1 times the CEC of the clay (PB.TO-P). The d-spacing of the first 2θ angles shown in Figure 4.9 did not change, but extra crystalline peaks appeared due to the presence of extra amount of TO-P Br salt. In addition, since TO-P Br salt is insoluble, and the PB modified with this salt was very sticky and PB.TO-P1.7 could not be ground for nanocomposite preparation.

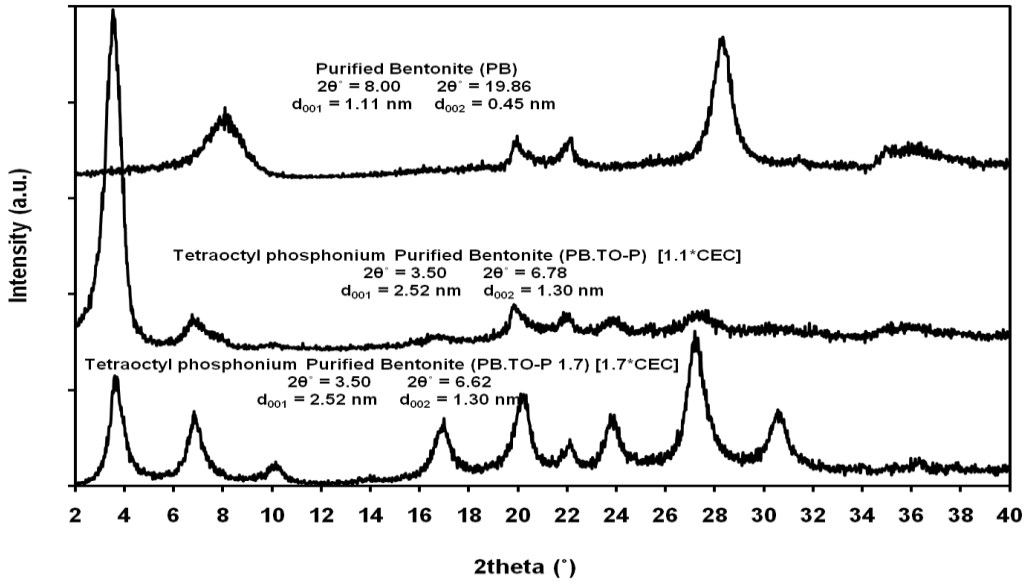

Figure 4.9 XRD patterns of purified bentonite (PB) modified by TO-P Br salt at 1.1*CEC (PB.TO-P) and 1.7*CEC (PB.TO-P 1.7)

4.2.1.1.2.2 Effects of the Salt Structure Used for Modification

The basal spacings determined for pristine clays B, PB and M increased, upon intercalating the TO-P Br salt inside the layers, from 1.19 nm, 1.11 nm and 1.24 nm up to 2.48 nm, 2.52 nm and 2.62 nm, respectively. According to the computer simulations of Torok et al. 1999, the TO-P Br modified clays indicate arrangements that are between pseudo-trilayers and paraffin-type of alkyl chains (5), (88).

Purified bentonites were modified with BZLTP-P Cl salt at 1.1 times the CEC of the clay (PB.BZLTP-P) and the XRD data are presented in Figure 4.10. The X-ray patterns of PB.BZLTP-P revealed a shift in the position of (001) planes (2θ changed from 8.00^{o} to 4.94^{o}), meaning an increase in the basal distance of these planes from 1.11 nm to 1.78 nm (60% increase).

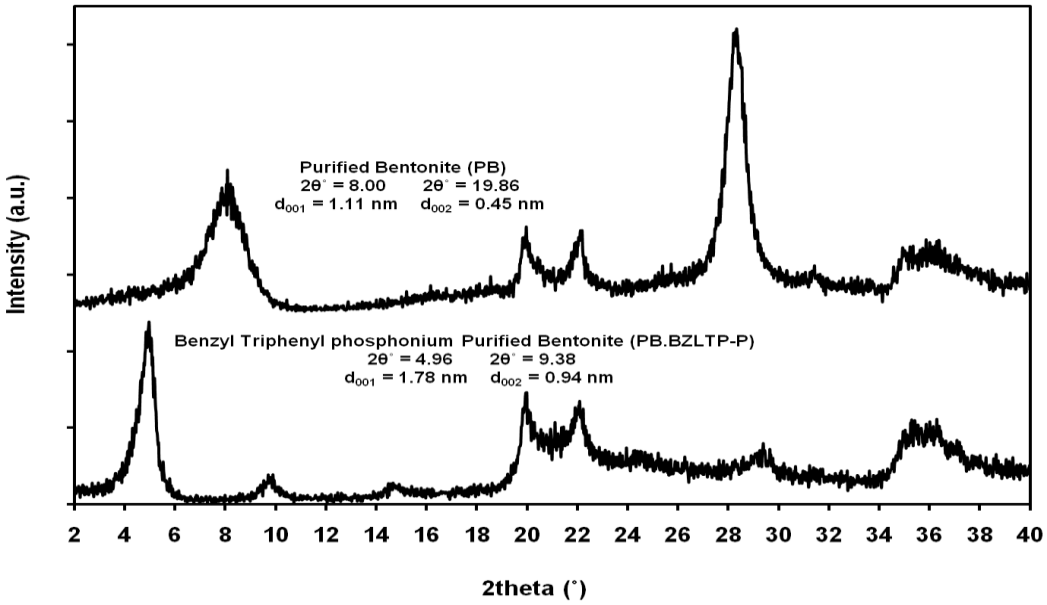

Figure 4.10 XRD patterns of purified bentonite (PB) and purified bentonite modified by BZLTP-P Cl salt at 1.1*CEC (PB.BZLTP-P)

Phosphonium organoclays exhibited a range of basal spacings from 1.80 to 2.52 nm. The low molecular weight surfactant (BZLTP-P Cl with the phenyl and benzyl groups) led to the smallest basal spacing (1.78 nm), corresponding to a bilayer arrangement of chains. High molecular weight surfactants (TO-P Br with long alkyl chains) produced organoclays with a higher basal spacing (2.52 nm). In addition, the higher basal spacing in the presence of the aliphatic phosphonium salt is known to facilitate the intercalation or even the exfoliation of the organo-montmorillonite in a polymer nanocomposite.

Purified bentonites were modified with four imidazolium salts (BZL-IM PF6), (BTL-IM PF6), (BTL-IM Cl) and (DCL-IM Cl) at 1.1 times the CEC of the clay and the products were abbreviated as (PB.BZL-IM), (PB.BTL-IM), (PB.BTL-IM') and

(PB.DCL-IM). Figures 4.11 - 4.13 present the X-ray patterns of these sets. The X-ray patterns of PB.BZL-IM revealed a shift in the position of (001) planes (2θ changed from 8.00^{o} to 6.16^{o}), meaning an increase in the basal distance of these planes from 1.11 nm to 1.43 nm, corresponding to an increase of 29%. The X-ray patterns of PB.BTL-IM and PB.BTL-IM' revealed the same shift in the position of (001) planes (2θ changed from 8.00^{o} to 6.6^{o}), with an increase in the basal distance from 1.11 nm to 1.34 nm, corresponding to an increase of only 21%. The X-ray patterns of PB.DCL-IM revealed a shift in the position of (001) planes (2θ changed from 8.00^{o} to 6.08^{o}), meaning an increase in the basal distance of these planes from 1.11 nm to 1.45 nm, corresponding to an increase of only 31%. Imidazolium modified organoclays exhibited a more compact structure than the phosphonium ones which exhibited up to 127% increase in the d-spacing presenting better intercalation. The increase in the cation molecular weight of the di-imidazolium surfactants resulted in slight increase in the basal spacing of the modified clays corresponding to monolayer arrangement of salt chains in all imidazolium organoclays. The increase in basal spacing based on the chain group attached to the first nitrogen atom in imidazolium salts was in the order of Butyl (BTL) < Benzyl (BZL) < Decyl (DCL). These results are in accordance with earlier studies on the effect of molecular weight and chemical structure on the resulting basal spacing of organoclays (7).

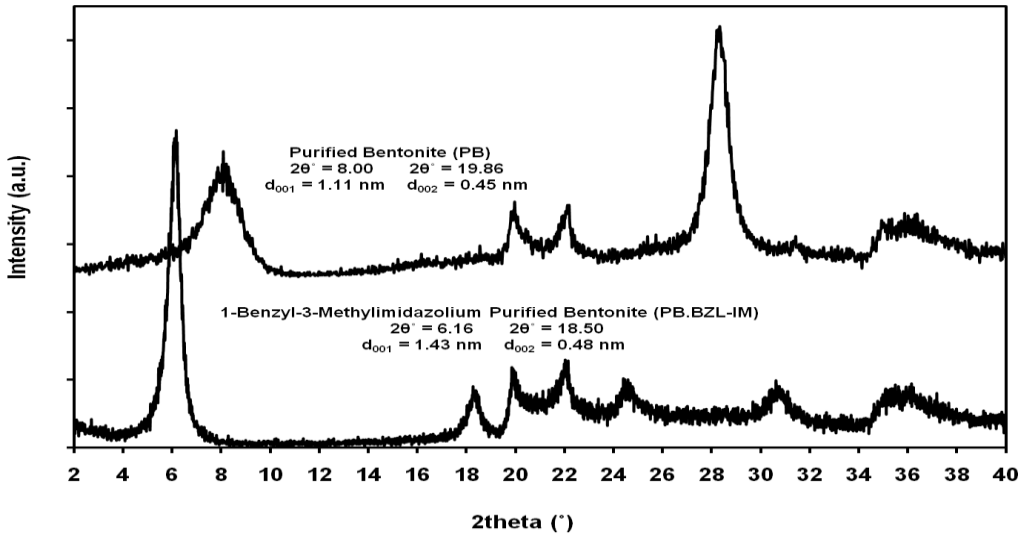

Figure 4.11 XRD patterns of purified bentonite (PB) unmodified and modified by BZL-IM PF6 salt (PB.BZL-IM)

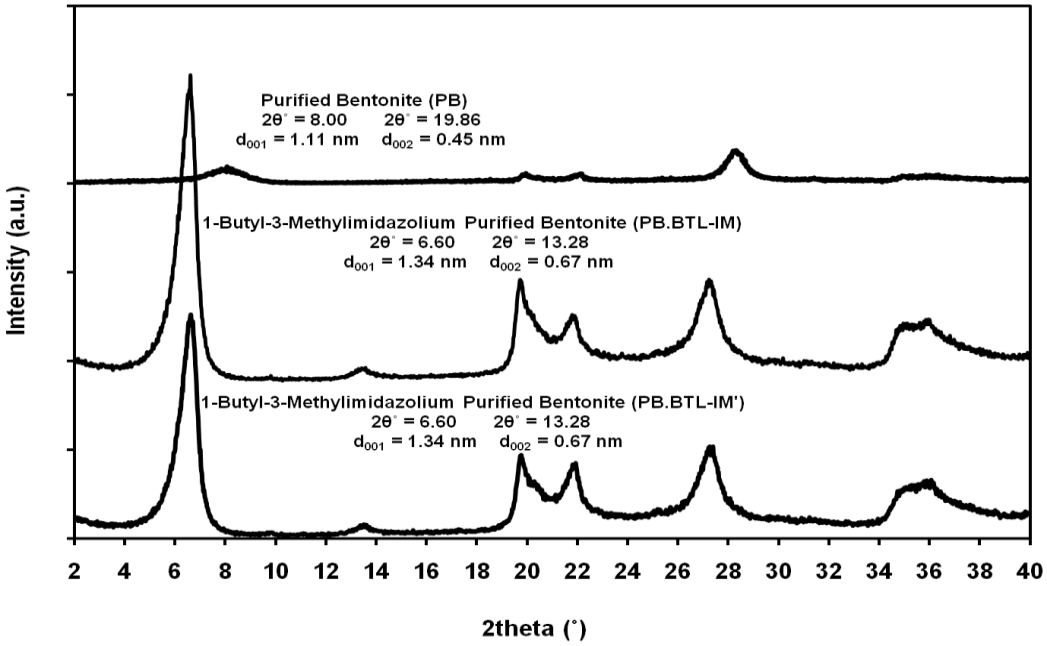

Figure 4.12 XRD patterns of purified bentonite (PB) unmodified and modified by BTL-IM PF6 salt (PB.BTL-IM) and by BTL-IM Cl salt (PB.BTL-IM')

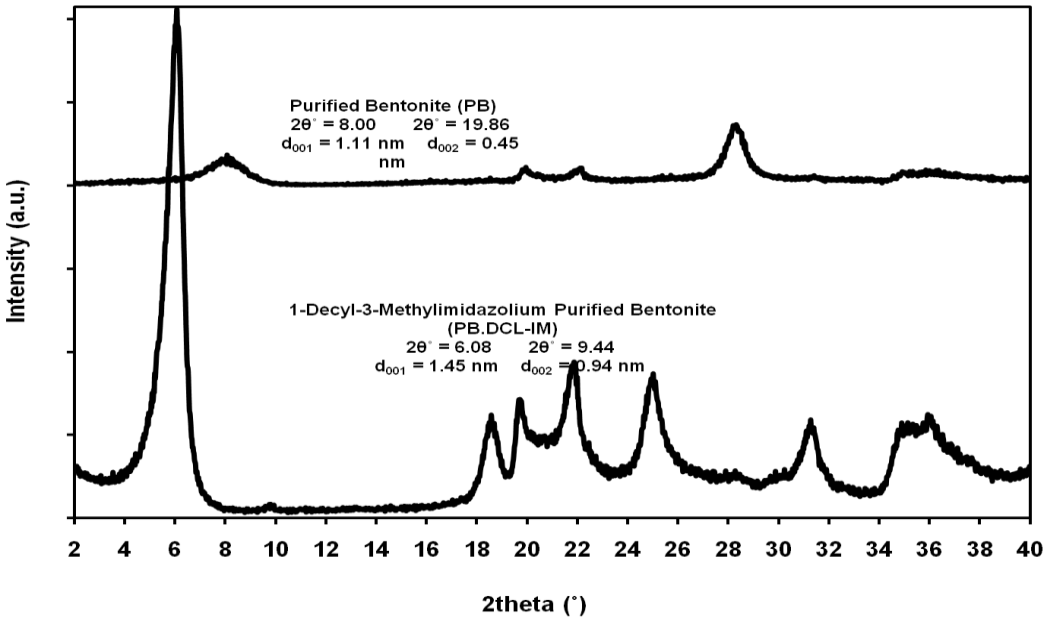

Figure 4.13 XRD patterns of purified bentonite (PB) modified by DCL-IM Cl salt (PB.DCL-IM)

4.2.1.2 X-Ray Diffraction Results of PA66 Nanocomposites

The d-spacings of PA66 binary and ternary nanocomposites having 1 and 2 wt % phosphonium organoclays and 5 wt % impact modifier are given in Table 4.6. The basal spacing differences with organoclays are summarized in Table 4.7.

Table 4.6 XRD results of PA66 compositions

Composition	1st Peak		2nd Peak	
	2 θ (˚)	d_{001} (nm)	2 θ (˚)	d_{002} (nm)
Polymer				
PA66 (Extruded Twice)	-	-	-	-
Organoclays				
PB.TO-P	3.50	2.52	6.78	1.30
PB.BZLTP-P	4.96	1.78	9.38	0.94
Polymer/Organoclay Binary Nanocomposites				
PA66/PB.TO-P	4.41	2.00	9.45	0.94
PA66/PB.BZLTP-P	4.65	1.90	9.43	0.94
Polymer/Organoclay/Elastomer Ternary Nanocomposites				
PA66/PB.TO-P/E-BA-MAH (1-S)	-	-	-	-
PA66/PB.TO-P/E-BA-MAH (1-P)	-	-	-	-
PA66/PB.TO-P/E-BA-MAH (2-P)	4.41	2.00	-	-
PA66/PB.TO-P/E-BA-MAH (2-S)	4.41	2.00	-	-
PA66/PB.TO-P/E-BA-MAH	4.41	2.00	9.58	0.92
PA66/PB.BZLTP-P/E-BA-MAH	4.65	1.90	9.53	0.93

Table 4.7 XRD results of PA66 compositions (basal spacing difference)

	d_{001} Initial (nm)	d_{001} PA66/OC (nm)	Δd (nm)	d_{001} PA66/OC/E (nm)	Δd (nm)
PB.TO-P (1-S)	2.52	-	-	-	-
PB.TO-P (1-P)	2.52	-	-	-	-
PB.TO-P (2-P)	2.52	2.00	-0.52	2.00	-0.52
PB.TO-P (2-S)	2.52	2.00	-0.52	2.00	-0.52
PB.TO-P	2.52	2.00	-0.52	2.00	-0.52
PB.BZLTP-P	1.78	1.90	0.12	1.90	0.12

OC: Organoclay, E: E-BA-MAH

The properties of polymer nanocomposites depend directly on the extent and quality of dispersion and on the degree of clay mineral exfoliation and/or polymer intercalation in the nanocomposite. The quality of adhesion at the polymer-clay interface is another important factor. The initial basal spacing in the organoclay is an important parameter for the determination of the potential for polymer intercalation and clay mineral delamination. Organoclays with smaller interlayer distances have reduced probabilities for polymer intercalation. Nevertheless, intercalated structures can also be prepared from clay mineral with smaller basal spacing via in-situ polymerization (6). In general, it is desirable to start with organoclays that exhibit large interlayer distances, in order to achieve desirable nanocomposites properties (5). However, if the salt is too big, then the polymers cannot diffuse into the interlayer spacing.

In the present study, it is important to note that the main objective is to prepare thermally stable organoclays and investigate the behavior of counter ion, aryl, (short and long) alkyl onium ions on the nanocomposite produced. Awad et al. in 2004 emphasized that using longer alkyl chains produces less thermally stable trialkyl imidazolium organoclays. In the present work, we concentrated on di-(alkyl, aryl) imidazolium salts as a part of the study.

4.2.1.2.1 Effects of Number of Extrusions and Injection Preparation Procedure

PB.TO-P organoclay was taken as the reference in order to investigate the effects of number extrusions (once or twice) and injection method (pelletized or simultaneous) on the various properties of the nanocomposites to be prepared using PA66 as the polymer and E-BA-MAH as the compatibilizer. For this purpose, PA66 (extruded twice), PA66 nanocomposites (PA66/1% PB.TO-P/5%E-BA-MAH) were extruded according to four procedures in order to determine the most effective way to have better intercalation of the polymers in between the clay layers.

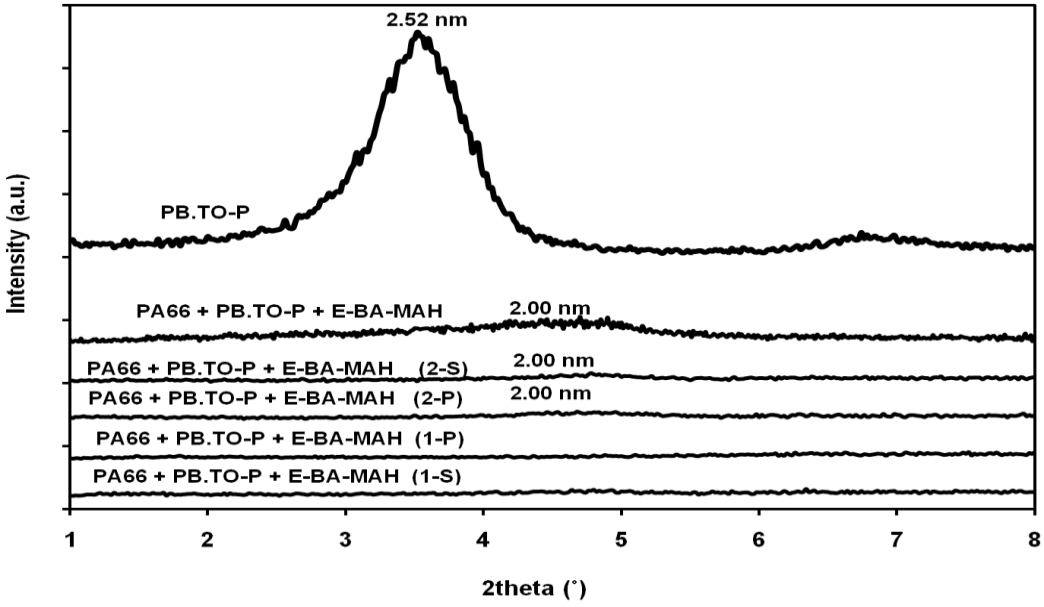

Figure 4.14 XRD patterns of PA66/1%PB.TO-P/E-BA-MAH and PA66/2%PB.TO-P/E-BA-MAH ternary nanocomposites

XRD patterns for (PB.TO-P) and the four nanocomposites 1-S, 1-P, 2-P and 2-S of (PA66/1% PB.TO-P/5%E-BA-MAH) are presented in Figure 4.14. The X-Ray diffraction patterns of the nanocomposites extruded only once (1-S and 1-P) did not show any reflection of the peaks. It may seem to the viewer as exfoliation, but X-ray beams may hit a non-uniformly dispersed region in a sample due to low concentration of the organoclay, or immiscibility and disorder in the sample may lead to elimination of a Bragg's reflection. Extrusion twice (2-P and 2-S) is known to

increase the effect of shear intensity on the organoclay dispersion. The XRD patterns of the nanocomposites extruded twice (2-P and 2-S) revealed a shift in the position of (001) planes (2θ changed from 3.52^{o} to 4.41^{o}), indicating a decrease in the basal distance of these planes from 2.52 nm to 2.00 nm.

4.2.1.2.2 Effects of Organoclay Content

The addition of 2 wt % of PB.TO-P organoclay did not improve the situation but presented clearer view of higher intensity of the angle at 4.41^{o}. XRD patterns for (PB.TO-P) and the nanocomposites produced by procedure 2-S (PA66/PB.TO-P) and (PA66/PB.TO-P/E-BA-MAH) are presented in Figure 4.15.

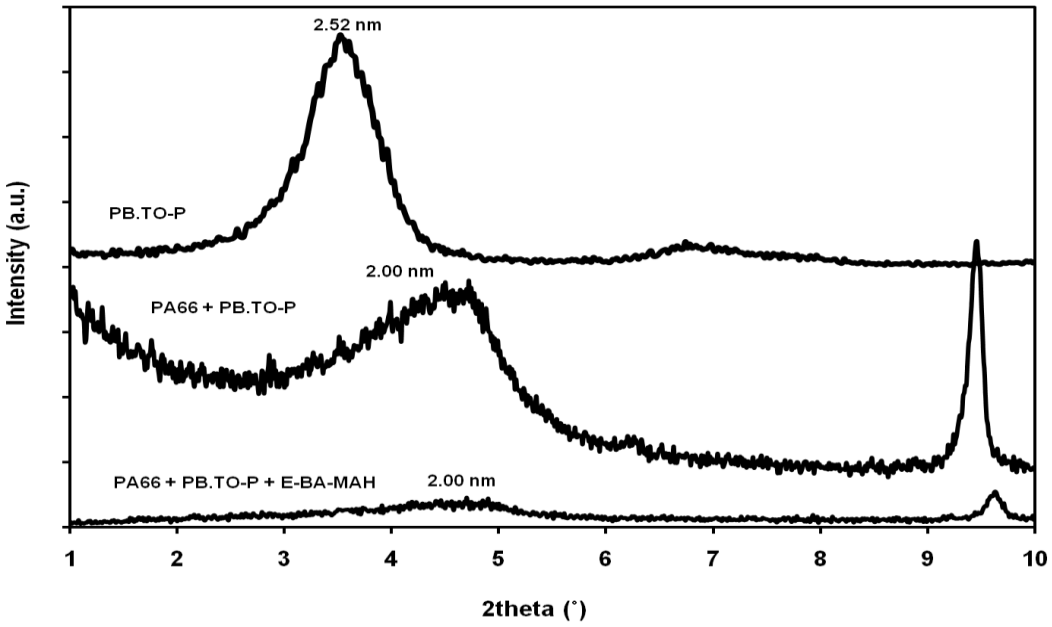

Figure 4.15 XRD patterns of PA66/PB.TO-P/E-BA-MAH binary and ternary nanocomposites

The procedure (2-S) involving extruding twice and simultaneous injection molding was applied, since it is the best way for nanocomposite production. Extrusion of the polymer matrix twice, and increasing the viscosity by adding elastomeric phase to the matrix increased the shear intensity and thereby facilitated the intercalation of the polymer chains into the van der Waals gallery of the clay (147), (1). Also, 2 wt % of clay is taken as the optimum organoclay content since 1% was not enough to

cause significant improvement in the preparation of nanocomposites as discussed in section 4.2.1.2.1. PA66/PB.TO-P binary and PA66/PB.TO-P/E-BA-MAH ternary nanocomposites revealed a shift in the peak from 3.5° to 4.41°. This shift from low-angle to higher angles after melting and cooling of organic-modified bentonite has been attributed to recrystallization which occurs during cooling after extrusion (6) or high temperature oxidative degradation. Another explanation is the evaporation of the organic phase while drying of the organoclay. A third possible argument is the high pressure which causes the clay layers to collapse during injection molding. Probably either one or a combination of these mechanisms took place. This shift indicates the poor miscibility of PB.TO-P with PA66. This is a clear indication that the compatibility of the clay modifier with the polymer matrix is very important (112).

XRD patterns for (PB.BZLTP-P) and the PA66 binary and ternary nanocomposites with PB.BZLTP-P and E-BA-MAH are presented in Figure 4.16. The X-Ray diffraction patterns of these nanocomposites revealed a slight increase in the basal distance of these planes from 1.78 nm to 1.90 nm (2θ changed from 4.96^{o} to 4.65^{o} for both) indicating that PB.BZLTP-P organoclay is not highly compatible with PA66. For this reason, the X-ray pattern indicates a slightly intercalated structure.

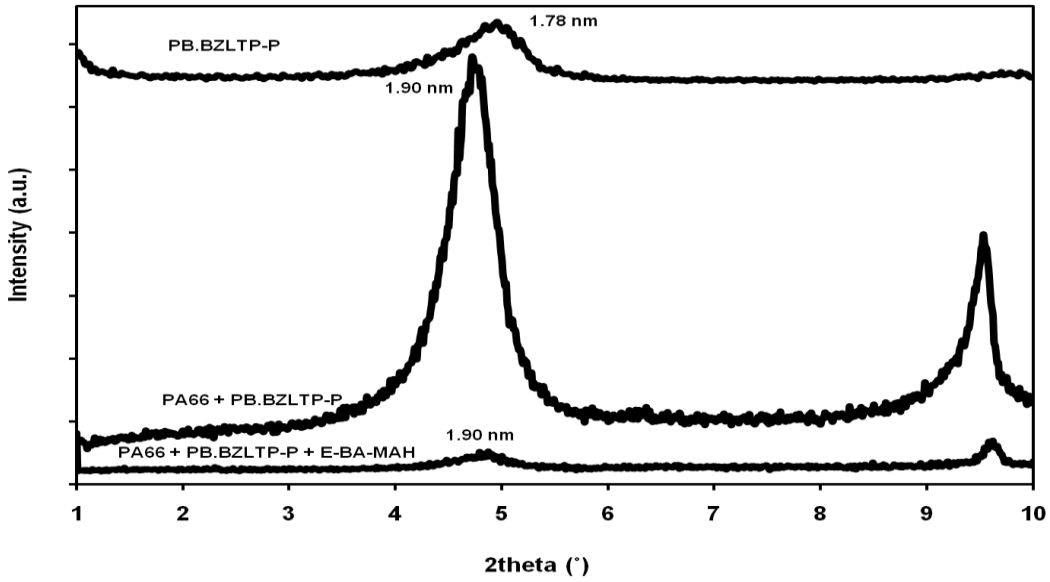

Figure 4.16 XRD patterns of PA66/PB.BZLTP-P/E-BA-MAH binary and ternary nanocomposites

4.2.1.3 X-Ray Diffraction Results of PET Nanocomposites

The d-spacings of organoclays, PET binary and ternary nanocomposites having 2 wt % phosphonium and imidazolium organoclays and 5 wt % impact modifier are given in Table 4.8. The basal spacing differences with organoclays are summarized in Table 4.9.

Table 4.8 XRD results of PET compositions

Composition	1st Peak		2nd Peak	
	2 θ (˚)	d_{001} (nm)	2 θ (˚)	d_{002} (nm)
Organoclays				
PB.TO-P	3.50	2.52	6.78	1.30
PB.BZLTP-P	4.96	1.78	9.38	0.94
PB.BZL-IM	6.16	1.43	18.50	0.48
PB.BTL-IM	6.60	1.34	13.28	0.67
PB.BTL-IM’	6.60	1.34	13.28	0.67
PB.DCL-IM	6.08	1.45	9.44	0.94
Polymer/Organoclay Binary Nanocomposites				
PET/PB.TO-P	3.74	2.36	7.59	1.16
PET/PB.BZLTP-P	4.50	1.96	9.24	0.96
PET/PB.BZL-IM	5.92	1.49	-	-
PET/PB.BTL-IM	6.20	1.43	-	-
PET/PB.BTL-IM’	6.20	1.43	-	-
PET/PB.DCL-IM	6.04	1.46	-	-
Polymer/Organoclay/Elastomer Ternary Nanocomposites				
PET/PB.TO-P/E-MA-GMA	3.92	2.25	-	-
PET/PB.BZLTP-P/E-MA-GMA	4.83	1.83	-	-
PET/PB.BZL-IM/E-MA-GMA	5.80	1.52	-	-
PET/PB.BTL-IM/E-MA-GMA	6.20	1.43	-	-
PET/PB.BTL-IM’/E-MA-GMA	6.20	1.43	-	-
PET/PB.DCL-IM/E-MA-GMA	6.02	1.47	-	-

Table 4.9 XRD results of PET compositions (basal spacing difference)

Organoclay	d_{001} Initial (nm)	d_{001} PET/OC (nm)	Δd (nm)	d_{001} PET/OC/E (nm)	Δd (nm)
PB.TO-P	2.52	2.36	-0.16	2.25	-0.27
PB.BZLTP-P	1.78	1.96	0.18	1.83	0.05
PB.BZL-IM	1.43	1.49	0.06	1.52	0.09
PB.BTL-IM	1.34	1.43	0.09	1.43	0.09
PB.BTL-IM’	1.34	1.43	0.09	1.43	0.09
PB.DCL-IM	1.45	1.46	0.01	1.47	0.02

OC: Organoclay, E: Elastomer (E-MA-GMA)

XRD patterns of PET/phosphonium organoclay/E-MA-GMA nanocomposites are given in Figures 4.17 - 4.18. XRD patterns for (PB.TO-P) and the PET binary and ternary nanocomposites with PB.TO-P and E-MA-GMA are presented in Figure 4.17. The XRD patterns of these nanocomposites revealed a slight decrease in the basal distance of these planes from 2.52 nm to 2.36 nm for the binary nanocomposite and 2.25 nm for the ternary nanocomposite. This shift from low-angle to higher angles after melting and cooling of organic-modified bentonite can be attributed to the reasons mentioned earlier for PA66/PB.TO-P/E-BA-MAH nanocomposite. PB.TO-P shows poor miscibility with PET, although the TEM images showed fair intercalation of the polymer into the organoclay layers. In fact, PB.TO-P organoclay was expected to exhibit good miscibility owing to the paraffin arrangement of the layers in the organoclays prior to compounding which is considered as the main factor for the polymer chains to penetrate easily between the clay layers.

XRD patterns for (PB.BZLTP-P) and the PET binary and ternary nanocomposites with PB.BZLTP-P and E-MA-GMA are presented in Figure 4.18. The XRD patterns of these nanocomposites revealed a slight increase in the basal distance of these planes from 1.78 nm to 1.96 nm for the binary nanocomposite and to 1.83 nm for the ternary nanocomposite with E-MA-GMA. The slight enhancement in the basal spacing of PB.BZLTP-P organoclay after compounding with PET does not reveal

delamination and TEM micrographs should give a better explanation of the structure of the composite.

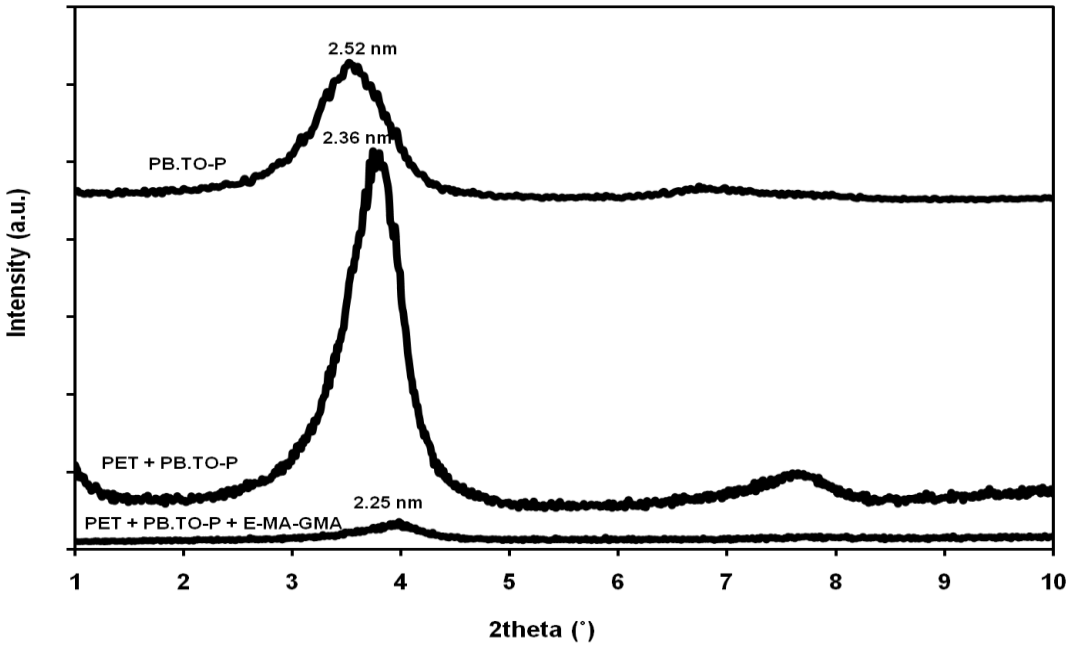

Figure 4.17 XRD patterns of PET/PB.TO-P/E-MA-GMA binary and ternary nanocomposites

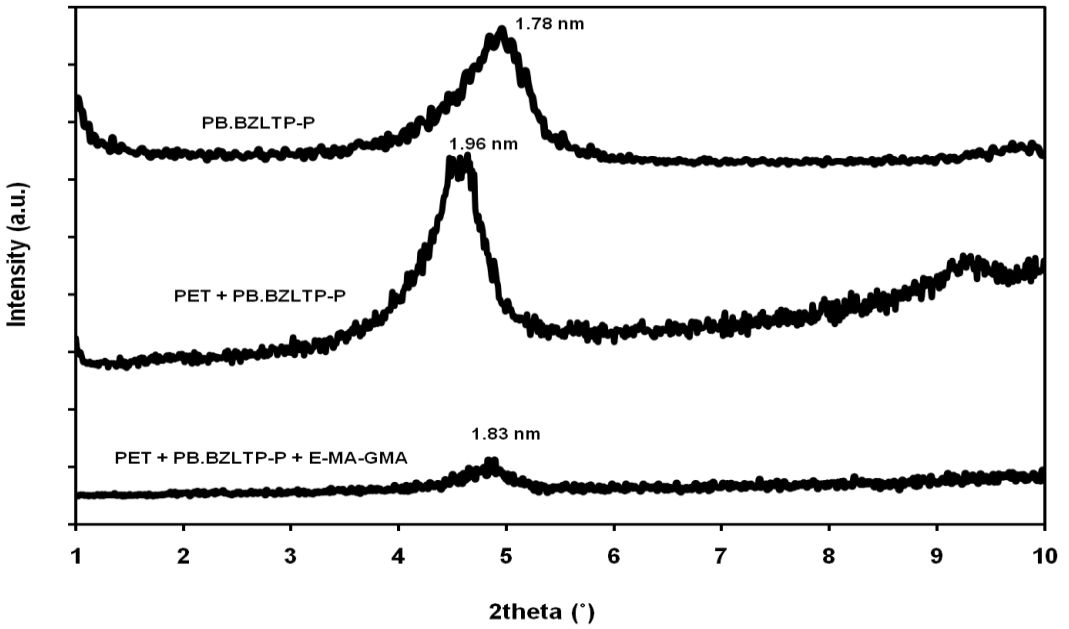

Figure 4.18 XRD patterns of PET/PB.BZLTP-P/E-MA-GMA binary and ternary nanocomposites

Two particular characteristics of layered silicates play an important role in the creation of nanocomposites: the first is the ability of silicate sheets to disperse into individual layers, and the second one is the possibility to modify their surface chemistry through ion exchange reactions with organic and inorganic cations. The simple mixing of polymer and layered silicates does not always result in the generation of a nanocomposite, as this usually leads to dispersion of stacked sheets. This failure is due to the weak interactions between the polymer and the inorganic component. If these interactions become stronger, then the inorganic phase can be dispersed in the organic matrix in nanometer scale (148). XRD patterns for PET/imidazolium organoclay/E-MA-GMA nanocomposites are given in Figures 4.19 - 4.21.

XRD patterns for (PB.BZL-IM) and the PET binary and ternary nanocomposites with PB.BZL-IM and E-MA-GMA are presented in Figure 4.19. The XRD patterns of these nanocomposites revealed a slight increase in the basal distance of these planes from 1.48 nm to 1.49 nm for the binary nanocomposite, 1.52 nm for the ternary nanocomposite and 1.53 nm for the ternary nanocomposite extruded three times.

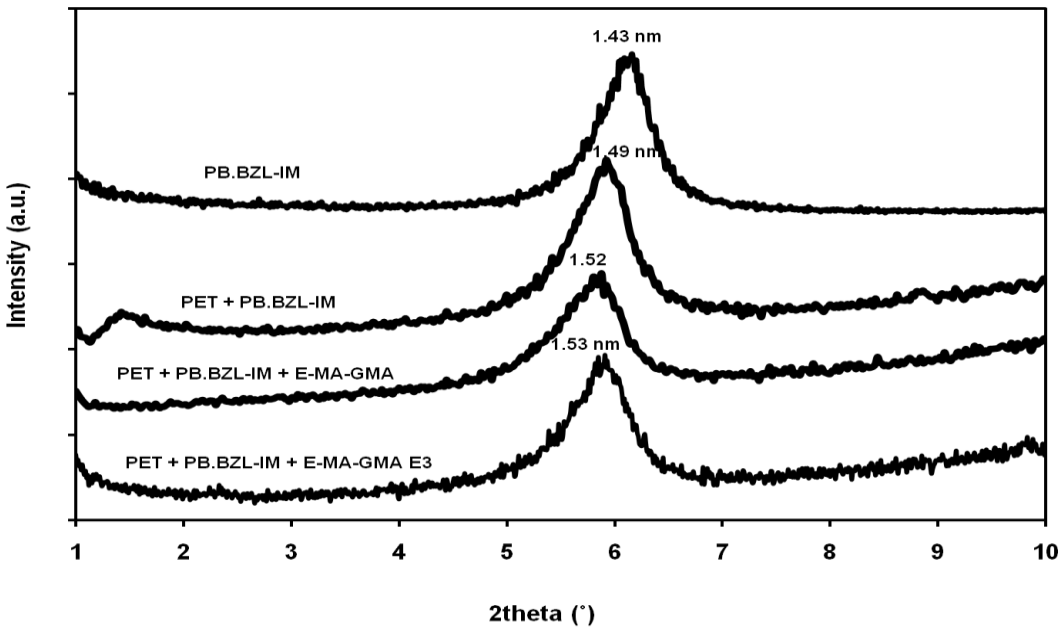

Figure 4.19 XRD patterns of PET/PB.BZL-IM/E-MA-GMA binary and ternary nanocomposites

XRD patterns for (PB.BTL-IM), (PB.BTL-IM'), and the PET binary and ternary nanocomposites with PB.BTL-IM, PB.BTL-IM' and E-MA-GMA are presented in Figure 4.20. PB.BTL-IM' exhibited the same patterns as PB.BTL-IM as expected. The XRD patterns of these nanocomposites revealed an increase in the basal distance of the planes from 1.34 nm to 1.43 nm for both the binary and ternary nanocomposites.

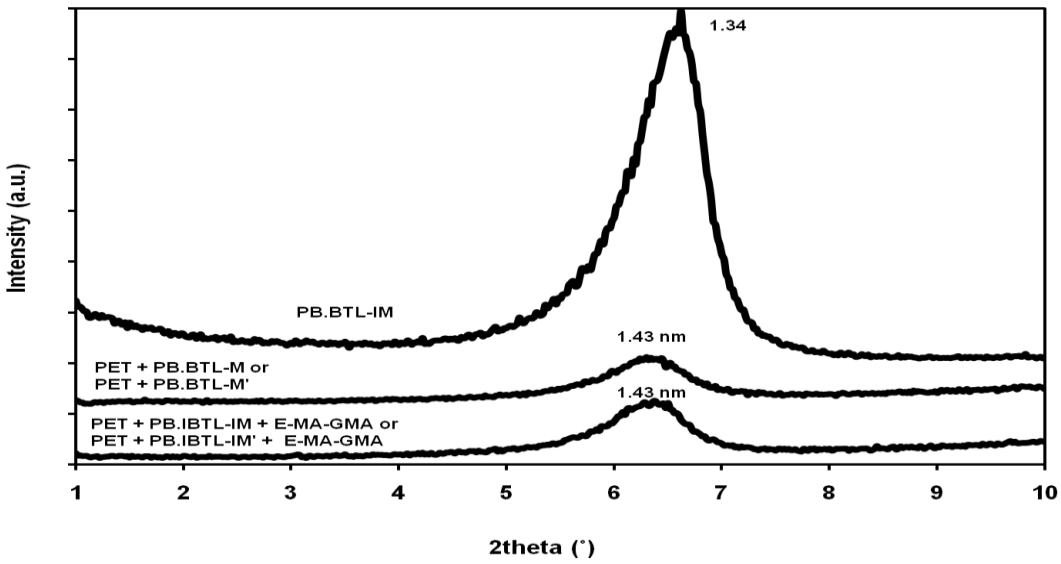

Figure 4.20 XRD patterns of PET/PB.BTL-IM & BTL-IM'/E-MA-GMA binary and ternary nanocomposites

XRD patterns for (PB.DCL-IM) and the PET binary and ternary nanocomposites with PB.DCL-IM and E-MA-GMA are presented in Figure 4.21. The XRD patterns of these nanocomposites revealed an increase in the basal distance of the planes from 1.44 nm to 1.46 nm for the binary nanocomposite and 1.47 nm for the ternary nanocomposite.

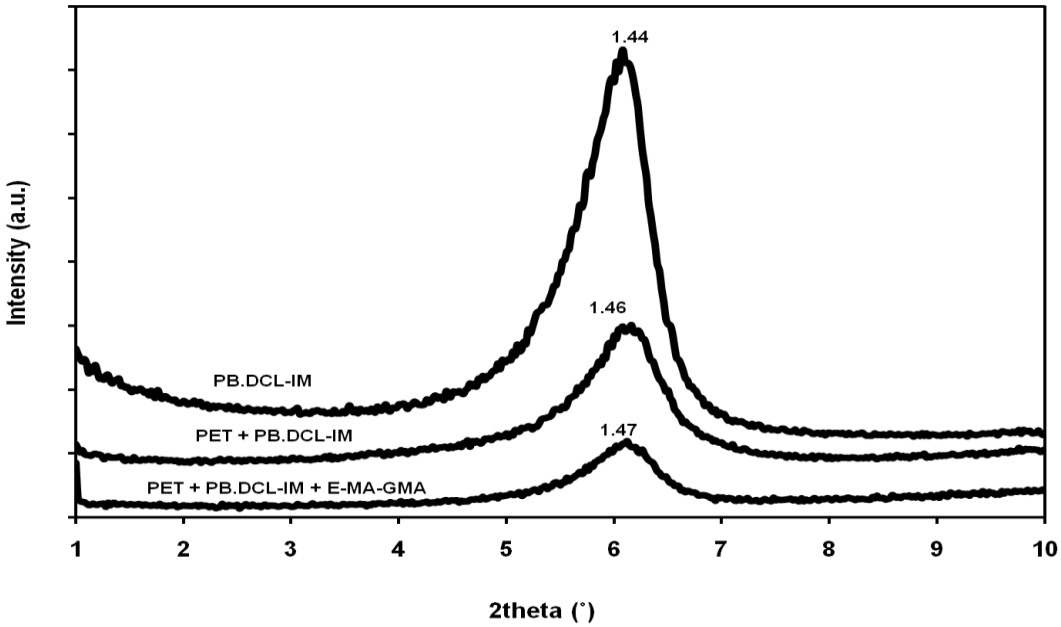

Figure 4.21 XRD patterns of PET/PB.DCL-IM/E-MA-GMA binary and ternary nanocomposites

The different structures of imidazolium organoclays did not exhibit significant difference upon compounding with PET in binary and ternary composites. The slight improvement in the basal spacing of the imidazolium organoclays after compounding with PET can be attributed mainly to the monolayer arrangement of the layers in the imidazolium organoclays prior to compounding which is counted as the main factor for the polymer chains to penetrate easily between the clay layers. The compatibility between the surfactant used for organoclays and the polymer matrix and the elastomer used can be also considered as the second reason. The d-spacings of PET/imidazolium organoclay nanocomposites increased slightly upon addition of the impact modifier. That can be ascribed to the presence of polar groups in the organoclay surfactant that can interact with the impact modifier.

Regarding the results, it can be concluded that organoclay delamination is affected by the structural and thermal properties of the organic modifier, number of extrusions and the interactions between clay layers, polymer matrix, impact modifier and organic modifier. Organic modifier polarity is highly effective in forming interactions with the polymer chains at the first step. However, packing density of

the organic modifier resulting from the interactions of the polar groups within its own structure and with the clay must allow passage of the polymer chains to interact with the clay surface for further separation of the clay layers, and the shear intensity has to be sufficient to yield higher dispersive forces for homogeneous dispersion of the organoclay.

4.2.2 Transmission Electron Microscopy

Transmission electron microscopy analysis is crucial in order to support and validate the X-ray diffraction analysis results which were performed to investigate the dispersion of silicate layer within the polymer matrix. TEM gives a clear distribution of the various phases through direct visualization at the internal nanometer scale. In the micrographs, the dark lines represent the thickness of individual clay layers or their agglomerates (tactoids), whereas the bright (gray/white) areas represent the polymer matrix. Several dark lines are observed indicating stacked silicate layers that are formed due to clustering and agglomeration.

4.2.2.1 TEM Results of PA66 Based Nanocomposites

Figures 4.22-4.24 display the TEM images of PA66/E-BA-MAH blend and PA66-phosphonium ternary nanocomposites (PA66/PB.TO-P/E-BA-MAH and PA66/PB.BZLTP-P/E-BA-MAH) at different magnifications. In Figure 4.22, the bright areas shown at both small and large magnifications stand for the polymer matrix, and the elastomeric phase is indicated by the darker area. The PA66/E-BA-MAH interphase is clear through the sharp line between both phases.

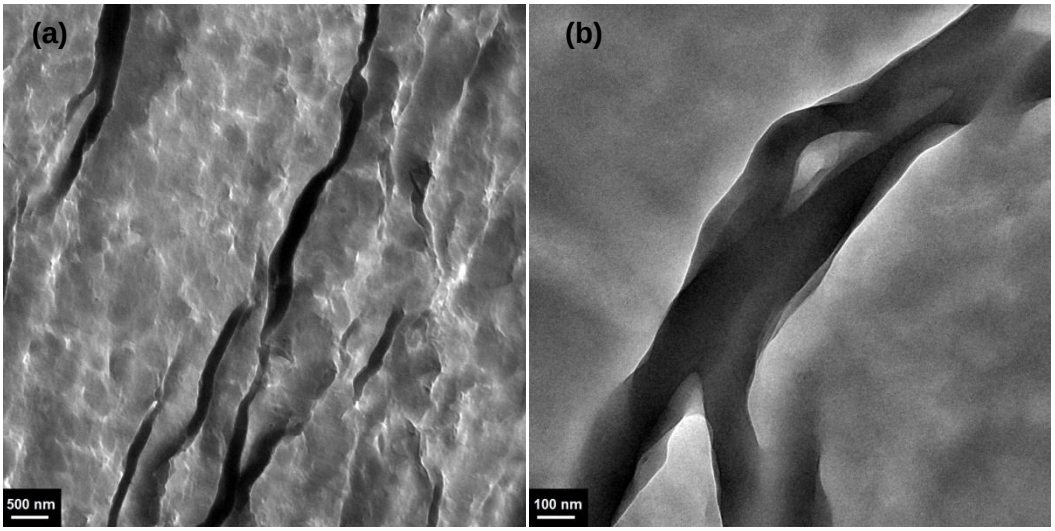

Figure 4.22 TEM micrograph of PA66/E-BA-MAH blend: (a) 500 nm, (b) 100 nm

In ternary nanocomposites, the visible black spots represent the clay agglomerates in TEM micrographs. The dark lines shown at high magnifications are the transverse sections of single or possibly multiple silicate platelets (104). For well dispersed structures, these spots appear as ribbons that indicate the delaminated layers of the filler. The gray areas show the polymer matrix, whereas, elastomeric phases are observed as dispersed white regions. The incorporation of the organoclays in polymer/elastomer/organoclay ternary nanocomposites is expected to reduce the interfacial tension between the polymer and elastomer. This reduction was clearly seen due to the organoclay addition which reduced the interfacial tension and led to an decreased elastomeric domain size (Figure 4.23 and 4.24). The organoclays particles are localized inside the elastomeric phase at the interphase between the PA66 and E-BA-MAH. Surprisingly, TEM micrographs show that PB.TO-P containing PA66 ternary nanocomposite exhibit better intercalation than PB.BZLTP-P containing PA66 ternary nanocomposite which contradicts with XRD results. It is also clear that PB.TO-P layers are intercalated and dispersed in the elastomeric phase, whereas PB.BZLTP-P exhibited more agglomerates rather than dispersed structure, but it was still intercalated. This can be attributed to the compatibility of the organoclay with PA66 matrix and the elastomer, in addition to the initial basal spacing of the organoclay PB.BZLTP-P (1.78 nm) which was smaller than the initial d-spacing of PB.TO-P (2.52 nm).

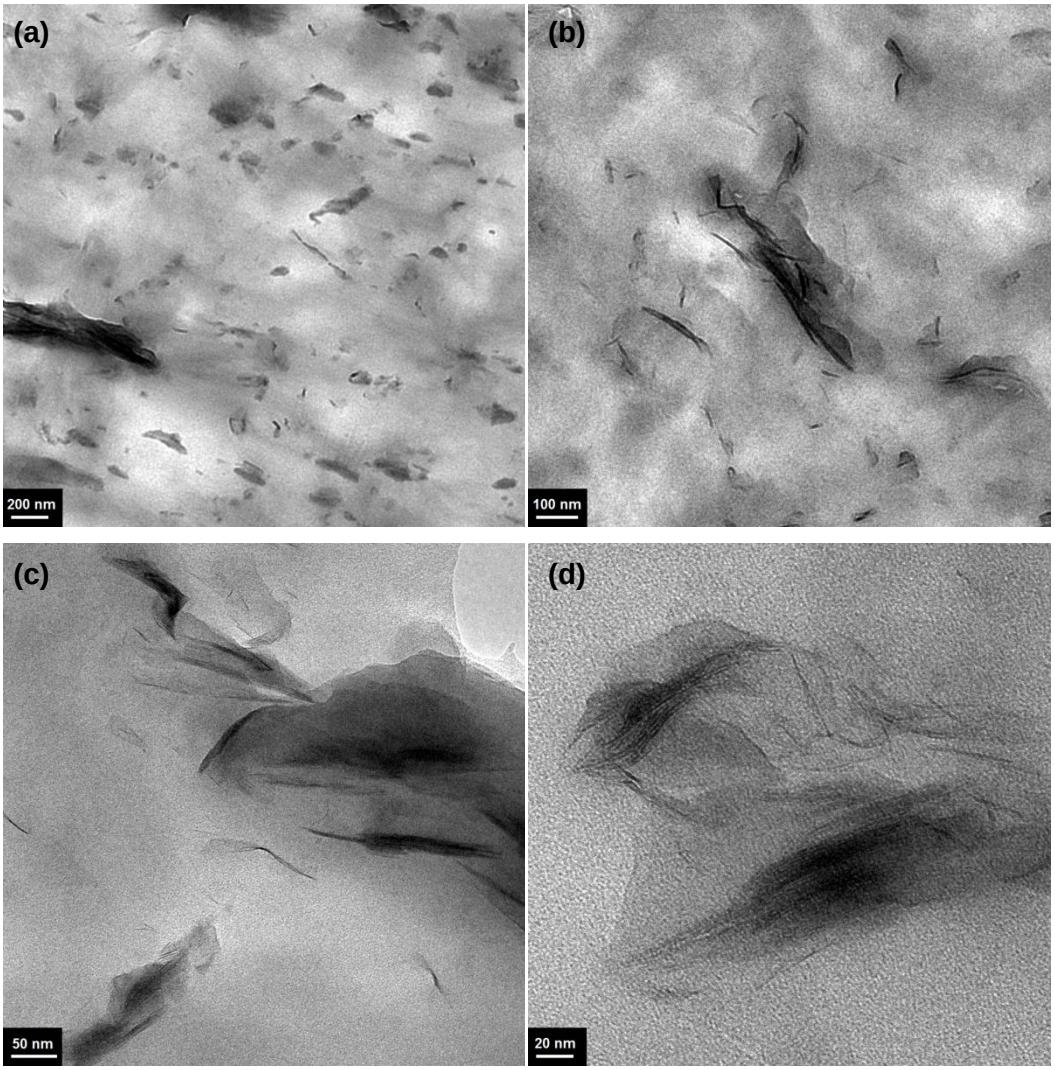

Figure 4.23 TEM micrographs of PA66/PB.TO-P/E-BA-MAH ternary nanocomposite (a) 200 nm, (b) 100 nm, (c) 50 nm, (d) 20 nm

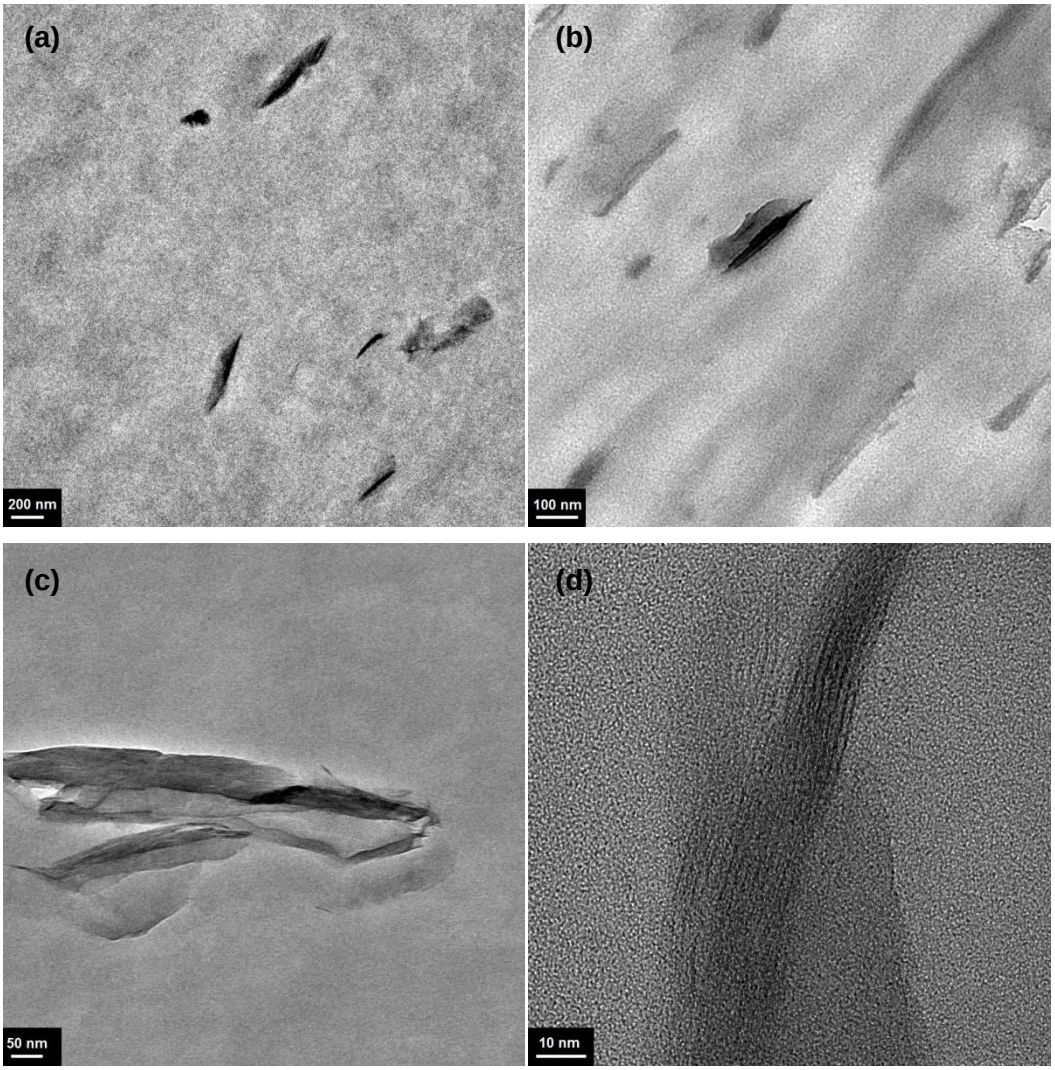

Figure 4.24 TEM micrographs of PA66/PB.BZLTP-P/E-BA-MAH nanocomposite (a) 200 nm, (b) 100 nm, (c) 50 nm, (d) 10 nm

4.2.2.2 TEM Results of PET Based Nanocomposites

Figures 4.25 and 4.26 show the TEM images of PET/PB.TO-P/E-MA-GMA and PET/PB.BZLTP-P/E-MA-GMA ternary nanocomposites, respectively at different magnifications. PB.TO-P organoclay incorporation in PET/E-MA-GMA/PB.TO-P ternary nanocomposites reduced the interfacial tension between the polymer and elastomer and led to an decrease in the elastomeric domain size. The intercalation of PB.TO-P layers is clear through their dispersion in the E-MA-GMA elastomeric phase, whereas PB.BZLTP-P exhibited weak dispersion and presented more

agglomerated structure, although it was still intercalated. Both organoclays exhibited similar behaviors with both polymers PA66 and PET. In addition, their behavior in the final composite is mainly attributed to the initial basal spacing of the organoclay although the presence of aromatic groups in PB.BZLTP-P organoclay was expected to exhibit good compatibility with PET containing aromatic groups.

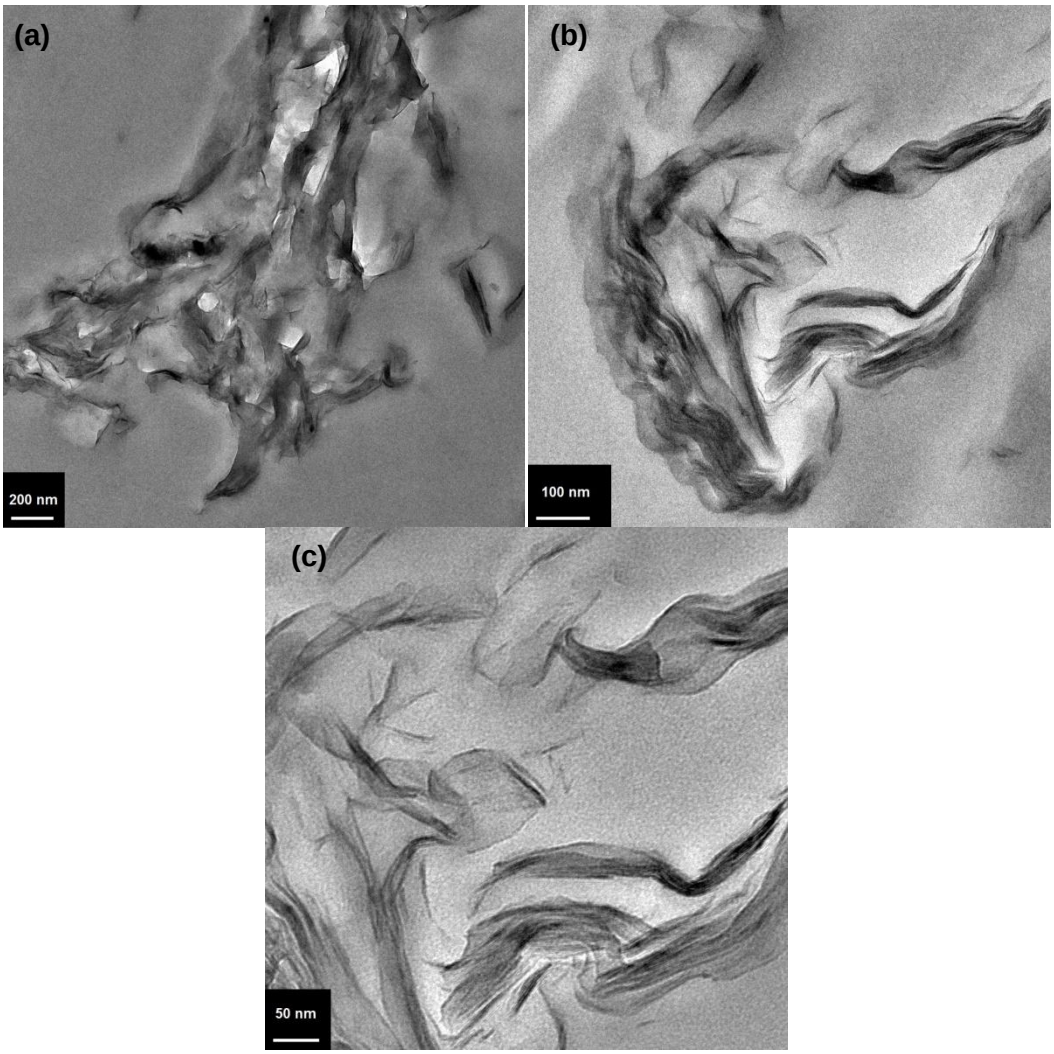

Figure 4.25 TEM micrographs of PET/PB.TO-P/E-MA-GMA Ternary nanocomposite (a) 200 nm, (b) 100 nm, (c) 50 nm

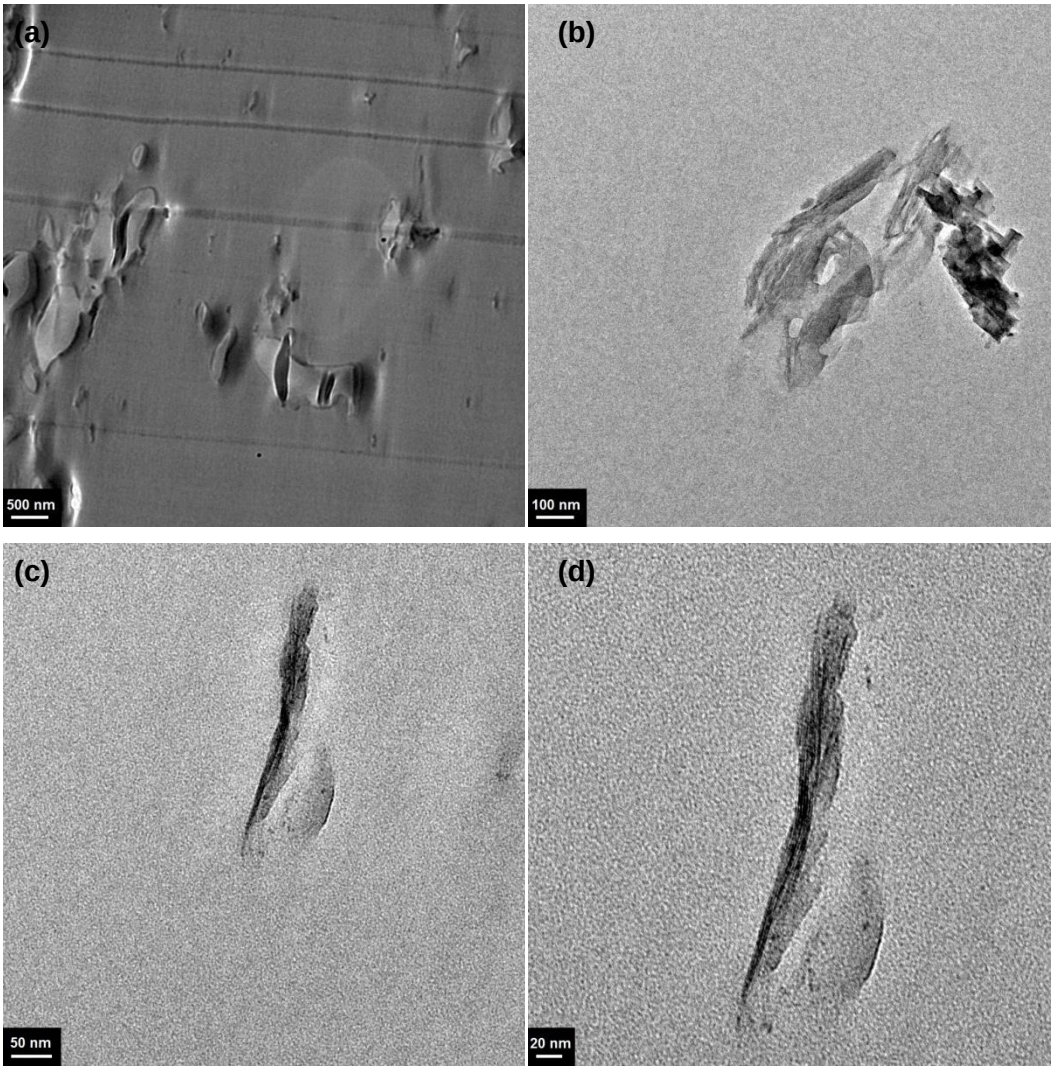

Figure 4.26 TEM micrographs of PET/PB.BZLTP-P/E-MA-GMA ternary nanocomposite (a) 500 nm, (b) 100 nm, (c) 50 nm, (d) 20 nm

In all of the imidazolium nanocomposites, primary particles of organoclay in the polymer matrix with closely stacked clay layers are observed. This indicates that the clay layers are not exfoliated, but simply intercalated by polymer chains. PET/PB.BZL-IM binary and PET/PB.BZL-IM/E-MA-GMA ternary nanocomposites are shown in Figures 4.27 and 4.28, respectively. In addition, the presence of the elastomer E-MA-GMA in the ternary nanocomposites provided better intercalation between the polymer and the organoclay.

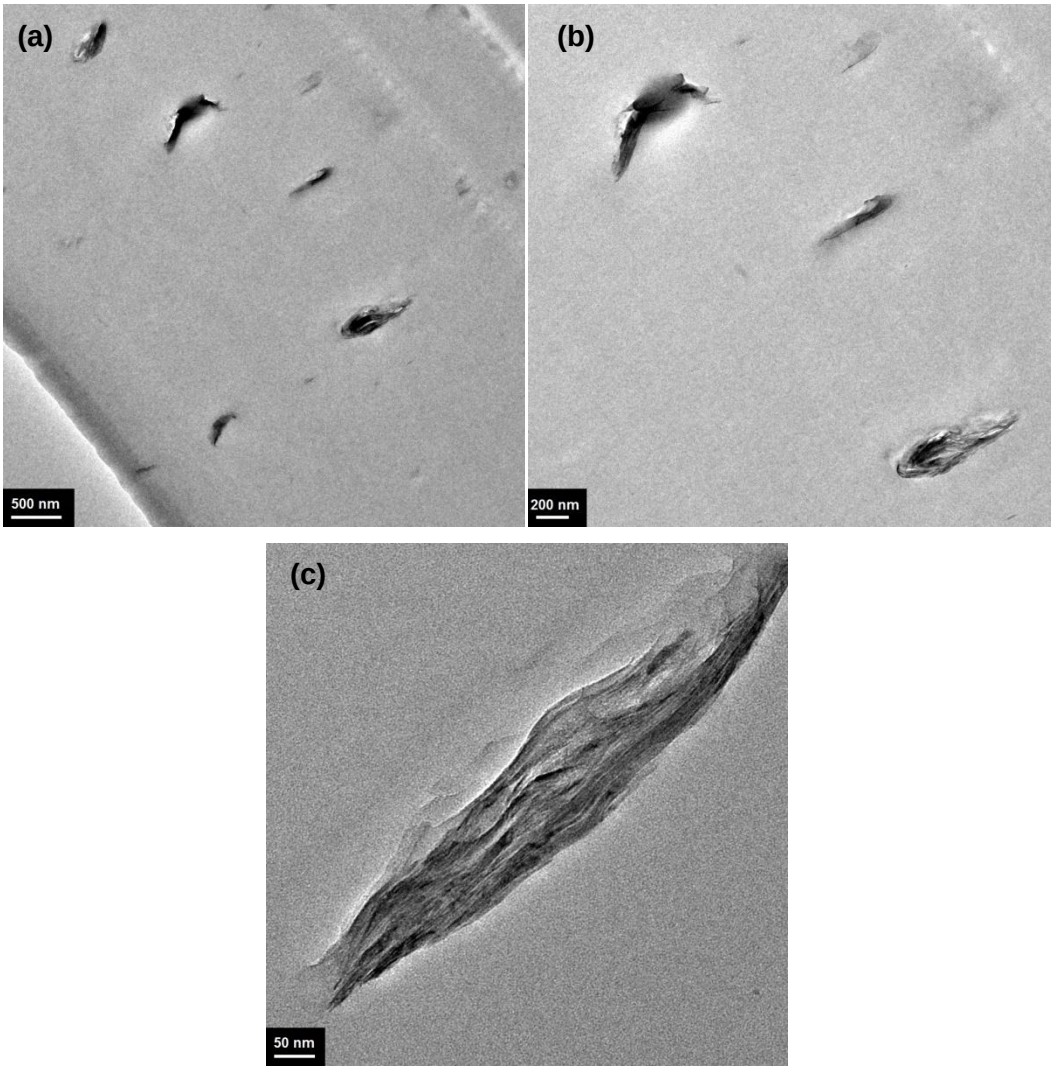

Figure 4.27 TEM micrographs of PET/PB.BZL-IM binary nanocomposite (a) 500 nm, (b) 200 nm, (c) 50 nm

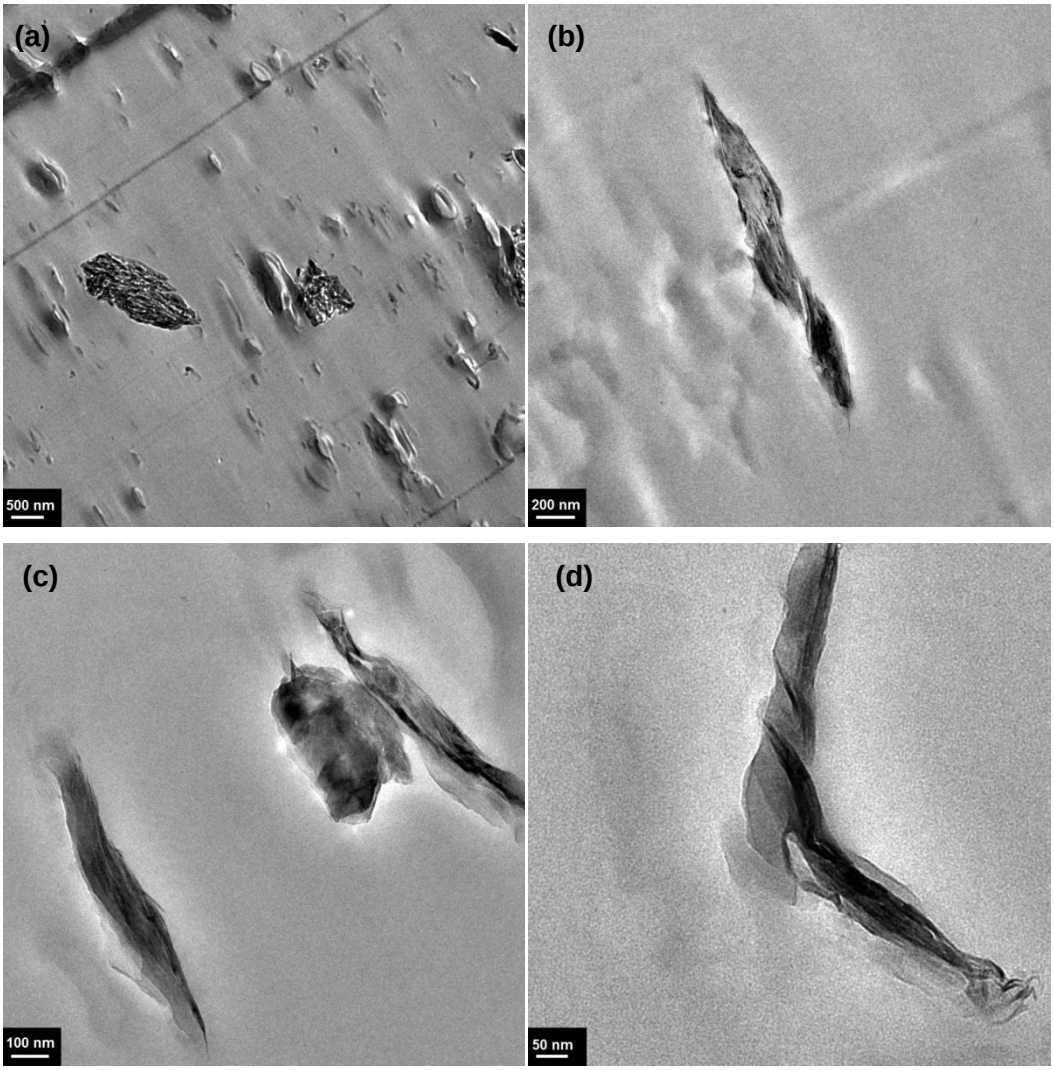

Figure 4.28 TEM micrographs of PET/PB.BZL-IM/E-MA-GMA ternary nanocomposite (a) 500 nm, (b) 200 nm, (c) 100 nm, (d) 50 nm

TEM micrographs of PET/PB.BTL-IM/E-MA-GMA and PET/PB.DCL-IM/E-MA-GMA ternary nanocomposites are shown in Figures 4.29 and 4.30, respectively. Tactoids can be clearly seen in composites with PB.BTL-IM organoclay, whereas PB.DCL-IM with longer chain length presented slightly better intercalation. This observation is also approved by XRD results which showed higher degree of intercalation for PB.DCL-IM organoclay.

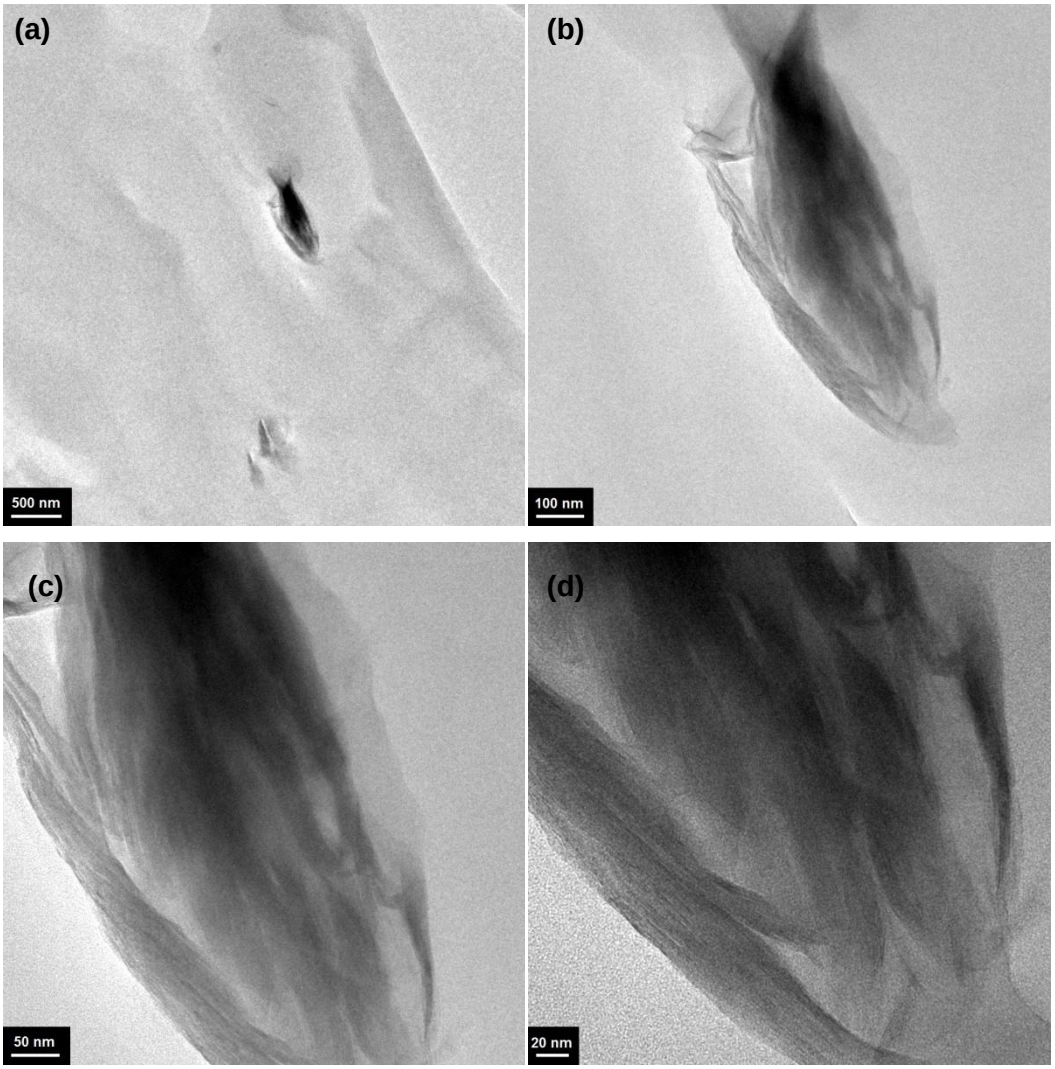

Figure 4.29 TEM micrographs of PET/PB.BTL-IM/E-MA-GMA ternary nanocomposite (a) 500 nm, (b) 100 nm, (c) 50 nm, (d) 20 nm

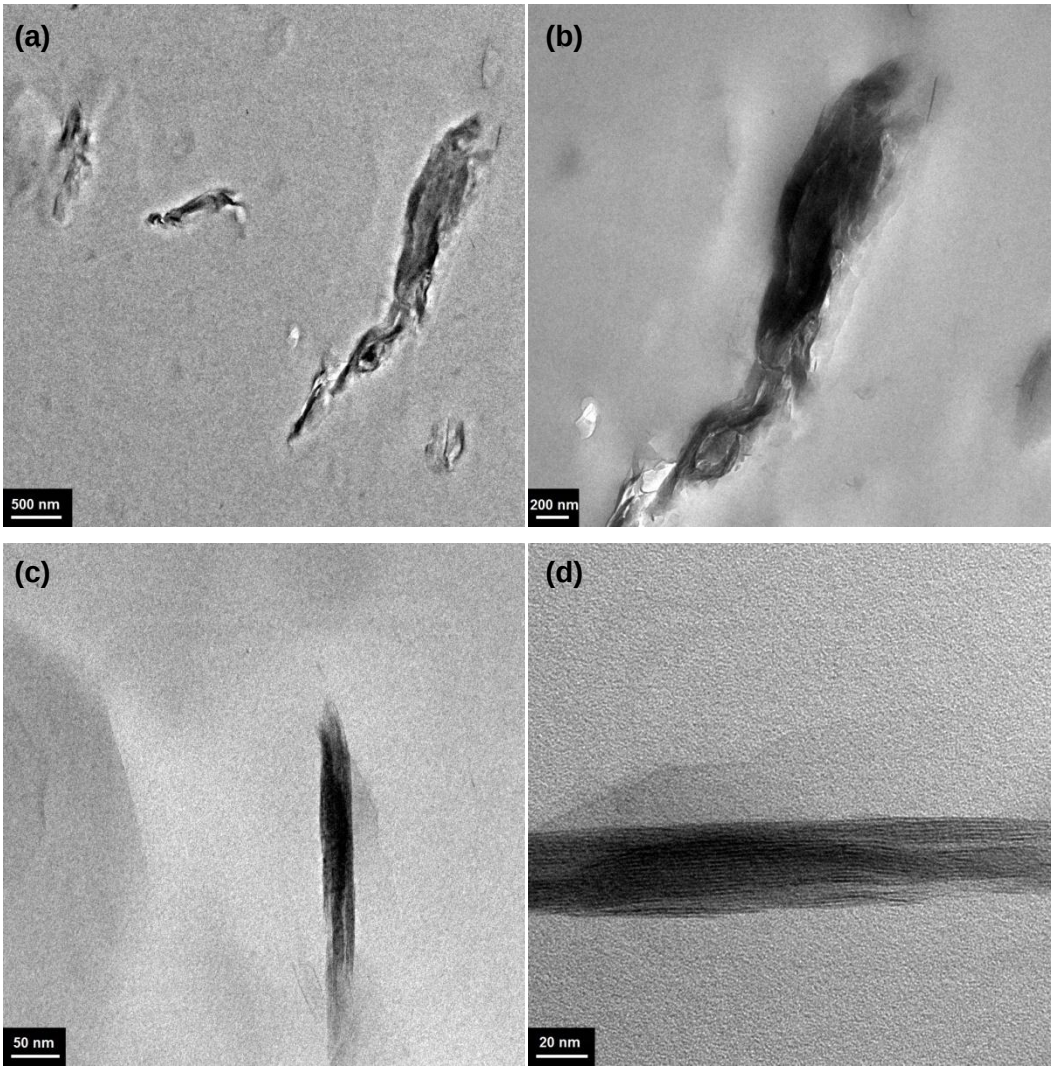

Figure 4.30 TEM micrographs of PET/PB.DCL-IM/E-MA-GMA ternary nanocomposite (a) 500 nm, (b) 200 nm, (c) 50 nm, (d) 20 nm

4.2.3 Scanning Electron Microscopy

SEM analyses were conducted to examine the morphology of polymer blends, and binary and ternary polymer nanocomposites at x250 and x4000 magnifications. The cavities in the SEM micrographs correspond to the elastomeric domains, which were selectively removed by etching with xylene for 6 hours before SEM observations, in order to gain a better understanding of their dispersion. The number of analyzed domains had to be kept at small values (50-100) to get an accurate dimension by Image J program. Average domain size (average diameter) was calculated by using Equations 4.1 and 4.2 where A_i and n_i represents the area and the number of domains that has an area of A_i respectively.

$$\overline{A} = \frac{\sum n_i . A_i}{\sum n_i} \quad (4.1)$$

$$\overline{d} = \sqrt{\frac{\overline{A} \times 4}{\pi}} \quad (4.2)$$

4.2.3.1 SEM Results of PA66 Nanocomposites

The average domain sizes calculated for PA66 samples are given in Table 4.10.

Table 4.10 Average domain sizes and impact strengths of PA66 samples

Composition	d_{av} (nm)	Impact Strength (kJ/m^2)
Polymer/Elastomer Blend		
PA66/E-BA-MAH	182.0	10.4
Polymer//Organoclay//Elastomer Ternary Nanocomposites		
PA66/PB.TO-P/E-BA-MAH (1-S)	174.9	10.2
PA66/PB.TO-P/E-BA-MAH (1-P)	171.2	8.2
PA66/PB.TO-P/E-BA-MAH (2-P)	167.4	9.4
PA66/PB.TO-P/E-BA-MAH (2-S)	163.6	10.5
PA66/PB.TO-P/E-BA-MAH	177.3	9.0
PA66/PB.BZLTP-P/E-BA-MAH	188.9	7.8

The SEM micrographs of the PA66 specimen and PA66/E-BA-MAH blend are given in Figures 4.31 and 4.32, respectively. Since PA66 is a tough material, tortuous lines can be seen for the pure samples taken at x250 magnification. Extensive ductile shearing is evident on the fracture surface of the unfilled PA66 system, indicating the well-known shear mechanisms of PA66. In the crack propagation direction, the bulk polymer is drawn and broken under tension.

The addition of E-BA-MAH compatibilizer to the unfilled PA66 system increased the tortuousity, shortened the crack propagation lines and resulted in porous structure due to the effect of cavitation (Figure 4.32). The addition of E-BA-MAH is known to form a graft copolymer during the blending process by the imidation reactions. This graft copolymer either forms at or migrates to the interface between the polymer and elastomer, lowering the interfacial energy and improving the interfacial adhesion. In this way, it contributes to the stability of the dispersed phase against segregation during further processing. Reaction reduces interfacial tension and retards particle coalescence (149). In addition, the compatibilizer used functions as an impact modifier which compensate for the decrease in toughness caused by the incorporation of the organoclay into the polymer matrix in nanocomposites. This effect is clearly seen in section 4.4.2 in which the toughness of PA66 increased from 7.0 kJ/m^2 to 10.4 kJ/m^2 upon blending with only 5 wt % of E-BA-MAH.

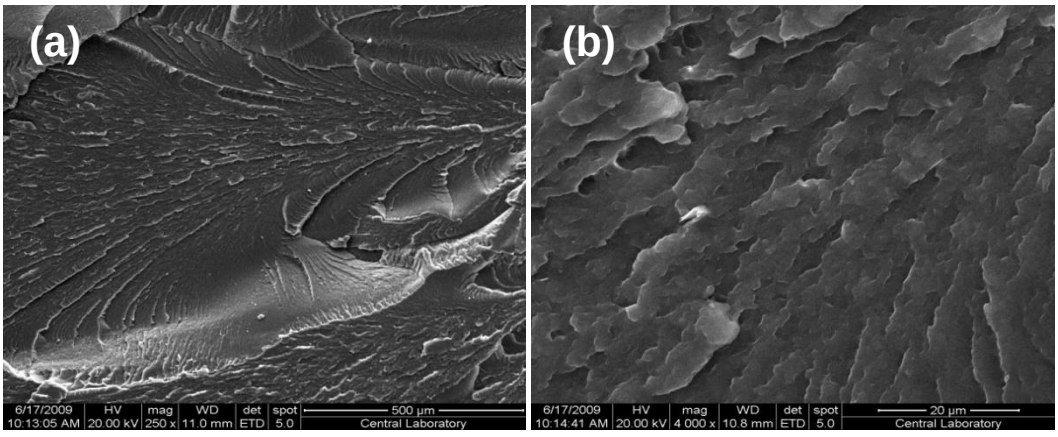

Figure 4.31 SEM micrographs of PA66 with (a) (x250) (b) (x4000) magnifications

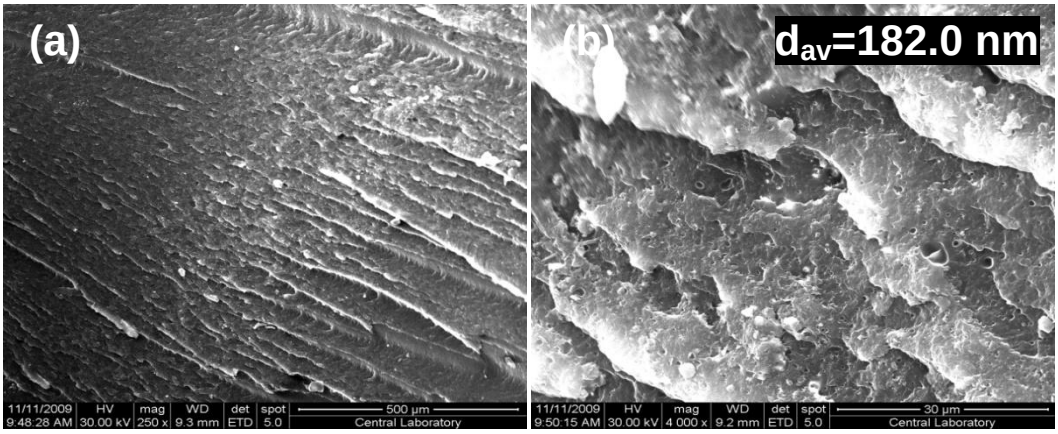

Figure 4.32 SEM micrographs of etched PA66/E-BA-MAH blend: (a) (x250), (b) (x4000)

The selection of a good balance between the viscosity and melt elasticity ratios of the components at the processing conditions and a certain level of grafting of the dispersed phase reduces the interfacial tension, increases the adhesion between the phases, and results in a finer dispersion and a more stable morphology. In addition, some requirements to achieve toughness include the following: an appropriate range of elastomer domain size and interparticle distance, uniform distribution of the elastomeric domains, low modulus ratio between the elastomer and the polyamide bulk phase, and high Poisson's ratios with low breaking stress of the dispersed phase. On the other hand, the main shortcoming of the elastomer-toughened blends is the significant reduction of their Young's modulus, which is caused mainly by the addition of an elastomeric phase with a low Young's modulus. The dispersion of minority phase (elastomer) during melt blending involves the stretching of drop-like particles until fibers are formed; then, the rupture of these filaments to form smaller drops and the coalescence of these drops to create larger ones follow. The balance of these processes determine the final particle size that is controlled by the viscosity and melt elasticity of the components, shear stresses and rates, the mobility of the interface, and the surface tension, since a lower tension promotes the stretching of even smaller drops producing a very fine morphology. This lower tension, in turn, is the result of the chemical reactions forming the interfacial copolymers and because of their presence the coalescence rate decreases, since they immobilize the interface thus reducing the final domain size (150).

The interaction between the polymer matrix, the organoclay and the elastomeric phase is expected to increase in the presence of MAH functional groups on the impact modifiers. The absence of adhesion between the phases can stop the stress transfer at the interface, and the material fails when reaching a strain value that only eliminates the physical union achieved during blending. In well dispersed blends, the stress transfer happens through the interface formed by the compatibilizing agent, which should ensure enough bonding to stop crack propagation.

PA66/organoclay binary and PA66/organoclay/E-BA-MAH ternary nanocomposites are shown in Figures 4.33-4.40. Although clay agglomeration can be observed in some of the nanocomposites which cause mechanical failure, the mechanical properties of the nanocomposites exhibited significant improvement. The toughness of the materials is dependent on the average domain size and interdomain distance (distance between two domains). Large elastomeric domains decrease toughness due to the effect of cavitation. The presence of ultrafine domains of the elastomers can also reduce toughness because of the reduced deformability caused by crosslinking or lower adhesion that arises from the absence of compatibilization (151). The presence of elastomeric domains of moderate size in the polymer matrix is considered as an advantage since ultrafine and large domains are not really effective in hindering the crack propagation and increasing the toughness in nanocomposites.

Clay platelets may act as barriers to prevent coalescence of dispersed phase and thus cause reduction in domain sizes because of their high aspect ratio (54). In addition, the elastomeric phase is known to increase the viscosity and the shear stress of the blend when incorporated into the polymer matrix. Thus, extra shear is needed in order to obtain good dispersion for blends and composites containing elastomeric materials. In the present work, the screw speed was fixed at a specified value and the elastomer content was same for all compositions. On the other hand, extrusion twice promoted the break of the elastomeric domains and resulted in reduction of domain sizes. This can be clearly seen in 1 wt % PB.TO-P ternary nanocomposites (Figures 4.35-4.38). In the 1 wt % PA66/PB.TO-P/E-BA-MAH (1-S) and (1-P) ternary nanocomposites, extrusion once decreased the domain sizes

from 182.0 nm to 174.9 nm and 171.2 nm, respectively owing to the incorporation of the organoclay. Increasing number of extrusions to two times in 1 wt % PA66/PB.TO-P/E-BA-MAH (2-P) and (2-S) decreased the domain sizes even more to 167.4 nm and 163.6 nm, respectively. Injection molding procedure (simultaneous or pelletized) had no significant effect on the domain sizes for all 1 wt % compositions. The incorporation of more clay in the 2 wt % PA66/PB.TO-P/E-BA-MAH ternary nanocomposite decreased the domain size to 177.3 nm.

The dispersion of the elastomeric domains in the polymer matrix is known to be improved using organoclays, which when well dispersed in the polymer matrix, suppress the agglomeration of the elastomeric domains. The E-BA-MAH domains in the PB.TO-P ternary nanocomposites in the present work (177.3 nm) were found to be smaller compared to the blend (182.0 nm). However, PB.BZLTP-P ternary nanocomposite (188.9 nm) showed the opposite effect. The reduction in the dispersed domain sizes might be attributed to the changes in melt flow index properties and barrier effect of clay, which prevent coalescence of the dispersed phase. The increase in domain size in PA66/PB.BZLTP-P/E-BA-MAH ternary nanocomposite can be attributed to the residence of incompatible organoclay particles, no matter whether it is well dispersed or not, at the interphase between the PA66 and E-BA-MAH. This is clearly seen in TEM analysis given earlier in section 4.2.2.1 (Figures 4.23 and 4.24).

To sum up, SEM micrographs taken at x250 magnification show that cracks propagate along tortuous paths for all composites explains the enhanced toughness results. According to the impact test results of PA66 compositions given in section 4.4.2.1, the highest toughness is obtained in PA66/PB.TO-P/E-BA-MAH (1-S) and (2-S) nanocomposites and the lowest in PA66/PB.BZLTP-P/E-BA-MAH nanocomposite. Table 4.10 shows that the domain sizes have to be at an optimum level and distance from each other to prevent crack propagation and increase the energy absorption during crack formation. The domain sizes of PA66/PB.TO-P/E-BA-MAH (1-S) and (2-S) nanocomposites are smaller than the domain sizes of PA66/PB.BZLTP-P/E-BA-MAH nanocomposite. The presence of MAH functional groups immobilized the interface and prevented the coalescence of elastomeric domains both in the nanocomposites and the blends by forming chemical bonds

with difunctional PA 66 matrix. MAH group is capable of reacting with the amine ends. PB.TO-P exhibited better compatibility with PA66 while PB.BZLTP-P exhibited lower toughness and mechanical properties.

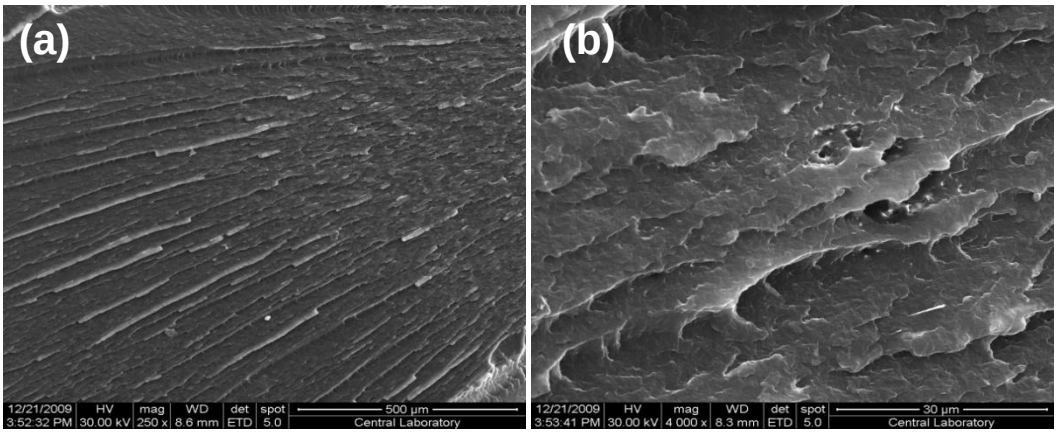

Figure 4.33 SEM micrographs of PA66/PB.TO-P binary nanocomposite: (a) (x250), (b) (x4000)

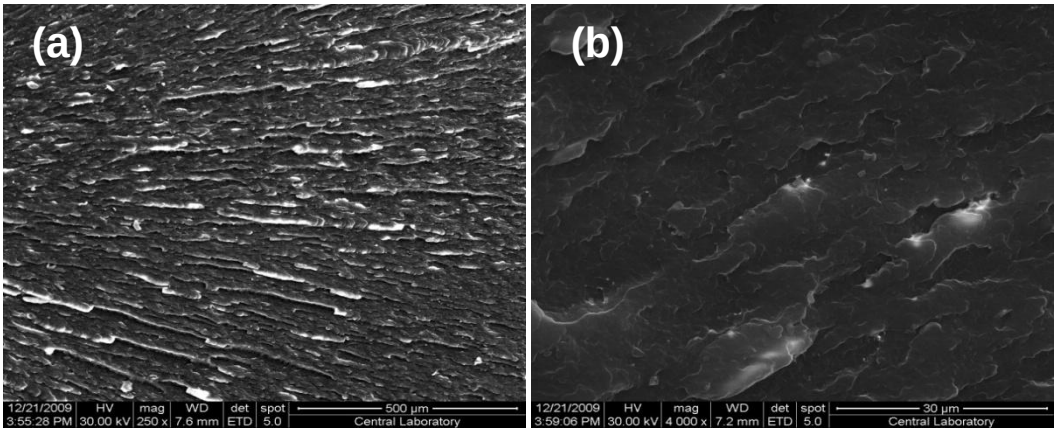

Figure 4.34 SEM micrographs of PA66/PB.BZLTP-P binary nanocomposite: (a) (x250), (b) (x4000)

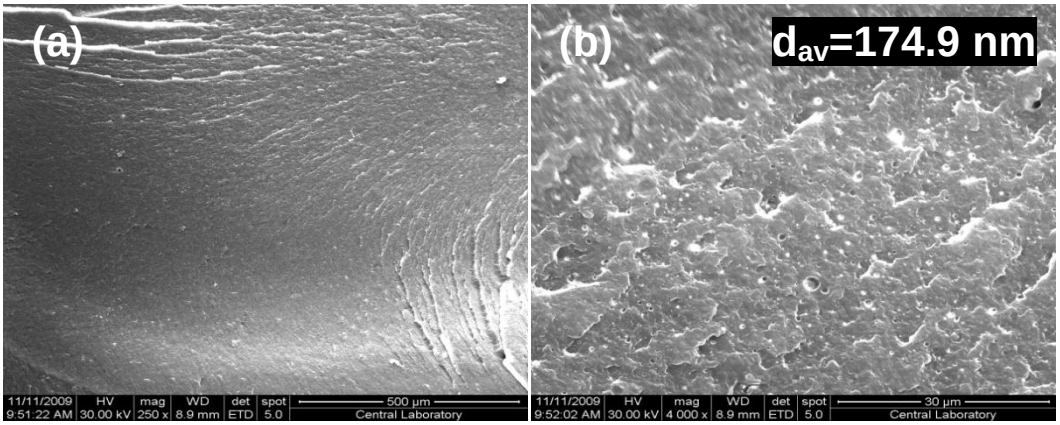

Figure 4.35 SEM micrographs of etched PA66/PB.TO-P/E-BA-MAH (1-S) ternary nanocomposite: (a) (x250), (b) (x4000)

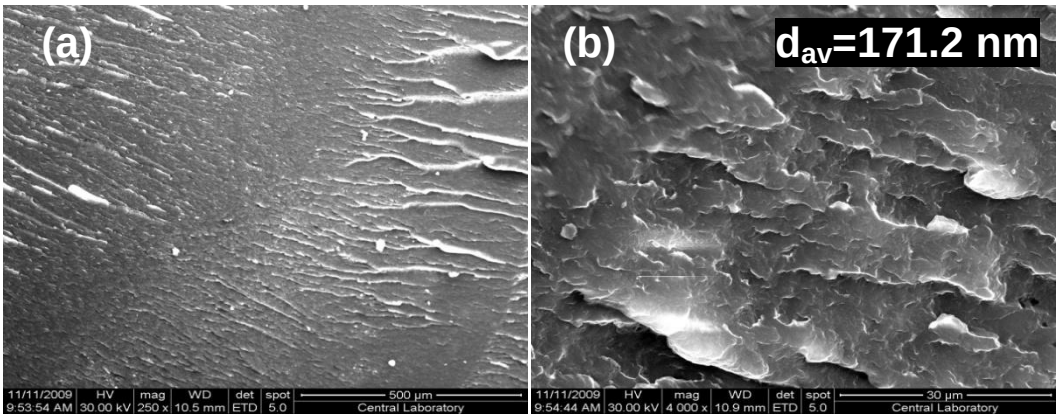

Figure 4.36 SEM micrographs of etched PA66/PB.TO-P/E-BA-MAH (1-P) ternary nanocomposite: (a) (x250), (b) (x4000)

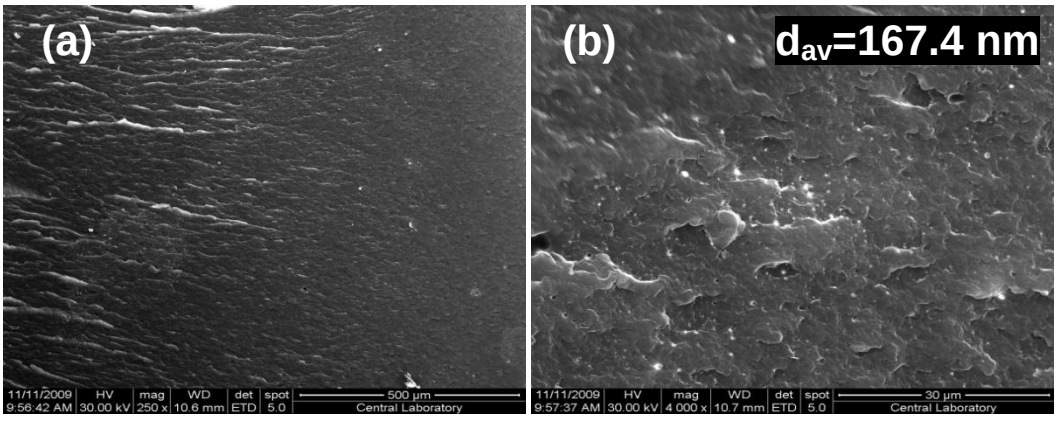

Figure 4.37 SEM micrographs of etched PA66/PB.TO-P/E-BA-MAH (2-P) ternary nanocomposite: (a) (x250), (b) (x4000)

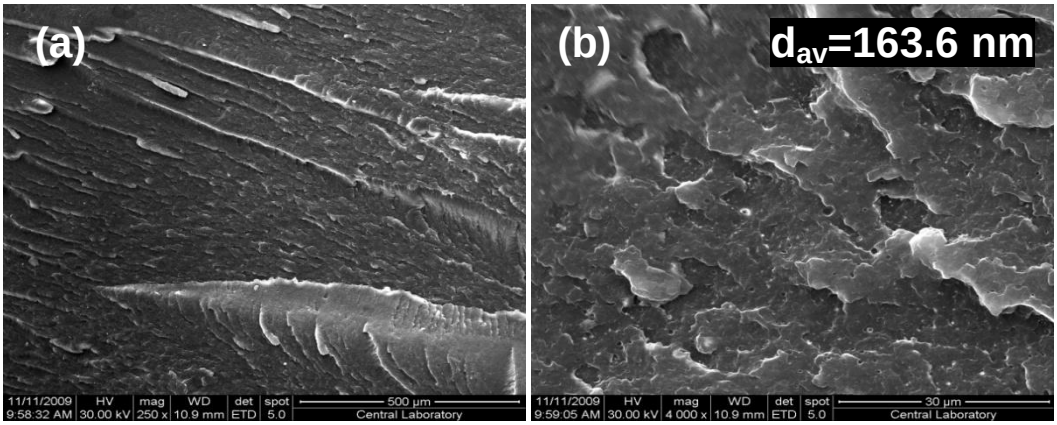

Figure 4.38 SEM micrographs of etched PA66/PB.TO-P/E-BA-MAH (2-S) ternary nanocomposite: (a) (x250), (b) (x4000)

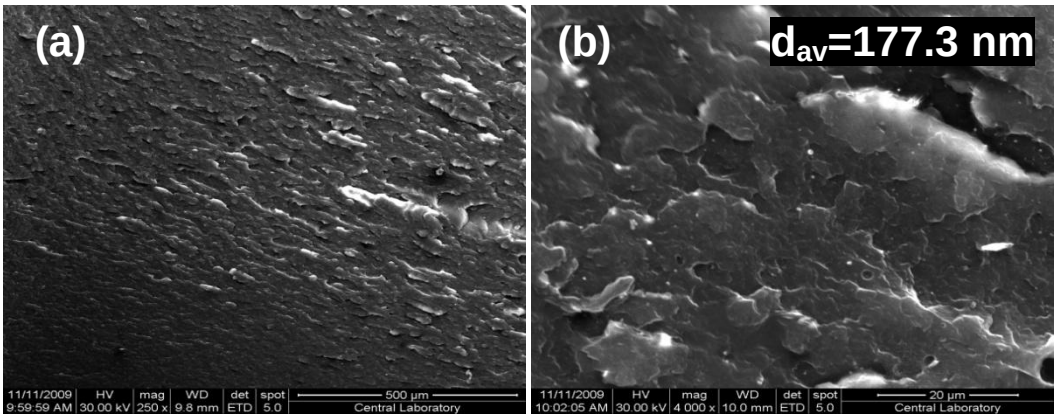

Figure 4.39 SEM micrographs of etched PA66/PB.TO-P/E-BA-MAH ternary nanocomposite: (a) (x250), (b) (x4000)

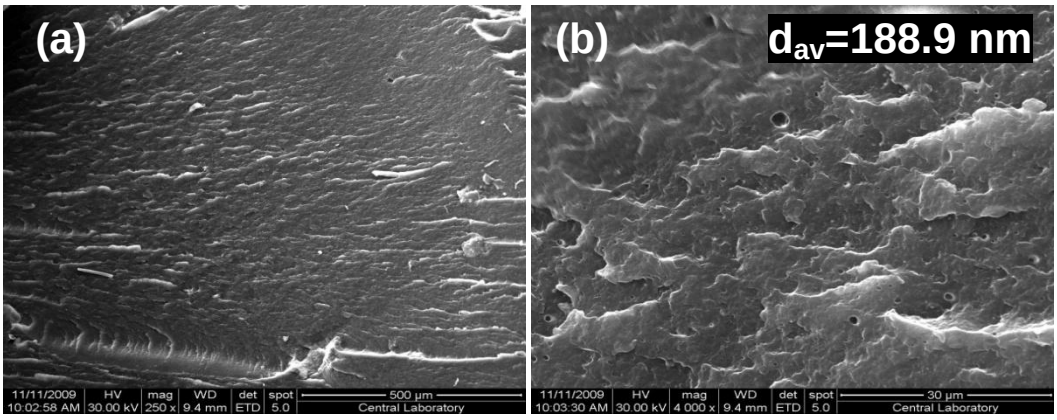

Figure 4.40 SEM micrographs of etched PA66/PB.BZLTP-P/E-BA-MAH ternary nanocomposite: (a) (x250), (b) (x4000)

4.2.3.2 SEM Results of PET Nanocomposites

The SEM micrographs of the PET, PET/E-MA-GMA blend and PET binary and ternary nanocomposites are given in Figures 4.41 - 4.55. The average domain size calculated for PET samples are given in Table 4.11.

Table 4.11 Average domain sizes and impact strengths of PET samples

Composition	d_{av} (nm)	Impact Strength (kJ/m^2)
Polymer/Elastomer Blend		
PET/E-MA-GMA	205.0	4.8
Polymer/Organoclay/Elastomer Ternary Nanocomposites		
PET/PB.TO-P/E-MA-GMA	192.2	4.7
PET/PB.BZLTP-P/E-MA-GMA	211.2	3.2
PET/PB.BZL-IM/E-MA-GMA	217.1	3.9
PET/PB.BZL-IM/E-MA-GMA (E3)	151.4	3.0
PET/PB.BTL-IM/E-MA-GMA	266.9	5.1
PET/PB.BTL-IM'/E-MA-GMA	270.7	4.8
PET/PB.DCL-IM/E-MA-GMA	287.9	6.0

From the SEM micrographs of the PET and PET/E-MA-GMA blend given respectively in Figures 4.41 and 4.42 at magnifications of x250 and x4000, the straight crack lines and smooth structure of PET indicates the brittle structure of PET with low impact strength. It is obvious that featureless structure of pure PET disappears and tortuous propagation lines appear when PET is melt blended with E-MA-GMA, and this can be clearly noticed in the significant increase in the impact strength from 2.9 kJ/m^2 for PET up to 4.8 kJ/m^2 for the blend. This improvement in the toughness of PET/E-MA-GMA blend is attributed to an optimum adhesion between PET and E-MA-GMA resulting from the intermolecular reactions between the two polymers. If the adhesion is high between the polymer and the elastomer, the cavitation mechanism is lowered and the impact strength could be low. E-MA-GMA is a functionalized polymer used as a compatibilizer in which the epoxy functionality of GMA reacts with the carboxyl and hydroxyl end groups of PET in the

melt phase to form a graft copolymer (55). E-MA-GMA reduces the effective area bearing the tensile load and created cavitation which is a major mechanism of the stress relief.

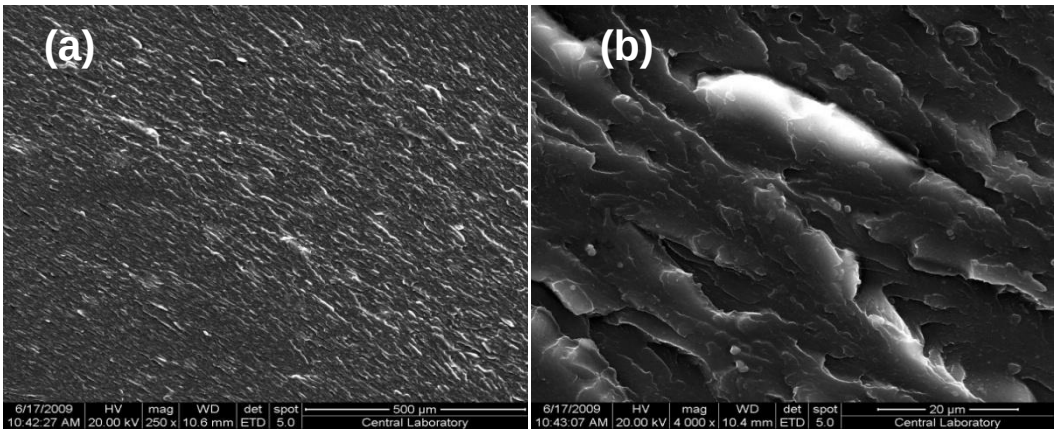

Figure 4.41 SEM micrographs of PET with (a) x250 (b) x4000 magnifications

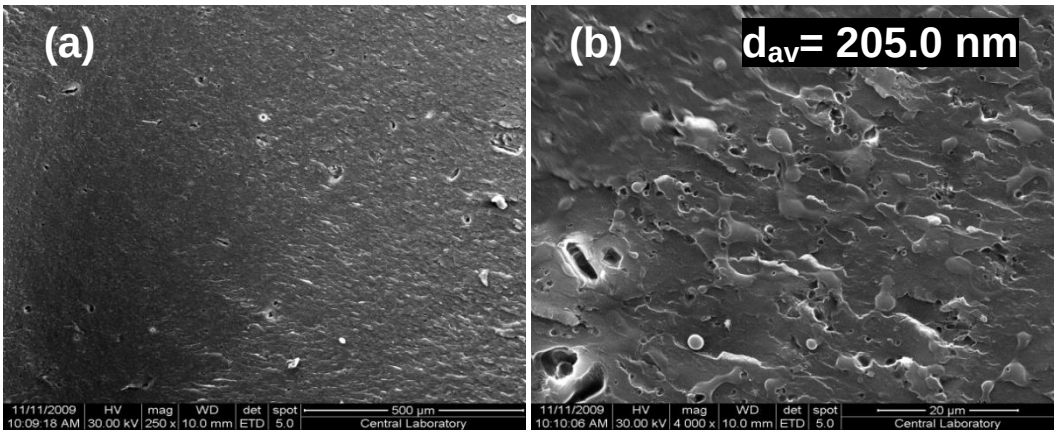

Figure 4.42 SEM micrographs of etched PET/E-MA-GMA blend: (a) (x250), (b) (x4000)

PET/phosphonium organoclay binary nanocomposites exhibited better interfacial interactions in Figures 4.43 – 4.44, while organoclay agglomerates can be clearly seen in all the imidazolium binary nanocomposites in Figures 4.45 – 4.48 especially for PET/PB.BZL-IM binary nanocomposite.

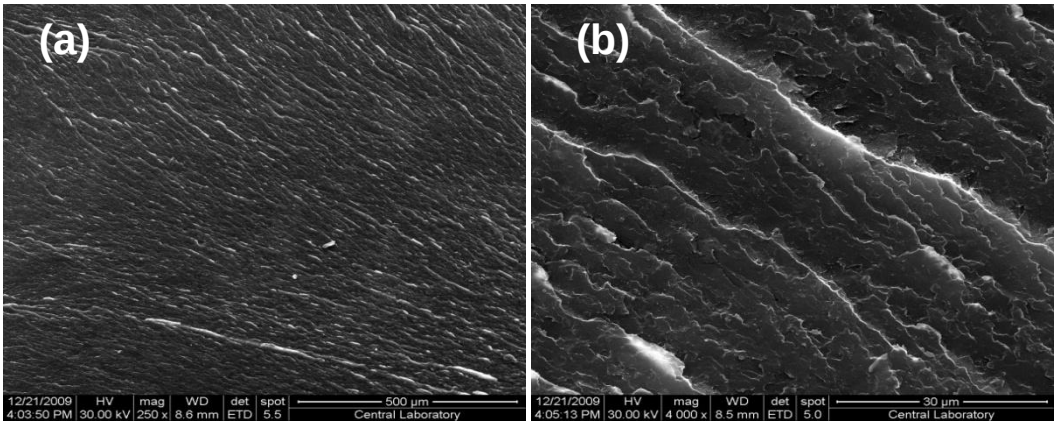

Figure 4.43 SEM micrographs of PET/PB.TO-P binary nanocomposite: (a) (x250), (b) (x4000)

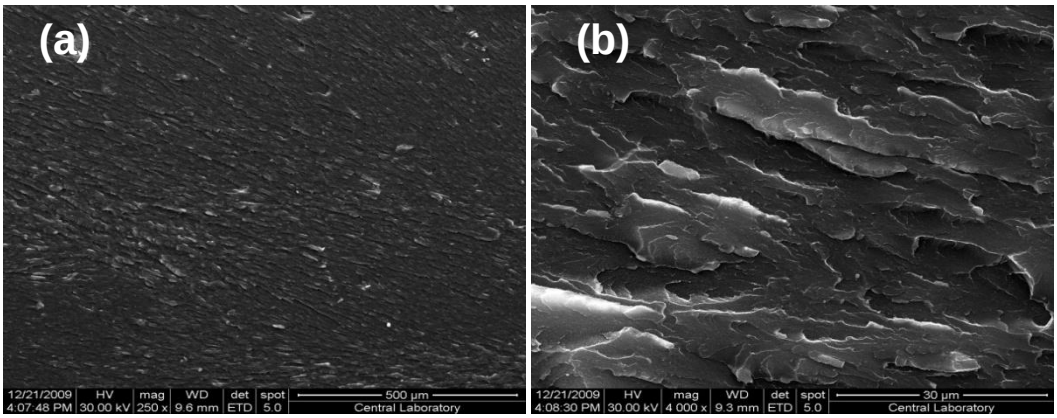

Figure 4.44 SEM micrographs of PET/PB.BZLTP-P binary nanocomposite: (a) (x250), (b) (x4000)

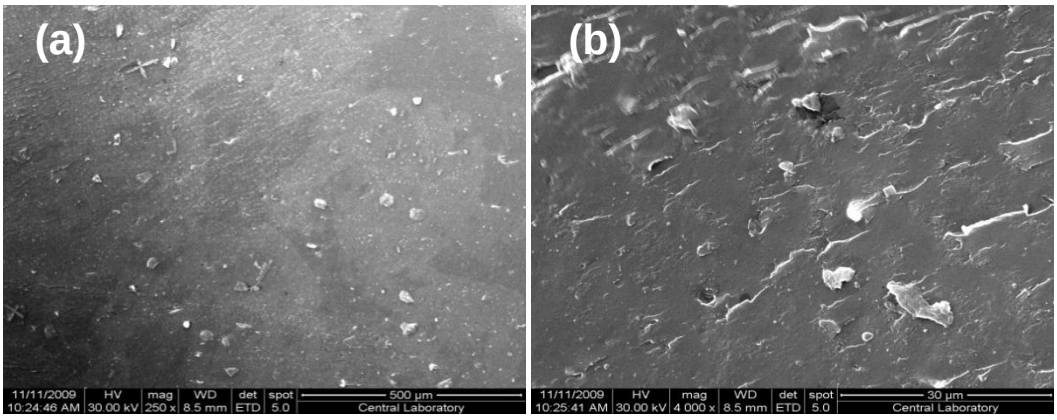

Figure 4.45 SEM micrographs of PET/PB.BZL-IM binary nanocomposite: (a) (x250), (b) (x4000)

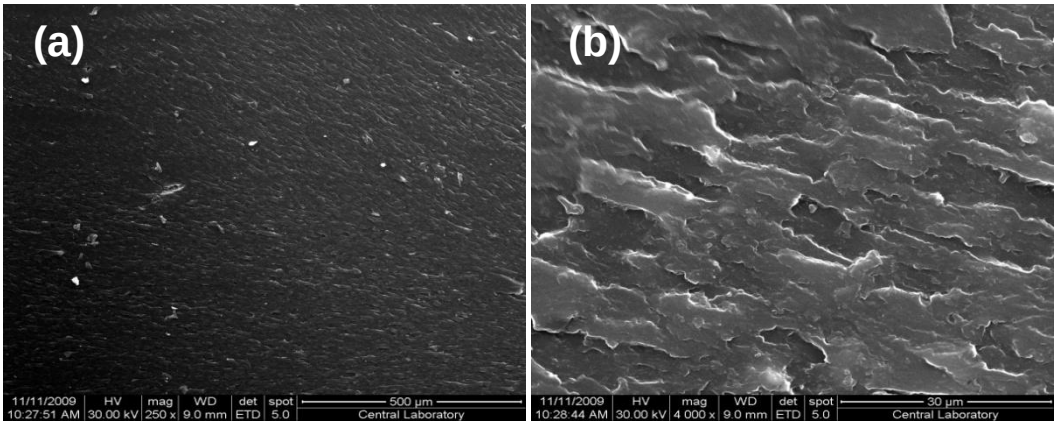

Figure 4.46 SEM micrographs of PET/PB.BTL-IM binary nanocomposite: (a) (x250), (b) (x4000)

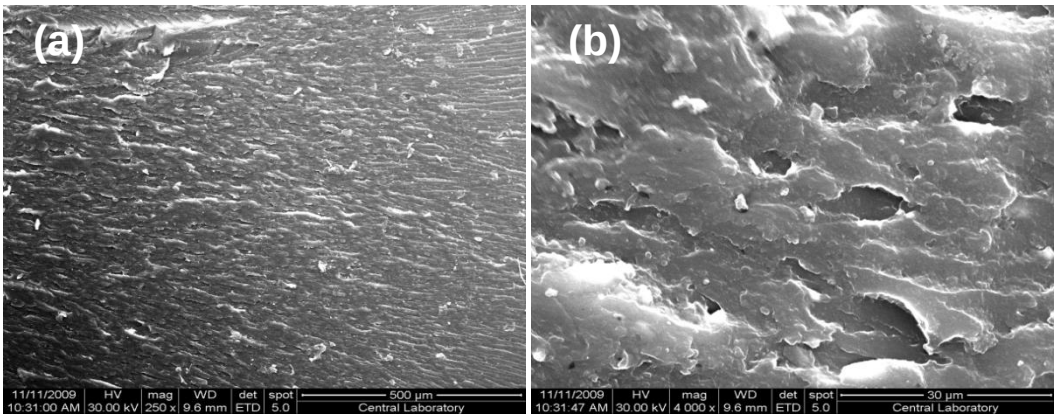

Figure 4.47 SEM micrographs of PET/PB.BTL-IM' binary nanocomposite: (a) (x250), (b) (x4000)

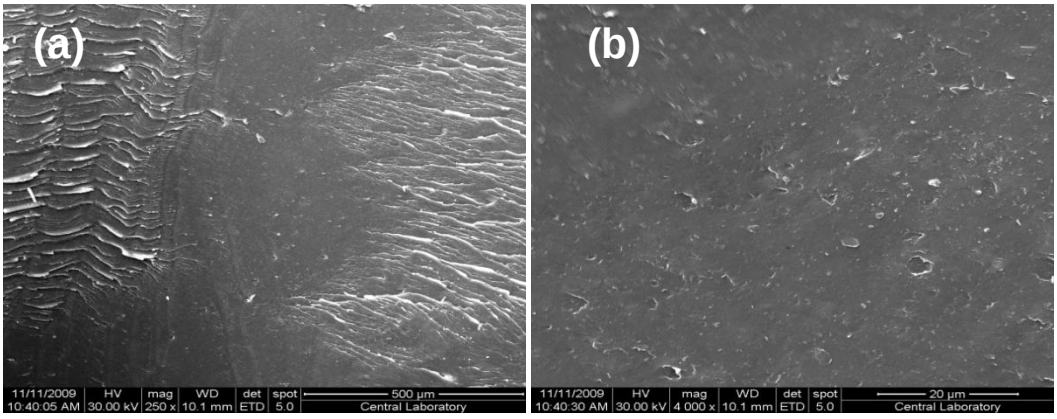

Figure 4.48 SEM micrographs of PET/PB.DCL-IM binary nanocomposite: (a) (x250), (b) (x4000)

The SEM micrographs of the PET/organoclay/E-MA-GMA ternary nanocomposites are shown in Figures 4.49 - 4.55. When cavitation and extensive deformation of the matrix occurs, the blend becomes tougher (57). SEM micrographs taken at x250 magnification show that cracks propagate along more tortuous paths in all nanocomposites compared to pure PET explaining the improvement in toughness results. An optimum value of the domain sizes is required in order to obtain best toughness improvement. Thus, the size of the domain should not be too small or too big. When there is high adhesion owing to great compatibilization, ultra-fine domains of elastomers are formed and cause low impact strength values, because crack propagation lines progress without touching the elastomer domains. Larger elastomeric domains also influence the toughness negatively since they form large regions that could not stop the crack propagation.

When compared to average domain size of the PET/E-MA-GMA binary blend, which has an average diameter of 205.0 nm, the ternary nanocomposites show an increase in their average domain sizes of all ternary nanocomposites except for PET/PB.TO-P/E-MA-GMA (192.2 nm) and PET/PB.BZL-IM/E-MA-GMA (E3) (151.4 nm). The incorporation of PB.TO-P in PET/PB.TO-P/E-MA-GMA ternary nanocomposite decreased the domain size from 205.0 nm for the PET/E-MA-GMA blend to 192.2 nm owing to the to the changes in melt flow index properties and the barrier effect of the good dispersed PB.TO-P organoclay, which prevent coalescence of the elastomeric domains. TEM analysis given in Figure 4.25 confirms the good dispersion of PB.TO-P in the ternary nanocomposite. The lowest decrease in domain sizes in PET/PB.BZL-IM/E-MA-GMA (E3) (151.4 nm) which exhibited also the lowest toughness (3.0 kJ/m^2) can be attributed to the incompatibility of benzyl groups of PB.BZLTP-P with the polymer matrix. TEM results exhibited better dispersion after extrusion three times of PB.BZL-IM containing ternary nanocomposite compared to extrusion twice. In fact, the presence of benzyl groups in both PB.BZLTP-P and PB.BZL-IM organoclays resulted in the lowest toughness in the binary and ternary nanocomposites. The toughness decreased in PET/PB.BZLTP-P/E-MA-GMA (3.4 kJ/m^2) and PET/PB.BZL-IM/E-MA-GMA (3.9 kJ/m^2) compared to PET/E-MA-GMA blend (4.8 kJ/m^2). The domain sizes in these two compositions increase slightly even though

they exhibit low dispersion since the silicate layers reside only at the interphase between PET and the elastomer.

The domain size and toughness of the E-MA-GMA elastomer is the highest in PET/PB.DCL-IM/E-MA-GMA (287.9 nm, 6.0 kJ/m^2) which is probably the optimum. The ternary nanocomposite of PB.BZL-IM has domain size and toughness (217.1nm, 3.9 kJ/m^2) which is significantly lower than that of PB.DCL-IM (287.9 nm, 6.0 kJ/m^2). This domain size is probably below the optimum size for enhancement of toughness. The domain sizes and toughness of the elastomer were lower in PET/PB.BTL-IM/E-MA-GMA (266.9 nm, 5.1 kJ/m^2) and PET/PB.BTL-IM'/E-MA-GMA (270.7 nm, 548 kJ/m^2) with shorter alkyl chain length compared to PET/PB.DCL-IM/E-MA-GMA with longer alkyl chain length. In this case, the silicate layers are dispersed at the interphase between PET and E-MA-GMA, and also inside the elastomeric domains. TEM micrographs of PET/PB.BTL-IM/E-MA-GMA and PET/PB.DCL-IM/E-MA-GMA ternary nanocomposites are shown earlier in Figures 4.29 and 4.30, respectively. Tactoids can be clearly seen in composites with PB.BTL-IM organoclay, whereas PB.DCL-IM with longer chain length exhibited slightly better dispersion. Thus, the present SEM results are in good agreement with TEM analysis.

The presence of GMA functional groups immobilized the interface and prevented the coalescence of elastomeric domains both in the nanocomposites and the blends by forming chemical bonds with PET matrix. In addition, for different types of phosphonium and imidazolium organoclays, a significant difference in the size of the domains can be observed for the samples. When the impact strengths of these nanocomposites and blend are considered, it can be seen that the SEM observations are consistent with impact tests. According to the impact test results of PET compositions extruded twice, the highest toughness is obtained for PET/PB.DCL-IM/E-MA-GMA nanocomposite containing longest alkyl chain and the lowest is obtained for PET/PB.BZLTP-P/E-MA-GMA nanocomposite containing benzyl groups.

To sum up, PET ternary nanocomposites with longer alkyl chains exhibited highest domain sizes and toughness. On the other hand, benzyl containing phosphonium

and imidazolium PET ternary nanocomposites exhibited the lowest toughness of all PET compositions. Phosphonium organoclay containing PET ternary nanocomposites exhibited different behavior than imidazolium containing PET ternary nanocomposites regarding domain sizes. The E-MA-GMA domain size decreased in phosphonium organoclay while it increased in imidazolium organoclay.

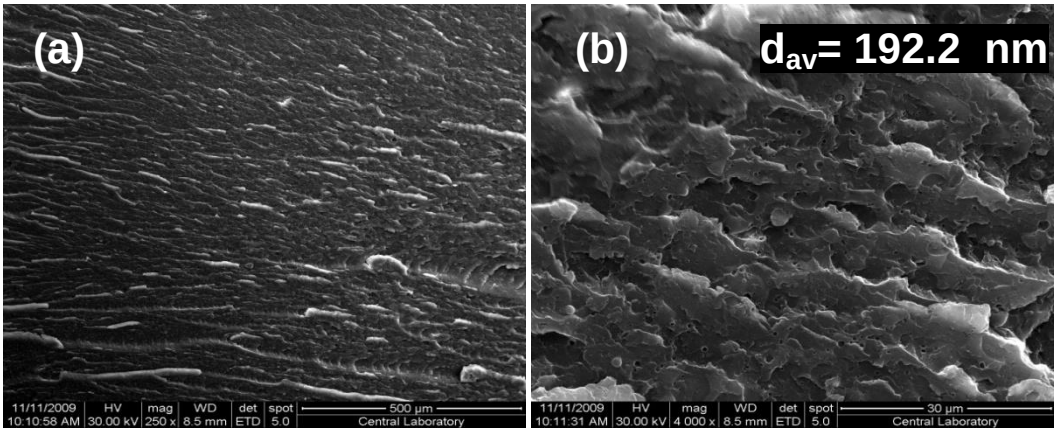

Figure 4.49 SEM micrographs of etched PET/PB.TO-P/E-MA-GMA ternary nanocomposite: (a) (x250), (b) (x4000)

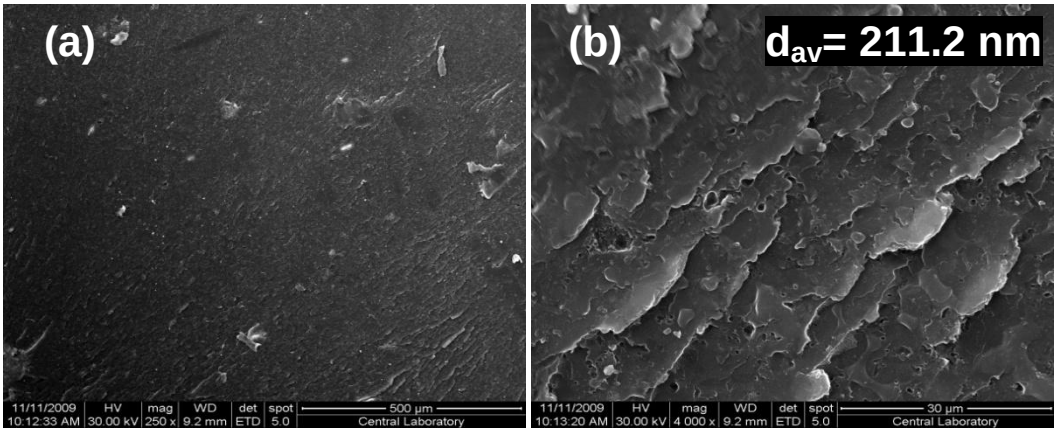

Figure 4.50 SEM micrographs of etched PET/PB.BZLTP-P/E-MA-GMA ternary nanocomposite: (a) (x250), (b) (x4000)

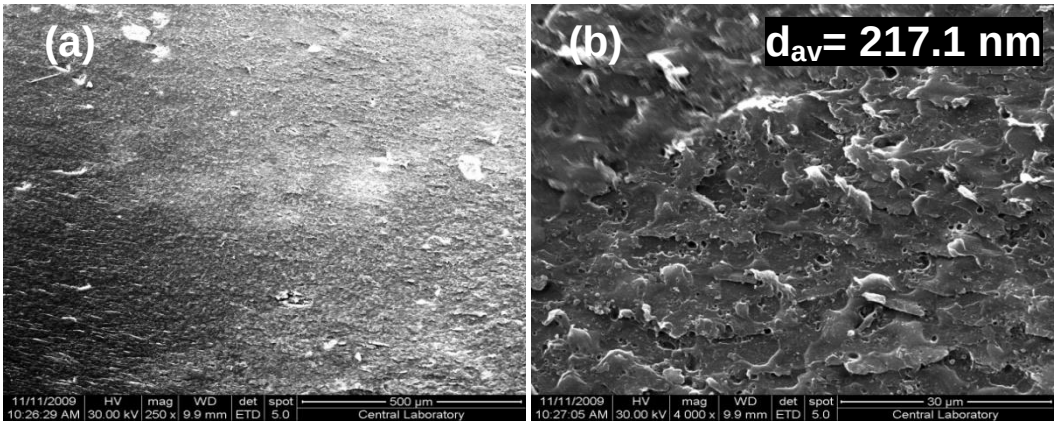

Figure 4.51 SEM micrographs of etched PET/PB.BZL-IM/E-MA-GMA ternary nanocomposite: (a) (x250), (b) (x4000)

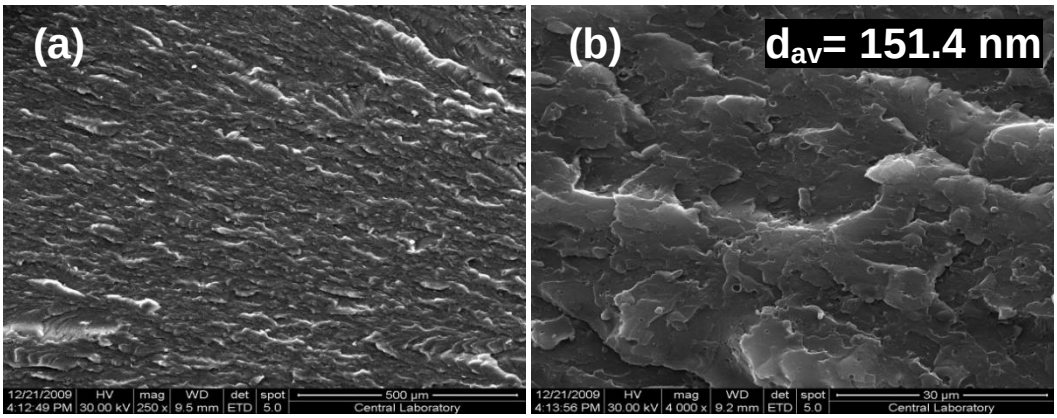

Figure 4.52 SEM micrographs of etched PET/PB.BZL-IM/E-MA-GMA (E3) ternary nanocomposite: (a) (x250), (b) (x4000)

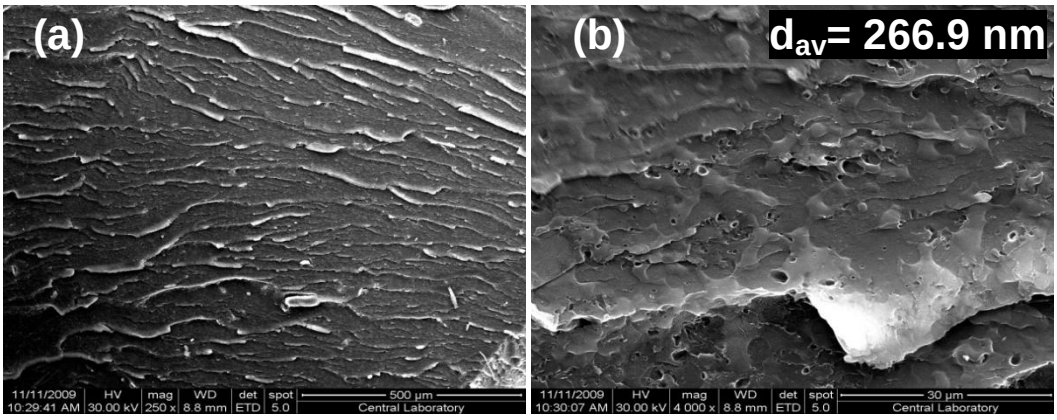

Figure 4.53 SEM micrographs of etched PET/PB.BTL-IM/E-MA-GMA ternary nanocomposite: (a) (x250), (b) (x4000)

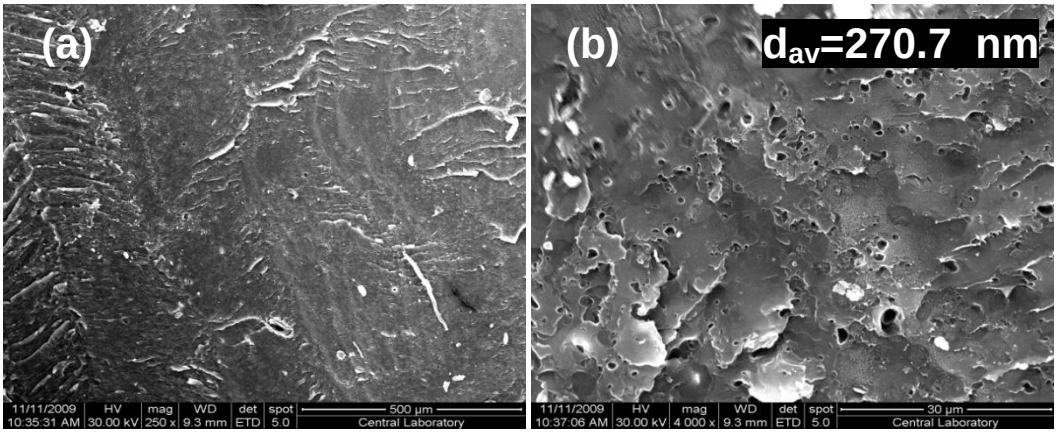

Figure 4.54 SEM micrographs of etched PET/PB.BTL-IM'/E-MA-GMA ternary nanocomposite: (a) (x250), (b) (x4000)

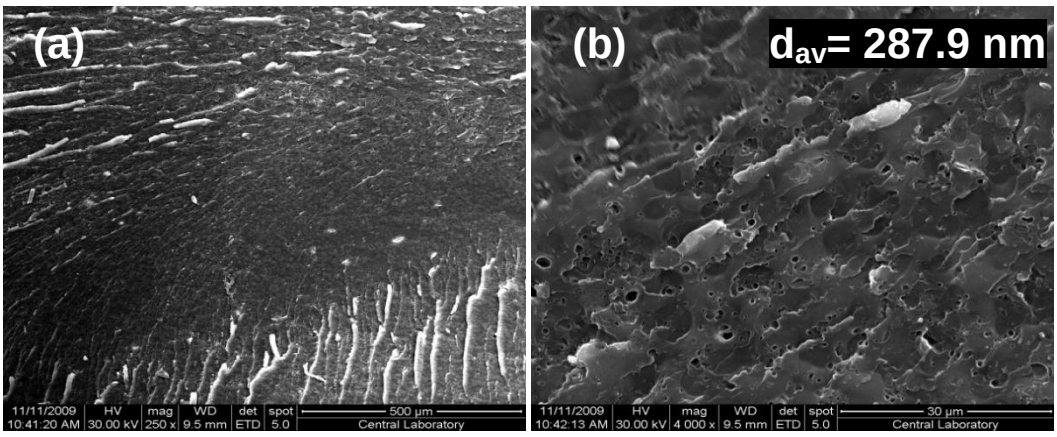

Figure 4.55 SEM micrographs of etched PET/PB.DCL-IM/E-MA-GMA ternary nanocomposite: (a) (x250), (b) (x4000)

4.3 Melt Flow Index Analysis

4.3.1 Melt Flow Index Measurements

To investigate the flow behavior of the materials, melt flow index (MFI) test was performed.

4.3.1.1 MFI Results of PA66 Nanocomposites

Melt flow index values of PA66 compositions obtained at 275°C using a load of 0.325 kg are given in Table 4.12.

Table 4.12 MFI results of PA66 Compositions

Composition	MFI (g/10min)	Standard deviation
Polymer		
PA66 (Not Extruded)	36.5	1.9
PA66 (Extruded Twice)	36.0	1.7
Elastomer		
E-BA-MAH	4.5	0.3
Polymer/Elastomer Blend		
PA66/E-BA-MAH	25.2	1.2
Polymer/Organoclay Binary Nanocomposites		
PA66/PB.TO-P	37.1	2.1
PA66/PB.BZLTP-P	38.0	2.0
Polymer/Organoclay/Elastomer Ternary Nanocomposites		
PA66/PB.TO-P/E-BA-MAH	24.5	2.6
PA66/PB.BZLTP-P/E-BA-MAH	24.8	1.0

The addition of organoclay can increase the viscosity of the polymer matrix due to the strong interaction between the organoclay and the polymer. This would lead to the reduction of melt viscosity difference between continuous polymer matrix and

the dispersed phase, thus improving the mixing properties of the blend. Melt flow index is inversely proportional to the melt viscosity and depends on the molecular weight of the polymer matrix, the presence of additives such as co-monomers, degree of chain branching as well as heat transfer and processing methods.

In the present study, the melt viscosity of PA66 did not change after extrusion twice indicating a high stability in the molecular structure of PA66 with negligible degradation during extrusion. The MAH group present in the elastomer E-BA-MAH with high melt viscosity (low MFI of 4.5 g/min) reacted with the amine ends of PA66 and resulted in a highly viscous PA66/E-BA-MAH blend with lower melt flow index (25.2 g/min) than that of PA66 extruded twice (36.0 g/min).

The addition of fillers into the polymer matrix retards the flow especially at low shear rates and causes an increase in the melt viscosity (decrease in MFI). This is mainly dependent on the shape, size and concentration of the filler. However, the melt viscosity decreased slightly (MFI increased) in PA66/phosphonium organoclay binary nanocomposites. This behavior can be ascribed to the slip between the polymer matrix and the dispersed clay platelets due to the ignorable change in the melt viscosity of extruded and pure PA66 (1), (152), (153). The MFI value of the blend is less than those of the binary nanocomposites as a result of the highest melt viscosity of the elastomer (lowest MFI).

The melt flow behavior of nanocomposites depends on the degree of dispersion of organoclay aggregates (i.e., morphology), which in turn depends, among many factors, on the degree of compatibility between polymer matrix and organoclay, as it is the case for polymer blends. A systematic correlation could not be found regarding the structure of the organoclays which exhibited close MFI values. The viscosity of the polymer matrix is an important factor that affects the dispersion of organoclays, since intercalation and/or exfoliation require the diffusion of polymer chains into the silicate layers or peel away the top and bottom layers as promoted by the polymer adsorption and by the application of shear stress (154). With increasing viscosity by organoclay incorporation, the shear stress applied to the platelets increases and leads the separation of layers. The incorporation of phosphonium organoclays in PA66 ternary nanocomposites exhibited the lowest

MFI values (highest viscosities) compared to pure PA66, PA66 blend and binary nanocomposites owing to the effect of organoclays which increased the viscosity.

4.3.1.2 MFI Results of PET Nanocomposites

Melt flow index values of PET compositions are given in Table 4.13. These data were obtained at 260°C using a load of 2.16 kg.

Table 4.13 MFI results of PET Compositions

Composition	MFI (g/10min)	Standard deviation
Polymer		
PET (Not Extruded)	357.5	18.7
PET (Extruded Twice)	486.8	31.2
Elastomer		
E-MA-GMA	7.0	0.7
Polymer/Elastomer Blend		
PET/E-MA-GMA	187.3	5.1
Polymer/Organoclay Binary Nanocomposites		
PET/PB.TO-P	420.2	12.0
PET/PB.BZLTP-P	423.4	9.5
PET/PB.BZL-IM	391.0	5.8
PET/PB.BTL-IM	323.3	12.3
PET/PB.DCL-IM	332.3	9.8
Polymer/Organoclay/Elastomer Ternary Nanocomposites		
PET/PB.TO-P/E-MA-GMA	240.4	16.3
PET/PB.BZLTP-P/E-MA-GMA	250.2	9.8
PET/PB.BZL-IM/E-MA-GMA	216.2	10.7
PET/PB.BTL-IM/E-MA-GMA	194.9	8.6
PET/PB.DCL-IM/E-MA-GMA	201.8	9.5

The melt viscosity of PET decreased significantly (MFI increased) after extrusion twice due to degradation and chain scission of the polymer. In this case, the molecular bond usually breaks shortening the overall chain (129).

The MFI of PET is much higher than that of E-MA-GMA under the same conditions. The epoxy functionality of GMA reacted with PET and formed a viscous PET/E-MA-GMA blend and resulted in lowering the MFI value down to approximately half of neat PET.

The concentration was the same (2 wt %) in all fillers incorporated into the PET/organoclay binary nanocomposites. Thus, the structure and size of organoclay particles and their compatibility with PET are the main factors for the effects of the fillers. In binary PET/organoclay nanocomposites, the addition of organoclay decreases the MFI (increases the viscosity) compared to the extruded twice PET as seen in Table 4.13. The decrease of MFI value in the presence of organoclays is basically due to intercalated/exfoliated layers and clusters formed by the organoclay. In addition, the change in viscoelastic behavior from liquid-like for the unfilled polymers to solid-like for nanocomposites with as little as 2 wt % layered silicate has been attributed to the formation, in the quiescent state, of a percolated network superstructure of the stacks (tactoids) of intercalated layers or exfoliated layers (155).

The compatibility between polymer matrix and the surfactant residing at the surface of organoclay and the gallery distance of the organoclays is crucial to interpret the melt flow behavior of the nanocomposites (154), (156). The binary nanocomposites have higher MFI (lower viscosity) than their corresponding ternary counterparts. The incorporation of elastomer reduced the MFI of all binary nanocomposites, owing to its low MFI as well as to the reaction between epoxy functionality of GMA and PET. In these ternary nanocomposites, generally, the addition of clay leads to a decrease in MFI with respect to the MFI of the PET/E-MA-GMA blend since organoclays increase the viscosity. The presence of elastomer suppresses the organoclay dispersion as seen in TEM Figures 4.25 and 4.29.

4.4 Mechanical Tests

The endurance of a material to various types of deformation mechanisms depends mainly on its individual mechanical properties. Tensile and impact tests were performed in this study to analyze the degree of improvement in the strength, stiffness, ductility and toughness of nanocomposites upon addition of the organoclays and compatibilizers which also serve as impact modifiers. These results are also demonstrated by the help of the graphs. The mechanical results obtained for all compositions are given in Appendix A.

4.4.1 Tensile Tests

Tensile tests were performed to obtain the response of the prepared nanocomposites to the applied force and the extent to which the specimens elongate before failure. Tensile strength, Young's modulus and elongation at break values were determined from the stress-strain curves.

4.4.1.1 Tensile Test Results of PA66 Nanocomposites

The tensile properties of the PA66 and E-BA-MAH are shown in Table 4.14. Tensile strength, Young's modulus and elongation at break of PA66 that was twice extruded were found to be 83.7 MPa, 2.734 GPa and 23.3 %, respectively. These values are within the range given by PolyOne Company for wet and dry as molded PA66. The tensile strength and Young's modulus values of PA66 compositions are given in Figures 4.56 and 4.57, respectively.

Table 4.14 Tensile properties of PA66 and E-BA-MAH

Property	PA66 (ISO 527)	E-BA-MAH (ISO 527)
Tensile strength (MPa)	83.7	12.0
Young's modulus (GPa)	2.734	-
Elongation at break (%)	23.3	600.0

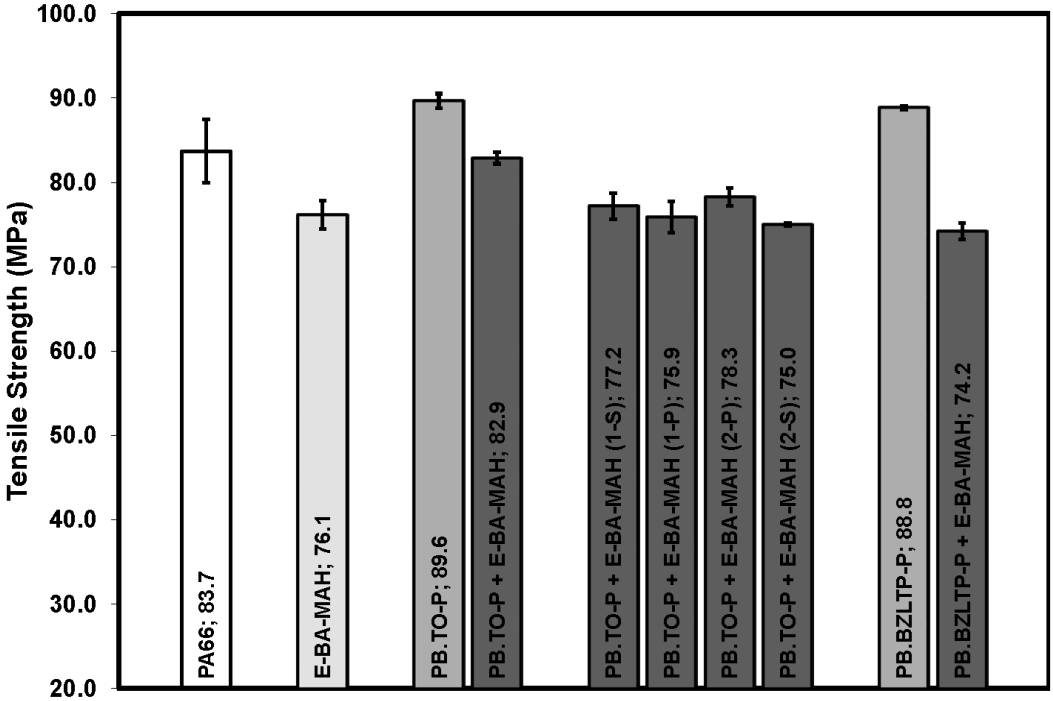

Figure 4.56 Tensile strength values (MPa) of PA66 compositions

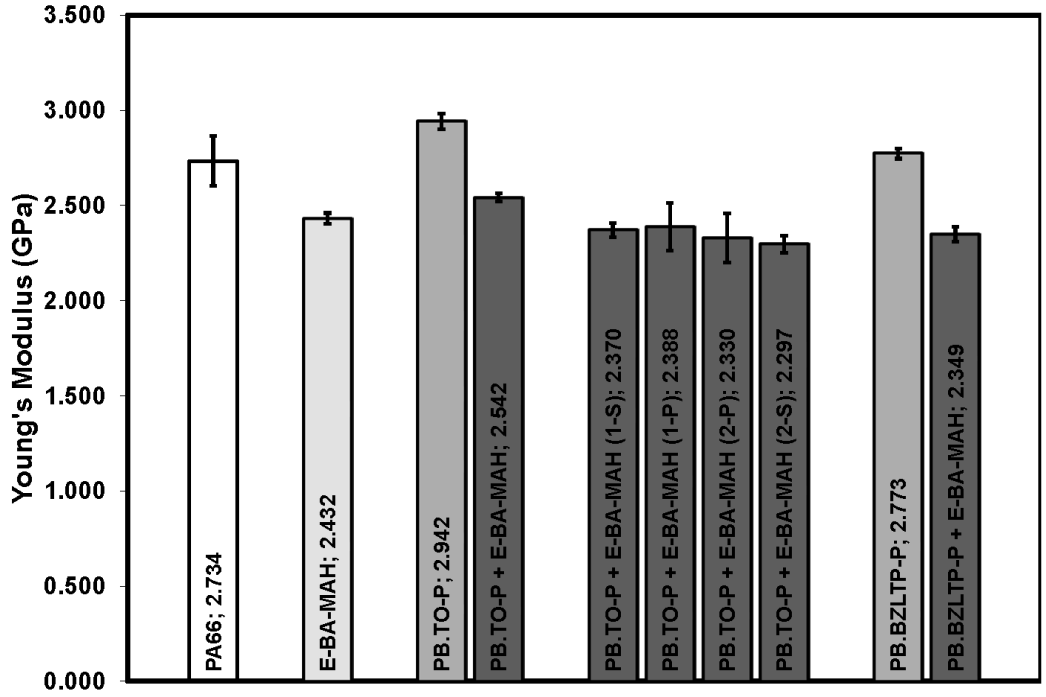

Figure 4.57 Young's modulus values (GPa) of PA66 Compositions

It is obvious from Figures 4.56 and 4.57 that addition of E-BA-MAH elastomer with low mechanical strength and Young's modulus decreases the tensile strength and Young's modulus of PA66/E-BA-MAH blend. Elastomeric materials enhance the bonding between the polymer and the organoclay. Also, the elastomeric phase has a lower Young's modulus compared to the matrix and it acts as stress concentrator during elongation. Thus, yielding or crazing occurs around the elastomeric domains and a higher amount of energy is absorbed by the polymer (150). On the other hand, phosphonium organoclays stiffen the matrix in PA66/PB.TO-P and PA66/PB.BZLTP-P binary nanocomposites, and thus they result in an increase in the tensile strength and Young's modulus indicating an increase in the rigidity of the material. The high aspect ratio of the organoclay contributes to the reinforcement effect because it creates a large contact area with the polymer matrix. The interfacial adhesion between PA66 and the organoclay is also significant in dispersing the clay homogeneously in the polymer matrix and increasing the strength of the material. This effect was observed better with PB.TO-P organoclays which exhibit higher tensile strength and Young's modulus than PB.BZLTP-P in the binary nanocomposites, due to the better dispersion of PB.TO-P in PA66. The compatibility of the organoclay with PA66 matrix and the elastomer, in addition to the initial basal spacing of the organoclay PB.BZLTP-P (1.78 nm) which was smaller than the initial d-spacing of PB.TO-P (2.52 nm) are well known to be crucial factors on the composite as a final product. These results are in good agreement with TEM analyses which showed that PB.TO-P layers are intercalated and dispersed in the elastomeric phase, whereas PB.BZLTP-P exhibited more agglomerates rather than dispersed structure, but still intercalated.

PA66/phosphonium organoclay/E-BA-MAH ternary nanocomposites exhibit the expected effect of the elastomer E-BA-MAH in lowering the strength and modulus increased by organoclays addition. The strength and modulus of 2 wt % PB.TO-P ternary nanocomposites are higher than strength and modulus of 1 wt % PB.TO-P ternary nanocomposites. This notice emphasizes the importance of adding an adequate amount of filler to obtain nanocomposites with higher mechanical properties. The compatibility of PB.BZLTP-P/PA66 again seems weaker than PB.TO-P/PA66 after the addition of E-BA-MAH compatibilizer.

In this study, increasing the organoclay content from 1 wt % to 2 wt % resulted in significant improvement in the mechanical properties, as it is a general fact that the stiffness of the nanocomposites increases with increasing clay content at the expenses of their impact strength and tensile ductility until an optimum organoclay concentration is reached (157). The tensile strength of 2 wt % PA66//PB.TO-P//E-BA-MAH (82.9 MPa) was higher than those of 1 wt % PA66/PB.TO-P/E-BA-MAH ranging between 75.0 and 78.3 MPa. Young's modulus of 2 wt % PA66/PB.TO-P/E-BA-MAH (2.542 GPa) was higher than those of 1 wt % PA66/PB.TO-P/E-BA-MAH ranging between 2.297 and 2.370 GPa. After this optimum content, further addition of organoclay hinders the separation of clay platelets, and clay particles are found as tactoids in the polymer matrix and the tensile properties cannot be improved. Thus, based on earlier investigations, in addition to the present brief study with (1 and 2 wt %), optimum amounts of 2 wt % organoclay and 5 wt % elastomeric phase were added to the polymer matrix in all the combinations after this point of the research in order to balance the stiffness and toughness of the materials.

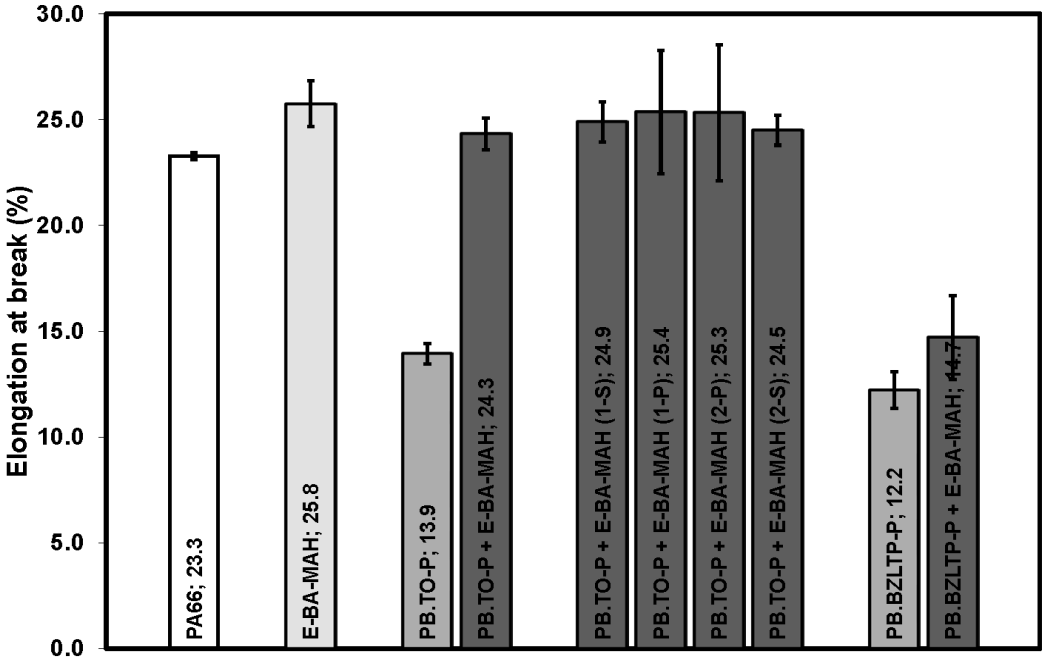

Figure 4.58 Elongation at break values (%) of PA66 compositions

The elongation at break values of PA66 compositions are given in Figure 4.58. E-BA-MAH caused about 9% increase in the elongation at break of the PA66 blend.

However, the high elongation at break value of PA66 diminished upon addition of organoclay in PA66 binary and ternary nanocomposites since inorganic silicate particles cannot be strained by external stresses. The spherulite size also decreases in PA66, upon addition of the organoclay, leading to brittle structure which is clearly seen in PA66/phosphonium organoclay binary nanocomposites. The decrease in the elongation at break is recovered and balanced by the addition of the elastomer E-BA-MAH in the phosphonium organoclay ternary nanocomposites. The elongation at break of PA66 ternary nanocomposite produced using PB.BZLTP-P organoclay showed less compatibility than that produced with PB.TO-P organoclay. This was also observed in tensile strength and Young's modulus results.

Elongation at break values drastically decreased due to increased stiffness and the formation of microvoids around clay particles during tensile testing. In summary, the main factor contributing to the enhancement of mechanical properties in PA66/organoclay nanocomposites was mainly the degree of dispersion and exfoliation of the clay particulates in the PA66 matrix.

4.4.1.2 Tensile Test Results of PET Nanocomposites

The tensile properties of the PET and E-MA-GMA are shown in Table 4.15. Tensile strength, Young's modulus and elongation at break of twice extruded PET were found to be 46.9 MPa, 1.749 GPa and 3.9 %, respectively.

Table 4.15 Tensile properties of PET and E-MA-GMA

Property	PET (ISO 527)	E-MA-GMA (ISO 527)
Tensile strength (MPa)	46.9	4.0
Young's modulus (GPa)	1.749	0.008
Elongation at break (%)	3.9	1100.0

The choice of the elastomer and its concentration are the main factors in preparing nanocomposites with optimum properties. Pure E-MA-GMA is reported to have

strain at break of 1100%, and it is also a suitable elastomer to be used with PET owing to its functional groups and epoxy functionality in GMA which can react with the carboxyl and hydroxyl end groups of PET in the melt phase to form a graft copolymer. The addition of elastomer decreases the tensile strength and Young's modulus. The concentration of the elastomer E-BA-MAH (5 wt %) owing to its balanced mechanical properties was chosen after an optimization work done in an earlier study by Alyamac et al. in 2007.

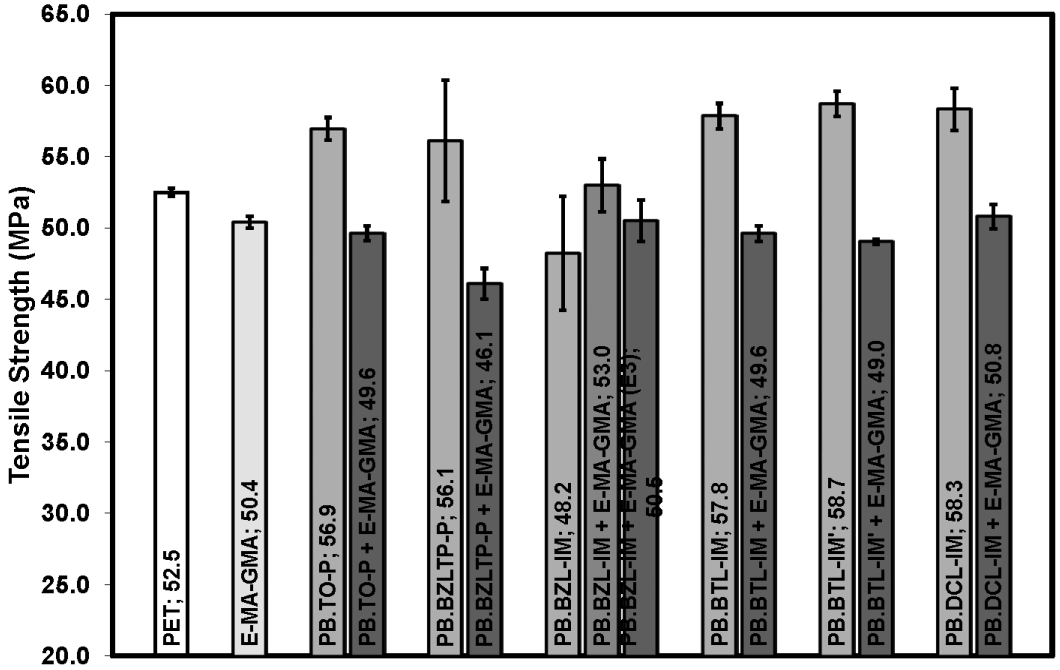

Figure 4.59 Tensile strength values (MPa) of PET compositions

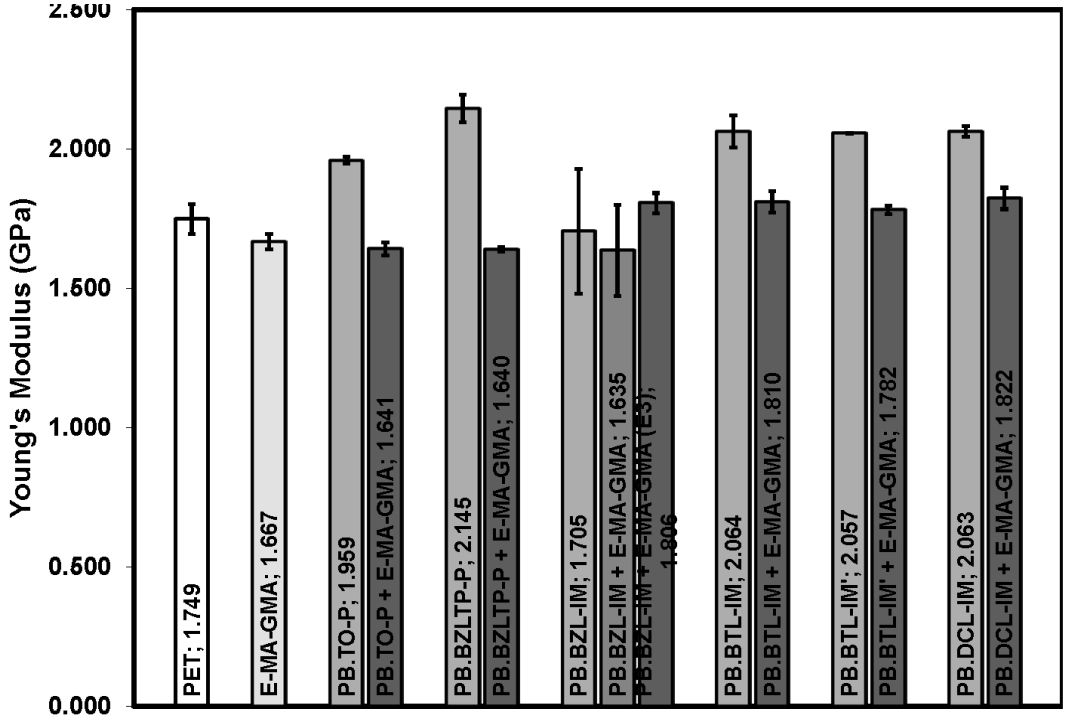

Figure 4.60 Young's modulus values (GPa) of PET compositions

Tensile strength and Young's modulus values of PET compositions are shown in Figures 4.59 and 4.60, respectively. The elastomeric effect showed the expected decrease in the tensile strength and Young's modulus of PET/E-MA-GMA blend in comparison to PET.

In general, organoclays, including phosphonium and imidazolium ones, stiffen the matrix in all PET/organoclay binary nanocomposites due to their high aspect ratio creating large contact area, and contributing to the reinforcement effect. This usually results in an increase in the tensile strength and Young's modulus resulting from the increase in the stiffness of the composites (158). This effect could be seen clearly in Figures 4.59 and 4.60 with the exception of PET/PB.BZL-IM binary and ternary nanocomposites which exhibited a slight decrease compared to other organoclays. As expected, the incorporation of the elastomer E-MA-GMA in PET/organoclay/E-MA-GMA ternary nanocomposites compensated for the decrease in tensile strength and Young's modulus caused by organoclays. The chemical structure in phosphonium organoclay binary and ternary nanocomposites did not exhibit significant differences in tensile strength and Young's modulus

values except for aryl phosphonium PB.BZLTP-P organoclay which exhibited a decrease in tensile strength value (46.1 MPa) compared to pure PET (52.5 MPa) due to the presence of benzyl groups. The alkyl chain length in alkyl Imidazolium organoclays (PB.BTL-IM, PB.BTL-IM' and PB.DCL-IM) had no effect on tensile and Young's strength values and they exhibit close results. The presence of benzyl groups in PB.BZL-IM caused decrease even in the PET binary nanocomposite extruded twice or three times.

The elongation at break values of PET compositions are given in Figure 4.61. Pure PET was brittle and fractured at about 5% strain. The presence of E-MA-GMA elastomer in PET/E-MA-GMA blend turned it ductile and neck propagation formed along the gauge section before break. A drastic reduction in the elongation at break value is commonly observed in thermoplastics associated with clay addition, because silicate particles cannot be strained by external stresses. Thus, rigid fillers in a rigid polymer generally decrease the elongation at break as well as the impact strength of a polymer (159).

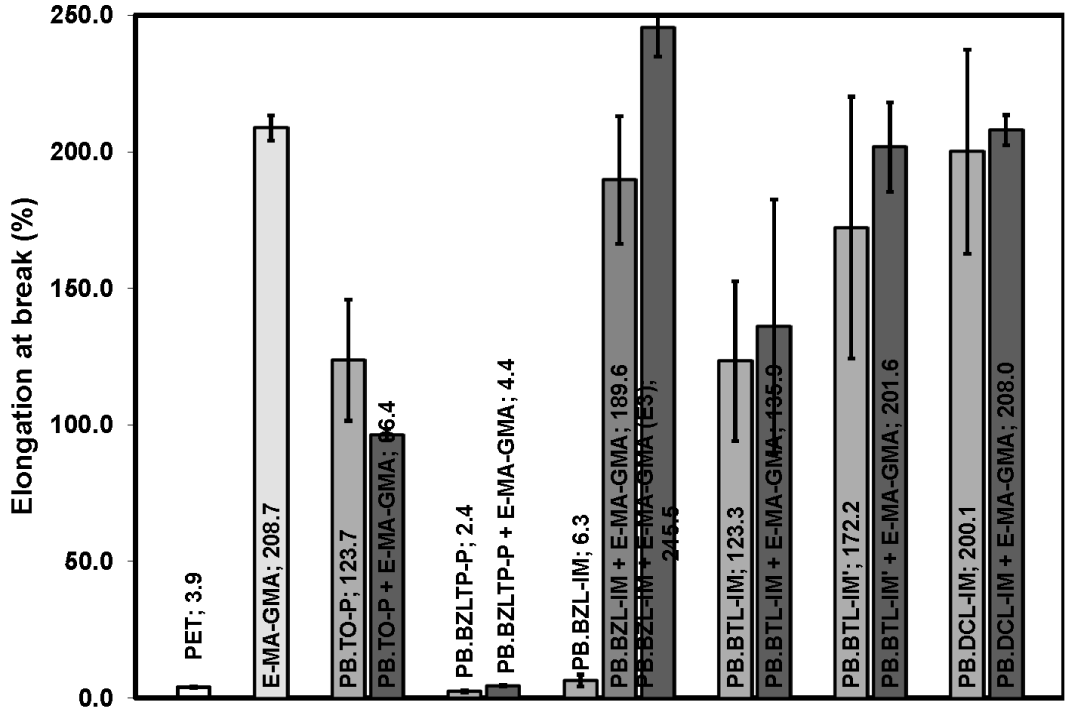

Figure 4.61 Elongation at break values (%) of PET compositions

The elongation at break of PET/PB.TO-P binary nanocomposite (123.7%) and of PET/PB.TO-P/E-MA-GMA ternary nanocomposite (86.4 %) is much higher than that of pure PET. However, elongation at break of PET/PB.BZLTP-P binary nanocomposite (2.4%) and of PET/PB.BZLTP-P/E-MA-GMA ternary nanocomposite (4.4 %) is lower than that or pure PET. The increase in PB.TO-P binary nanocomposites can be attributed to the better dispersion of the PB.TO-P organoclay in PET matrix and confirms the incompatibility of PB.BZLTP-P with PET. The ductility role of E-MA-GMA was also inhibited by the incompatible PB.BZLTP-P organoclays.

The elongation at break values of imidazolium organoclay containing binary and ternary nanocomposites are also much higher than that of pure PET, except PET/PB.BZL-IM binary nanocomposite (6.3 %).

4.4.2 Impact Test

Charpy notched impact strength tests were carried out to measure the toughness of polymer (PA66, PET) blends and nanocomposites. In nanocomposites, toughness usually decreases upon the addition of an organoclay into the polymer matrix because the organoclay with stiff structure decreases the molecular mobility due to its interaction with the polymer matrix. On the other hand, the elastomeric phase increases the interfacial adhesion between the polymer and the organoclay in addition to its impact modification properties.

Toughness of polymer nanocomposites is mainly affected by polymer/elastomer interactions, an appropriate range of elastomeric domain size and interparticle distance, uniform distribution of the elastomeric domains, low modulus ratio between the elastomer and the polymer bulk phase, and high Poisson's ratios with low breaking stress of the dispersed phase (150). Polymer/elastomer interactions are mainly interrelated to the other factors mentioned above. The better these interactions are, the less the interfacial tension between the elastomer and the polymer become. In addition, the stabilization of the surface mobility is considered as a third main factor which results in a preferred decrease in the domain size of the elastomer domains. The range of elastomer particle size and interparticle

distance (interdomain distance) must be optimized in a reasonable range to increase toughness fairly and not cause a decrease in other properties. The size of the elastomeric domains is also influenced by the mobility of the interface, melt viscosity of the matrix, shear stresses and surface tension. High shear stresses and melt viscosity are efficient in uniform dispersion of the elastomeric domains and promoting the formation of finer elastomeric domains (150). Interdomain distance is affected both by intrinsic parameters (interfacial adhesion, modulus of the matrix, modulus of the matrix/modulus of the elastomer ratio) and extrinsic parameters (impact speed, test temperature and mode of deformation). The critical interdomain distance becomes lower with an increase in the modulus of the matrix and increases as the modulus of the elastomeric phase decreases (118). In the present work, intrinsic parameters are more dominant since extrinsic parameters were kept constant.

4.4.2.1 Impact Test Results of PA66 Nanocomposites

Polyamides have great industrial importance owing to their excellent tensile properties, chemical and abrasion resistance and high melting point. The toughness of PA66 made it a preferred polymer in many industrial applications requiring impact resistance. In addition, toughening of semicrystalline polymers is known to be a complex mechanism including the initial elastic loading of the polymer/elastomer blend, the internal or external cavitation of the dispersed elastomer particles, followed by craze initiation and shear banding of the matrix (100). Impact strengths of PA66, PA66 blend and PA66 nanocomposites are shown in Figure 4.62. Impact strength of PA66/E-BA-MAH blend increased from 7.0 kJ/m^2 for pure PA66 to 10.4 kJ/m^2 owing to cavitation mechanism introduced by the elastomer.

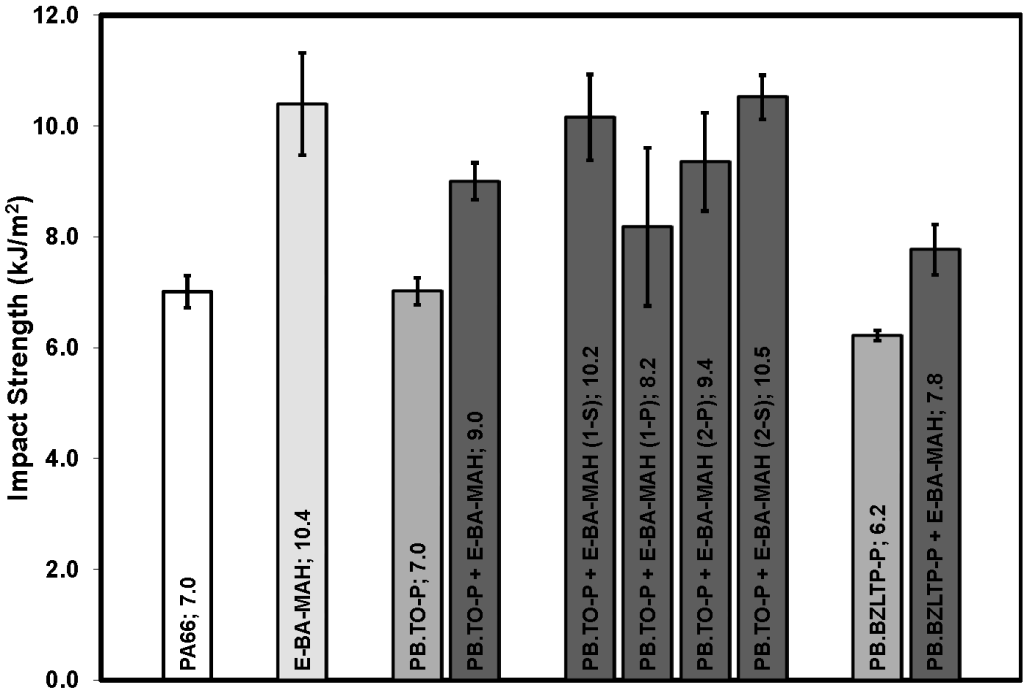

Figure 4.62 Impact strength values (kJ/m^2) of PA66 compositions

The impact strength of PA66/organoclay binary nanocomposites decreased slightly using PB.BZLTP-P, while it stayed constant upon using PB.TO-P organoclay. Significant decreases in the impact strength can be usually seen at higher organoclay contents. For PA66 ternary nanocomposites, PB.TO-P exhibited an impact strength value 9.0 kJ/m^2 which is higher than that of PB.BZLTP-P which exhibited a lower value 7.8 kJ/m^2. On the other hand, PA66 ternary nanocomposites prepared with 1 wt % of PB.TO-P exhibited higher values in comparison to those prepared with 2 wt % organoclays. In addition, simultaneous injection molding exhibited better results for PA66/PB.TO-P/E-BA-MAH (1-S) and PA66/PB.TO-P/E-BA-MAH (2-S) sets, while pelletizing before injection molding exhibited lower values for (1-P) and (2-P) due to thermal degradation resulting from melting the sample three times.

The organoclay dispersion was better in PB.TO-P than PB.BZLTP-P containing PA66 binary and ternary nanocomposites and this was clearly reflected on the toughness of the nanocomposites. This observation was also approved by TEM and SEM analyses discussed earlier. Although exfoliation of the organoclays was

not totally achieved, the intercalated regions shown by TEM propose that a fair percent of the clay agglomerates were broken down and the polymer chains could penetrate between the clay platelets although they were not completely separated. Thus, the toughness of the PA66 ternary nanocomposites was improved with respect to the binary nanocomposites. Also, in the ternary nanocomposites the mechanism of cavitation can take place.

4.4.2.2 Impact Test Results of PET Nanocomposites

Impact strengths of PET, PET blend and PET nanocomposites are shown in Figure 4.63. Impact strength of PET/E-MA-GMA blend increased from 2.9 kJ/m^2 for pure PET to 4.8 kJ/m^2 owing to the cavitation mechanism usually introduced by the elastomeric domains.

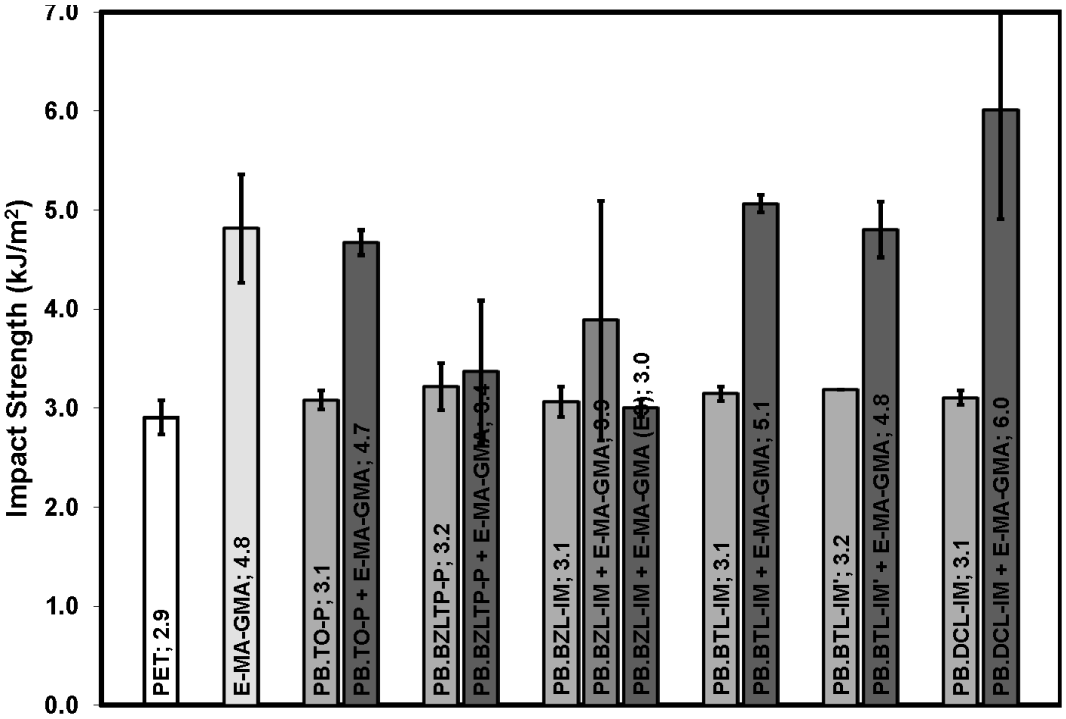

Figure 4.63 Impact strength values (kJ/m^2) of PET compositions

The addition of organoclay makes the PET matrix stiffer by decreasing the molecular mobility of the polymer chains due to the interaction between the matrix and clay surface, and the toughness of the rigid polymer matrix increases. The

impact strength of PET/organoclay binary nanocomposites increased slightly upon the addition of organoclay from 2.9 kJ/m^2 to values in the range between 3.1 and 3.2 kJ/m^2 for all binary nanocomposites. In addition to the impact modification role of the elastomer through compensating the reduced impact strength with organoclay addition, it acts as a compatibilizer which increases the compatibility between organoclay and the polymer matrix to aid the intercalation of polymer chains between the silicate layers. For PET ternary nanocomposites, PB.TO-P exhibited an impact strength value 4.7 kJ/m^2 which is higher than that PB.BZLTP-P which exhibited a lower value 3.4 kJ/m^2 owing to the better compatibility and dispersion of alkyl phosphonium organoclay (PB.TO-P) compared to aryl phosphonium organoclay (PB.BZLTP-P) with PET matrix.

PB.BZL-IM containing ternary nanocomposites exhibited an increase in toughness with values 3.9 kJ/m^2. This value decreased upon extrusion three times in PET/PB.BZL-IM/E-MA-GMA (E3). The presence of benzyl groups in both PET/PB.BZLTP-P/E-MA-GMA and PET/PB.BZL-IM/E-MA-GMA resulted in lowest toughness values among all compositions. PB.BTL-IM and PB.BTL-IM' containing ternary nanocomposites exhibited close results with values 5.1 kJ/m^2 and 4.8 kJ/m^2, respectively. PB.DCL-IM containing ternary nanocomposite with longer alkyl chain exhibited best improvement in impact strength results among all compositions. PET/PB.DCL-IM/E-MA-GMA ternary nanocomposite containing longer alkyl chains exhibited better improvement than PET/PB.BTL-IM/E-MA-GMA with short alkyl chain.

The better the organoclay is dispersed in the polymer matrix, the more these organoclays act as barriers and hinder the coalescence of the elastomeric domains. In PET compositions studied, the addition of organoclays increased the average domain size and this was attributed to the dispersion of clay particles at the interface between PET and elastomeric phase.

4.5 Thermal Analyses

4.5.1 Thermogravimetric Analysis

The thermal gravimetric analyses of surfactants, clays, phosphonium and imidazolium organoclays, PA66 nanocomposites and PET nanocomposites were performed in order to investigate the effects of salts used on the clay and the resulting nanocomposites.

4.5.1.1 TG/DrTGA Analysis of Surfactants

Prior to discussion concerning the thermal stability of phosphonium and imidazolium-intercalated organoclays, one should focus on the thermal decomposition process of imidazolium salts and the role of their chemical structure. The chemical structures of the two phosphonium and four di-imidazolium surfactants are briefly discussed below:

1. PH1 Surfactant (TO-P Br): Four long octyl chain groups attached to the phosphonium cation with bromide counter ion.
2. PH2 Surfactant (BZLTP-P): One benzyl and 3 phenyl groups attached to the phosphonium cation with chloride counter ion.
3. IM1 Surfactant (BZL-IM PF6): The chain group attached to the first nitrogen atom is aromatic with hexafluorophosphate counter ion.
4. IM2 Surfactant (BTL-IM PF6): The chain group attached to the first nitrogen atom is short aliphatic with hexafluorophosphate counter ion.
5. IM3 Surfactant (BTL-IM Cl): The chain group attached to the first nitrogen atom is short aliphatic with chloride counter ion.
6. IM4 Surfactant (DCL-IM Cl): The chain group attached to the first nitrogen atom is long aliphatic with chloride counter ion.

Thermogravimetric measurements (TG/DrTGA) were carried out on phosphonium and imidazolium salts under nitrogen atmosphere. The TGA and DrTGA thermograms of the salts are given in Figures 4.64 and 4.65, respectively.

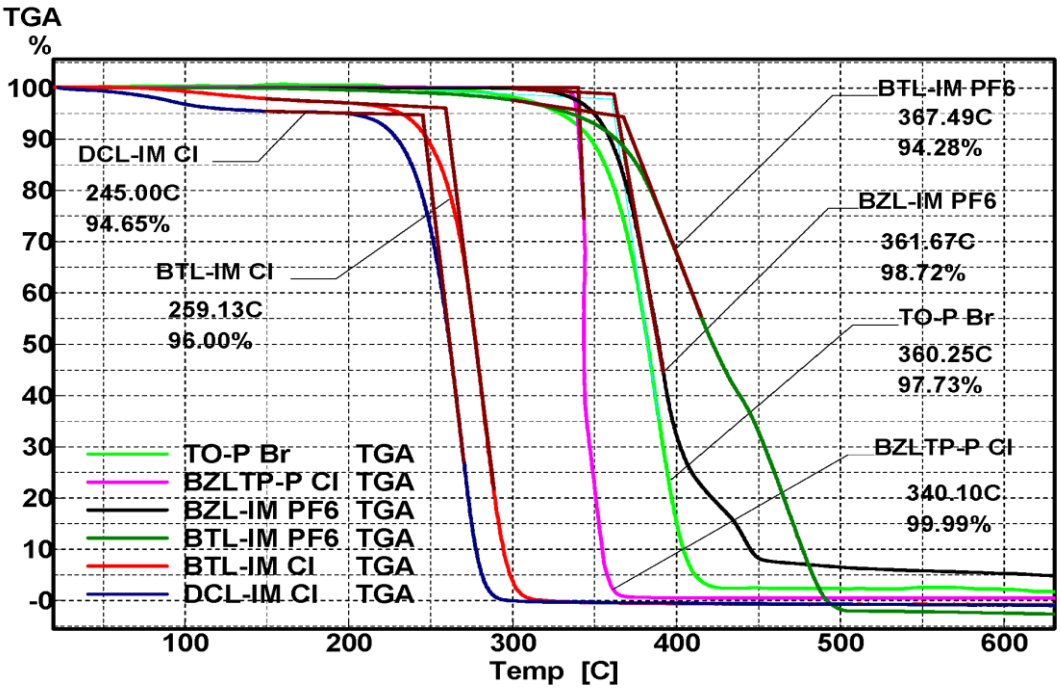

Figure 4.64 TGA Thermograms of salts (onset decomposition temperatures and mass % indicated)

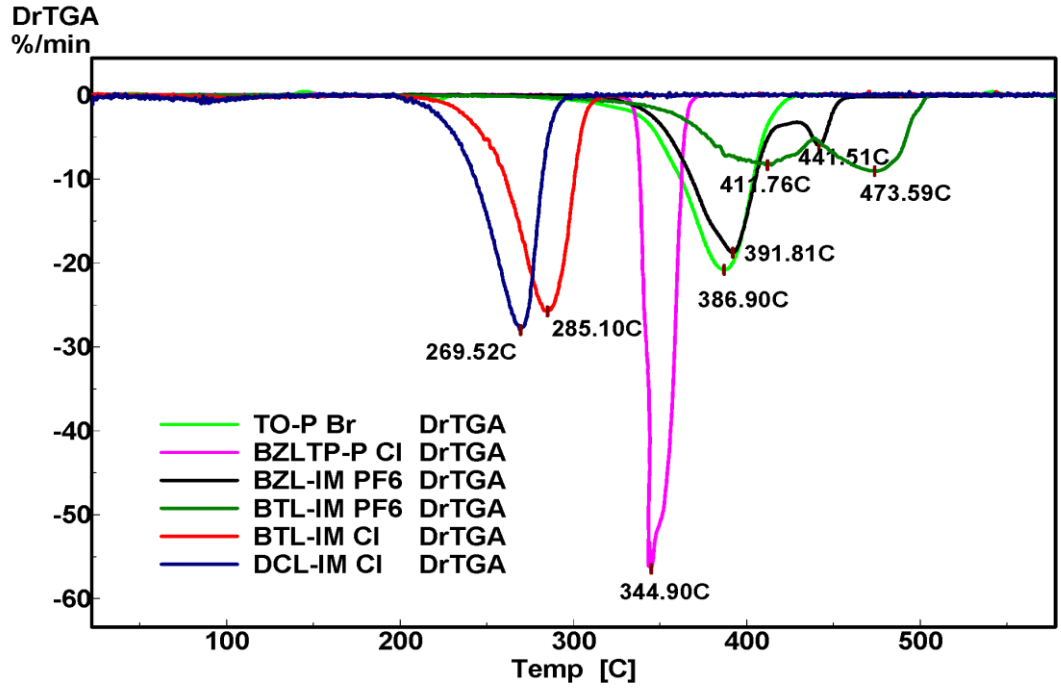

Figure 4.65 DrTGA thermograms of salts

The results are reported in terms of onset decomposition temperature and peak decomposition temperature from derivative thermograms in Table 4.16. Onset decomposition temperature has been defined in the literature as the temperature at 5% mass loss. Other researchers compared the thermal stability of organoclays by taking the maximum decomposition temperature found from derivative TGA peaks. A more accurate definition is the temperature corresponding to the cross-section of the two tangents around the main degradation point. This definition was taken as the reference in the present study. The temperature at the onset of the first (prominent) peak is taken to represent the point at which the surfactant begins to decompose. The regions of interest were chosen for analysis. The weight loss at 200°C was chosen to compare the results to conventional ammonium salts which mainly start to degrade at temperatures less than 200°C. On the other hand, the thermal stability of the salts and their subsequent organoclays should also be analyzed at 275°C which is the processing temperature of polymers used in this study.

Phosphonium Salts: TGA shows that the thermal decomposition of phosphonium surfactants occurred in one step. However, the derivative TGA indicates that the thermal decomposition of the alkyl salt (TO-P Br) occurred in two steps, while the aryl salt (BZLTP-P Cl) exhibited one decomposition step. TO-P Br exhibited its first mass loss at 100°C-280°C due to the probable evaporation of water and/or impurities. The second mass loss occurred above 280°C in both salts, due to the main onset thermal decomposition. The alkyl phosphonium salt exhibited a higher onset decomposition temperature of 360°C (2.3% mass loss) compared to the aryl phosphonium salt with an onset decomposition temperature of 340°C (0.1% mass loss). The higher thermal stability of the alkyl phosphonium salt can be attributed to the higher molecular weight of the alkyl salt. The thermal decomposition of TO-P Br and BZLTP-P Cl (temperature at 5% mass loss) started at 329°C and 339°C, respectively. On the other hand, the maximum decomposition rate from derivative TGA curves was 387°C for TO-P Br and 345°C for BZLTP-P Cl. At 200°C, both surfactants exhibited no mass loss, and at 275°C only TO-P Br exhibited 0.66% mass loss. Thus, phosphonium surfactants exhibited superior thermal stability, considering normal polymer processing temperatures in the range of 200°C-300°C.

Table 4.16 Decomposition results of surfactants

Surfactant	D.T. at 2% M.L. (°C)	D.T. at 5% M.L. (°C)	% M.L. at 200°C	% M.L. at 275°C	T_{onset}	% M.L. at T_{onset}	Temperature at max decomposition rate, (°C)
TO-P Br	302	329	0.00	0.66	360	2.3	387
BZLTP-P Cl	338	339	0.00	0.00	340	0.1	345
BZL-IM PF6	336	350	0.13	0.20	362	1.3	392
BTL-IM PF6	289	335	0.48	1.61	367	5.7	412
BTL-IM Cl	141	232	3.02	44.25	259	4.0	285
DCL-IM Cl	84	186	5.00	85.28	245	5.3	270

D.T.: Decomposition Temperature

M.L.: Mass Loss

T_{onset}: Temperature corresponding to the cross-section of the two tangents around the main degradation point in TGA thermogram

Imidazolium Salts: The derivative TGA shows that the thermal decomposition of aryl (BZL-IM PF6) and alkyl (BTL-IM PF6) surfactants occurred in two steps as seen in Figure 4.65. The onset decomposition temperatures for aryl (BZL-IM PF6) and alkyl (BTL-IM PF6) were 362°C (1.3% mass loss) and 367°C (5.7% mass loss), respectively. The thermal decomposition of BZL-IM PF6 and BTL-IM PF6 (temperature at 5% mass loss) started at 350°C and 335°C, respectively. In addition, the maximum decomposition rate from derivative TGA curves was 392°C for BZL-IM PF6 and 412°C for BTL-IM PF6. At 200°C, the mass loss of the aryl (BZL-IM PF6) and alkyl (BTL-IM PF6) surfactants were 0.13 and 0.48 %, respectively. At 275°C, the mass loss of the aryl (BZL-IM PF6) and alkyl (BTL-IM PF6) surfactants were 0.20% and 1.61%, respectively. Although the onset decomposition temperature of BZL-IM PF6 was lower, the weight % values confirmed the better thermal stability of the aryl (BZL-IM PF6) compared to the alkyl (BTL-IM PF6). BTL-IM PF6 decomposed much faster than BZL-IM PF6 which contained benzyl groups with higher molecular weight and rigid chemical structure.

The type of the anion has an effect on the thermal stability of the di-alkyl imidazolium salts. The di-alkyl imidazolium salts with hexafluorophosphate anions exhibited more than 105°C increase in the onset decomposition temperature compared to the di-alkyl imidazolium salts with halide anions. The thermal stability increases in the order: PF6 > Cl, Br. The pyrolysis of the quaternary salts involves nucleophilic substitution SN1 or SN2 mechanism. Imidazolium quaternary salt most likely proceeds via SN2 process and the present results seem to support this understanding since the order of nucleophilicity is: $Br^- > Cl^- > F^-$. Awad et al. (7) showed similar results by using tri-alkyl imidazolium salts with about 100°C increase in the onset decomposition temperature for the hexafluorophosphate anions compared to the tri-alkyl imidazolium salts with halide anions. As expected, the presence of halide in BTL-IM Cl caused lower decomposition compared to BTL-IM PF6 with hexafluorophosphate anion. The onset decomposition temperatures for BTL-IM PF6 and BTL-IM Cl were 367°C (5.7% mass loss) and 259°C (4.0% mass loss), respectively. In addition, the maximum decomposition rate from derivative TGA curves was 412°C for BTL-IM PF6 and 285°C for BTL-IM Cl. The thermal decomposition of BTL-IM PF6 and BTL-IM Cl (temperature at 5% mass loss) started at 335°C and 232°C, respectively. At 200°C, the mass loss of the BTL-IM

PF6 and BTL-IM Cl surfactants were 0.48 and 3.02 %, respectively. At 275°C, the mass loss of BTL-IM PF6 and BTL-IM Cl surfactants were 1.61% and 44.25%, respectively. In addition to the above observations, the drastic mass loss of the halide salt confirms that the presence of halides cause drastic deterioration in the thermal stability of the salt and subsequently on the modified organoclay. Thus, their removal by washing after the ion exchange process is crucial.

BTL-IM Cl and DCL-IM Cl surfactants were compared according to the chain length attached to the first nitrogen atom. DCL-IM Cl with longer chain exhibited lower thermal stability and decomposed at earlier temperatures. The onset decomposition temperatures for BTL-IM Cl and DCL-IM Cl were 259°C (4.0% mass loss) and 245°C (5.3% mass loss), respectively. In addition, the maximum decomposition rate from derivative TGA curves was 285°C for BTL-IM Cl and 270°C for DCL-IM Cl. The thermal decomposition of BTL-IM Cl and DCL-IM Cl (temperature at 5% mass loss) started at 232°C and 186°C, respectively. At 200°C, the mass loss of the BTL-IM Cl and DCL-IM Cl surfactants were 3.02% and 5.00%, respectively. At 275°C, the mass loss of the BTL-IM Cl and DCL-IM Cl surfactants were 44.25% and 85.28%, respectively. This highlights the relationship observed between the chain length of the alkyl group and the thermal stability: as the chain length increased from butyl to decyl, the stability decreased.

4.5.1.2 TG/DrTGA Analysis of Clays/Organoclays

Clays: The thermal stability of the clay itself as a starting material is of great importance in the preparation of thermally stable organoclays. In addition, the purity and the drying conditions are crucial factors. The impurities available in the raw bentonite negatively affect its cation exchange capacity and thermal stability. From Figure 4.66, it is seen that the TGA thermograms of B, PB and M dried at 80°C exhibited a clear weight loss around 100°C due to the presence of water. PB dried at 80°C exhibited the expected less weight loss compared to B dried at 80°C, and both B and PB exhibited better results compared to M dried at 80°C. After drying B and PB at 120°C, the weight loss around 100°C due to moisture was minimized and the thermograms of B and PB shifted up with an approximate increase of 4 wt %. All thermograms, showed main decomposition temperatures in the range of 600°C

and 700°C. After purification, the thermal stability of the bentonite clay increased significantly. PB became more stable than before owing to the release of inorganic minerals that cause thermal instability of the clay. In Figure 4.67, the onset decomposition temperatures for B and PB were 628°C (3.0% mass loss) and 653°C (2.42% mass loss), respectively. In addition, the maximum decomposition rate from derivative TGA curves was 689°C for B and 728°C for PB. The thermal decomposition of B and PB (temperature at 5% mass loss) started at 666°C and 769°C, respectively. These results confirm the importance of purification of the raw bentonites before the ion exchange process.

In an attempt to understand the thermal degradation of the phosphonium and imidazolium-treated montmorillonite, the decomposition of the pristine bentonite should be considered first. The degradation process of intercalated montmorillonite reveals significant differences. For instance, pure montmorillonite does not exhibit any significant mass loss due to decomposition processes up to 300°C. Figure 4.67 shows the thermogravimetric analysis (TGA) and its derivative (Dr TGA), curves up to 900°C for the raw bentonite and purified bentonite. The large internal surface area of bentonite leads to the naturally occurring minerals being highly hydrated and hence releasing free water (water between particles and sorbed on the external surfaces of crystals) in the region up to 200°C. The weight loss in the TGA curves, and the derivative TGA peaks in this range may be attributed to the dehydration of interlayer water associated with the exchangable Na^{+} and Ca^{2+} ions (90°C to 135°C) with a minor contribution from physisorbed ‘free’ water (not bonded OH) held in interparticle pores. Between 200°C and 500°C, the organic substances evolve. The weight loss and the peaks at 500-800°C are associated with the loss of structural water (bonded OH that undergoes dehydroxylation) through dehydroxylation of the montmorillonite layers. In this range and above 700°C, the evolution of products associated with residual organic carbonaceous residue occurs up to 1000°C.

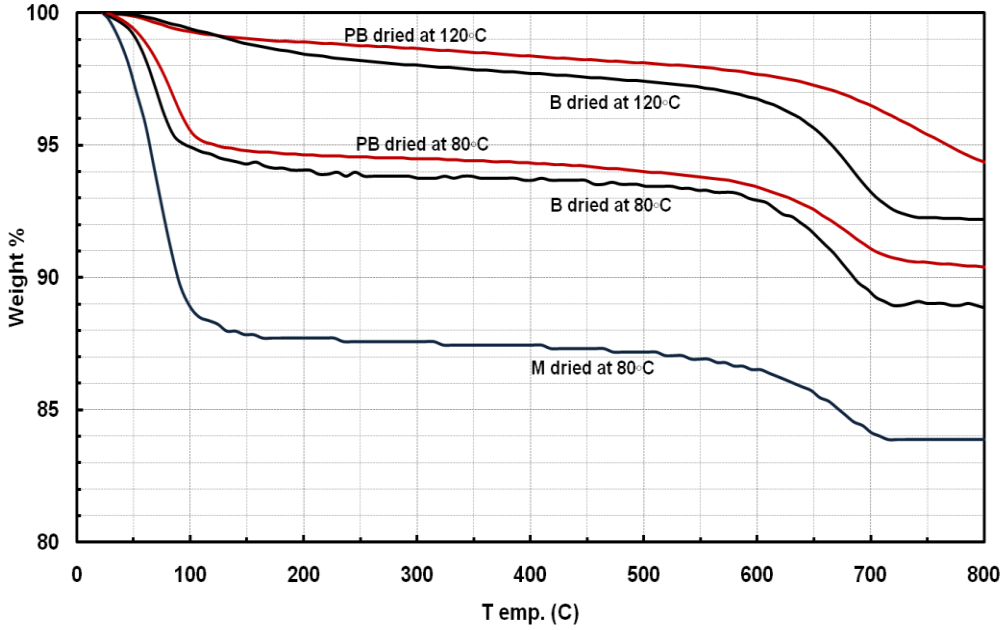

Figure 4.66 TGA thermograms of raw bentonite (B), purified bentonite (PB) and commercial montmorillonite (M) dried at different temperatures.

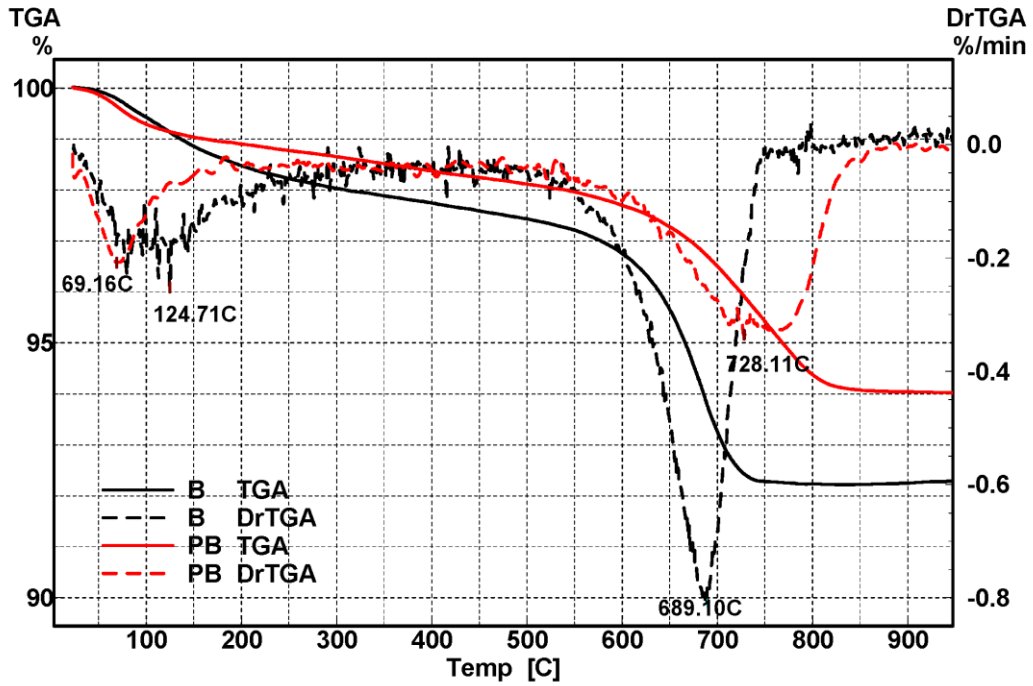

Figure 4.67 TG/DrTGA Thermograms of B and PB clays (Dried at 120°C)

Organoclays: Thermogravimetric measurements (TG/DrTGA) were carried out under nitrogen atmosphere on purified bentonites modified with phosphonium and imidazolium salts. The results are reported in terms of onset decomposition temperature and peak decomposition temperature from derivative thermograms in Table 4.17. The thermograms of the purified bentonites and organoclays are given in Figures 4.68 and 4.69, respectively.

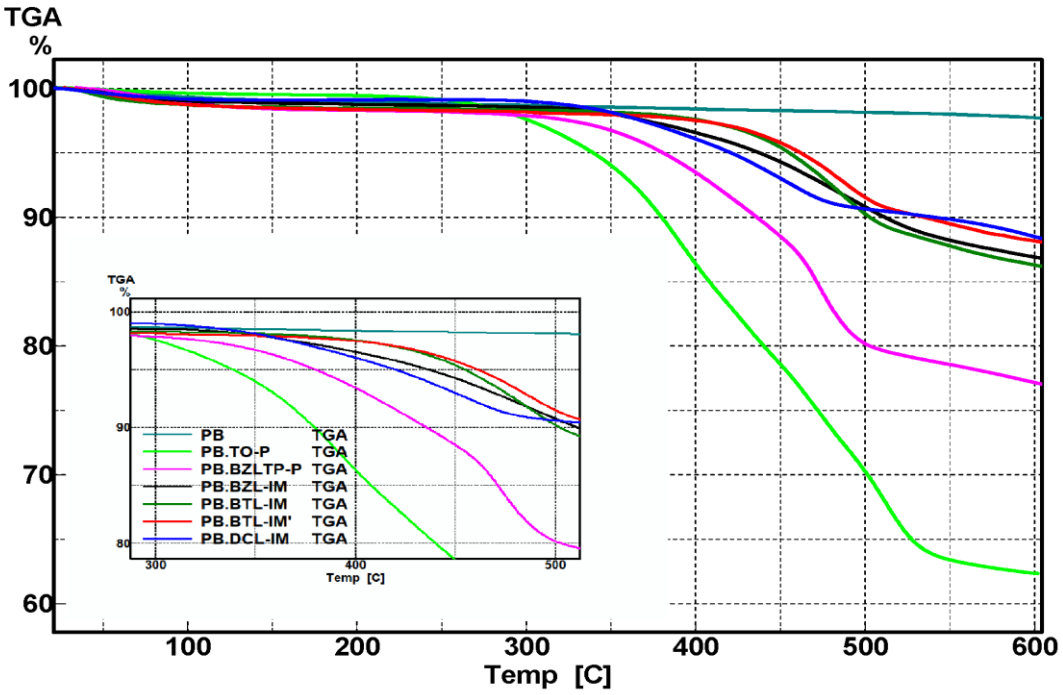

Figure 4.68 TGA thermograms of purified bentonite, and phosphonium and imidazolium organoclays

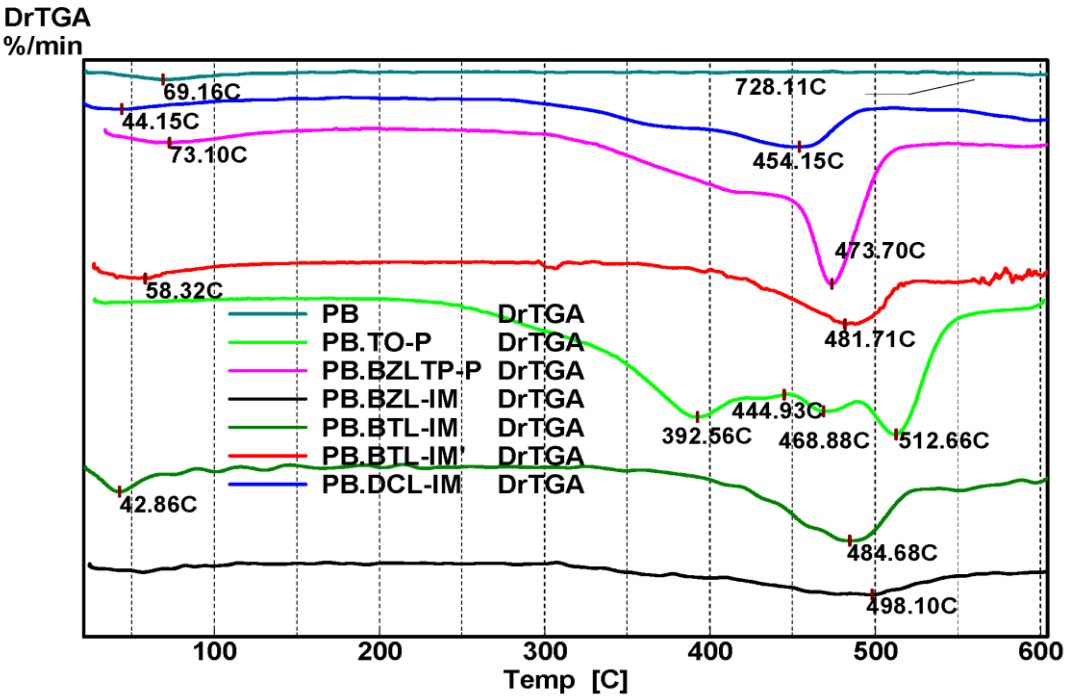

Figure 4.69 DrTGA thermograms of purified bentonite, and phosphonium and imidazolium organoclays

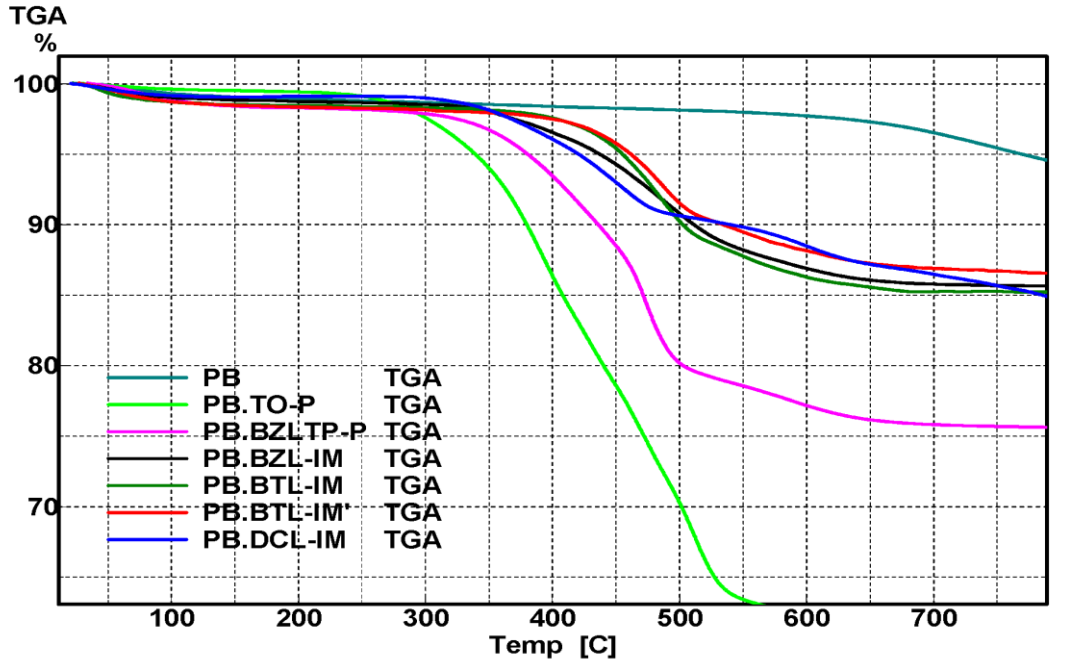

Figure 4.70 TGA thermograms of purified bentonite, and phosphonium and imidazolium organoclays (Up to 800°C)

Table 4.17 Decomposition results of bentonite clays and organoclays

Clay /Organoclay	D.T. at 2% M.L. (°C)	D.T. at 5% M.L. (°C)	% M.L. at 200°C	% M.L. at 275°C	T_{onset}	% M.L. at T_{onset}	Temperature at max Decomposition rate, (°C)
B	299	666	1.54	1.90	628	3.00	689
PB	533	769	1.10	1.31	653	2.42	728
PB.TO-P	290	338	0.66	1.45	327	0.88	513
PB.TOP 1.7	310	356	0.66	1.17	368	1.60	404
PB.BZLTP-P	284	380	1.73	1.95	354	2.75	474
PB.BZL-IM	349	438	1.26	1.40	380	1.70	498
PB.BTL-IM	371	454	1.54	1.68	433	2.51	485
PB.BTL-IM'	308	461	1.70	1.85	437	2.36	482
PB.DCL-IM	352	420	0.91	1.01	337	0.97	454

D.T.: Decomposition Temperature, M.L.: Mass Loss

Phosphonium Organoclays: The enhancement of thermal stability of phosphonium modified clay mean that it could be useful for polymers, which must be processed at temperatures above which the ammonium clays undergo degradation. From earlier studies, it is a well known fact that the onset temperature of the degradation of phosphonium modified clay is higher than that of ammonium clay, this difference is important in the melt compounding of some polymers melting above 200°C.

Thermal decomposition of ammonium salts generally follows either a Hoffmann elimination reaction or an SN2 nucleophilic substitution. Phosphonium-modified MMT decompose at higher temperatures than ammonium organoclays, although phosphonium surfactants are susceptible to similar reactions. Hoffmann elimination occurs in the presence of basic anions, such as hydroxyl groups, which extract hydrogen from the alkyl chain of the quaternary ammonium, yielding an olefinic and tertiary amino group (8).

The non-isothermal decomposition of quaternary phosphonium modified montmorillonite (PB.TO-P and PB.BZLTP-P) given in Figures 4.68 and 4.69 can be briefly considered in the regions mentioned before for the thermal decomposition of montmorillonites. Below 180°C, the evolution of absorbed water and gaseous species, such as physiabsorbed CO_2 and N_2, occurs. Between 250°C and 500°C, organic substances evolve. Dehydroxylation of the aluminosilicate occurs from 500°C to 700°C, and evolution of products associated with residual organic carbonaceous residue occurs between 700°C and 1000°C (8). The regions of interest for the production of polymer/organoclay nanocomposites exist below 500°C, where the release of small molecules associated with fabrication and storage of the phosphonium organoclay or the evolution of decomposition products may modify interfacial energies between the silicate and polymer.

After the intercalation of purified bentonite with phosphonium salts, the bentonite gained thermal stability depending on the structure of the salt. The onset decomposition temperatures for PB.TO-P and PB.BZLTP-P organoclays were 327°C (0.88% mass loss) and 354°C (2.65% mass loss), respectively. The aryl group substituted phosphonium organoclay (PB.BZLTP-P) showed a higher thermal

stability of 380°C (5% decomposition) in comparison to 338°C for the alkyl substituted phosphonium organoclay (PB.TO-P). For the salts, the molecular weight was dominant whereas for the organoclays, the phenyl and benzyl substituted organoclay PB.BZLTP-P exhibited better thermal stability. On the other hand, the maximum decomposition rate from derivative TGA curves was 513°C for PB.TO-P and 474°C for PB.BZLTP-P. At 200°C, the mass loss of the aryl (PB.BZLTP-P) and alkyl (PB.TO-P) substituted phosphonium organoclays were 0.66% and 1.73%, respectively. At 275°C, the mass loss of PB.BZLTP-P and alkyl PB.TO-P organoclays were 1.45% and 1.95%, respectively. These results are in good agreement with the alkyl and/or aryl phosphonium organoclays study done by Patel et al. in 2007 (71). In addition, these values are quite higher than the processing temperatures of PA66 and PET matrices used in this study. Using excess amount of TO-P Br salt (1.7*CEC) in PB.TO-P1.7 caused a significant improvement in the thermal stability (T_{onset} = 356°C) compared to PB.TO-P (1.1*CEC) (T_{onset} = 327°C) as shown in Figure 4.71.

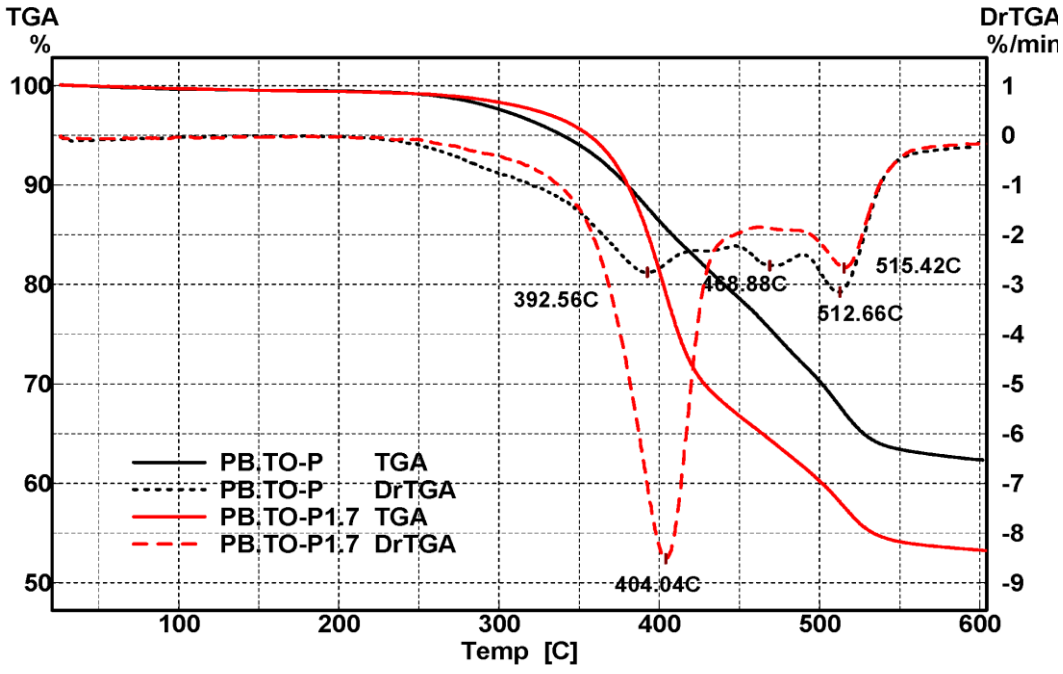

Figure 4.71 DrTGA thermograms of PB.TO-P and PB.TO-P1.7 organoclays

Imidazolium Organoclays: The TG/DrTGA graphs (Figures 4.68-4.69) show the outstanding thermal stability of di-imidazolium salts even after intercalation into the purified bentonite, as compared to phosphonium salts which are also more thermally stable than ammonium based organoclays.

The onset decomposition temperatures for PB.BZL-IM and PB.BTL-IM organoclays were 380°C (1.7% mass loss) and 433°C (2.5% mass loss), respectively. Interestingly, the benzyl group in PB.BZL-IM did not exhibit higher thermal stability in comparison to PB.BTL-IM. On the other hand, the onset decomposition temperatures of the salts BZL-IM PF6 and BTL-IM PF6 were 362°C (1.3% mass loss) and 367°C (5.7% mass loss), respectively.

BTL-IM PF6 and BTL-IM Cl have the same molecular weight (after exchange of the PF6 and Cl groups) and their subsequent organoclays exhibited close thermal decomposition results. The onset decomposition temperatures for PB.BTL-IM and PB.BTL-IM' organoclays were 433°C (2.5% mass loss) and 437°C (2.4% mass loss), respectively. On the other hand, it seems that there is no significant improvement in the thermal stability of the intercalated hexafluorophosphate salts; this may be due to the weak nucleophilicity of PF_6^- anions.

The onset decomposition temperatures for PB.BTL-IM' and PB.DCL-IM organoclays were 437°C (2.4% mass loss) and 337°C (1.0% mass loss), respectively. Both, PB.BTL-IM' and PB.DCL-IM organoclays exhibited highly significant increase in the thermal stability in a similar manner to the salts BTL-IM Cl and DCL-IM Cl confirming that the increase in the chain length of the alkyl group also decreases the thermal stability of organoclays which is in agreement with tri-alkyl imidazolium organoclays study done by Awad et al. (7).

The dramatic increase in the thermal stability of both phosphonium (PB.TO-P and PB.BZLTP-P) and imidazolium (PB.BTL-IM and PB.DCL-IM) organoclays as compared to their salts can be attributed to the crucial removal of the halide. This reflects the importance of getting rid of the entire halide residue that may contaminate the intercalated product after the ion exchange.

To sum up, the discussion of various phosphonium and imidazolium surfactant and organoclays with good thermal stability confirms the superior thermal stability of these materials considering polymer processing temperatures in the range of 200°C - 350°C. The onset decomposition temperatures of the organoclays ranged between 327 - 437°C. The weight losses of the phosphonium and imidazolium substituted organoclays were in the range of 1.01 - 1.95 % at the processing temperature of 275°C for the polymers PA66 and PET used in this study. The maximum decomposition temperatures found from derivative TGA thermograms were in the range 454 - 513°C which is quite higher from both the processing temperatures of PA66 and PET, and the conventional quaternary alkylammonium organoclays mainly used in the production of polymer layered silicate nanocomposites.

4.5.1.3 TGA/DTA Results of PA66 Compositions

The thermal stability of the surfactant molecules used is crucial in the production of high melting PA66 nanocomposites. The most commonly used quaternary ammonium surfactants are not very stable at temperatures above 200°C. It has been shown that the combination of high processing temperatures in combination and high shear stresses causes even more degradation than high temperatures without shear. For short processing times the degradation is not much of a problem in the case of PA6 (processed at 240°C), but at the temperatures required for PA66 melt processing (minimum 270°C) the problem is much more serious. It has been reported that PA66 nanocomposites cannot be made via the same process and with the same modified silicates while other authors have shown that it is possible, with reasonably good results (116).

The thermal decomposition data of all PA66 compositions taken under nitrogen atmosphere are given in Table 4.18. The TG/DrTG/DTA graphs of each composition are given in Appendix B.1.

Table 4.18 Thermal decomposition results of PA66 compositions

Composition	T onset (°C)	D.T. at 2% M.L. (°C)	D.T. at 5% M.L. (°C)	M.L. at 275°C (%)	C.Y. at 600°C (%)
Polymer					
PA66	408	365	392	1.20	4.1
Polymer/Elastomer Blend					
PA66/E-BA-MAH	403	370	392	0.89	2.4
Polymer/Organoclay Binary Nanocomposites					
PA66/PB.TO-P	432	378	408	0.34	9.0
PA66/PB.BZLTP-P	427	381	410	0.59	3.5
Polymer/Organoclay/Elastomer Ternary Nanocomposites					
PA66/PB.TO-P/E-BA-MAH	415	380	400	0.66	3.0
PA66/PB.BZLTP-P/E-BA-MAH	412	368	397	1.16	3.1

Decomposition Temperature: D.T., Mass Loss: M.L., Char Yield: C.Y.

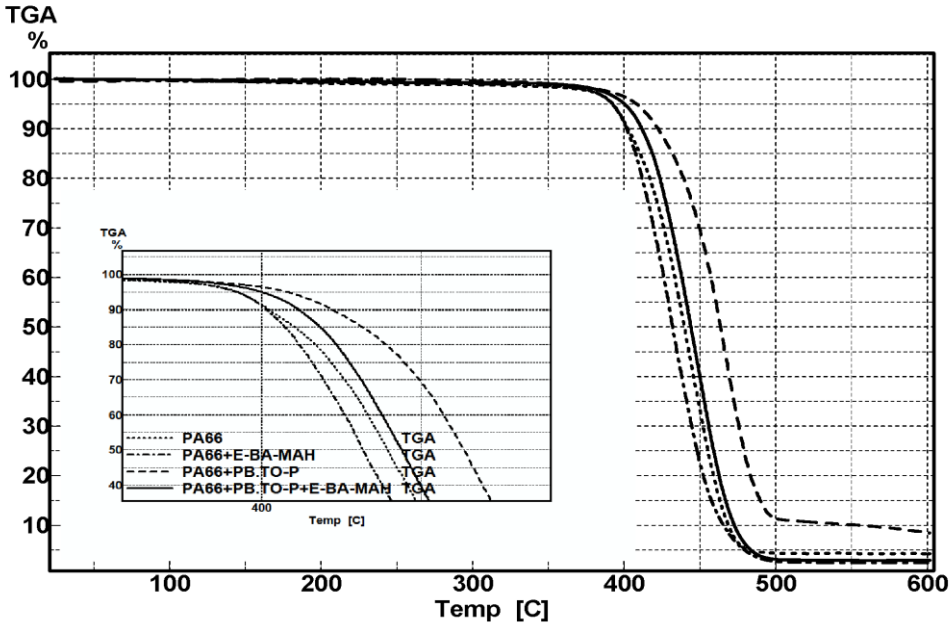

Figure 4.72 TGA thermograms of PA66, PA66/E-BA-MAH, PA66/PB.TO-P, PA66/PB.TO-P/E-BA-MAH

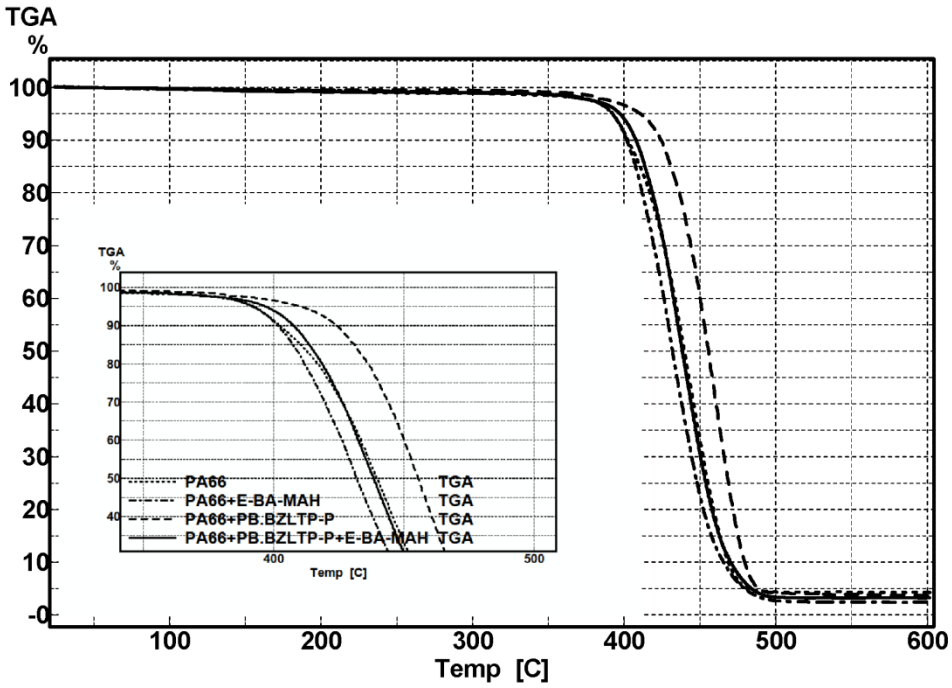

Figure 4.73 TGA thermograms of PA66, PA66/E-BA-MAH, PA66/PB.BZLTP-P, PA66/PB.BZLTP-P/E-BA-MAH

Figures 4.72 and 4.73 present the TGA graphs of PB.TO-P and PB.BZLTP-P containing nanocomposites compared to pure PA66 and PA66/E-BA-MAH blend. It can be clearly seen that the addition of the E-BA-MAH elastomer into PA66 causes an earlier decomposition of the PA66/E-BA-MAH blend. This decrease resulting from using the elastomer is mainly compensated by higher mechanical properties and especially higher toughness of the blend. Qin et al. (2003) studied the thermal stability and flammability of PA 66/ammonium organoclay nanocomposites. When compared to the pristine polymer, the onset decomposition temperature of the binary nanocomposite was 10°C lower than that of pure PA 66 in nitrogen atmosphere. The thermal behavior of the nanocomposites in N_2 atmosphere indicated that the addition of MMT accelerated the thermal decomposition of PA 66 matrix, a fact the researchers associated to the catalysis of water evolved from MMT (adsorbed or from dehydroxylation) (40). However, in our case, using thermally stable phosphonium organoclays revealed that the barrier effect of the silicate layers was dominant due to the formation of carbonaceous-silicate char on the surface of nanocomposite in which the onset decomposition temperature was

22°C and 17°C higher for PA66/PB.TO-P and PA66/PB.BZLTP-P binary nanocomposites, respectively. The onset decomposition temperatures for PA66/PB.TO-P and PA66/PB.BZLTP-P binary nanocomposites were 432°C and 427°C, respectively. On the other hand, PA66/phosphonium organoclay/E-BA-MAH ternary nanocomposites exhibited improvement in the thermal stability compared to the pristine PA66 polymer, and a decrease in the onset decomposition temperature compared to PA66 binary nanocomposites owing to the presence of the elastomer. The onset decomposition temperatures for PA66/PB.TO-P/E-BA-MAH and PA66/PB.BZLTP-P/E-BA-MAH ternary nanocomposites were 415°C and 412°C, respectively.

4.5.1.4 TGA/DTA Results of PET Compositions

Polyester-based nanocomposites are considered as novel materials with promising properties for e.g. packaging applications. PET nanocomposites are often prepared at elevated processing temperatures above 280°C. Since the thermal stability of organoclays with alkyl-ammonium cations has caused severe problems during processing of PET, the present research has been directed toward the preparation of organoclays that are thermally stable at high temperatures. For instance, polyester/clay nanocomposites prepared through in-situ polymerization resulted in high levels of dispersion and improved physical properties; however, a more commercially viable approach with conventional polymer processing led to poorly dispersed clay in the polymer matrix. The researchers attributed this phenomenon to the low decomposition temperature (250°C) of the organic modifier bound to the clay surface.

The thermal decomposition data of all PET compositions taken under nitrogen atmosphere are given in Table 4.19. The TG/DrTG/DTA graphs of all the compositions are given in Appendix B.2.

Table 4.19 Thermal decomposition results of PET compositions

Composition	T onset (°C)	D.T. at 2% M.L. (°C)	D.T. at 5% M.L. (°C)	M.L. at 275°C (%)	C.Y. at 600°C (%)
Polymer					
PET (Extruded Twice)	413	386	400	0.41	14.0
Polymer/Elastomer Blend					
PET/E-MA-GMA	412	391	401	0.10	12.6
Polymer/Organoclay Binary Nanocomposites					
PET/PB.TO-P	420	345	396	1.92	8.2
PET/PB.BZLTP-P	424	395	409	0.29	15.9
PET/PB.BZL-IM	423	393	407	0.30	12.9
PET/PB.BTL-IM	423	398	411	0.30	18.0
PET/PB.BTL-IM’	427	400	412	0.14	17.5
PET/PB.DCL-IM	422	397	409	0.07	17.3
Polymer/Organoclay/Elastomer Ternary Nanocomposites					
PET/PB.TO-P/E-MA-GMA	410	382	395	0.16	11.3
PET/PB.BZLTP-P/E-MA-GMA	423	394	408	0.18	13.5
PET/PB.BZL-IM/E-MA-GMA	422	397	410	0.09	12.7
PET/PB.BZL-IM/E-MA-GMA (E3)	422	396	408	0.46	13.0
PET/PB.BTL-IM/E-MA-GMA	428	400	411	0.07	14.8
PET/PB.BTL-IM’/E-MA-GMA	417	389	405	0.29	3.4
PET/PB.DCL-IM/E-MA-GMA	422	396	409	0.40	14.0

Decomposition Temperature: D.T., Mass Loss: M.L., Char Yield: C.Y.

Figures 4.74 and 4.75 show the TGA graphs of PB.TO-P and PB.BZLTP-P containing nanocomposites compared to pure PET and PET/E-MA-GMA blend. It can be clearly seen that the addition of the E-MA-GMA elastomer into PET caused no significant change on the decomposition of the PET/E-MA-GMA blend. Bandyopadhyay et al. (2007) investigated the thermal stability of PET/ammonium organoclay nanocomposites. The onset decomposition temperatures of the binary

nanocomposites were 10°C lower than pure PET in nitrogen atmosphere. The thermal behavior of the nanocomposites in N_2 atmosphere indicated that the addition of alkylammonium organoclays accelerated the thermal decomposition of PET matrix, which is attributed to the catalysis of water evolved from MMT. The onset decomposition temperatures for PET/PB.TO-P and PET/PB.BZLTP-P binary nanocomposites were 420°C and 424°C, respectively. The thermally stable phosphonium organoclays revealed that the barrier effect of the silicate layers was dominant due to the formation of carbonaceous-silicate char on the surface of nanocomposites, thus the onset decomposition temperature was 7°C and 11°C higher for PET/PB.TO-P and PET/PB.BZLTP-P binary nanocomposites, respectively. On the other hand, PET/phosphonium organoclay/E-MA-GMA ternary nanocomposites exhibited improvement in the thermal stability compared to the pristine polymer, without any decrease in the onset decomposition temperature compared to PET binary nanocomposites owing to the presence of the elastomer, except for PB.TO-P containing ternary nanocomposite which exhibited lower onset decomposition temperature (410°C), whereas the onset decomposition temperature for PET/PB.BZLTP-P/E-MA-GMA ternary nanocomposite was 423°C.

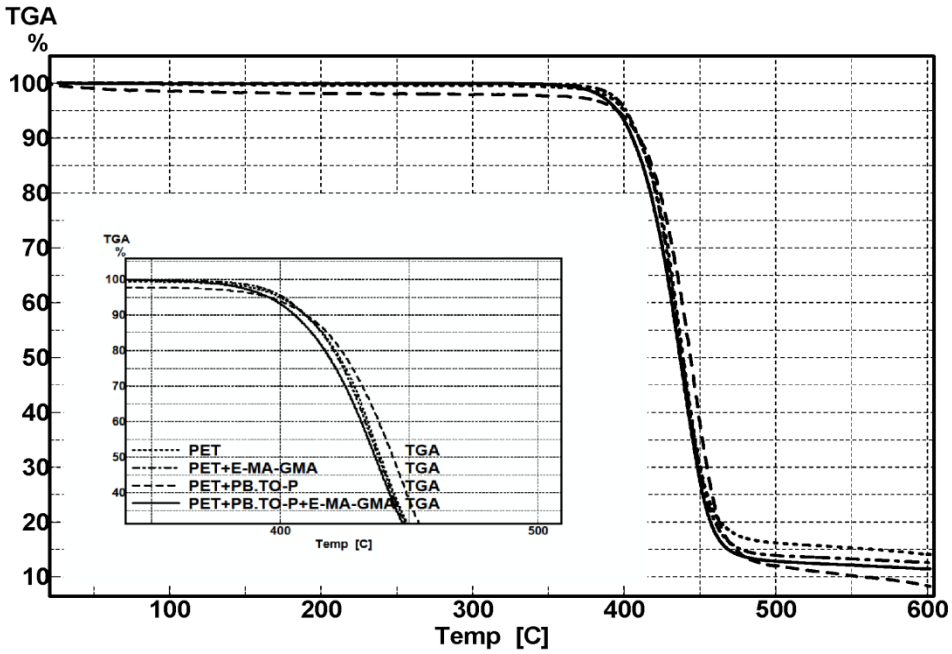

Figure 4.74 TGA thermograms of PET, PET/E-MA-GMA, PET/PB.TO-P, PA66/PB.TO-P/E-MA-GMA

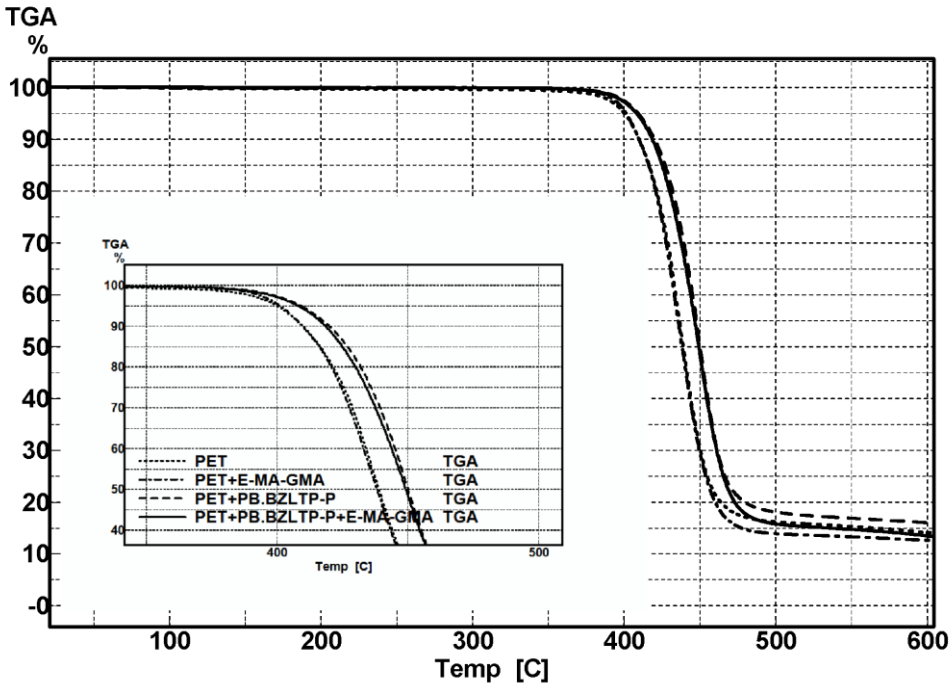

Figure 4.75 TGA thermograms of PET, PET/E-MA-GMA, PET/PB.BZLTP-P, PA66/PB.BZLTP-P/E-MA-GMA

Figures 4.76 through 4.79 present the TGA graphs of PB.BZL-IM, PB.BTL-IM, PB.BTL-IM' and PB.DCL-IM containing nanocomposites compared to pure PET and PET/E-MA-GMA blend. From these figures and Table 4.19, it is clearly seen that the onset decomposition temperatures of all binary and ternary nanocomposites increased by 5 to 15°C indicating the superior effect of thermally stable imidazolium organoclays used.

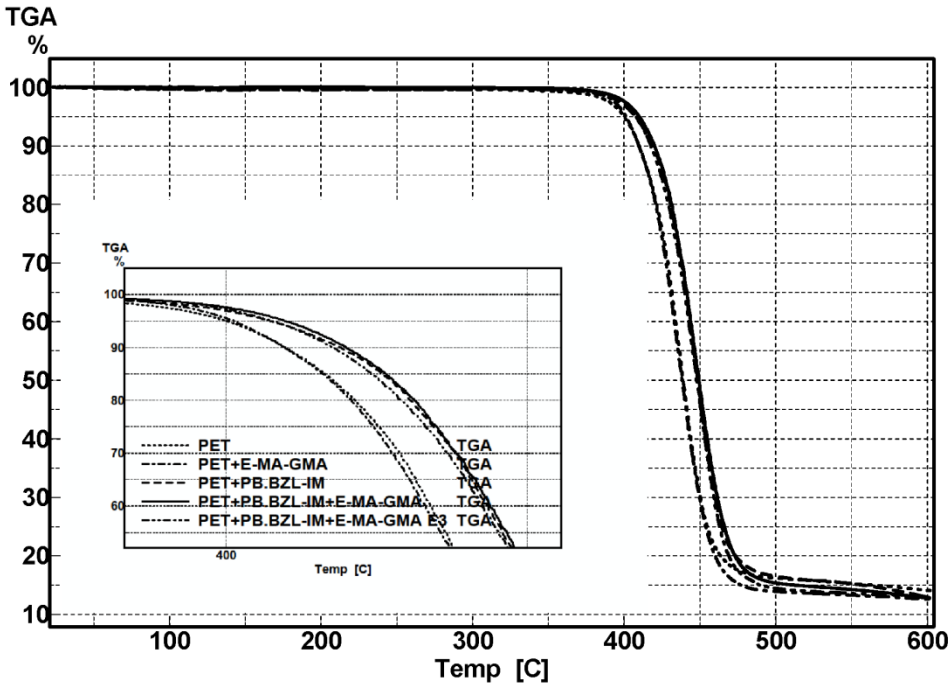

Figure 4.76 TGA thermograms of PET, PET/E-MA-GMA, PET/PB.BZL-IM, PET/PB.BZL-IM/E-MA-GMA, PET/PB.BZL-IM/E-MA-GMA (E3)

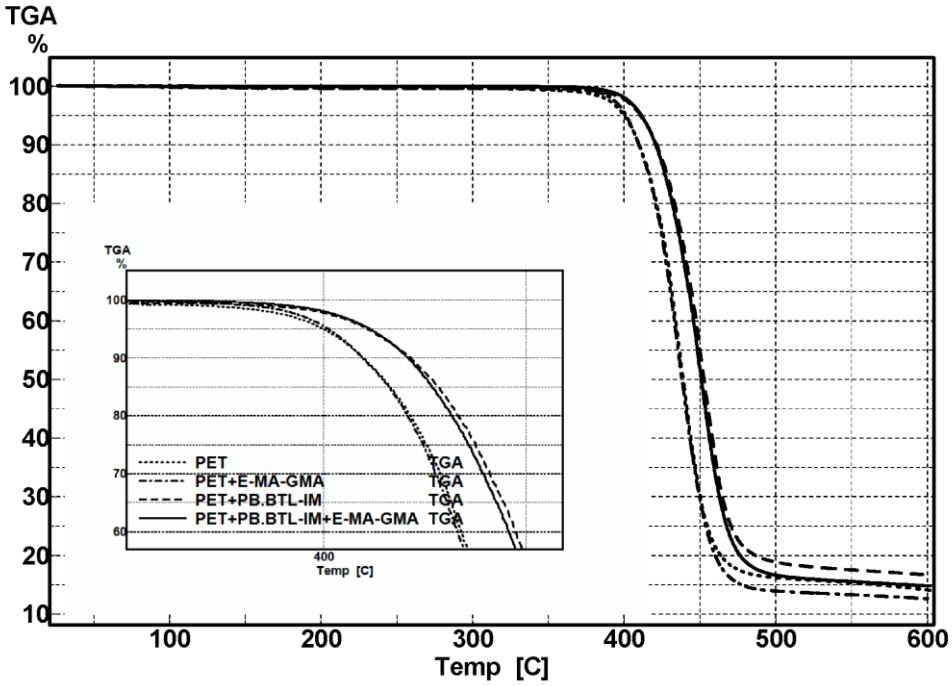

Figure 4.77 TGA thermograms of PET, PET/E-MA-GMA, PET/PB.BTL-IM, PET/PB.BTL-IM/E-MA-GMA

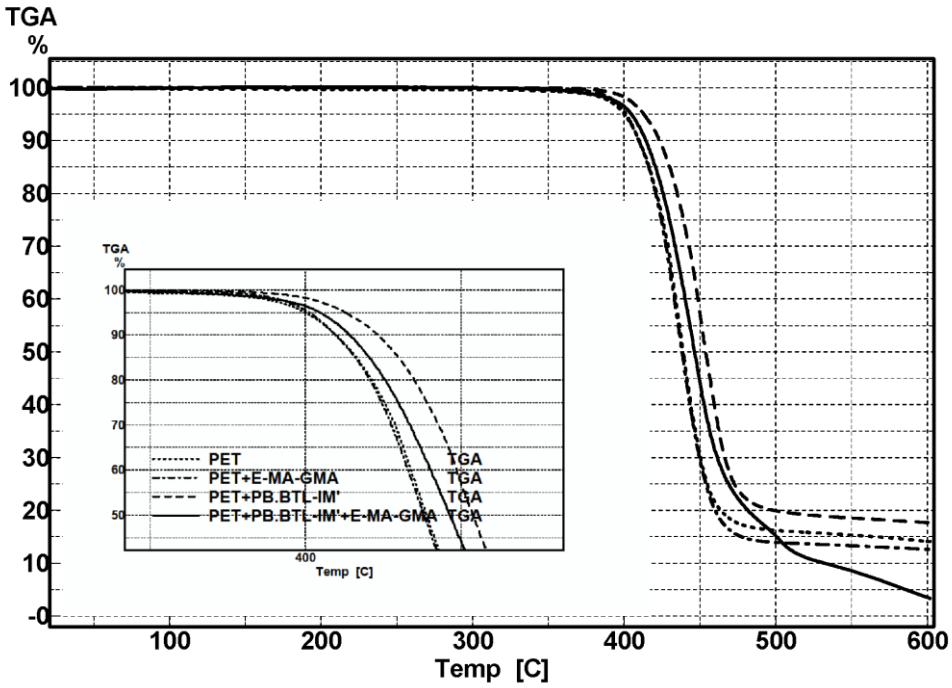

Figure 4.78 TGA thermograms of PET, PET/E-MA-GMA, PET/PB.BTL-IM', PET/PB.BTL-IM'/E-MA-GMA

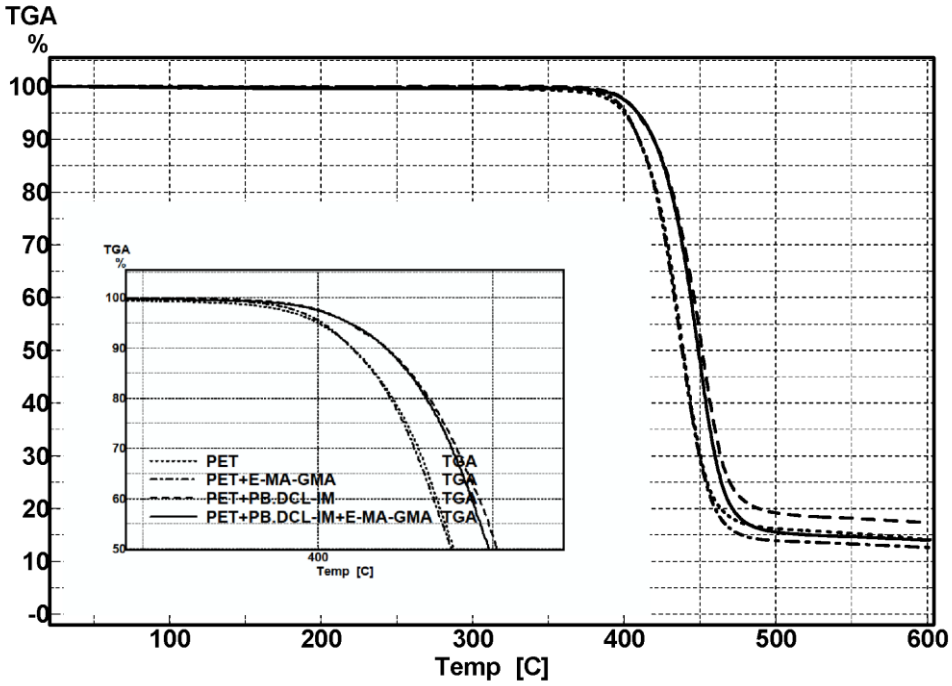

Figure 4.79 TGA thermograms of PET, PET/E-MA-GMA, PET/PB.DCL-IM, PET/PB.DCL-IM/E-MA-GMA

In all compositions for PA66 and PET, it can be seen that the nanocomposites containing organoclay exhibit thermal stability superior to the pristine polymer. This suggests that in the range of the processing temperatures used, the degradation of the system did not occur. The thermal stability of the organoclays and the onset decomposition temperature for all compositions were improved. Apparently, organoclays have two opposing functions in the thermal stability of the nanocomposites, one is due to barrier property to the oxygen and the other is due to the catalysis effect which speeds the degradation of the polymer, but the barrier effect is predominant with the addition of low fraction of clay to the polymer matrix, as observed in this work. Although the XRD results showed slight improvement in the basal spacing of the bentonite clays after treatment for imidazolium salts, the thermally stable phosphonium and imidazolium surfactants exhibited significant thermal improvement in the resulting organoclays and thus in the polymer nanocomposites prepared by these organoclays.

4.5.2 Differential Scanning Calorimetry Analysis

The degree of crystallinity is the most important characteristic of a polymer in that it determines mechanical properties, such as yield stress, elastic modulus and impact resistance (160). The percent crystallinity of the polyamide phase is calculated as the ratio of the heat of fusion of the sample (ΔH_f), divided by the weight fraction of polyamide in the nanocomposite and the heat of fusion of the pure crystalline form of polyamide-6 (ΔH_f^o).

The melting point and crystallinity were studied to determine the effects of the organoclay and elastomer additives, which are expected to influence the percentage crystallinity and consequently the mechanical properties and deformation mechanisms in PA66.

4.5.2.1 DSC Results of PA66 Nanocomposites

DSC thermograms of pure PA66, PA66/E-BA-MAH blend, binary and ternary nanocomposites are listed in Appendix C, Figures C. 1 through C.10. Crystallinity of

the polyamide phase in all the combinations was determined by DSC analysis and the results are given below in Table 4.20.

Table 4.20 Thermal properties of all PA66 compositions

Composition	T_m (°C)	ΔH_f (J/g)	Crystallinity (%)
Polymer			
PA66 (Extruded Twice)	264.9	53.4	25.9
Polymer/Elastomer Blend			
PA66/E-BA-MAH	263.6	74.8	38.2
Polymer/Organoclay Binary Nanocomposites			
PA66/PB.TO-P	263.5	66.6	33.0
PA66/PB.BZLTP-P	265.9	66.6	33.0
Polymer/Organoclay/Elastomer Ternary Nanocomposites			
PA66/PB.TO-P/E-BA-MAH (1-S)	263.3	57.3	29.6
PA66/PB.TO-P/E-BA-MAH (1-P)	264.5	65.3	33.7
PA66/PB.TO-P/E-BA-MAH (2-P)	264.5	56.0	28.9
PA66/PB.TO-P/E-BA-MAH (2-S)	265.7	63.0	32.5
PA66/PB.TO-P/E-BA-MAH	265.5	61.7	32.2
PA66/PB.BZLTP-P/E-BA-MAH	267.3	68.6	35.8

The melting temperature of PA66 did not significantly change upon blending with E-BA-MAH in PA66/E-BA-MAH blend. However, the crystallinity increased significantly implying acceleration of the crystallization process in the presence of E-BA-MAH, probably because of enhanced nucleation.

The degree of crystallinity was found to be dependent on additives such as the organoclay and the elastomer in PA66 nanocomposites. The melting point did not change significantly in PA66/phosphonium organoclay binary nanocomposites. The crystallinity of PA66 is increased by 7% upon adding the phosphonium organoclays (33.0 %) compared to 25.9 % for pure PA66, which is attributed to the heterogeneous nucleation of montmorillonite organoclays. The crystallization of

PA66/organoclay nanocomposites proceeds mainly via heterogeneous nucleation since the number of clay layers is so large, whereas neat PA66 proceeds via both heterogeneous and homogeneous nucleation mechanisms. Homogeneous nucleation requires a low temperature to form stable nucleation since it starts spontaneously by chain aggregation below the melting point. On the other hand, heterogeneous nuclei form simultaneously as soon as the sample reaches the crystallization temperature. Thus, the temperature to reach the maximum crystallization rate in neat PA66 is expected to be lower than that of PA66/organoclay binary nanocomposites (108). In general, the overall crystallization process is governed by two processes, diffusion and nucleation. Diffusion is controlled by the activation energy for transporting a polymer segment to a growing crystal and nucleation is related to the thermodynamic driving force required to nucleate new layers on the crystal (53).

In general, it has been shown that the clay layers affected the formation of the lamellae, spherulites, crystallization rate, and also the crystalline phase. It was proposed by many authors that an increase in crystallinity or spherulite size in polymeric materials could increase the tensile strength and Young's modulus, and decrease impact strength and elongation at break. These effects are clearly seen in the mechanical properties of PA66 binary nanocomposites in addition to the mechanical effects of the clay. The tensile strengths and Young's moduli of PA66/PB.TO-P (89.6 MPa, 2.942 GPa) and PA66/PB.BZLTP-P (88.8 MPa, 2.773 GPa) binary nanocomposites increased compared to pure PA66 (83.7 MPa, 2.734 GPa). The elongation at break and impact strength values of PA66/PB.TO-P (13.9 %, 7.0 kJ/m^2) and PA66/PB.BZLTP-P (12.2 %, 6.2 kJ/m^2) binary nanocomposites decreased compared to pure PA66 (23.3 %, 7.0 kJ/m^2).

Considering the differences in the percentage crystallinity of neat PA66, binary and ternary nanocomposites after blending with elastomer or reinforcing with phosphonium organoclay in PA66, it is thought that the balanced mechanical properties of the ternary nanocomposites (Sections 4.4.1.1 and 4.4.2.1) are also affected by the additives. The correlation of property and structure is complicated and depends on morphology and processing factors that affect both the inorganic/organic filler and polymer, such as the orientation of silicate layers, their

effect on polymer conformation and morphology, and the dispersion of fillers in the matrix.

The tensile strengths and Young's moduli of PA66/PB.TO-P/E-BA-MAH (82.9 MPa, 2.542 GPa) and PA66/PB.BZLTP-P/E-BA-MAH (74.2 MPa, 2.349 GPa) ternary nanocomposites decreased compared to pure PA66 and binary nanocomposites due to the presence of the elastomeric phase.

The elongation at break values increased in PA66/PB.TO-P/E-BA-MAH (24.3 %) and decreased in PA66/PB.BZLTP-P/E-BA-MAH (14.7 %) ternary nanocomposites. PB.TO-P containing ternary nanocomposites (wt% 1 and 2) exhibited impact strength values ranging from 8.4 to 10.4 kJ/m^2 and directly proportional to crystallinity values (values range from 28.9 to 33.7 %). The more the crystallinity increased, the impact strength decreased. On the other hand, PA66/PB.BZLTP-P/E-BA-MAH ternary nanocomposite with highest crystallinity (35.8 %) exhibited lowest impact strength of 7.8 kJ/m^2. The chemical structure of the organoclay PB.BZLTP-P with aromatic groups showed less compatibility with PA66 compared to PB.TO-P with aliphatic groups. In PB.TO-P ternary composite with 1 wt % organoclay, the crystallinity increased substantially indicating the nucleating behavior of organoclays. Also it is known that for uniform organoclay content, the more the organoclay is exfoliated, the higher crystallinity would be owing to the nucleating effect. A correlation could not be found regarding pelletizing procedure or number of extrusions but the effect of clay content was clearly seen in mechanical properties in which PA66/PB.TO-P/E-BA-MAH (with 2 wt %) exhibited slightly higher values in tensile strength and Young's modulus, and slightly lower values in elongation at break and impact strength compared to 1 wt % compositions.

4.5.2.2 DSC Results of PET Nanocomposites

Amorphous PET is of little commercial value since it has poor mechanical properties, low dimensional stability and high gas permeation rate. On the other hand, crystalline PET has higher strength, good dimensional stability and chemical resistance. It is widely used in the production of fibers and in carbonated beverage

containers because of its strength and low gas permeability, especially to carbon dioxide and oxygen (160). The importance of crystallinity was thus clearly vital on the properties of a composite when produced as a final product. The effect of MMT on the crystallization behavior of PET during heating is examined by DSC. DSC thermograms of pure PET, PET/E-MA-GMA blend, and binary and ternary nanocomposites are listed in Appendix C, Figures C.11 through C.25. Crystallinity values of the PET phase in all the combinations are given in Table 4.21.

Table 4.21 Thermal properties of all PET compositions

Composition	T_m (°C)	ΔH_f (J/g)	Crystallinity (%)
Polymer			
PET (Extruded Twice)	254.5	54.9	40.4
Polymer/Elastomer Blend			
PET/E-MA-GMA	253.3	49.5	38.3
Polymer/Organoclay Binary Nanocomposites			
PET/PB.TO-P	253.0	52.6	39.5
PET/PB.BZLTP-P	252.7	55.9	41.9
PET/PB.BZL-IM	255.7	46.3	34.7
PET/PB.BTL-IM	256.2	46.4	34.8
PET/PB.BTL-IM’	255.9	38.6	29.0
PET/PB.DCL-IM	256.4	36.3	27.2
Polymer/Organoclay/Elastomer Ternary Nanocomposites			
PET/PB.TO-P/E-MA-GMA	256.3	43.5	34.4
PET/PB.BZLTP-P/E-MA-GMA	252.8	46.0	36.4
PET/PB.BZL-IM/E-MA-GMA	254.8	40.1	31.7
PET/PB.BZL-IM/E-MA-GMA (E3)	253.7	51.8	40.9
PET/PB.BTL-IM/E-MA-GMA	254.7	36.8	29.1
PET/PB.BTL-IM’/E-MA-GMA	255.0	39.4	31.1
PET/PB.DCL-IM/E-MA-GMA	256.1	33.5	26.5

The crystallinity decreased slightly upon the addition of E-MA-GMA elastomer in PET/E-MA-GMA blend (38.3 %) implying the retardation of the crystallization process compared to pure PET (40.4 %). The melting point also decreased due to the dilution effect of the elastomer, similar to freezing point depression.

A strong nucleating effect of organoclays in polymer/MMT nanocomposites is usually expected, due to the dispersion of the clay at the nanometric scale, providing a large interfacial area susceptible to promote heterogeneous crystallization. The clay dispersion (weak or strong) at the nanometric level cannot be the only factor influencing the crystallization in polymer/montmorillonite composites. Amorphous PET molded under glass transition temperatures usually have slow crystallization rate (11), and the usage of organoclay did not promote the nucleation process in the present study. The results obtained in the present work suggest that the clay/polymer interface properties also affect crystalline structure formation. Phosphonium based binary nanocomposites did not show significant effects as nucleating agents, whereas imidazolium based binary nanocomposites decreased the crystallinity. The nature of the salt as intercalating agent might have influenced the crystallization kinetics by affecting the clay dispersion level and the organoclay/polymer interface properties. PET/imidazolium organoclay composites present comparable clay dispersion levels but different crystallization rates. In addition, the thermal decomposition of the salt and thus organoclay might also play a role in the crystallization process, although it is difficult to quantify it. The mold temperature can be increased up to 140^{o}C and nucleating agents can be used in order to promote the nucleation process.

The presence of additives such as organoclay and elastomer affected the crystallinity in PET nanocomposites slightly. The melting point did not change significantly in PET/phosphonium organoclay binary nanocomposites. The crystallinity of PET/PB.TO-P binary nanocomposite (39.5 %) decreased slightly, and PET/PB.BZLTP-P (41.9 %) increased slightly compared to pure PET extruded twice (40.4 %). The mechanical behavior of these composites was in good agreement with DSC results. However, crystallinity is not the only factor affecting the mechanical properties. The tensile strengths and Young's moduli of PET/PB.TO-P (56.9 MPa, 1.959 GPa) and PET/PB.BZLTP-P (56.1 MPa, 2.145

GPa) binary nanocomposites increased compared to pure PET (52.5 MPa, 1.749 GPa). The elongation at break values and impact strengths of PET/PB.TO-P (123.7 %, 3.1 kJ/m^2) and PET/PB.BZLTP-P (2.4 %, 3.2 kJ/m^2) binary nanocomposites changed substantially compared to pure PET (3.9 %, 2.9 kJ/m^2). PB.BZLTP-P based binary nanocomposite exhibited higher crystallinity and PB.TO-P based binary nanocomposites exhibited lower crystallinity than pure PET. It should be noted that PB.TO-P based binary composites extended much more than pure PET. The mechanical behavior is in good agreement with the crystallinity regarding elongation at break whereas impact strength values changed slightly.

The incorporation of imidazolium organoclay in PET binary nanocomposites decreased the crystallinity which is mainly attributed to the polymer/organoclay interactions related to chemical structure of the organoclay. PB.DCL-IM with long alkyl chain exhibited the lowest crystallinity among imidazolium based binary nanocomposites. The presence of benzyl groups in PB.BZL-IM resulted in the maximum deterioration in all mechanical properties such as, the decrease in tensile strength and Young's modulus values and the least increase in elongation at break values among all binary nanocomposites. Impact strength values ranged between 3.1 to 3.2 kJ/m^2 for all the imidazolium based compositions. PB.BTL and PB.BTL-IM' exhibited comparable mechanical values with small difference in crystallinity values.

The mechanical properties of the ternary nanocomposites (Sections 4.4.1.2 and 4.4.2.2) are due to the effects of the organoclay and elastomer additives. PB.BZLTP-P based ternary nanocomposite exhibited higher crystallinity values compared to PB.TO-P based ternary nanocomposite, and the reflection of this on mechanical behavior is clearly observed in the strength and toughness results, except for tensile strengths which exhibited opposite results. The tensile strengths and Young's moduli of PET/PB.BZLTP-P/E-MA-GMA (46.1 MPa, 1.641 GPa) and PET/PB.TO-P/E-MA-GMA (49.6 MPa, 1.640 GPa) ternary nanocomposites were decreased by the presence of the organoclay and elastomeric phase compared to pure PET extruded twice. The elongation at break and impact strength values of PET/PB.TO-P/E-MA-GMA (96.4 %, 4.7 kJ/m^2) and PET/PB.BZLTP-P/E-MA-GMA (4.4 %, 3.4 kJ/m^2) ternary nanocomposites changed in accordance with crystallinity.

The presence of benzyl groups in PB.BZL-IM exhibited the maximum deterioration in all mechanical properties of binary and ternary PET nanocomposites such as, a decrease in tensile strength and Young's modulus values and the least increase in elongation at break values and impact strength among all imidazolium based ternary PET nanocomposites. Impact strength values ranged between 3.9 to 5.2 kJ/m^2 for all imidazolium based ternary nanocomposites owing to the presence of the elastomer which acts as an impact modifier.

Increasing number of extrusion to three times in PET/PB.BZL-IM/E-MA-GMA (E3) ternary nanocomposite increased the crystallinity among imidazolium based ternary nanocomposites. However, the strength and elongation at break values in this nanocomposite behaved oppositely. On the other hand, the Young's modulus increased and the impact strength decreased from 3.9 to 3.0 kJ/m^2 as expected.

PB.BTL and PB.BTL-IM' exhibited comparable mechanical values with small difference in crystallinity values for all imidazolium based PET ternary nanocomposites. PB.DCL-IM based ternary PET nanocomposite exhibited the least crystallinity and highest increase in elongation at break and impact strength.

CHAPTER 5

CONCLUSIONS

Effects of Clay Purification

XRF results indicated that the weight percents of non-clay minerals were minimized, if not totally removed. FTIR analysis showed that the characteristic vibrations of various hydroxyl groups associated with octahedral cations, silicates and water present in the clay did not show significant change upon purification. In addition, cation exchange capacity analysis exhibited good improvement, and the CEC of the bentonite clays increased from 67.5 meq/100g clay to 95 meq/100g clay after purification.

The XRD results of this investigation showed that the clay deposits from Reşadiye mainly consists of montmorillonite with some amount of cristobalite impurity. The unpurified bentonite clay (B) also contained analcime, calcite, clinoptilolite, dolomite feldspar, quartz, Illite, opal-C and α-cristobalite as non-clay minerals. After purification, these minerals did not exist except for negligible amounts of quartz and α-cristobalite. The interlayer distance of bentonite of 1.19 nm changed slightly after purification. (PB) had an interlayer spacing of 1.11 nm.

The purity and drying conditions were crucial factors in analyzing the thermal stability of the bentonite clay. The impurities available in raw bentonites caused less thermal stability (5% more weight loss) compared to the purified clays. In addition, TGA thermograms of B and PB dried at two different temperatures 80°C and 120°C showed that drying the clays at 120°C was more suitable owing to moisture evaporation. After purification, the thermal stability of the bentonite clay increased

significantly (5% less weight loss) owing to the release of inorganic minerals that cause thermal instability of the clay.

Effects of Clay Modification

The intercalation of phosphonium and imidazolium salts in the purified bentonite layers was proven from the observations of FTIR analysis which exhibited new peaks for the intercalated salt cations between the silicate layers.

The low molecular weight surfactant (BZLTP-P Cl with the phenyl and benzyl groups) led to a basal spacing of 1.78 nm, corresponding to a bilayer arrangement of alkyl chains. High molecular weight surfactant (TO-P Br with long alkyl chains) produced an organoclay with a higher basal spacing (2.52 nm) indicating arrangement between pseudo-trilayers and paraffin-type of alkyl chains. The interlayer spacing of the imidazolium-bentonites was between 1.35 nm and 1.45 nm indicating a more compact structure than the phosphonium ones. The increase in the molecular weight with different chemical structures of the di-imidazolium surfactants, regardless of the molecular weight of the anion, resulted in slight increase in the basal spacing of the modified clays corresponding to monolayer arrangement of chains. The increase in the basal spacing, based on the chain group attached to the first nitrogen atom in imidazolium salts, was in the order of Butyl < Benzyl < Decyl.

TGA analysis indicated that the thermal stability of (alkyl, aryl) phosphonium and di-(alkyl, aryl) imidazolium organoclays were superior to conventionally used quaternary alkyl ammonium organoclays. For the salts, the molecular weight was the dominant factor, whereas for the organoclays, the chemical structure controlled the thermal stability. It seemed that there was no significant improvement in the thermal stability of the intercalated hexafluorophosphate salts; this may be due to the weak nucleophilicity of PF_6 anions. A relationship, from TGA analysis of BTL-IM Cl and DCL-IM Cl, was also observed between the chain length of the alkyl group and the thermal stability; as the chain length increased from butyl to decyl, the stability decreased. The dramatic increase in the thermal stability of halide containing phosphonium and imidazolium organoclays as compared to their salts

can be attributed to the crucial removal of the halide that may contaminate the intercalated clay after the ion exchange by forming NaCl halite as impurity from exchanged sodium cations, and thus blocks the polymer chains paths' to intercalate within the layers of the organoclay.

Phosphonium and imidazolium surfactants and organoclays confirmed the superior thermal stability of these materials considering polymer processing temperatures in the range of 200 - 350°C. The onset decomposition temperatures of the organoclays ranged between 327 - 437°C. The weight losses of the phosphonium and imidazolium substituted organoclays were in the range of 1.01 - 1.95 % at the processing temperature of 275°C for the polymers PA66 and PET used in this study.

Effects of Phosphonium Organoclays in PA66 Nanocomposites

The procedure (2-S) involving extruding twice and simultaneous injection molding was applied for all PA66 compositions with 2 wt % organoclay, since it was found to be the best way for nanocomposite production. 1 wt % of clay was not enough to cause significant improvement in the mechanical properties. Extrusion of the polymer matrix twice, and increasing the viscosity by adding elastomeric phase to the matrix increased the shear intensity and thereby facilitated the intercalation of the polymer chains into the gallery of the clay. The initial basal spacing was the dominant factor in PA66/phosphonium organoclay based ternary nanocomposites. PB.TO-P layers were intercalated and dispersed in the elastomeric phase, whereas PB.BZLTP-P exhibited more agglomerates rather than dispersed structure, but it was still intercalated.

In 1 wt % PA66/PB.TO-P/E-BA-MAH ternary nanocomposites, extrusion twice promoted the break of the elastomeric domains and resulted in reduction of the domain sizes compared to those extruded once, and the PA66/E-BA-MAH blend. Injection molding procedure (simultaneous or pelletized) had no significant effects on the domain sizes for all the compositions with 1 wt % organoclay. The domain size in 2 wt % PA66/PB.TO-P/E-BA-MAH ternary nanocomposite decreased compared to the blend whereas it increased in PB.BZLTP-P based ternary nanocomposite. Enhanced toughness of all PA66 compositions except for the

PA66/PB.BZLTP-P binary nanocomposite was clearly observed from the crack propagation along tortuous paths. SEM results were confirmed by TEM micrographs and toughness results: PB.TO-P exhibited higher compatibility with PA66 while PB.BZLTP-P based ternary composite exhibited lower toughness and mechanical properties.

The melt viscosity decreased slightly in PA66/phosphonium organoclay binary nanocomposites. The MFI value of the blend was less than those of the binary nanocomposites as a result of the highest melt viscosity of the elastomer. The incorporation of phosphonium organoclays in PA66 ternary nanocomposites exhibited the lowest MFI values compared to pure PA66, PA66 blend and binary nanocomposites owing to the effect of organoclays which increases the viscosity.

The significance of interfacial adhesion between PA66 and the organoclay in dispersing the clay homogeneously in the polymer matrix and increasing the strength of the material was observed better with PB.TO-P organoclays which exhibited higher tensile strength and Young's modulus than PB.BZLTP-P in the binary and ternary nanocomposites, due to the better dispersion of PB.TO-P in PA66. These results were in good agreement with TEM analyses which showed that PB.TO-P layers were intercalated and dispersed in the elastomeric phase, whereas PB.BZLTP-P exhibited more agglomerates rather than dispersed structure, but still intercalated.

Earlier studies with PA66/ammonium organoclay nanocomposites lowered the onset decomposition temperature of the binary nanocomposites by 10°C in nitrogen atmosphere compared to pure PA 66. However, in our case using thermally stable phosphonium organoclays revealed that the barrier effect of the silicate layers was dominant due to the formation of carbonaceous-silicate char on the surface of nanocomposite in which the onset decomposition temperature was 22°C and 17°C higher for PA66/PB.TO-P and PA66/PB.BZLTP-P binary nanocomposites, respectively. Also, phosphonium ternary nanocomposites exhibited improvement in the thermal stability compared to the pristine PA66 polymer, and a decrease in the onset decomposition temperature ~6°C compared to PA66 binary nanocomposites owing to the presence of the elastomer.

The degree of crystallinity was found to be dependent on additives such as the organoclay and the elastomer in PA66 nanocomposites. The melting point did not change significantly in PA66/phosphonium organoclay binary nanocomposites. The crystallinity of PA66 increased upon adding the phosphonium organoclay, which was attributed to the heterogeneous nucleation of montmorillonite organoclays.

Effects of Phosphonium/Imidazolium Organoclays in PET Nanocomposites

XRD results indicated that PB.BZLTP-P organoclay exhibited higher dispersion with PET in phosphonium based ternary nanocomposite compared to PB.TO-P whereas TEM analysis exhibited different behavior. This was attributed to the paraffin arrangement of the layers in the PB.TO-P organoclay prior to compounding. The slight improvement in the basal spacing of the imidazolium organoclays after compounding with PET can also be attributed mainly to the monolayer arrangement of the layers in the imidazolium organoclays prior to compounding which was counted the main factor for the polymer chains to disperse well between the clay layers. In addition, better intercalated structures could be prepared from clay mineral with small basal spacing via in-situ polymerization.

PET ternary nanocomposites with longer alkyl chains exhibited highest domain sizes and toughness. On the other hand, benzyl containing phosphonium and imidazolium PET ternary nanocomposites resulted in the lowest toughness values among all PET compositions. Phosphonium organoclay containing PET ternary nanocomposites exhibited different behavior than imidazolium containing PET ternary nanocomposites regarding domain sizes. The E-MA-GMA domain size decreased in phosphonium organoclay while it decreased in imidazolium organoclay.

MFI results showed that extrusion twice caused degradation and chain scission of pure PET and thus a significant increase in MFI. However, the epoxy functionality of GMA reacted with PET and formed a viscous PET/E-MA-GMA blend and resulted in lowering the MFI value down to approximately half of neat PET. The binary nanocomposites had higher MFI than their corresponding ternary counterparts. The

incorporation of elastomer reduced the MFI of all binary nanocomposites, owing to its low MFI as well as to the reaction between epoxy functionality of GMA and PET.

The chemical structure in phosphonium organoclay binary and ternary nanocomposites did not exhibit significant differences in tensile strength and Young's modulus values, except for aryl phosphonium PB.BZLTP-P organoclay which exhibited a decrease in tensile strength value compared to pure PET due to the presence of benzyl and phenyl groups. The alkyl chain length in alkyl Imidazolium organoclays (PB.BTL-IM, PB.BTL-IM' and PB.DCL-IM) had no effect on tensile and Young's strength values and they exhibited close results. The presence of benzyl groups in PB.BZL-IM caused decrease even in the PET binary nanocomposite extruded twice or three times.

SEM results showed that the better the organoclay was dispersed in the polymer matrix, the more these organoclays acted as barriers and hindered the coalescence of the elastomeric domains. In PET compositions studied, the addition of organoclays increased the average domain size and this was attributed to the dispersion of clay particles at the interface between PET and elastomeric phase.

TGA results indicated that the barrier effect of the silicate layers due to the formation of carbonaceous-silicate char on the surface of nanocomposite was dominant in the thermally stable phosphonium and imidazolium organoclays. In all PET compositions, it can be seen that the nanocomposite containing organoclay exhibited thermal stability superior to the pristine polymer. The onset decomposition temperature increased in the range of 7°C and 11°C for PET/phosphonium organoclay binary nanocomposites compared to pure PET. On the other hand, phosphonium organoclay based ternary nanocomposites exhibited improvement in the thermal stability without any decrease in the onset decomposition temperature due to the presence of elastomer. The onset decomposition temperatures of all imidazolium based binary and ternary nanocomposites increased with little difference in the range of 5 to 15°C indicating the superior effect of thermally stable imidazolium organoclays used. Although the XRD results showed slight improvement in the basal spacing of the bentonite clays after treatment for imidazolium salts, the thermally stable phosphonium and imidazolium surfactants

from TGA analysis exhibited significant thermal improvement in the resulting organoclays and thus in the PET nanocomposites prepared by these organoclays. Thus, incorporation of imidazolium salts with longer chains would have promoted the basal spacing of the organoclay and resulted in better dispersion with the polymer and as a result better mechanical and thermal properties could be achieved.

Amorphous PET molded under glass transition temperatures usually had slow crystallization rate, and the usage of organoclay did not promote the nucleation process in the present study. DSC results obtained in the present work suggested that the clay/polymer interface properties also affected crystalline structure formation. Phosphonium based binary nanocomposites did not show significant effects as nucleating agents, whereas imidazolium based binary nanocomposites decreased the crystallinity. The nature of the salt as intercalating agent might have influenced the crystallization kinetics by affecting the clay dispersion level and the organoclay/polymer interface properties. PET/imidazolium organoclay composites presented comparable clay dispersion levels but different crystallization rates. In addition, the thermal decomposition of the salt and thus organoclay might also play a role in the crystallization process, although it was difficult to quantify it. The mold temperature can be increased up to 140^{o}C and nucleating agents or plasticizers can be used in order to promote the nucleation process.

REFERENCES

1. Processing and properties of modified polyamide66-organoclay nanocomposites. Mert, M. and Yilmazer, U. 2008, Journal of Applied Polymer Science, Vol. 108, pp. 3890-3900.
2. Polymer-layered silicate nanocomposites: synthesis, properties and applications. Giannelis, E.P. 1998, Applied Organometallic Chemistry, Vol. 12, pp. 675-680.
3. Organo-bentonites with quaternary alkylammonium ions. Favre, H and Lagaly, G. 1991, Clay Minerals, Vol. 26, pp. 19-32.
4. Surface modification of clay minerals. Bergaya, F. and Lagaly, G. Applied Clay Science : s.n., 2001, Vol. 19, pp. 1-3.
5. Thermally stable phosphonium-montmorillonite organoclays. Calderon, J.U., Lennox, B. and Kamal, M.R. 2008, Applied Clay Science, Vol. 40, pp. 90-98.
6. Polymer/layered silicate nanocomposites from thermally stable trialkylimidazolium-treated montmorillonite. Gilman, Jeffrey W., et al. 2002, Chemistry of Materials, Vol. 14, pp. 3776-3785.
7. Thermal Degradation studies of alkyl-imidazolium salts and their application in nanocomposites. Awad, W. H., et al. 2004, Thermochimica Acta, Vol. 409, pp. 3-11.
8. Thermal stability of quaternary phosphonium modified Montmorillonites. Xie, W., et al. 2002, Chemistry of Materials, Vol. 14, pp. 4837-4845.
9. Isolation and characterization of a smectite as a micro-mesoporous material from a bentonite. Onal, M., et al. 2003, Turkish Journal of Chemisrty, Vol. 27, pp. 683-693.
10. Grim, RE. Clay Mineralogy. s.l. : Mc Graw-Hill Company, Inc., 1953.
11. Material properties of nanoclay PVC composites. Awad, W. H., et al. 2009, Polymer, Vol. 50, pp. 1857-1867.
12. Thermal stability and flammability of polyamide 66/montmorillonite nanocomposites. Qin, H., et al. 2003, Polymer, Vol. 44, pp. 7533-7538.
13. Kroschwitz, J. I. and Mark, H. F. Encyclopedia of Polymer Science and Technology. New Jersey : Wiley Interscience, Hoboken, 2003. Vol. 3rd Ed.
14. Auerbach, S.M., Carrado, K.A. and Dutta, P.K. Handbook of Layered Materials. 1st Edition. New York : Marcel Dekker, Inc., 2004.
15. Bergaya, F., Theng, B.K.G and Lagaly, G. Handbook of Clay Science. 1st Edition. s.l. : Elsevier Science, 2006.

16. Clauer, N. and Chaudhuri, S. Clays in Crustal Environments, Isotope Dating and Tracing. Berlin : Springer-Verlag, 1995.
17. Wikipedia. [Online] Wikipedia. http://en.wikipedia.org/wiki/Silicate_minerals.
18. Moore, D.M. and Reynolds, R.C. X-ray Diffraction and the Identification and Analysis of Clay Analysis of Clay Minerals. 1st Edition. Oxford : Oxford University Press, 1997.
19. Polymer-layered silicate nanocomposites: preparation, properties, and uses of a new class of materials. Alexandre, M. and Dubios, P. 2000, Materials Science and Engineering, Vol. 28, pp. 1-63.
20. Boccaleri, E. Synthesis, functionalisation and charatcerisation of nanostructured materials. Torino : Università del Piemonte Orientale “A. Avogadro”, Centro Interdisciplinare NanoSiSTeMI, July 10, 2007.
21. Kornmann, X. Synthesis and Characterization of Thermoset-Clay Nanocomposites. Luleå, Sweden : Division of Polymer Engineering, Luleå University of Technology, 2001.
22. Utracki, L.A. Clay-Containing Polymeric Nanocomposites. Shropshire : Rapra Technology Limited, 2004. p. 1st Edition.
23. MTA. VIII. Beş Yıllık Kalkınma Planı, Madencilik Özel İhtisas Komisyonu Raporu. Maden Tetkik ve Arama Genel Müdürlüğü. Ankara : s.n., 2001.
24. Türkiye Bentonit Envanteri. Evinç, H. 70, Ankara : MTA Eğt. Serisi, 1982, Vol. 184.
25. Advances in Nanomer Additives for Clay/Polymer Nanocomposites. Lan, T., et al. San Francisco, CA : s.n., 1999. Proceeding of Additives 99.
26. Polymer-layered silicate nanocomposites: an overview. LeBaron, P.C., Wang, Z. and Pinnavaia, T.J. 1999, Applied Clay Science, Vol. 15, pp. 11-29.
27. Structure and dynamics of polymer-layered silicate nanocomposites. Krishnamoorti, R., Vaia, R. and Giannelis, E.P. 1996, Chemistry of Materials, Vol. 8, pp. 1728-1734.
28. Organoclays: Properties, preparation and applications. Paiva, L. B., Morales, A. R. and Diaz, F. R. V. 2008, Applied Clay Science, Vol. 42, pp. 8-24.
29. Callister Jr., W.D. Materials Science and Engineering: An Introduction. 6th Edition. New York : John Wiley & Sons, 2003.
30. Staab, George H. Laminar Composites. 1st Edition. Woburn, MA : Butterworth-Heinemann, 1999.

31. Mazumdar, S.K. Composites Manufacturing: Materials, Product, and Process Engineering. Washington, D.C. : CRC Press LLC, 2001.
32. Chawla, K. Composite Materials Science and Engineering. 2nd Edition. New York : Springer - Verlag, 1998.
33. Xanthos, M. Functional Fillers for Plastics. 1st Edition. Weinheim, Germany : Wiley-VCH, 2005.
34. General approach to nanocomposite preparation. Ishida, H., Campbell, S. and Blackwell, J. 2000, Chemistry of Materials, Vol. 12, pp. 1260-1267.
35. Di Ventra, M., Evoy, S. and Heflin, Jr., J.R. Introduction to Nanoscale Science and Technology. Boston : Kluwer Academic Publishers, 2004.
36. Clay-based polymer nanocomposites: research and commercial development. Zeng, Q. H., et al. 2005, Journal of Nanoscience and Nanotechnology, Vol. 5, pp. 1574-1592.
37. A review on polymer–layered silicate nanocomposites. Pavlidou, S. and Papaspyrides, C.D. 2008, Progress in Polymer Science, Vol. 33, pp. 1119-1198.
38. Synthesis and properties of two dimensional nanostructures by direct intercalation of polymer melts in layered silicates. Vaia, R. A., Ishii, H. and Giannelis, E. P. 1993, Chemistry of Materials, Vol. 5, pp. 1694-1696.
39. Polymer layered silicate nanocomposites. Zanetti, M., Lomakina, S. and Camino, G. 279, 2000, Macromolecular Materials and Engineering.
40. Polymer/montmorillonite nanocomposites with improved thermal properties Part I. Factors influencing thermal stability and mechanisms of thermal stability improvement. Leszczynska, A., et al. 2007, Thermochimica Acta, Vol. 453, pp. 75-96.
41. Effect of melt processing conditions on the extent of exfoliation in organoclay-based nanocomposites. Dennis, H.R., et al. 2001, Polymer, Vol. 42, pp. 9513-9522.
42. Billmeyer, F.W. Textbook of Polymer Science. 1st Edition. New York : John Wiley & Sons, 1984.
43. Seymour, B.S. and Carraher, C.E. Structure and Property Relationships in Polymers. 1st Edition. New York : Plenum Press, 1984.
44. Kirk-Othmer. Kirk-Othmer Encyclopedia of Chemical Technology. s.l. : John Wiley and sons Inc., 2001. Vol. 6.
45. Ebewele, R.O. Polymer Science and Technology. New York : CRC Press, 1996. Vol. 1.

46. Kohan, M.I. Nylon Plastics. 1973 : John Wiley & Sons, 1973. Vol. 1.
47. Salamone, J. C. Polymeric Materials Encyclopedia. Boca Raton : CRC Press, 1996. Vol. 8.
48. Characterization of poly(ethylene terephthalate) after multiple processing cycles. Silva Spinace, M. A. and De Paoli, M. A. 2001, Journal of Applied Polymer Science, Vol. 80, pp. 20-25.
49. Surface characterization of polyethylene terephthalate/silica nanocomposites. Parvinzadeh, M., et al. 2010, Applied Surface Science, Vol. 256, pp. 2792-2802.
50. Lee, N. C. Plastic Blow Molding Handbook. London : Chapman and Hall, 1990.
51. Lu, M., et al. Atlanta : s.n., 1998. 58th Annual Technical Conference of SPE.
52. PSLC. Polymer Science Learning Center. [Online] http://pslc.ws/mactest/pet.htm.
53. Micro- and nano-scale deformation behavior of nylon 66-based binary and ternary nanocomposites. Dasari, A., et al. 2006, Composites Science and Technology, Vol. 66, pp. 3097-3114.
54. Maleic anhydride polyethylene octene elastomer toughened polyamide 6/polypropylene nanocomposites: mechanical and morphological properties. Hassan, A., et al. 2006, Macromolecular Symposia, Vol. 239, pp. 182-191.
55. Arkema Chemicals. Arkema Chemicals. [Online] http://www.atofinachemicals.com.
56. Ultimate mechanical properties of rubber toughened semicrystalline PET at room temperature. Loyens, W. and Groeninckx, G. 2002-a, Polymer, Vol. 43, pp. 5679-5691.
57. Impact modification of poly(ethylene terephthalate). Chapleau, N. and Huneault, M.A. 2003, Journal of Applied Polymer Science, Vol. 90, pp. 2919-2932.
58. Raunwendaal, C. Polymer Extrusion. 3rd Edition. New York : Hanser/Gardner Publishers, 1994.
59. Mert, M. Impact Modified Nylon 66-Organolcay Nanocomposites. Ankara : s.n., 2007. MS Thesis.
60. Harper, C. A. Modern Plastics Handbook. Ohaio : McGraw-Hill, 2000.
61. Fisher, E.G. Extrusion of Plastics. London : Newness-Butterworths, 1976. Vol. 3.
62. Rodriguez, F., et al. Principles of Polymer Systems. 1st Edition. New York : Taylor & Francis, 2003.
63. Middleman, S. Fundamentals of Polymer Processing. 1st Edition. New York : McGraw-Hill, 1977.
64. Margolis, J.M. Engineering Plastics Handbook. New York : McGraw-Hill, 2006.

65. Matthews, F. L. and Rowlings, R. D. Composite Materials, Engineering & Science. New York : Chapman & Hall, 1994.

66. Expansion characteristics of organoclay as a precursor to nanocomposites. Lee, S. Y. and Kim, S. J. 2002, Colloids and Surfaces A: Physicochem. Eng. Aspects, Vol. 211, pp. 19-26.

67. Adsorption properties of tetradecyl- and hexadecyl trimethylammonium bentonites. Yilmaz, N. and Yapar, S. 2004, Applied Clay Science, Vol. 27, pp. 223-228.

68. Influence of clay modification process in PA6-layered silicate nanocomposite properties. Gracia-Lopez, D., et al. 2005, Polymer, Vol. 26, pp. 2758-2765.

69. Beneficiation of montmorillonite from ores by dispersion processing. Song, S., et al. 2005, Journal of Dispersion Science and Technology, Vol. 26, pp. 375-379.

70. Determination of structural modification in acid activated montmorillonite clay by FT-IR spectroscopy. Tyagi, B., Chudasama, C. D. and Jasra, R. V. 2006, Spectrochimica Acta Part A, Vol. 64, pp. 273-278.

71. Preparation and characterization of phosphonium montmorillonite with enhanced thermal stability. Patel, H., et al. 2007, Applied Clay Science, Vol. 35, pp. 194-200.

72. Structural charachteristics of organo-modified bentonites of different origins. Tabak, A., et al. 2, 2007, Journal of Thermal Analysis and Calorimetry, Vol. 87, pp. 375-381.

73. Use of different alkylammonium salts in clay surface modification for epoxy-based nanocomposites. Nakaş, G. I. and Kaynak, C. 2009, Poymer Composites, pp. 357-363.

74. Thermal degradation chemistry of alkyl quaternary ammonium montmorillonite. Xie, W., et al. 2001-b, Chemistry of Materials, Vol. 13, pp. 2979-2990.

75. Nanocomposites based on poly (ε-Caprolactone) (PCL)/clay hybrid: polystyrene, high impact polystyrene, ABS, polypropylene and polyethylene. Zheng, X. and Wilkie, C.A. 2003, Polymer Degradation and Stability, Vol. 82, pp. 441-450.

76. Thermal characterization of organically modified Montmorillonite. Xie, W., et al. 2001-a, Thermochimica Acta, Vol. 367, pp. 339-350.

77. Singh, A. and Haghighat, R. High-temperature polymer/inorganic nanocomposites. United States Patent 6057035, 2000.

78. Combustion behaviour of epoxide based nanocomposites with ammonium and phosphonium bentonites. Hartwig, A., et al. 2003, Macromolecular Chemistry and Physics, Vol. 204, pp. 2247-2257.

79. Styrene-acrylonitrile (SAN) layered silicate nanocomposites prepared by melt compounding. Chu, Lih-Long, et al. 2004, Polymer, Vol. 45, pp. 4051-4061.
80. Poly(ethylene naphthalate)/clay nanocomposites based on thermally stable trialkylimidazolium-treated montmorillonite:thermal and dynamic mechanical properties. Chua, Y.C., Wu, S. and Lu, X. 12, 2006, Journal of nanoscience and nanotechnology, Vol. 6, pp. 3985-3988.
81. Novel organic modification of montmorillonite in hydrocarbon solvent using ionic liquid-type surfactant for the preparation of polyolefin–clay nanocomposites. Ding, Y., et al. 2006, Journal of Applied Polymer Science, Vol. 102, pp. 4314-4320.
82. Surface characteristics of layered silicates: influence on the properties of clay/polymer nanocomposites. Kadar, F., et al. 2006, Langmuir, Vol. 22, pp. 7848-7854.
83. Modification of cationic nanoclays with ionic liquids. Kim, N.H., Malhotra, S.V. and Xanthos, M. 2006, Microporous and Mesoporous Materials, Vol. 96, pp. 29-35.
84. Synthesis of imidazolium salts and their application in epoxy montmorillonite nanocomposites. Langat, J., et al. 2006, Polymer, Vol. 47, pp. 6698-6709.
85. Phosphonium-modified layered silicate epoxy resins nanocomposites and their combinations with ATH and organo-phosphorus fire retardants. Schartel, B., et al. 2006, Polymers for Advanced Technologies, Vol. 17, pp. 281-293.
86. Ionic liquid modification of layered silicates for enhanced thermal stability. Byrne, C. and McNally, T. 2007, Macromolecular Rapid Communications, Vol. 28, pp. 780-784.
87. Benzimidazolium surfactants for modification of clays for use with styrenic polymers. Costache, M. C., et al. 2007, Polymer Degradation and Stability, Vol. 92, pp. 1753-1762.
88. Thermal analysis of montmorillonites modified with quaternary phosphonium and ammonium surfactants. Hedley, C. B., Yuan, G. and Theng, B. K. G. 2007, Applied Clay Science, Vol. 35, pp. 180-188.
89. The effect of mechanical treatment on the structure of montmorillonite. Hrachova, J., Komadel, P. and Fajnor, V. S. 2007, Materials Letters, Vol. 61, pp. 3361-3365.
90. Nanohybrid materials from the intercalation of imidazolium ionic liquids in kaolinite. Letaief, S. and Detellier, C. 2007, Journal of Materials Chemistry, Vol. 17, pp. 1476-1484.

91. Gas permeation and mechanical properties of polypropylene nanocomposites with thermally-stable imidazolium modified clay. Mittal, V. 2007, European Polymer Journal, Vol. 43, pp. 3727-3736.

92. PET/imidazolium-based OMMT nanocomposites via in situ polymerization: morphological, thermal, and nonisothermal crystallization studies. Monemian, S.A., et al. 4, 2007, Advances in Polymer Technology, Vol. 26, pp. 247-257.

93. Kinetic study of the thermal degradation of PS/MMT nanocomposites prepared with imidazolium surfactants. Abate, L., et al. 3, 2008, Journal of Thermal Analysis and Calorimetry, Vol. 91, pp. 681-686.

94. Enhanced thermal stability and structural characteristics of different MMT-Clay/epoxy-nanocomposite materials. Lakshmi, M., Narmadha, B. and Reddy, B. S. R. 2008, Polymer Degradation and Stability, Vol. 93, pp. 201-213.

95. Modification of bentonite with diphosphonium salts: synthesis and characterization. Makhoukhi, B., Didi, M. A. and Villemin, D. 2008, Materials Letters, Vol. 62, pp. 2493-2496.

96. Imidazolium-modified clay-based ABS nanocomposites:a comparison between melt-blending and solution-sonication processes. Modesti, M., et al. 2008, Polymers for Advanced Technologies, Vol. 19, pp. 1576-1583.

97. Thermal decomposition of various alkyl onium organoclays: effect on polyethylene terephthalate nanocomposites' properties. Stoeffler, K., Lafleur, P. G. and Denault, J. 2008, Polymer Degradation and Stability, Vol. 93, pp. 1332-1350.

98. Phosphonium salt intercalated montmorillonites. Avalos, F., et al. Applied Clay Science : s.n., 2009, Vol. 43, pp. 27-32.

99. Influence of montmorillonite nano-dispersion on polystyrene photo-oxidation. Bottino, F. A., et al. 2009, Polymer Degradation and Stability, Vol. 94, pp. 369-374.

100. Rubber toughening of glass fiber reinforced nylon-6,6 with functionalized block copolymer SEBS-g-MA. Karayannidis, G. P., et al. 2002, Advances in Polymer Technology, Vol. 21, pp. 153-163.

101. Polymorphism in polyamide 66/clay nanocomposites. Liu, X., Wu, Q. and Berglund, L. A. 2002, Polymer, Vol. 43, pp. 4967-4972.

102. Toughness of nanoscale and multiscale polyamide-6,6 composites. Nair, S.V., Goettler, L.A. and Lysek, B.A. 2002, Polymer Engineering and Science, Vol. 42, pp. 1872-1882.

103. Predicting the binding energy for nylon 6,6 nanocomposites by molecular modeling. Tanaka, G. and Goettler, L.A. 2002, Polymer, Vol. 43, pp. 541-553.
104. Preparation and characterization of nylon 66/montmorillonite nanocomposites with co-treated montmorillonites. Han, B., et al. 2003, European Polymer Journal, Vol. 39, pp. 1641-1646.
105. Phase transition in polyamide-66/montmorillonite nanocomposites on annealing. Liu, X., et al. Part B: Polymer Physics, 2003, Journal of Polymer Science, Vol. 41, pp. 63-67.
106. Morphology and properties of ternary polyamide 6/ polyamide 66/ elastomer blends. Tomova, D. and Radusch, H. J. 2003, Polymers for Advanced Technologies, Vol. 14, pp. 19-26.
107. Dispersion and distribution of organically modified montmorillonite in nylon-66 matrix. Yu, Z. Z., et al. Part B: Polymer Physics, 2003, Journal of Polymer Science, Vol. 41, pp. 1234-1243.
108. Multiple melting and crystallization of nylon-66/montmorillonite nanocomposites. Zhang, Q. X., et al. Part B: Polymer Physics, 2003, Journal of Polymer Science, Vol. 41, pp. 2861-2869.
109. Studies on crystallization behaviors and crystal morphology of polyamide 66/clay nanocomposites. Kang, X., et al. 2005, Journal of Applied Polymer Science, Vol. 95, pp. 756-763.
110. Comparison of nanocomposites based on nylon 6 and nylon 66. Chavarria, F. and Paul, D.R. 2004, Polymer, Vol. 45, pp. 8501-8515.
111. Influence of thermal processing on the perfection of crystals in polyamide 66 and polyamide 66/clay nanocomposites. Lu, Y., et al. 2004, Polymer, Vol. 45, pp. 8999-9009.
112. Melt processing of PA-66/clay, HDPE/clay and HDPE/PA-66/clay nanocomposites. Mehrabzadeh, M. and Kamal, M. 2004, Polymer Engineering and Science, Vol. 44, pp. 1151-1161.
113. Nanoindentation and morphological studies on nylon 66-organoclay nanocomposites. II. Effect of strain rate,, . Shen, L., et al. 2004, Polymer, Vol. 45, pp. 3341-3349.
114. Mechanical and dynamic mechanical properties of nylon 66/montmorillonite nanocomposites fabricated by melt compounding. Yu, Z. Z., et al. 2004, Polymer International, Vol. 53, pp. 1093-1098.

115. Effect of blending sequence on microstructure of ternary nanocomposites . Dasari, A., Yu, Z. Z. and Mai, Y. W. 2005, Polymer, Vol. 46, pp. 5986-5991.
116. A comparison of the temperature dependence of the modulus, yield stress and ductility of nanocomposites based on high and low MW PA6 and PA66. Vlasveld, D. P. N., et al. 2005, Polymer, Vol. 46, pp. 3452-3461.
117. Embrittlement mechanisms of nylon 66/organoclay nanocomposites prepared by melt-compounding process. Chen, L., et al. 2006, Materials and Manufacturing Processes, , Vol. 22, pp. 153-158.
118. Rubber-toughened polyamide 6/clay nanocomposites. Gonzáles, I., Eguiazábal, J.I. and Nazábal, J. 2006, Composites Science and Technology, Vol. 66, pp. 1833-1843.
119. Morphology, thermal, and mechanical properties of polyamide 66/clay nanocomposites with epoxy-modified organoclay. Gyoo, P. M., Venkataramani, S. and Kim, S. C. 2006, Journal of Applied Polymer Science, Vol. 101, pp. 1711-1722.
120. Crystallisation behaviour of Polyamide-6 and Polyamide-66 nanocomposites. Hedicke, K., et al. 2006, Composites Science and Technology, Vol. 66, pp. 571-575.
121. Melt preparation and investigation of properties of toughened Polyamide 66 with SEBS-g-MA and their nanocomposites. Farahani, R.D. and Ramazani S.A., A. 2008, Materials and Design, Vol. 29, pp. 105-111.
122. Polyamide 66/Brazilian clay nanocomposites. Araujo, E. M., et al. s.l. : Hindawi Publishing Corporation, 2009, Journal of Nanomaterials.
123. Compatibilization of polymer blends by reactive processing. Xanthos, M. and Dagli, S.S. 1991, Polymer Engineering and Science, Vol. 31, pp. 929-935.
124. Comparison of compatibilizer effectiveness for PET/HDPE blends. Kalfoglou, N.K., Skafidas, D.S. and Kallitsis, J.K. 1995, Polymer, Vol. 36, pp. 4453-4462.
125. Phase morphology development in reactively compatibilised polyethylene terephthalate/elastomer blends. Loyens, W. and Groeninckx, G. 2002-b, Macromolecular Chemistry and Physics, Vol. 203, pp. 1702-1714.
126. Effects of melt-processing conditions on the quality of poly(ethylene terephthalate) montmorillonite clay nanocomposites. Davis, C.H., et al. 2002, Journal of Polymer Science: Part B: Polymer Physics, Vol. 40, pp. 2661-2666.

127. Preparation and characterization of poly(ethylene terephthalate)/clay nanocomposites by melt blending using thermally stable surfactants. Costache, M.C., et al. 2006, Polymers for Advanced Technologies, Vol. 17, pp. 764-771.

128. Study on mechanical properties, thermal stability and crystallization behavior of PET/MMT nanocomposites. Wang, Y., et al. 2006, Composites: Part B, Vol. 37, pp. 399-407.

129. Reactive extrusion of poly(ethylene terephthalate)–(Ethylene/Methyl Acrylate/Glycidyl Methacrylate)–organoclay nanocomposites. Alyamac, E. and Yilmazer, U. 2, 2007, Polymer Composites, Vol. 28, pp. 251-258.

130. Thermal and thermo-mechanical properties of poly(ethylene terephthalate) nanocomposites. Bandyopadhyay, J., Ray, S.S. and Bousmina, M. 4, 2007, J. Ind. Eng. Chem., Vol. 13, pp. 614-623.

131. Morphology and thermomechanical properties of recycled PET–organoclay nanocomposites. Bizarria, M.T.M., et al. 2007, Journal of Applied Polymer Science, Vol. 104, pp. 1839-1844.

132. Nanocomposite fibers of poly(ethylene terephthalate) with montmorillonite and mica: thermomechanical properties and morphology. Chang, J. and M.K., Mun. 2007, Polymer International, Vol. 56, pp. 57-66.

133. Synthesis of thermally stable organosilicate for exfoliated poly(ethylene terephthalate) nanocomposite with superior tensile properties. Kim, K.H., et al. 2, 2007, Macromolecular Research, Vol. 15, pp. 178-184.

134. Recycled PET-organoclay nanocomposites with enhanced processing properties and thermal stability. Kracalık, M., et al. 2007, Journal of Applied Polymer Science,, Vol. 106, pp. 2092-2100.

135. Thermal stability of surfactants with amino and imido groups in poly(Ethylene Terephthalate)/clay composites. Yuan, X., et al. 2008, Journal of Applied Polymer Science, , Vol. 109, pp. 4112-4120.

136. Degradation of poly(ethylene terephthalate)/clay nanocomposites during melt extrusion: effect of clay catalysis and chain extension. Xu, X., et al. 2009, Polymer Degradation and Stability, Vol. 94, pp. 113-123.

137. New insight into the crystallization behavior of poly(ethylene terephthalate)/clay nanocomposites. Guan, G., et al. 2008, Journal of Polymer Science: Part B: Polymer Physics, Vol. 46, pp. 2380-2394.

138. The effect of organic modifier of the clay on morphology and crystallization properties of PET nanocomposites. Calcagno, C.I.W., et al. 2007, Polymer , Vol. 48, pp. 966-974.

139. The heat of fusion of poly(ethylene Terephthalate). Starkweather Jr., H. W., Zoller, P. and Jones, G. A. 2, Delaware : s.n., 2003, Journal of Polymer Science: Polymer Physics Edition, Vol. 21, pp. 295-299.

140. FTIR techniques in clay mineral studies. Madejova, J. 2003, Vibrational Spectroscopy, Vol. 31, pp. 1-10.

141. Coates, J. Interpretation of Infrared Spectra, A Practical Approach. [book auth.] R.A. Meyers. Encyclopedia of Analytical Chemistry. s.l. : John Wiley & Sons Ltd., 2000, Vol. 18, pp. 10815-10837.

142. Brindley, G.W. and Brown, G. Crystal Structures of Clay Minerals and their X-Ray Identification. 1st Edition. London : Mineralogical Society, 1980.

143. Structural and mechanical properties of polymer nanocomposites. Tjong, S.C. 2006, Materials Science and Engineering, Vol. 53, pp. 73-197.

144. Microstructural evolution of melt intercalated polymer-organically modified layered silicates nanocomposites. Vaia, R.A., et al. 1996, Chem. Mater, Vol. 8, pp. 2628-2635.

145. Traditional and new applications for kaolin smectite and palygorskite: a general overview. Murray, H. 2000, Applied Clay Science, Vol. 17, pp. 207-221.

146. Thermal stability of nanocomposites based on polypropylene and bentonite. Ramos Filho, F. G., et al. 2005, Polymer Degradation and Stability, Vol. 89, pp. 383-392.

147. Nylon-6 nanocomposites from alkylammonium-modified clay: the role of alkyl tails onexfoliation. Fornes, T.D., Hunter, D.L. and Paul, D. R. 2004, Macromolecules, Vol. 37, pp. 1793-1798.

148. Permeability of polymer/clay nanocomposites: A review. Choudalakis, G. and Gotsis, A.D. 2009, European Polymer Journal, Vol. 45, pp. 967-984.

149. In situ compatibilization of polyamide 6/natural rubber blends with maleic anhydride. Carone Jr, E., et al. 2000, Polymer, Vol. 41, pp. 5929-5935.

150. Characterization and tensile properties of ternary blends with PA-6 nanocomposites. Contreras, V., et al. 2006, Polymer Engineering and Science, Vol. 46, pp. 1111-1120.

151. Polyamide nanocomposites with improved toughness. Kelnar, I., et al. 2005, Journal of Applied Polymer Science, Vol. 96, pp. 288-293.
152. Nylon 6 nanocomposites by melt compounding. Cho, J. W. and Paul, D. R. 2001, Polymer, Vol. 42, pp. 1083-1094.
153. Exfoliated PA6,6 nanocomposites by modification with PA6. Gonzalez, I., Eguiazabal, J. I. and Nazabal, J. 2005, Polymer , Vol. 46, pp. 2978-2985.
154. Rheology of organoclay nanocomposites: effects of polymer matrix/organoclay compatibility and the gallery distance of organoclay. Lee, K. M. and Han, C.D. 2003, Macromolecules, Vol. 36, pp. 7165-7178.
155. Rheology of polymer layered silicate nanocomposites. Krishnamoorti, R. and Yurekli, K. 2001, Current Opinion in Colloid & Interface Science , Vol. 6, pp. 464-470.
156. Melt rheology of organoclay and fumed silica nanocomposites. Cassagnau, P. 9, 2008, Polymer, Vol. 49, pp. 2183-2196.
157. The relationship between nano- and micro-structures and mechanical properties in PMMA-epoxy-nanoclay composites. Park, J.H. and Jana, S.C. 2003, Polymer, Vol. 44, pp. 2091-2100.
158. Seymour, R.B. Polymer Chemistry: An Introduction. 4th Edition. New York : Marrel Dekker, 1996.
159. Nielsen, L. and Landel, R. Mechanical properties of polymers and composites. 2nd Edition. s.l. : USA: Marcel Dekker, 1993.
160. The measurement of the crystallinity of polymers by DSC. Kong, Y. and Hay, J.N. 2002, Polymer, Vol. 43, pp. 3873-3878.

APPENDIX A

MECHANICAL TEST RESULTS

A.1 Mechanical Test Results of PA66 Compositions

Table A. 1 Tensile strength (MPa) data of all PA66 compositions

Composition	Tensile Strength (MPa)	Standard deviation
Polymer		
PA66 (Extruded Twice)	83.7	3.7
Polymer/Elastomer Blend		
PA66/E-BA-MAH	76.1	1.7
Polymer/Organoclay Binary Nanocomposites		
PA66/PB.TO-P	89.6	0.9
PA66/PB.BZLTP-P	88.8	0.2
Polymer/Organoclay/Elastomer Ternary Nanocomposites		
PA66/PB.TO-P/E-BA-MAH (1-S)	77.2	1.5
PA66/PB.TO-P/E-BA-MAH (1-P)	75.9	1.8
PA66/PB.TO-P/E-BA-MAH (2-P)	78.3	1.1
PA66/PB.TO-P/E-BA-MAH (2-S)	75.0	0.2
PA66/PB.TO-P/E-BA-MAH	82.9	0.7
PA66/PB.BZLTP-P/E-BA-MAH	74.2	1.0

Table A. 2 Young's modulus (GPa) data of all PA66 compositions

Composition	Young's Modulus (GPa)	Standard deviation
Polymer		
PA66 (Extruded Twice)	2.734	0.131
Polymer/Elastomer Blend		
PA66/E-BA-MAH	2.432	0.028
Polymer/Organoclay Binary Nanocomposites		
PA66/PB.TO-P	2.942	0.040
PA66/PB.BZLTP-P	2.349	0.040
Polymer/Organoclay/Elastomer Ternary Nanocomposites		
PA66/PB.TO-P/E-BA-MAH (1-S)	2.370	0.037
PA66/PB.TO-P/E-BA-MAH (1-P)	2.388	0.124
PA66/PB.TO-P/E-BA-MAH (2-P)	2.330	0.129
PA66/PB.TO-P/E-BA-MAH (2-S)	2.297	0.046
PA66/PB.TO-P/E-BA-MAH	2.542	0.022
PA66/PB.BZLTP-P/E-BA-MAH	2.349	0.040

Table A. 3 Elongation at break (%) data of all PA66 compositions

Composition	Elongation at Break (%)	Standard deviation
Polymer		
PA66 (Extruded Twice)	23.3	0.2
Polymer/Elastomer Blend		
PA66/E-BA-MAH	25.8	1.1
Polymer/Organoclay Binary Nanocomposites		
PA66/PB.TO-P	13.9	0.5
PA66/PB.BZLTP-P	12.2	0.9
Polymer/Organoclay/Elastomer Ternary Nanocomposites		
PA66/PB.TO-P/E-BA-MAH (1-S)	24.9	1.0
PA66/PB.TO-P/E-BA-MAH (1-P)	25.4	2.9
PA66/PB.TO-P/E-BA-MAH (2-P)	25.3	3.2
PA66/PB.TO-P/E-BA-MAH (2-S)	24.5	0.7
PA66/PB.TO-P/E-BA-MAH	24.3	0.8
PA66/PB.BZLTP-P/E-BA-MAH	14.7	2.0

Table A. 4 Impact strength (kJ/m^2) data of all PA66 compositions

Composition	Impact Strength (kJ/m^2)	Standard deviation
Polymer		
PA66 (Extruded Twice)	7.0	0.3
Polymer/Elastomer Blend		
PA66/E-BA-MAH	10.4	0.8
Polymer/Organoclay Binary Nanocomposites		
PA66/PB.TO-P	7.0	0.2
PA66/PB.BZLTP-P	6.2	0.1
Polymer/Organoclay/Elastomer Ternary Nanocomposites		
PA66/PB.TO-P/E-BA-MAH (1-S)	10.2	0.8
PA66/PB.TO-P/E-BA-MAH (1-P)	8.2	1.4
PA66/PB.TO-P/E-BA-MAH (2-P)	9.4	0.4
PA66/PB.TO-P/E-BA-MAH (2-S)	10.5	0.4
PA66/PB.TO-P/E-BA-MAH	9.0	0.3
PA66/PB.BZLTP-P/E-BA-MAH	7.8	0.5

A.2 Mechanical Test Results of PET Compositions

Table A. 5 Tensile strength (MPa) data of all PET compositions

Composition	Tensile Strength (MPa)	Standard deviation
Polymer		
PET (Extruded Twice)	52.5	0.3
Polymer/Elastomer Blend		
PET/E-MA-GMA	50.4	0.4
Polymer/Organoclay Binary Nanocomposites		
PET/PB.TO-P	56.9	0.8
PET/PB.BZLTP-P	56.1	4.3
PET/PB.BZL-IM	48.2	4.0
PET/PB.BTL-IM	57.8	0.9
PET/PB.BTL-IM’	58.7	0.9
PET/PB.DCL-IM	58.3	1.5
Polymer/Organoclay/Elastomer Ternary Nanocomposites		
PET/PB.TO-P/E-MA-GMA	49.6	0.5
PET/PB.BZLTP-P/E-MA-GMA	46.1	1.1
PET/PB.BZL-IM/E-MA-GMA	53.0	1.9
PET/PB.BZL-IM/E-MA-GMA (E3)	50.5	1.4
PET/PB.BTL-IM/E-MA-GMA	49.6	0.5
PET/PB.BTL-IM’/E-MA-GMA	49.0	0.2
PET/PB.DCL-IM/E-MA-GMA	50.8	0.8

Table A. 6 Young's modulus (MPa) data of all PET compositions

Composition	Young's Modulus (GPa)	Standard deviation
Polymer		
PET (Extruded Twice)	1.749	0.053
Polymer/Elastomer Blend		
PET/E-MA-GMA	1.667	0.027
Polymer/Organoclay Binary Nanocomposites		
PET/PB.TO-P	1.959	0.013
PET/PB.BZLTP-P	2.145	0.049
PET/PB.BZL-IM	1.705	0.224
PET/PB.BTL-IM	2.064	0.058
PET/PB.BTL-IM'	2.057	0.001
PET/PB.DCL-IM	2.063	0.019
Polymer/Organoclay/Elastomer Ternary Nanocomposites		
PET/PB.TO-P/E-MA-GMA	1.641	0.023
PET/PB.BZLTP-P/E-MA-GMA	1.640	0.008
PET/PB.BZL-IM/E-MA-GMA	1.635	0.164
PET/PB.BZL-IM/E-MA-GMA (E3)	1.806	0.036
PET/PB.BTL-IM/E-MA-GMA	1.810	0.039
PET/PB.BTL-IM'/E-MA-GMA	1.782	0.015
PET/PB.DCL-IM/E-MA-GMA	1.822	0.038

Table A. 7 Elongation at break (%) data of all PET compositions

Composition	Elongation at break (%)	Standard deviation
Polymer		
PET (Extruded Twice)	3.9	0.3
Polymer/Elastomer Blend		
PET/E-MA-GMA	208.7	4.7
Polymer/Organoclay Binary Nanocomposites		
PET/PB.TO-P	123.7	22.2
PET/PB.BZLTP-P	2.4	0.3
PET/PB.BZL-IM	6.3	2.2
PET/PB.BTL-IM	123.3	2.2
PET/PB.BTL-IM’	172.2	48.0
PET/PB.DCL-IM	200.1	37.3
Polymer/Organoclay/Elastomer Ternary Nanocomposites		
PET/PB.TO-P/E-MA-GMA	96.4	2.1
PET/PB.BZLTP-P/E-MA-GMA	4.4	0.2
PET/PB.BZL-IM/E-MA-GMA	189.6	23.4
PET/PB.BZL-IM/E-MA-GMA (E3)	245.5	10.6
PET/PB.BTL-IM/E-MA-GMA	135.9	46.7
PET/PB.BTL-IM’/E-MA-GMA	201.6	16.4
PET/PB.DCL-IM/E-MA-GMA	208.0	5.5

Table A. 8 Impact strength (kJ/m^2) data of all PA66 compositions

Composition	Impact Strength (kJ/m^2)	Standard deviation
Polymer		
PET (Extruded Twice)	2.9	0.2
Polymer/Elastomer Blend		
PET/E-MA-GMA	4.8	0.5
Polymer/Organoclay Binary Nanocomposites		
PET/PB.TO-P	3.1	0.1
PET/PB.BZLTP-P	3.2	0.2
PET/PB.BZL-IM	3.1	0.2
PET/PB.BTL-IM	3.1	0.1
PET/PB.BTL-IM’	3.2	0.0
PET/PB.DCL-IM	3.1	0.1
Polymer/Organoclay/Elastomer Ternary Nanocomposites		
PET/PB.TO-P/E-MA-GMA	4.7	0.1
PET/PB.BZLTP-P/E-MA-GMA	3.4	0.7
PET/PB.BZL-IM/E-MA-GMA	3.9	1.2
PET/PB.BZL-IM/E-MA-GMA (E3)	3.0	0.1
PET/PB.BTL-IM/E-MA-GMA	5.1	0.1
PET/PB.BTL-IM’/E-MA-GMA	4.8	0.3
PET/PB.DCL-IM/E-MA-GMA	6.0	1.1

APPENDIX B

TGA ANALYSIS

B.1 TG/DrTG/DTA Thermograms of Clays and Organoclays

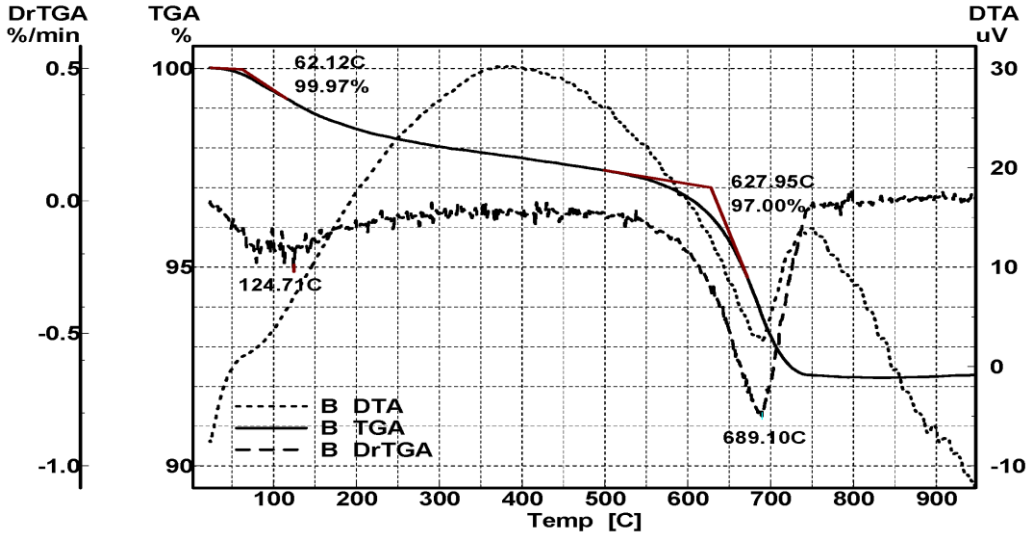

Figure B. 1 TG/DrTG/DTA thermogram of bentonite (B)

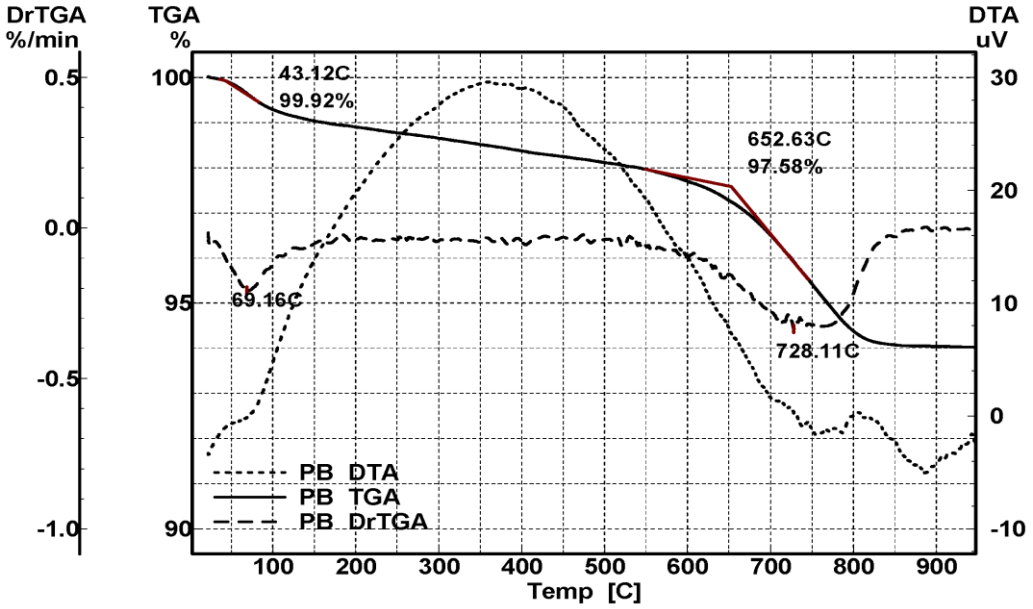

Figure B. 2 TG/DrTG/DTA thermogram of purified bentonite (PB)

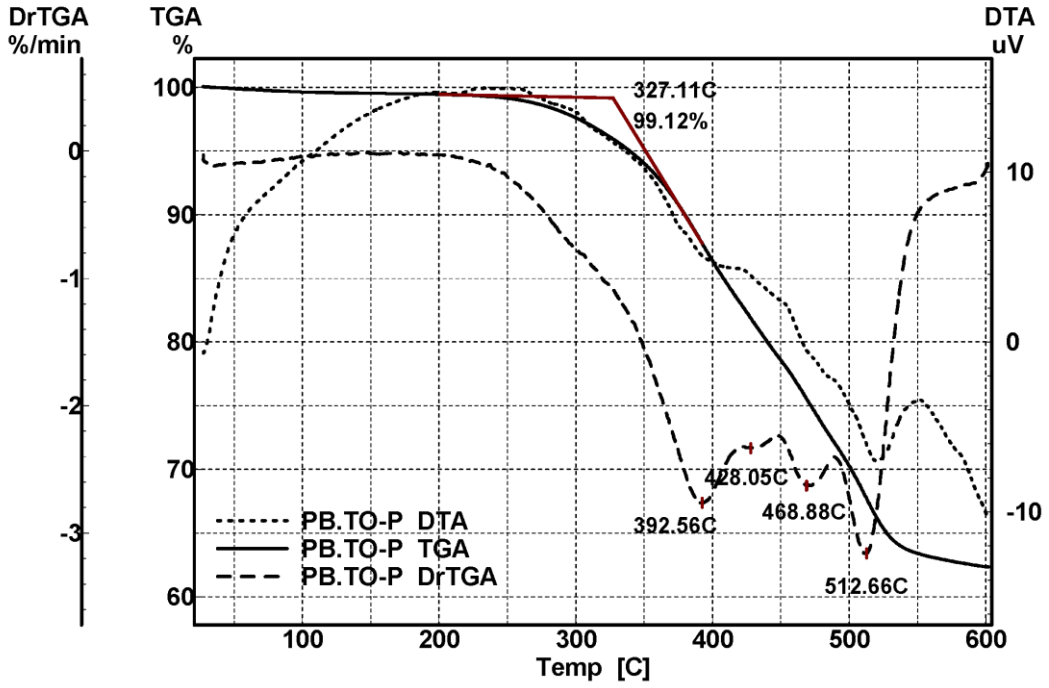

Figure B. 3 TG/DrTG/DTA thermogram of PB.TO-P

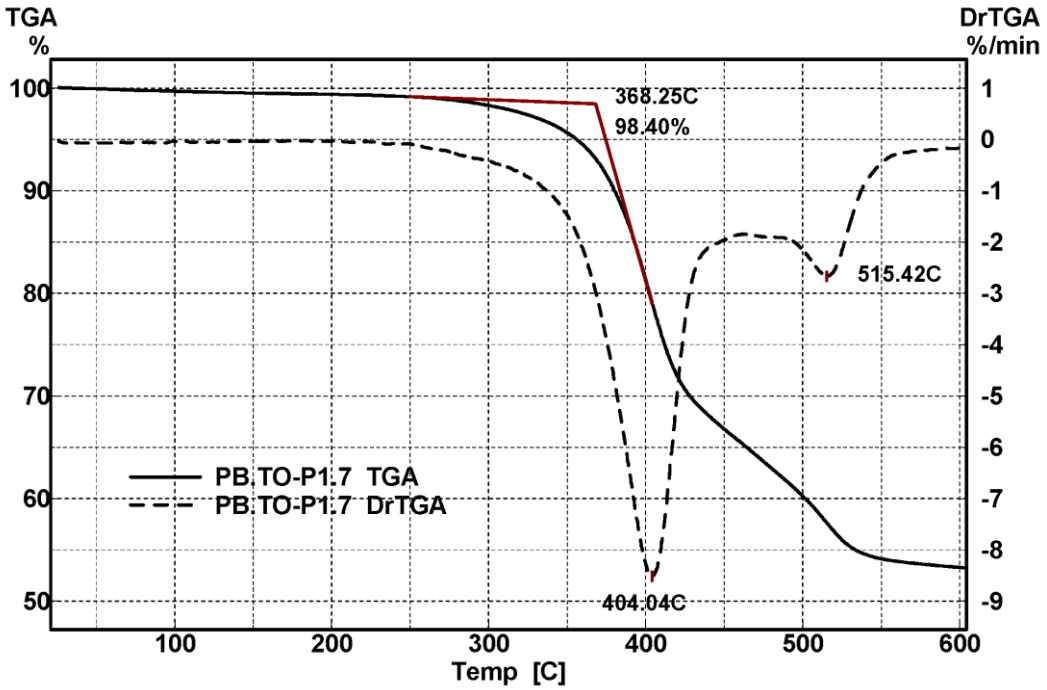

Figure B. 4 TG/DrTG/DTA thermogram of PB.TO-P1.7

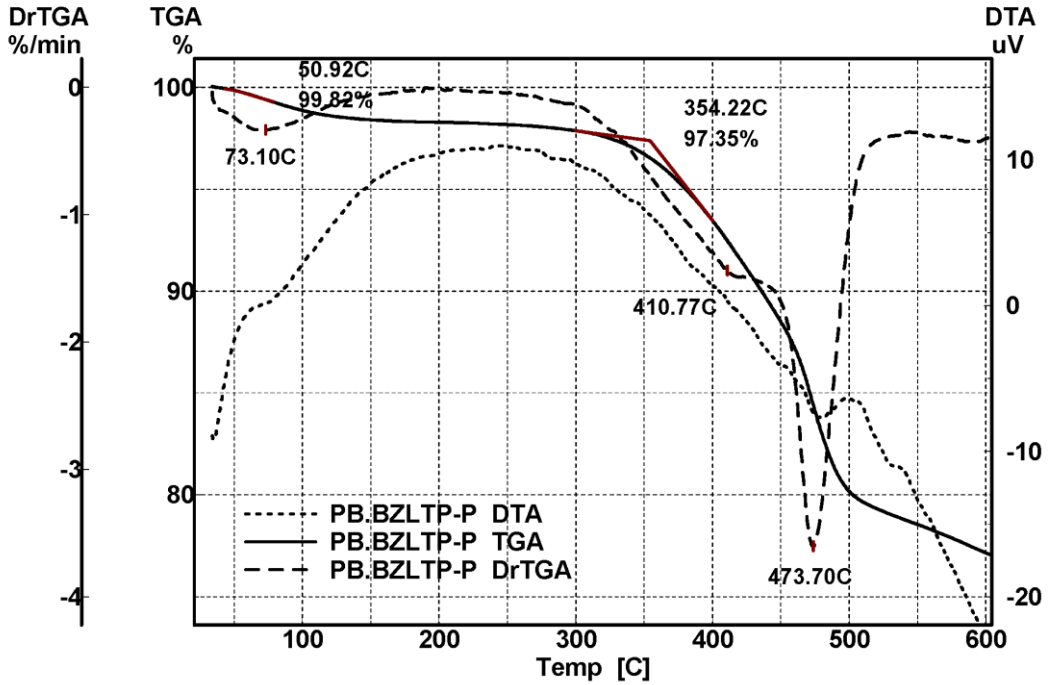

Figure B. 5 TG/DrTG/DTA thermogram of PB.BZLTP-P

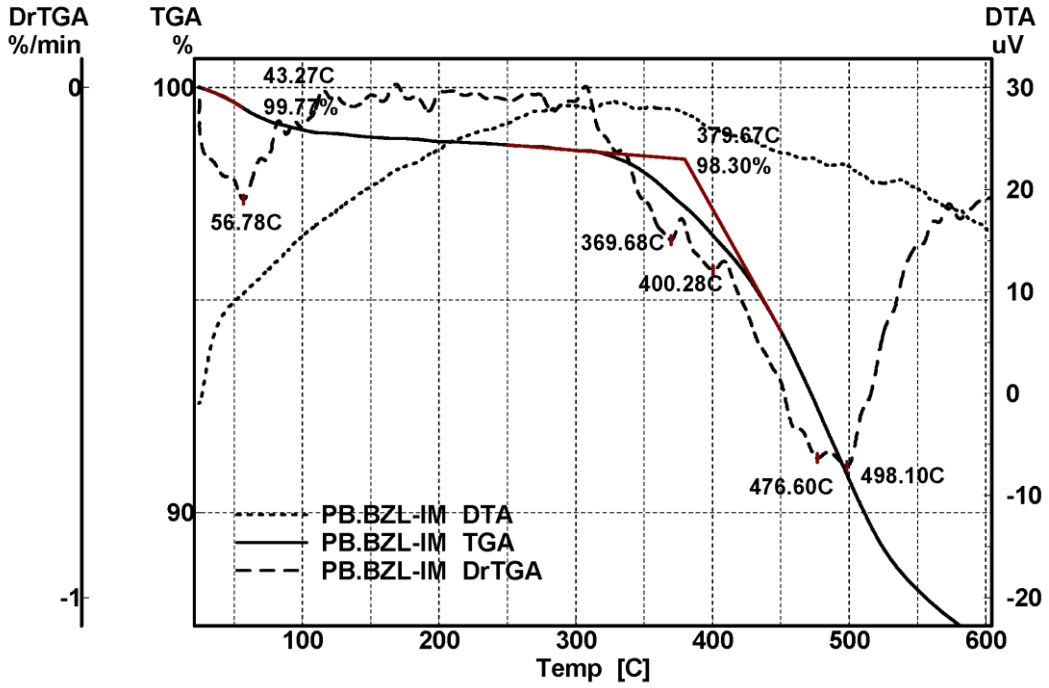

Figure B. 6 TG/DrTG/DTA thermogram of PB.BZL-IM

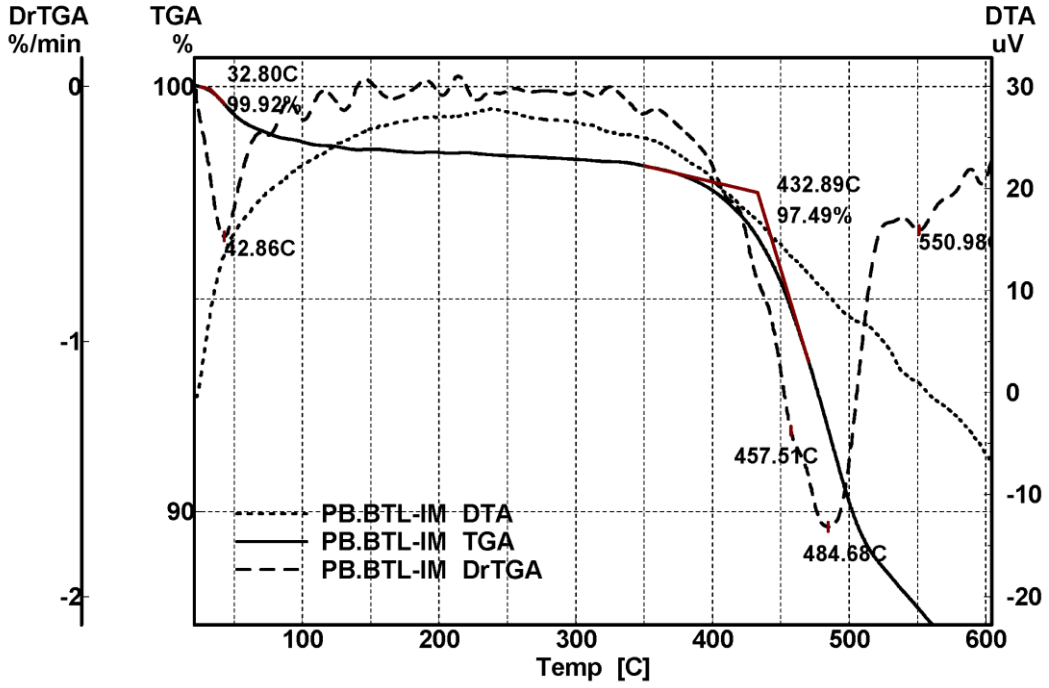

Figure B. 7 TG/DrTG/DTA thermogram of PB.BTL-IM

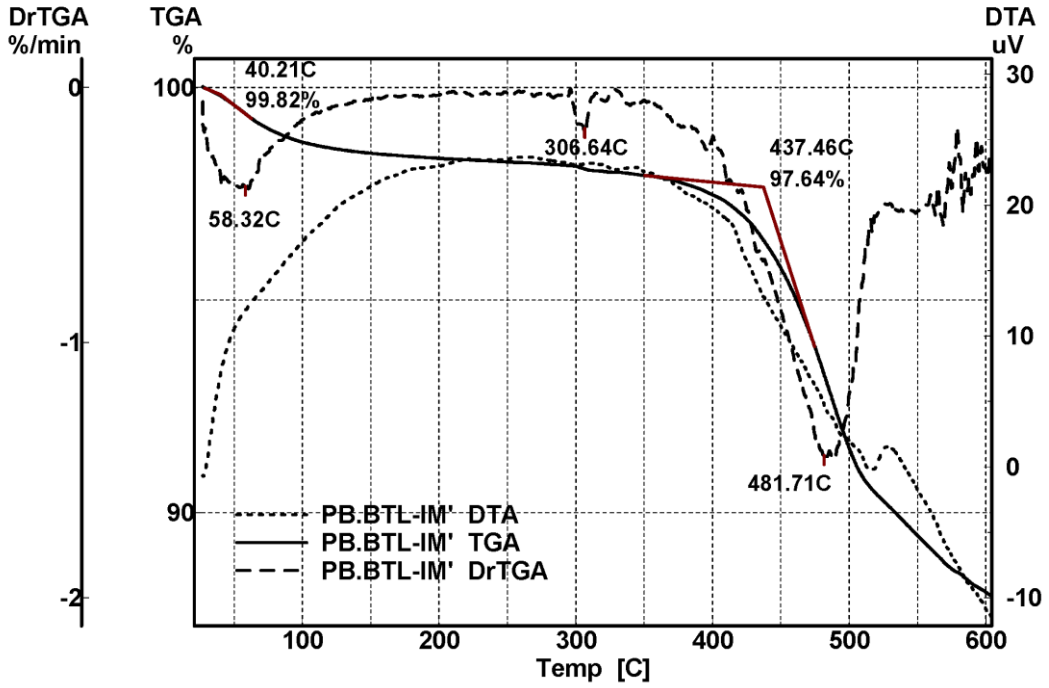

Figure B. 8 TG/DrTG/DTA thermogram of PB.BTL-IM’

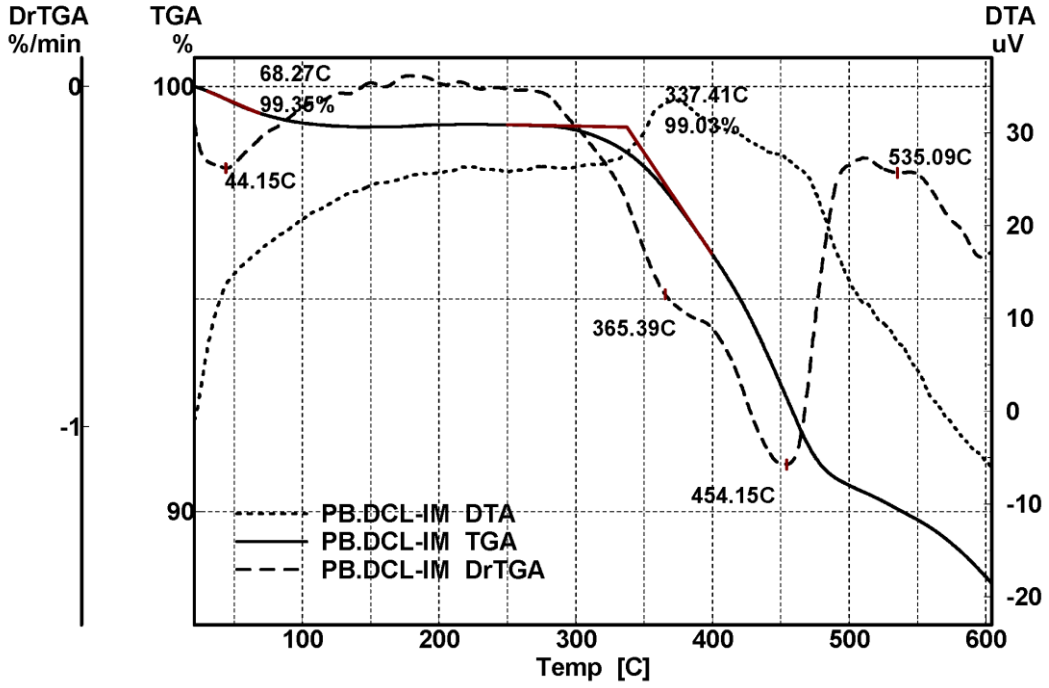

Figure B. 9 TG/DrTG/DTA thermogram of PB.DCL-IM

B.2 TG/DrTGA Thermograms of PA66 Compositions

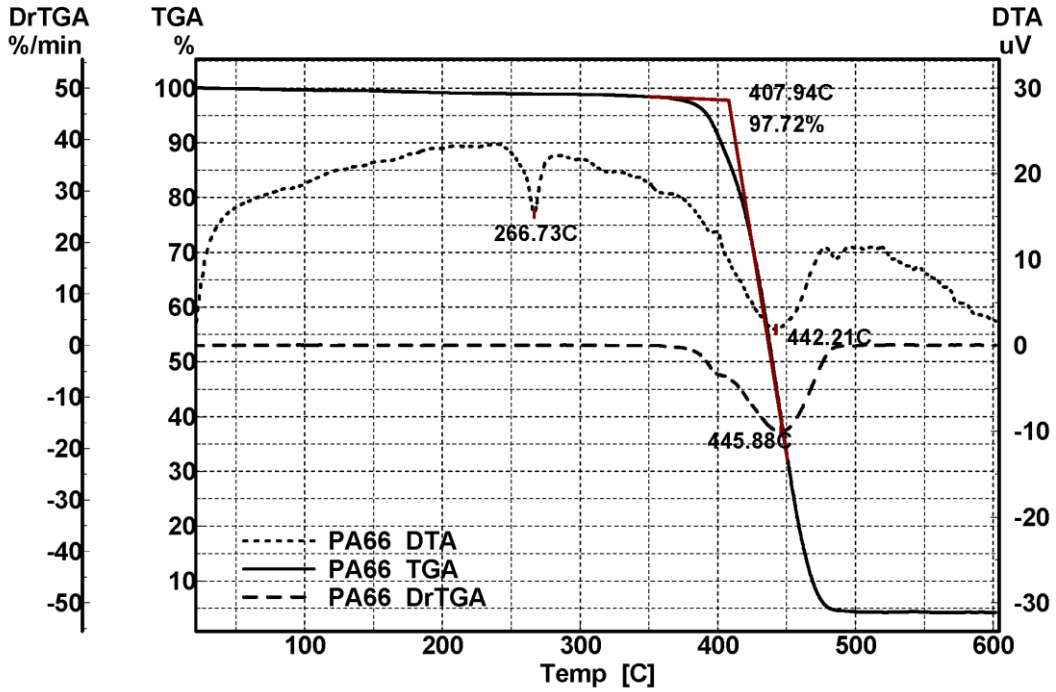

Figure B. 10 TG/DrTG/DTA thermogram of PA66

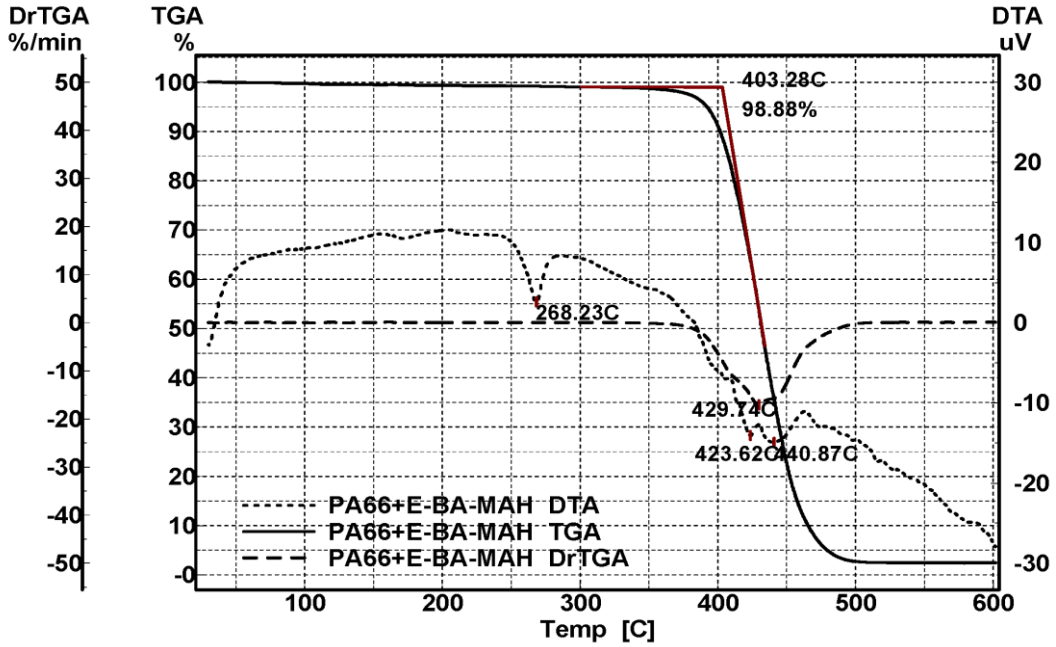

Figure B. 11 TG/DrTG/DTA thermogram of PA66/E-BA-MAH

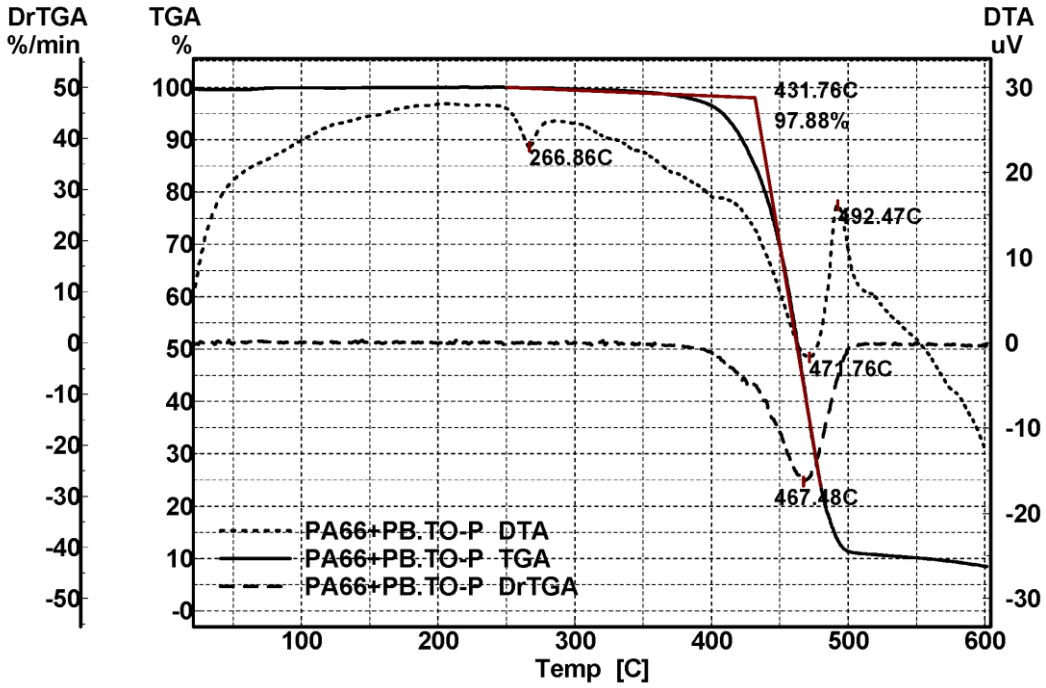

Figure B. 12 TG/DrTG/DTA thermogram of PA66/PB.TO-P

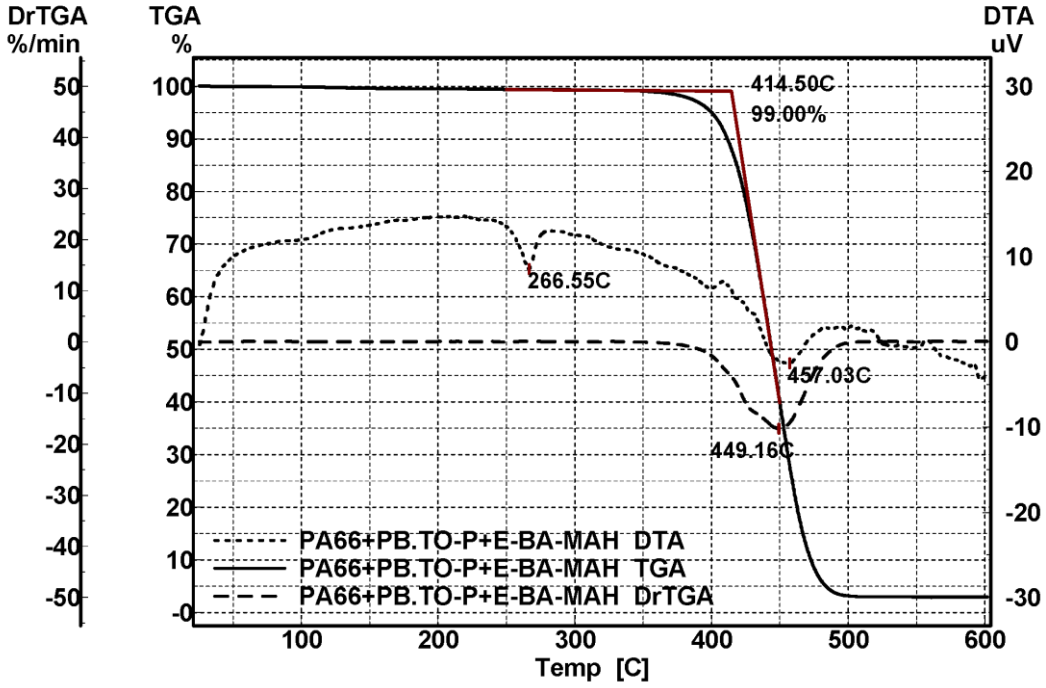

Figure B. 13 TG/DrTG/DTA thermogram of PA66/PB.TO-P/E-BA-MAH

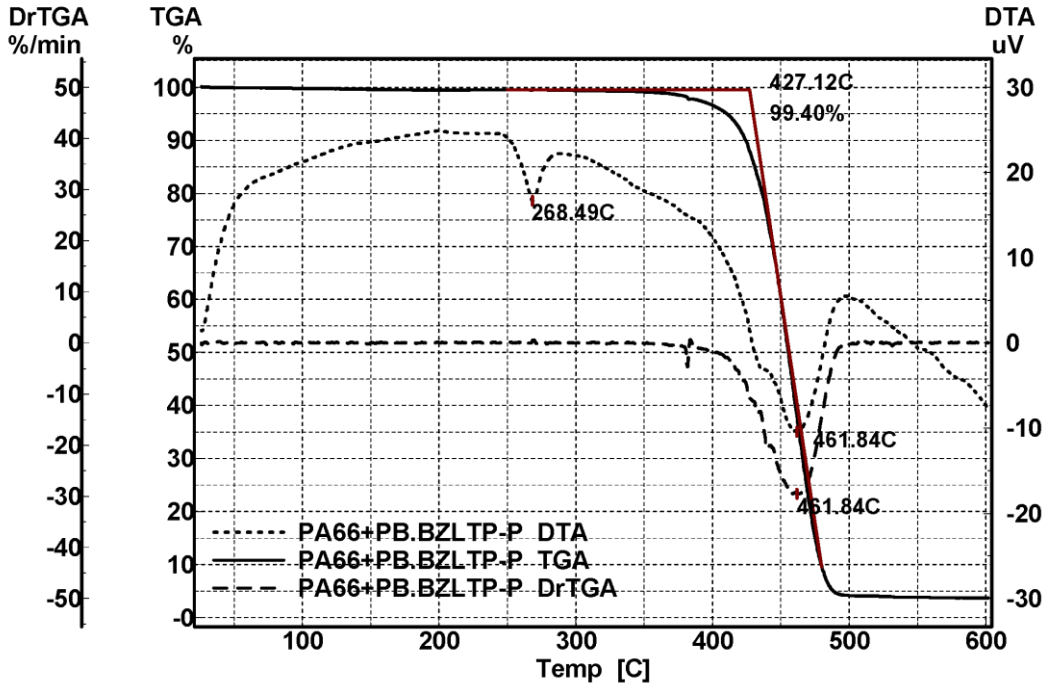

Figure B. 14 TG/DrTG/DTA thermogram of PA66/PB.BZLTP-P

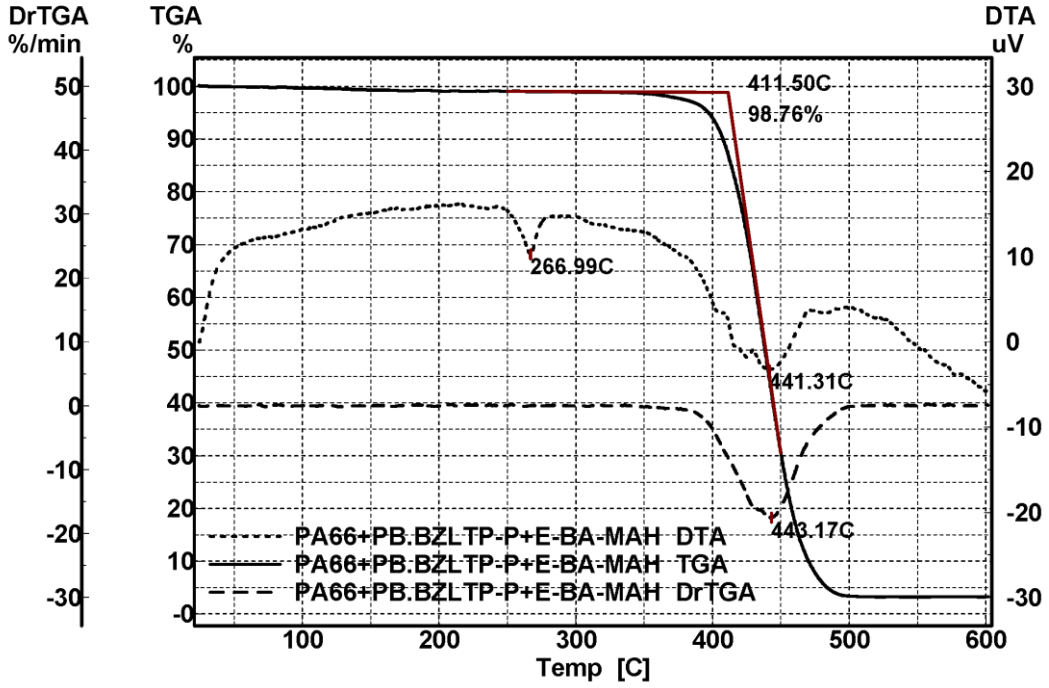

Figure B. 15 TG/DrTG/DTA thermogram of PA66/PB.BZLTP-P/E-BA-MAH

B.3 TG/DrTGA Thermograms of PET Compositions

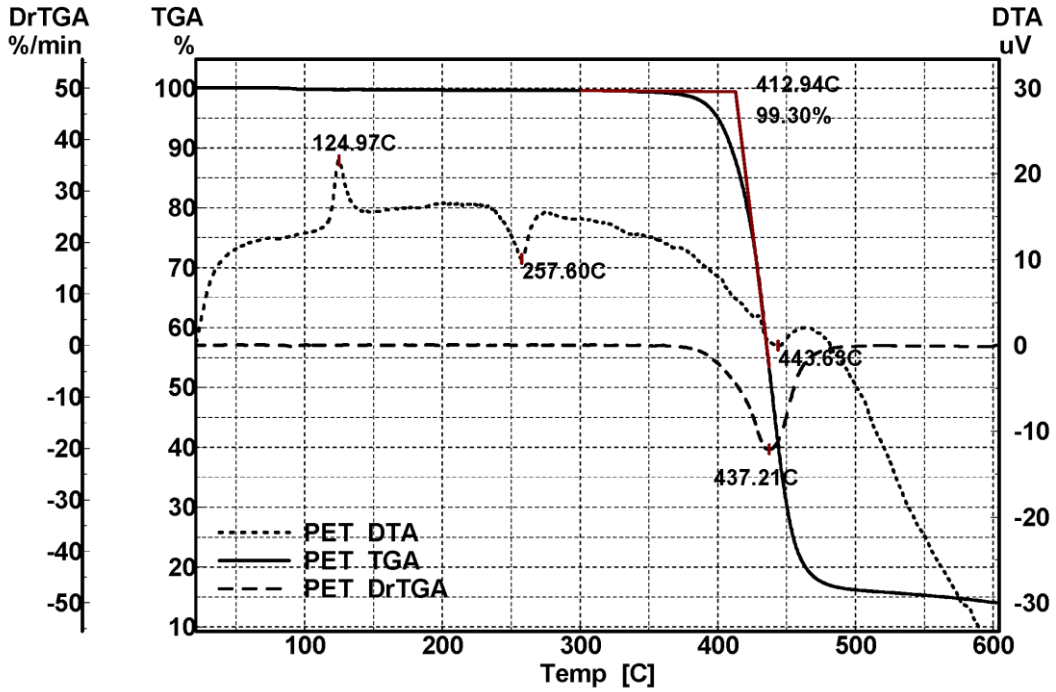

Figure B. 16 TG/DrTG/DTA thermogram of PET

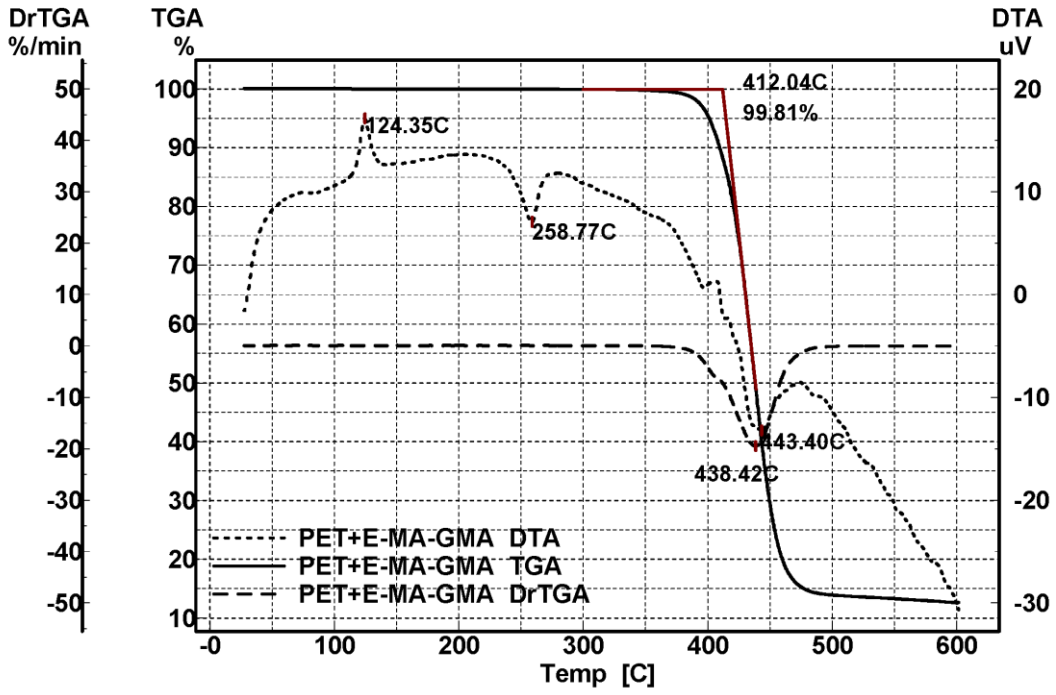

Figure B. 17 TG/DrTG/DTA thermogram of PET/E-MA-GMA

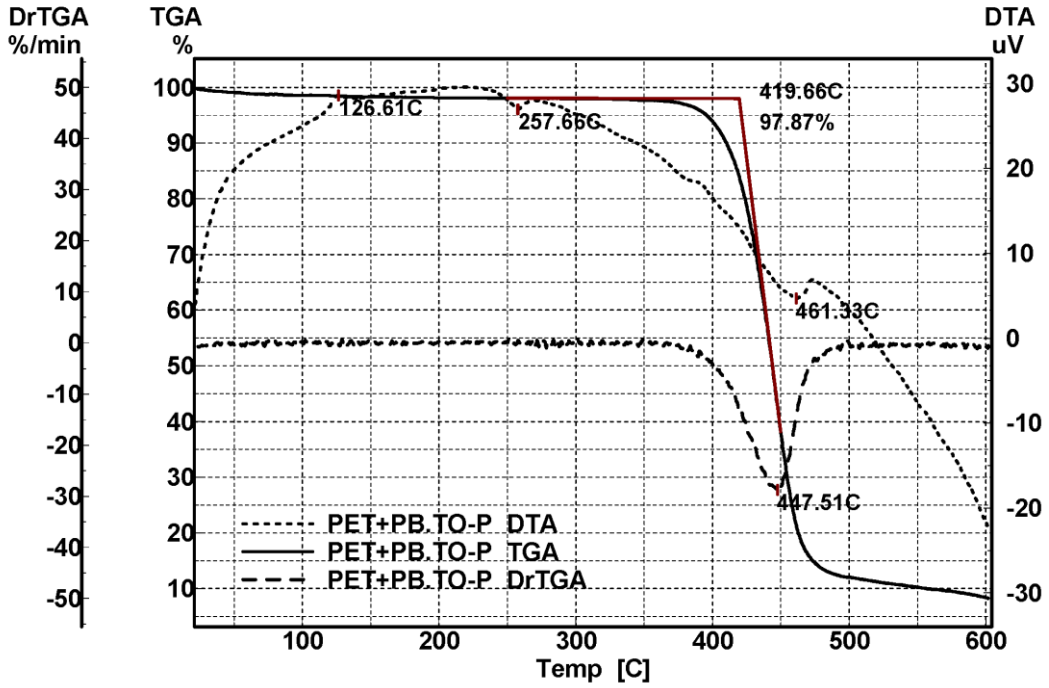

Figure B. 18 TG/DrTG/DTA thermogram of PET/PB.TO-P

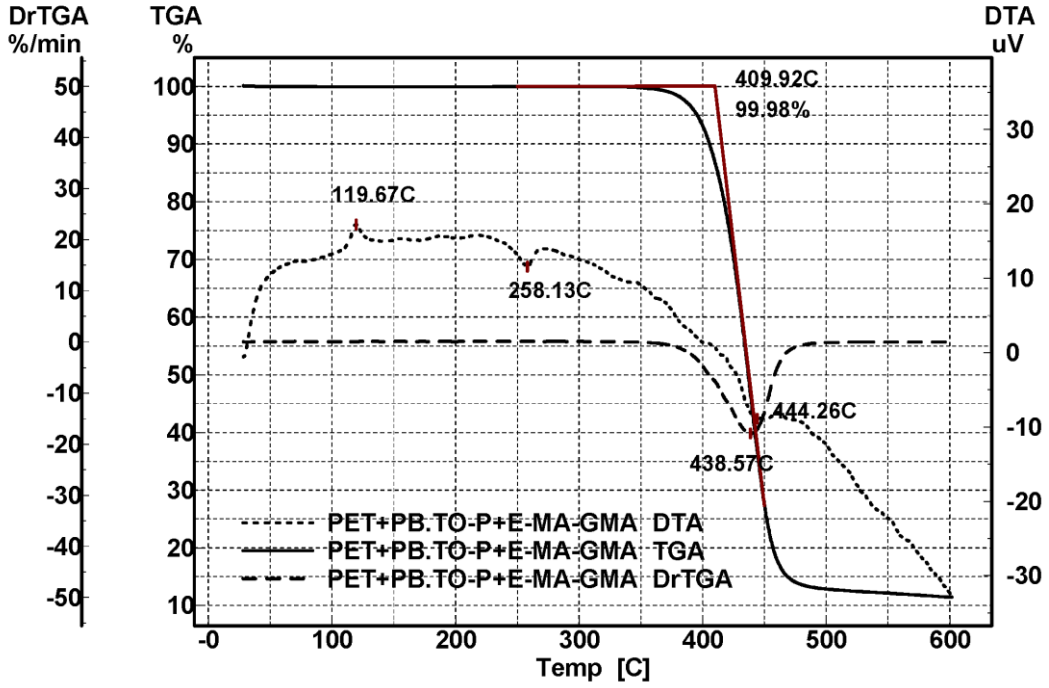

Figure B. 19 TG/DrTG/DTA thermogram of PET/PB.TO-P/E-MA-GMA

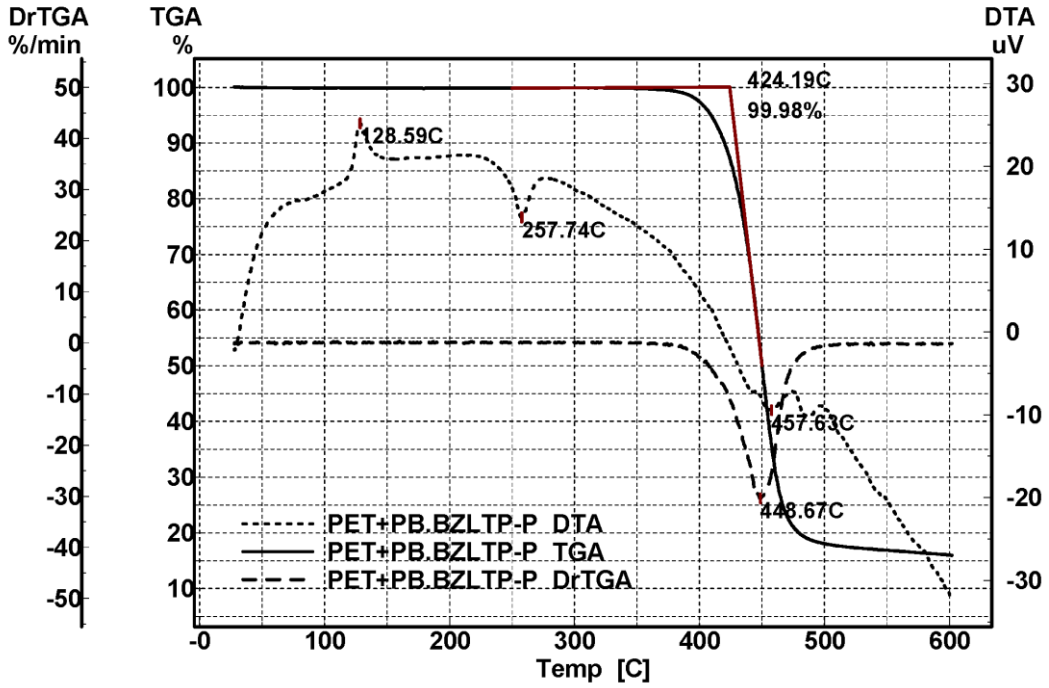

Figure B. 20 TG/DrTG/DTA thermogram of PET/PB.BZLTP-P

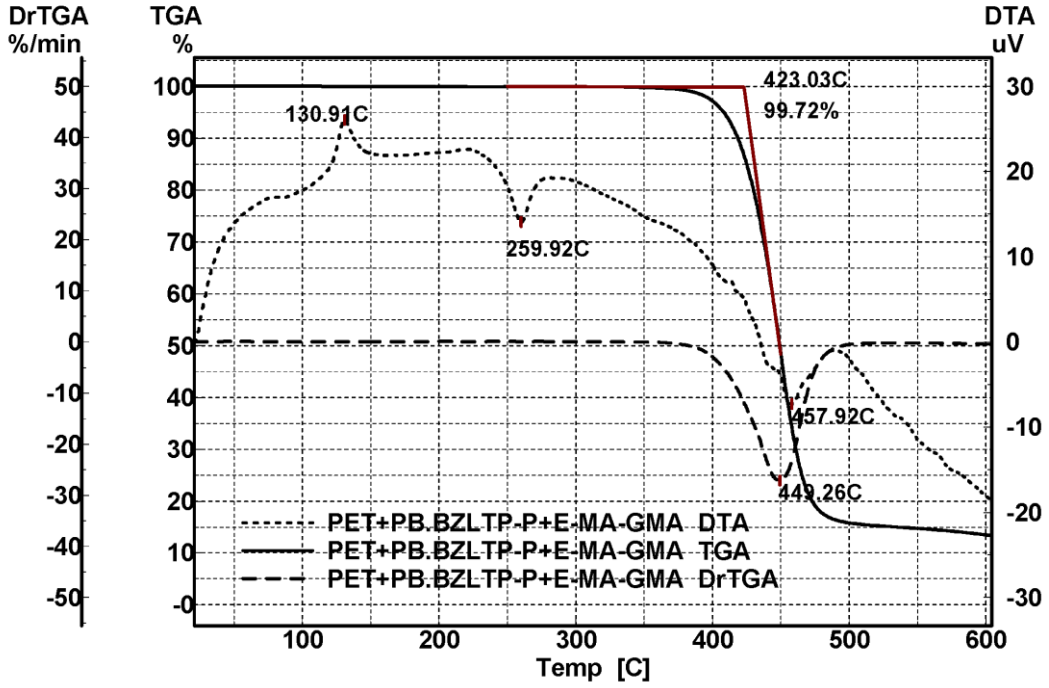

Figure B. 21 TG/DrTG/DTA thermogram of PET/PB.BZLTP-P/E-MA-GMA

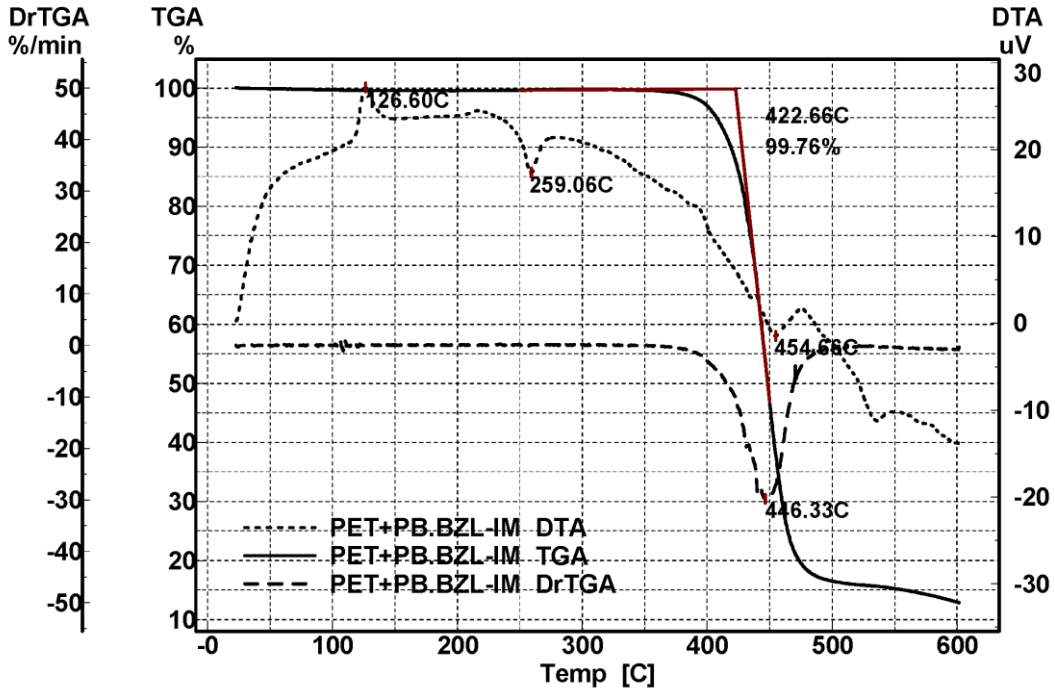

Figure B. 22 TG/DrTG/DTA thermogram of PET/PB.BZL-IM

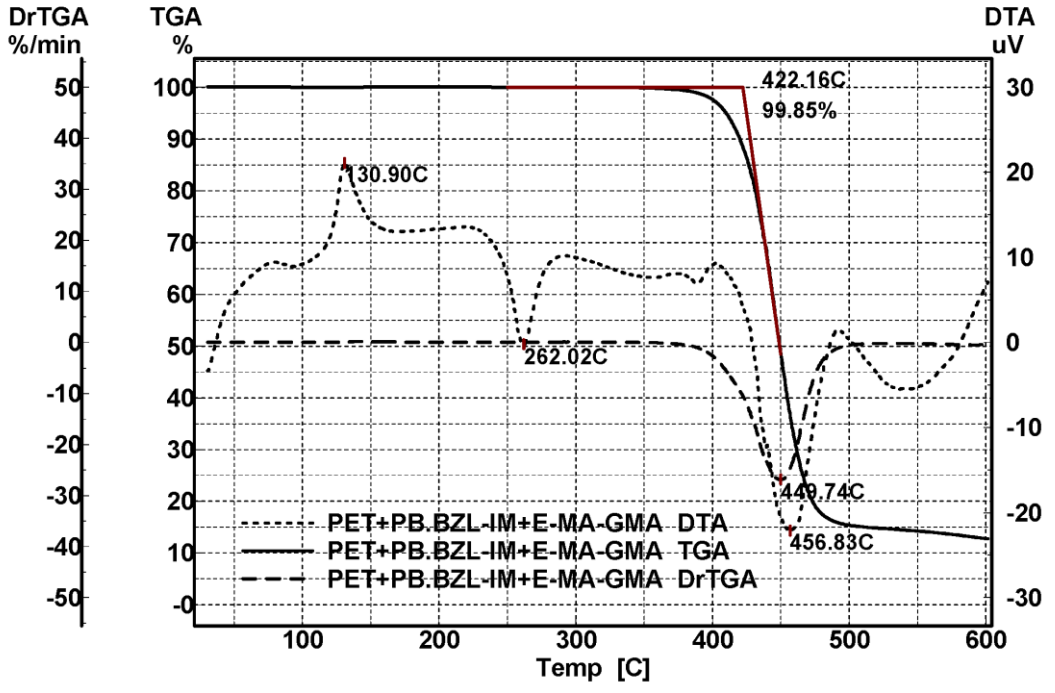

Figure B. 23 TG/DrTG/DTA thermogram of PET/PB.BZL-IM/E-MA-GMA

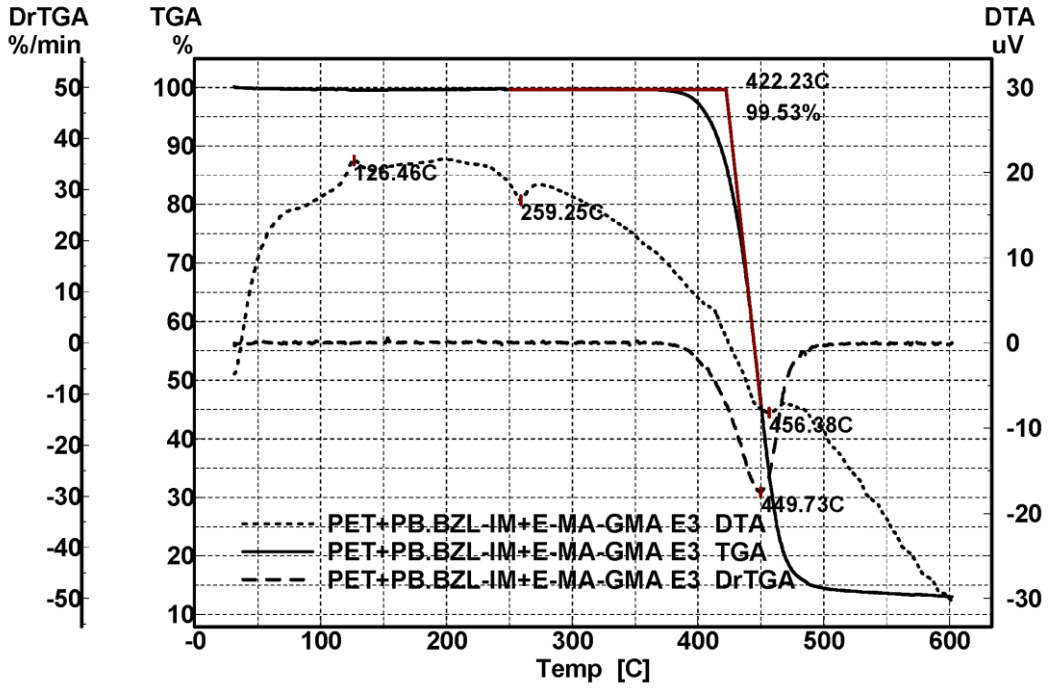

Figure B. 24 TG/DrTG/DTA thermogram of PET/PB.BZL-IM/E-MA-GMA (E3)

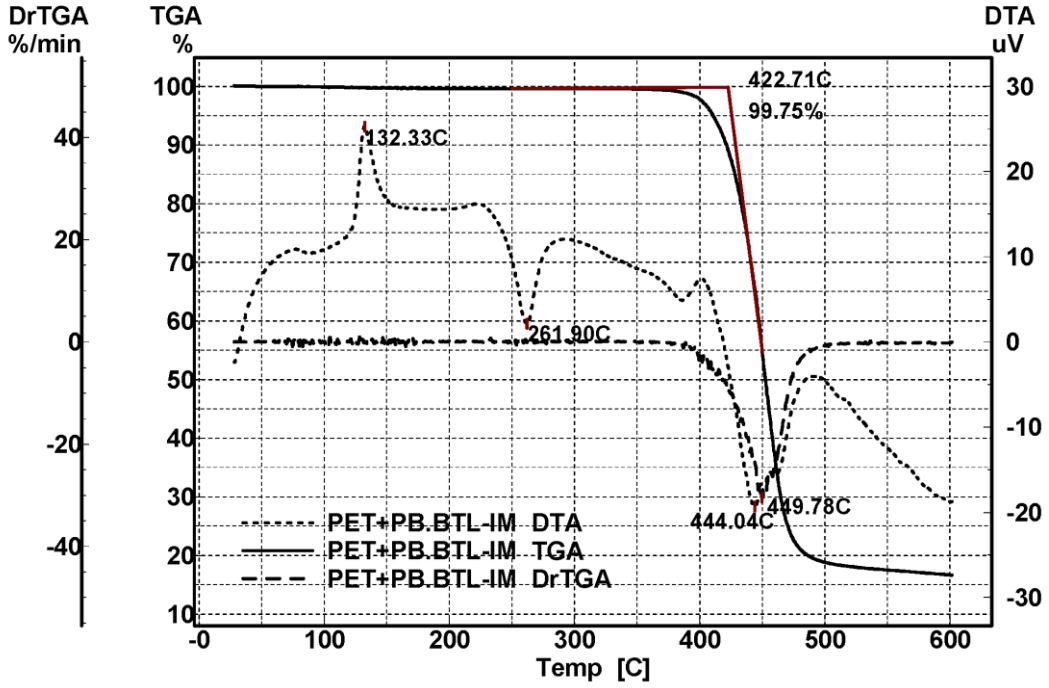

Figure B. 25 TG/DrTG/DTA thermogram of PET/PB.BTL-IM

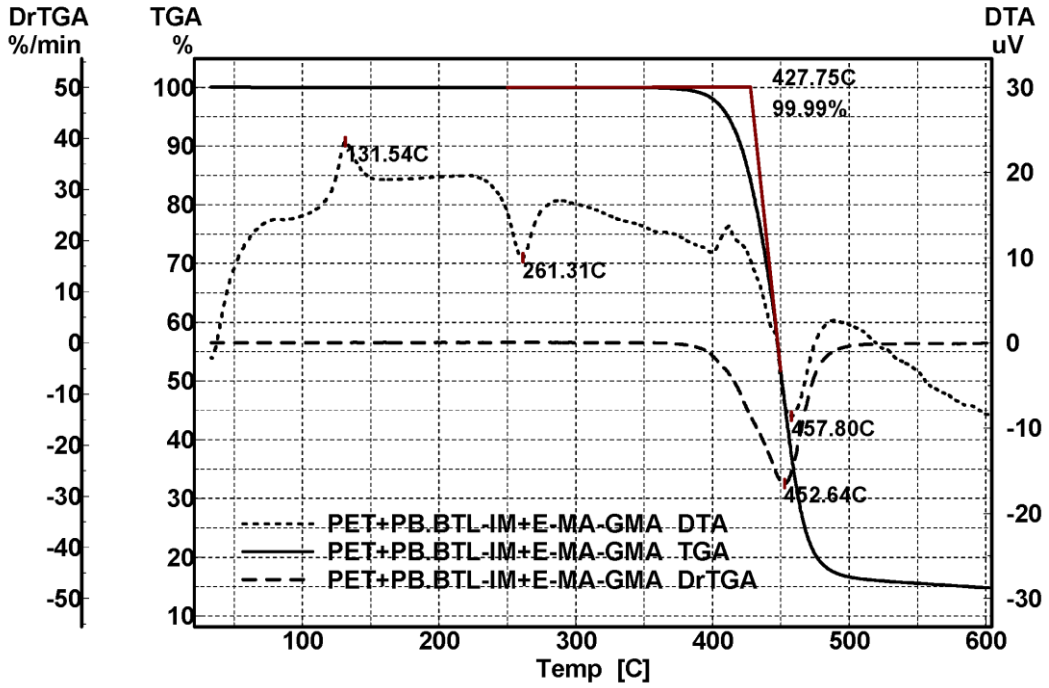

Figure B. 26 TG/DrTG/DTA thermogram of PET/PB.BTL-IM/E-MA-GMA

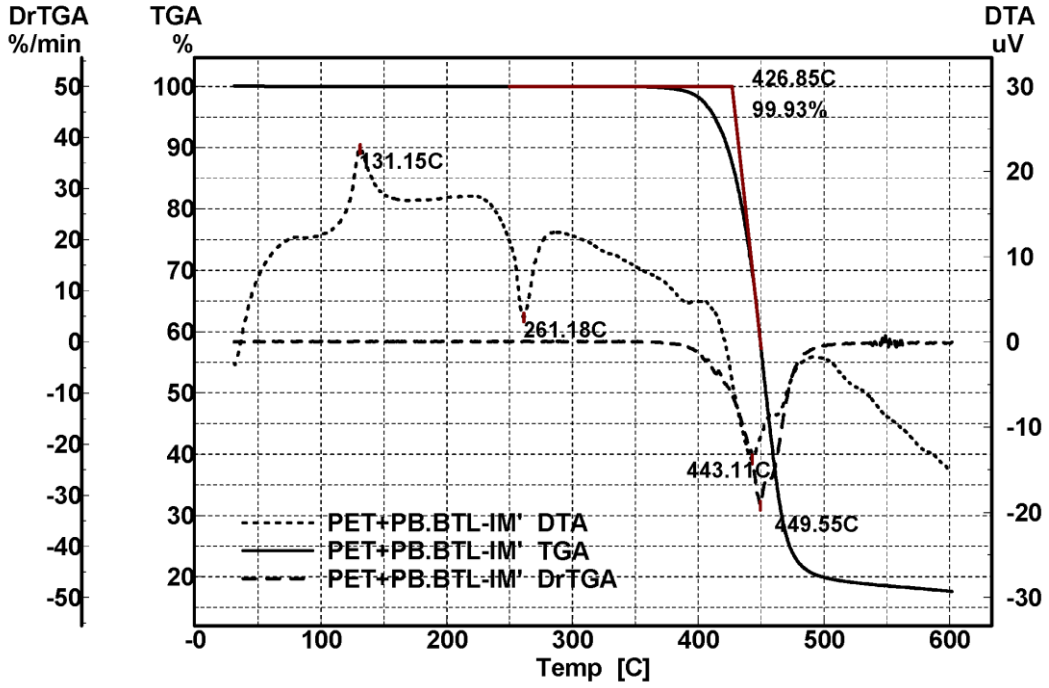

Figure B. 27 TG/DrTG/DTA thermogram of PET/PB.BTL-IM'

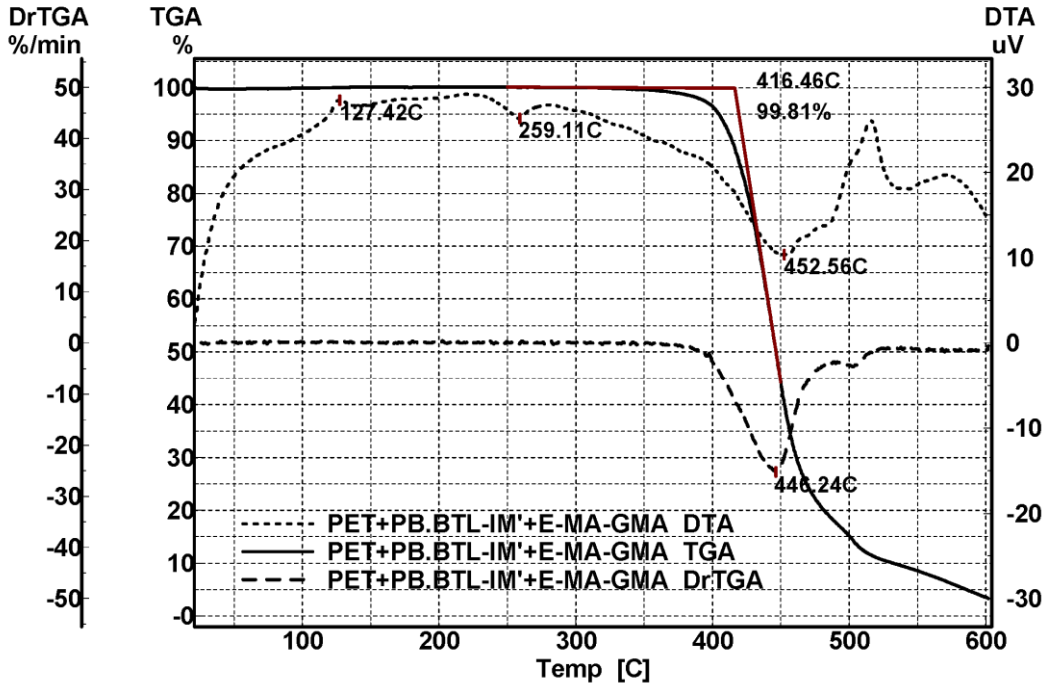

Figure B. 28 TG/DrTG/DTA thermogram of PET/PB.BTL-IM'/E-MA-GMA

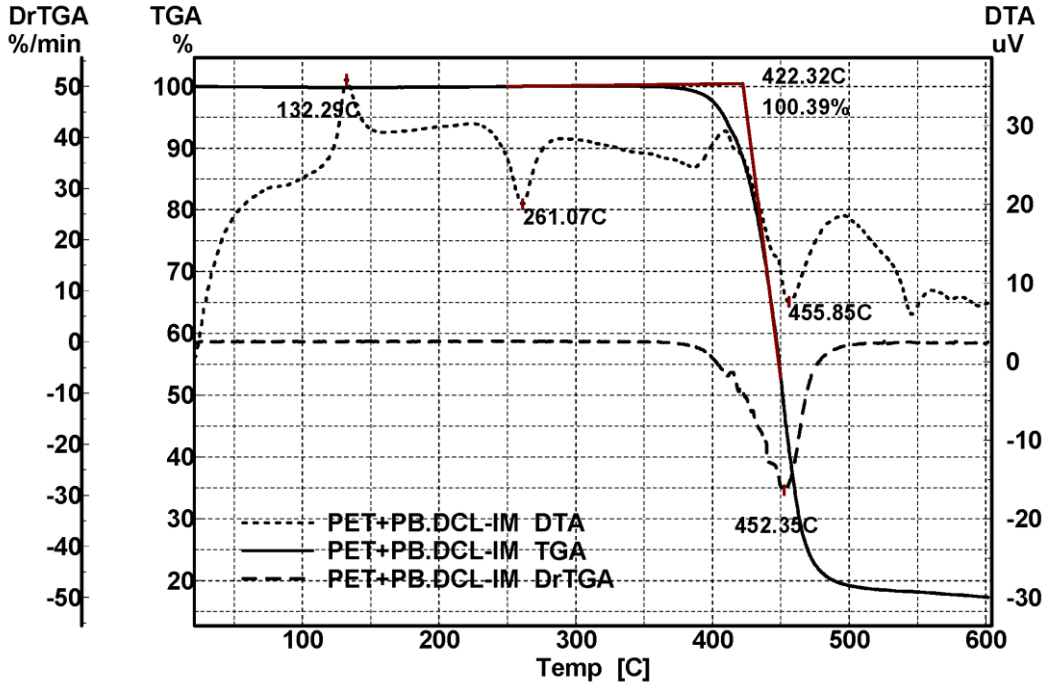

Figure B. 29 TG/DrTG/DTA thermogram of PET/PB.DCL-IM

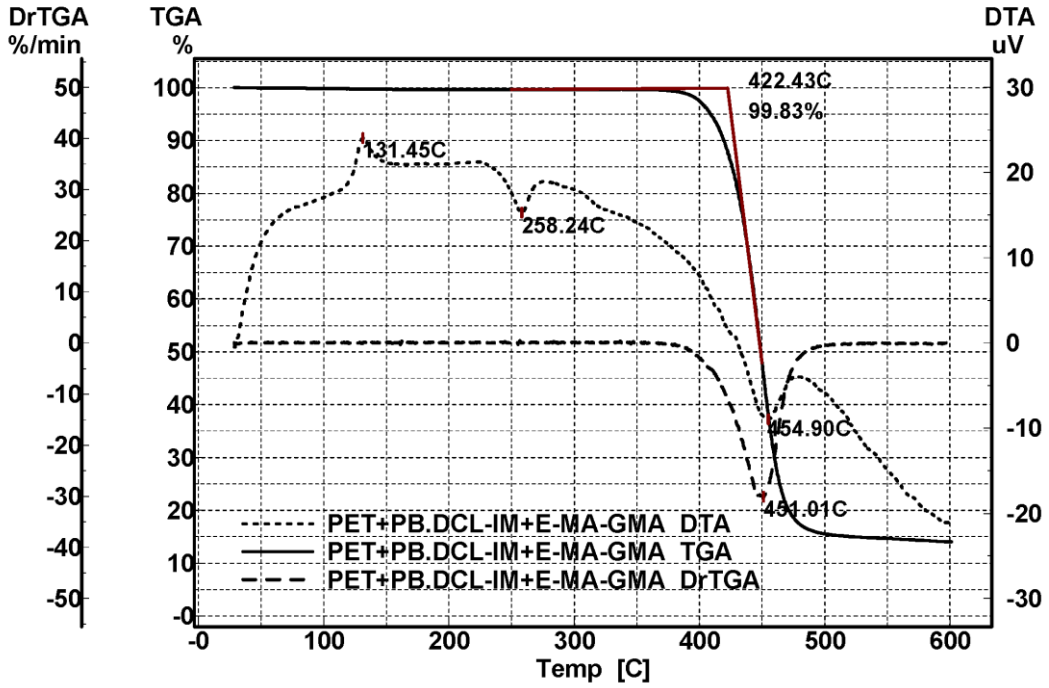

Figure B. 30 TG/DrTG/DTA thermogram of PET/PB.DCL-IM/E-MA-GMA

APPENDIX C

DSC ANALYSIS

C.1 DSC Thermograms of PA66 Compositions

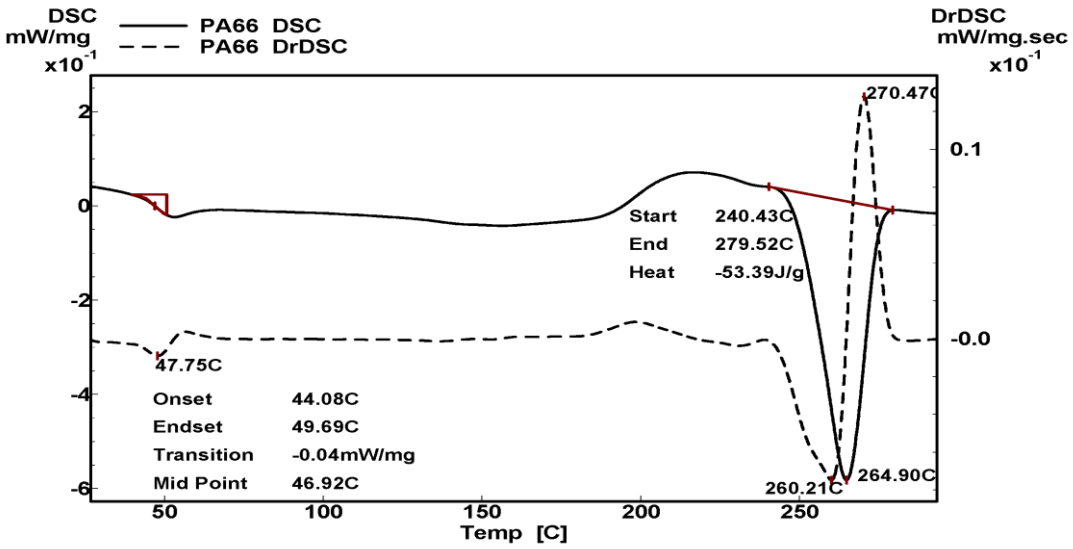

Figure C. 1 DSC thermogram of pure PA66

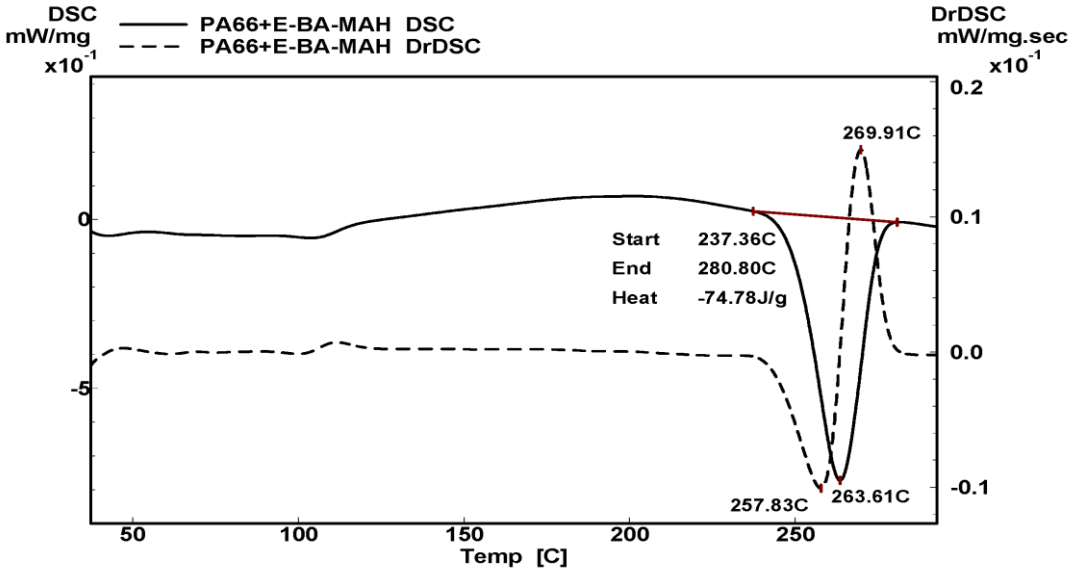

Figure C. 2 DSC thermogram of PA66/E-BA-MAH blend

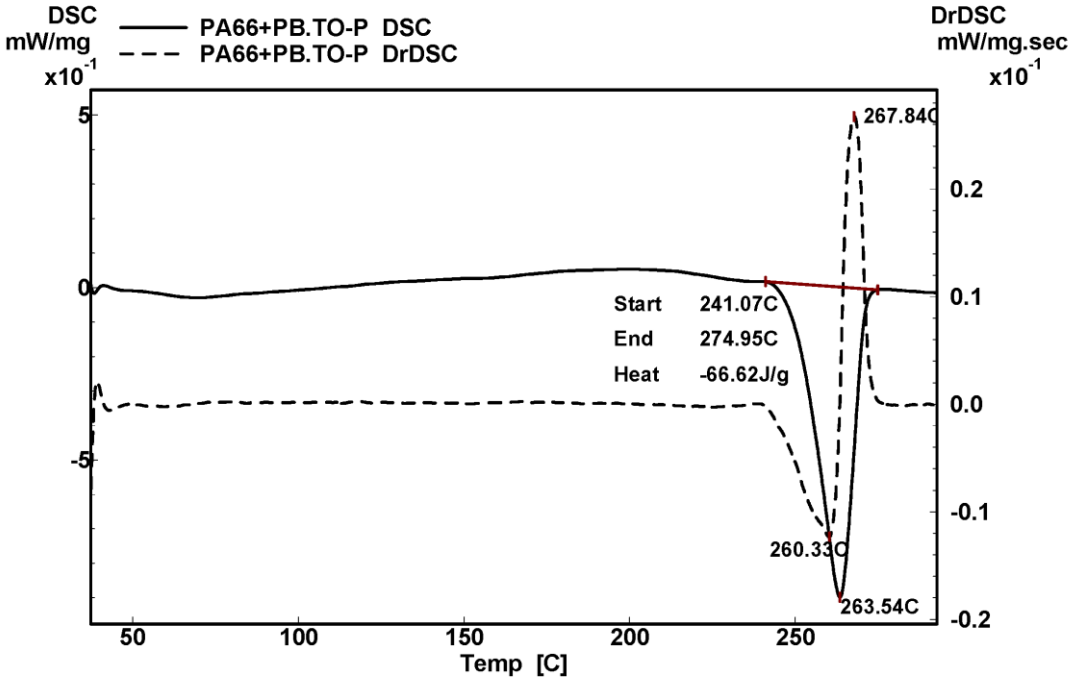

Figure C. 3 DSC thermogram of PA66/PB.TO-P

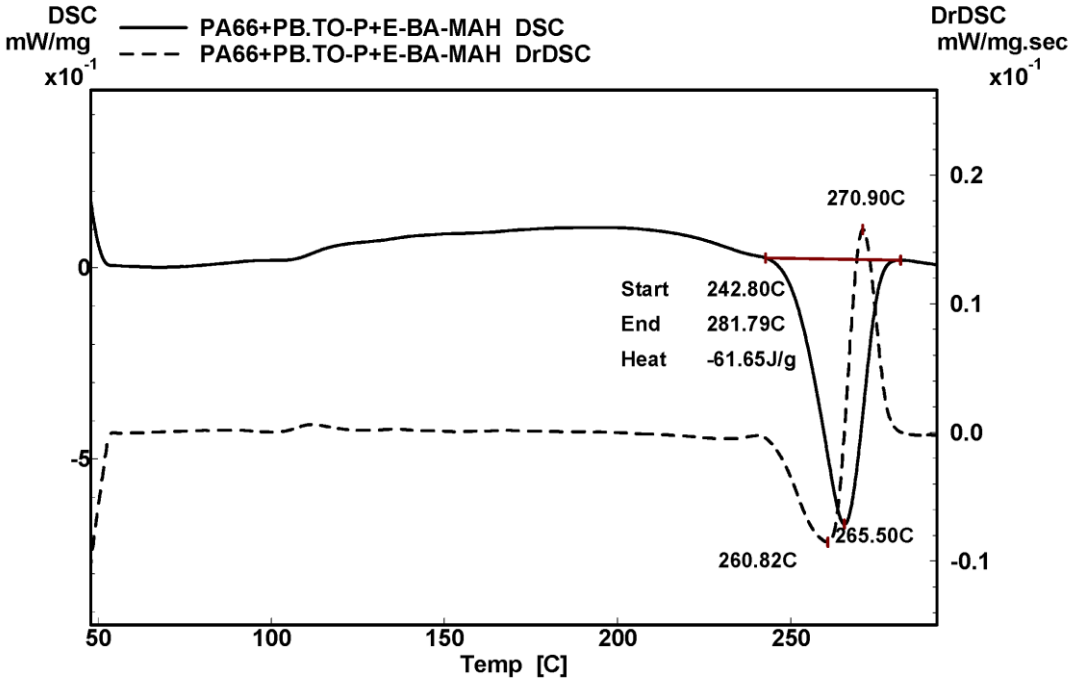

Figure C. 4 DSC thermogram of PA66/PB.TO-P/E-BA-MAH

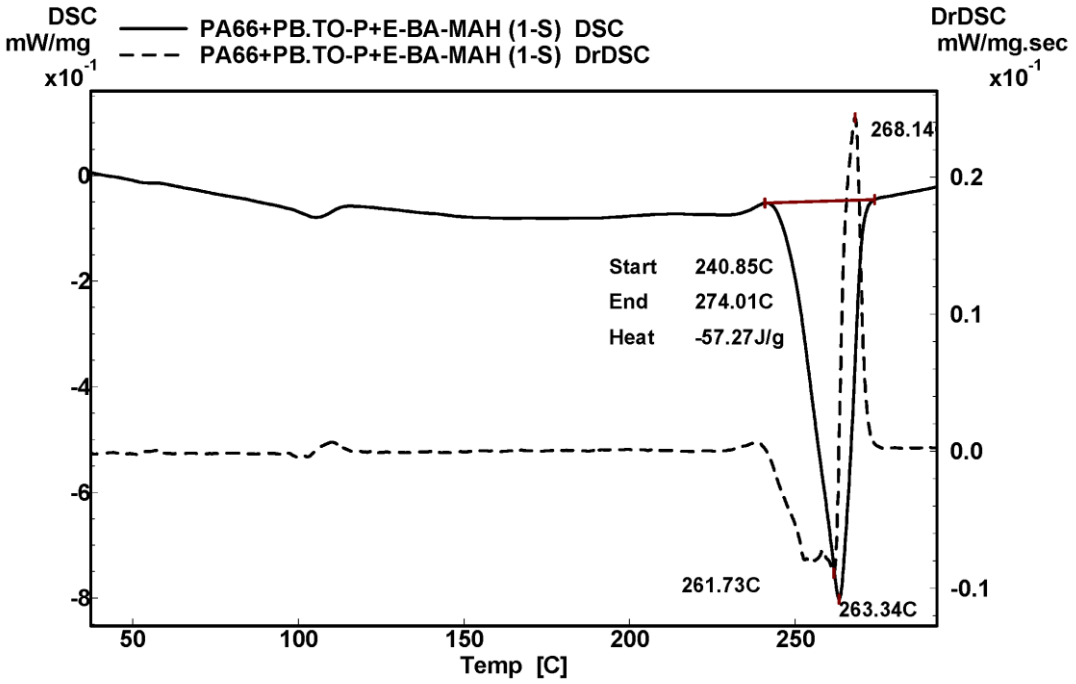

Figure C. 5 DSC thermogram of PA66/PB.TO-P/E-BA-MAH (1-S)

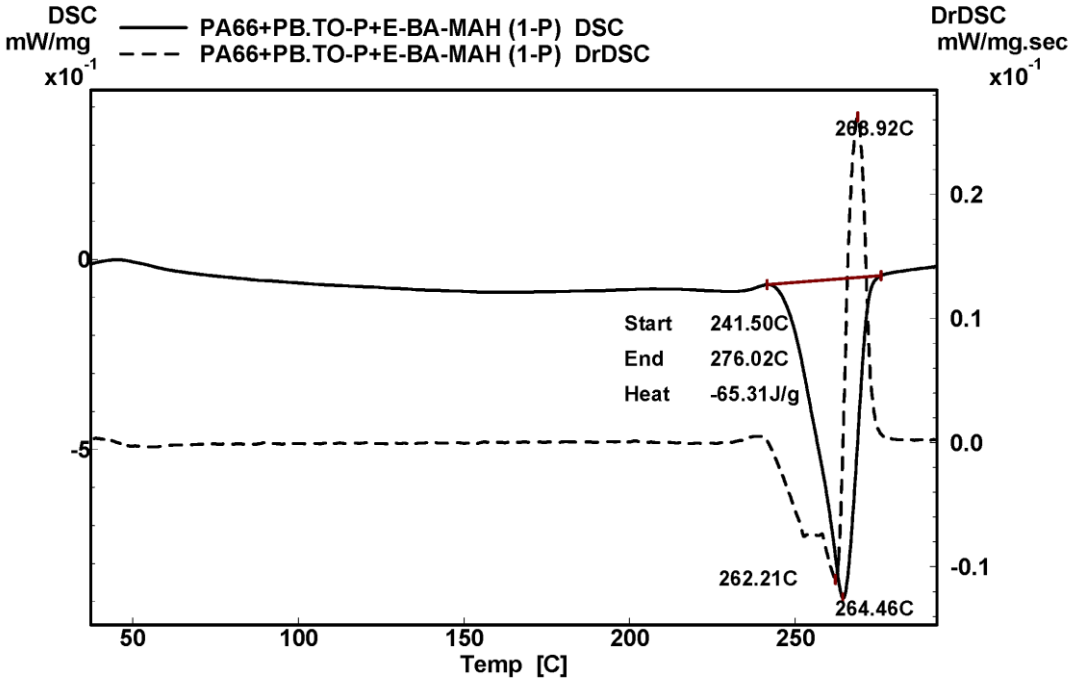

Figure C. 6 DSC thermogram of PA66/PB.TO-P/E-BA-MAH (1-P)

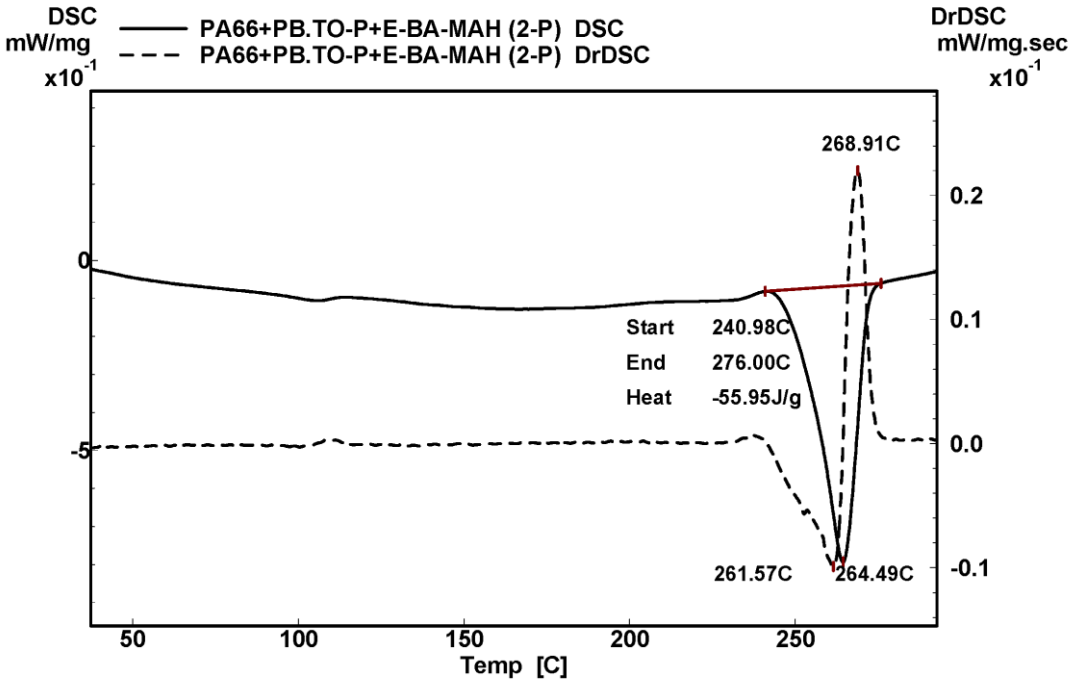

Figure C. 7 DSC thermogram of PA66/PB.TO-P/E-BA-MAH (2-P)

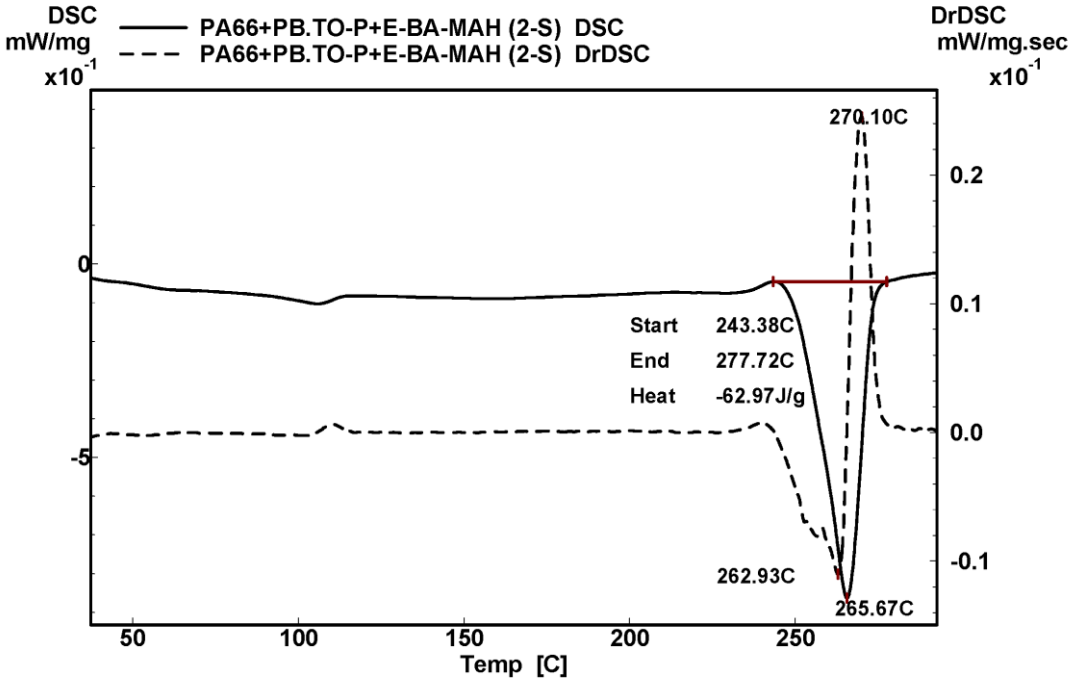

Figure C. 8 DSC thermogram of PA66/PB.TO-P/E-BA-MAH (2-S)

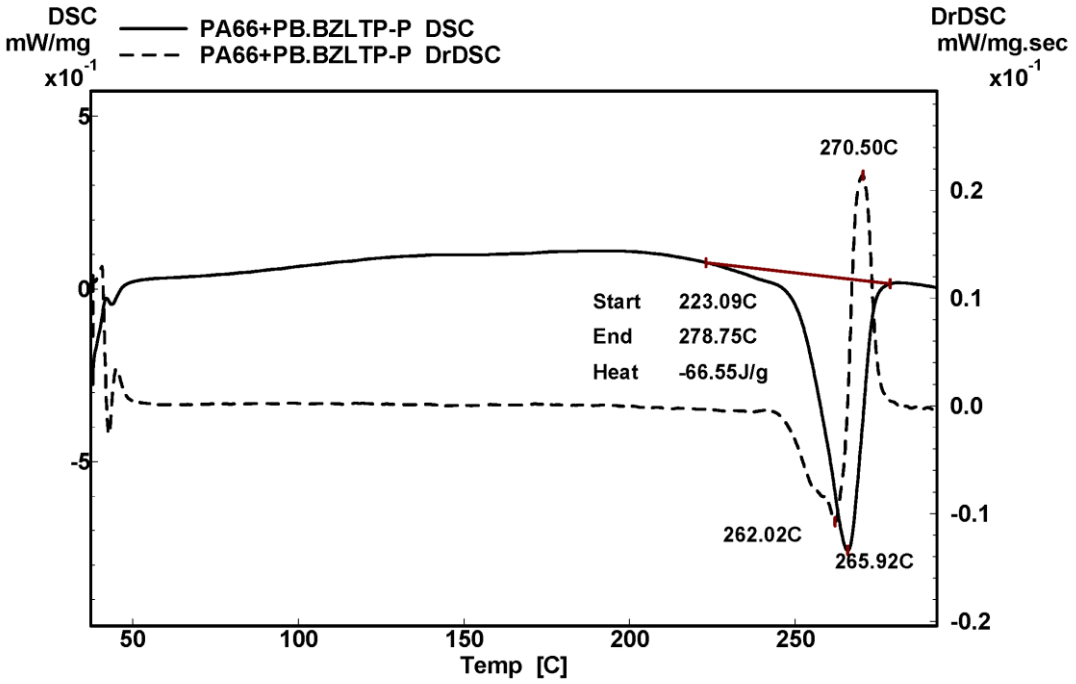

Figure C. 9 DSC thermogram of PA66/PB.BZLTP-P

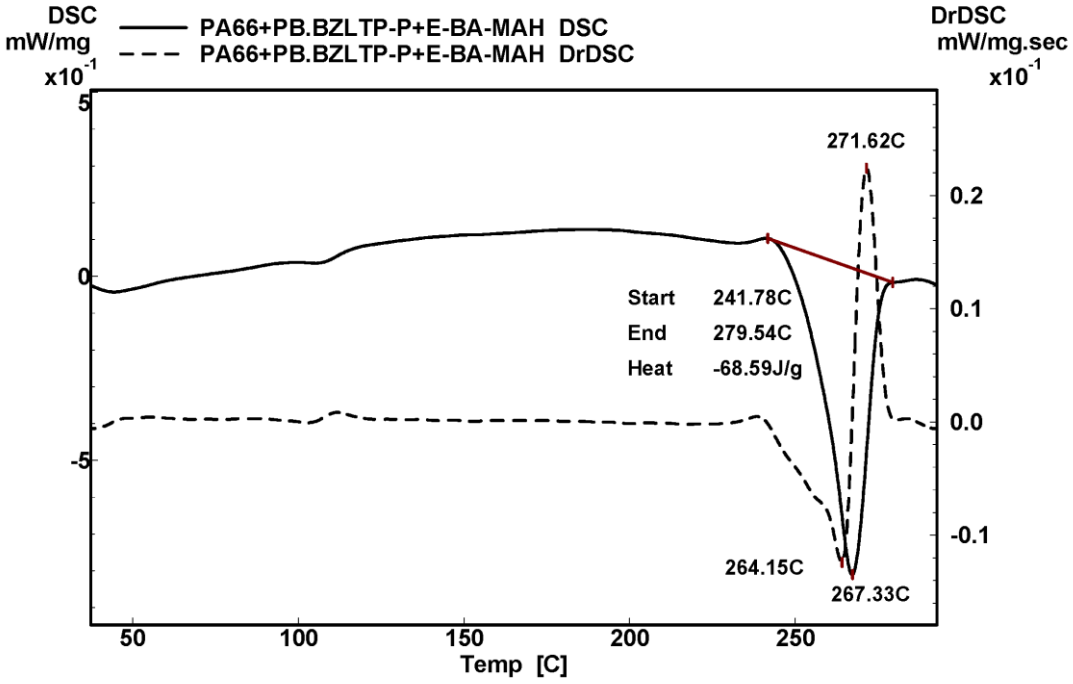

Figure C. 10 DSC thermogram of PA66/PB.BZLTP-P/E-BA-MAH

C.2 DSC Thermograms of PET Compositions

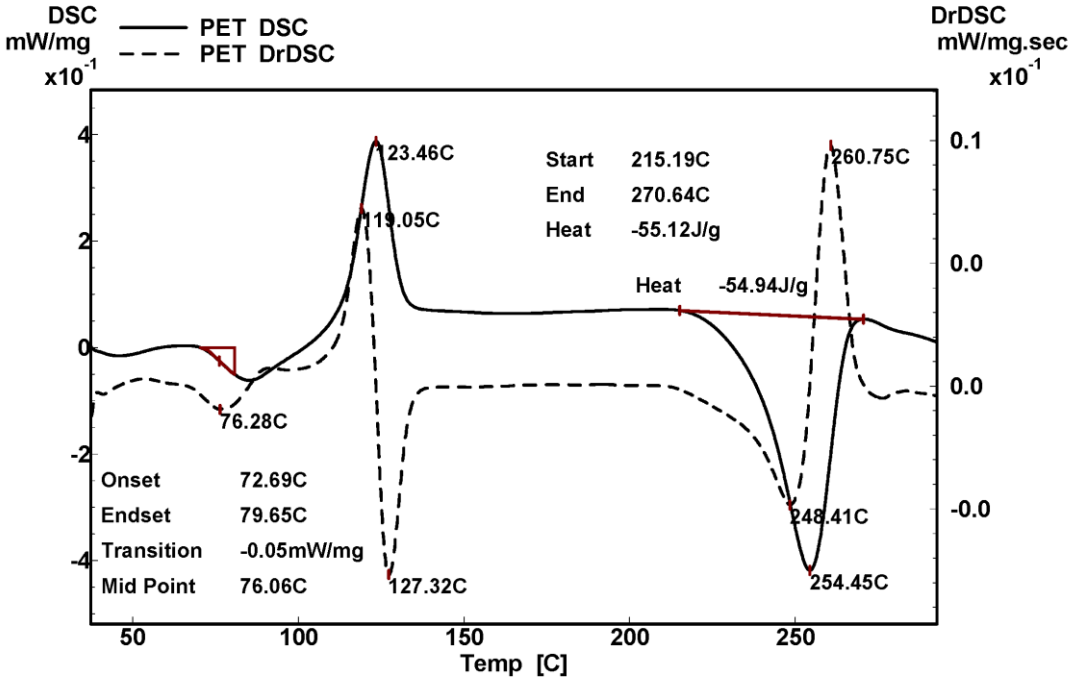

Figure C. 11 DSC thermogram of PET

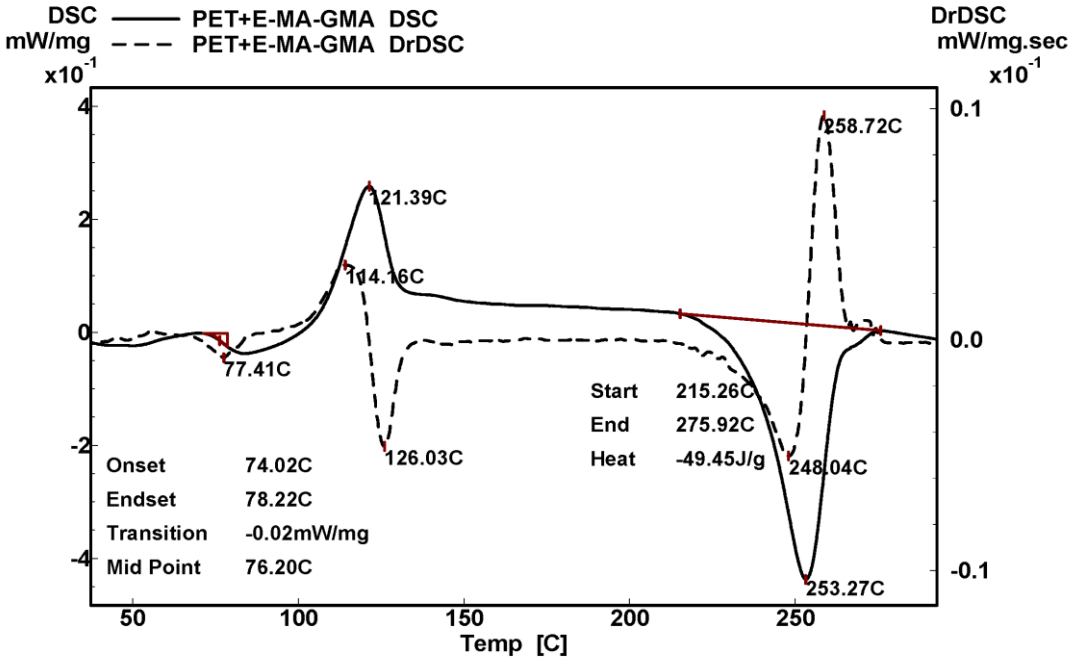

Figure C. 12 DSC thermogram of PET/E-MA-GMA

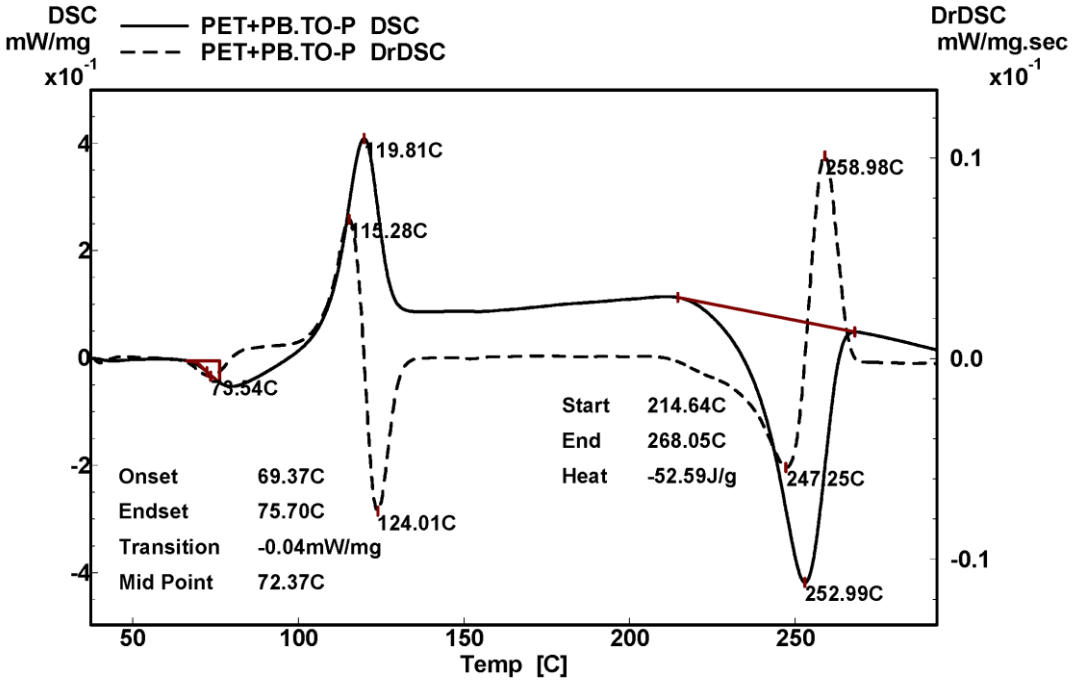

Figure C. 13 DSC thermogram of PET/PB.TO-P

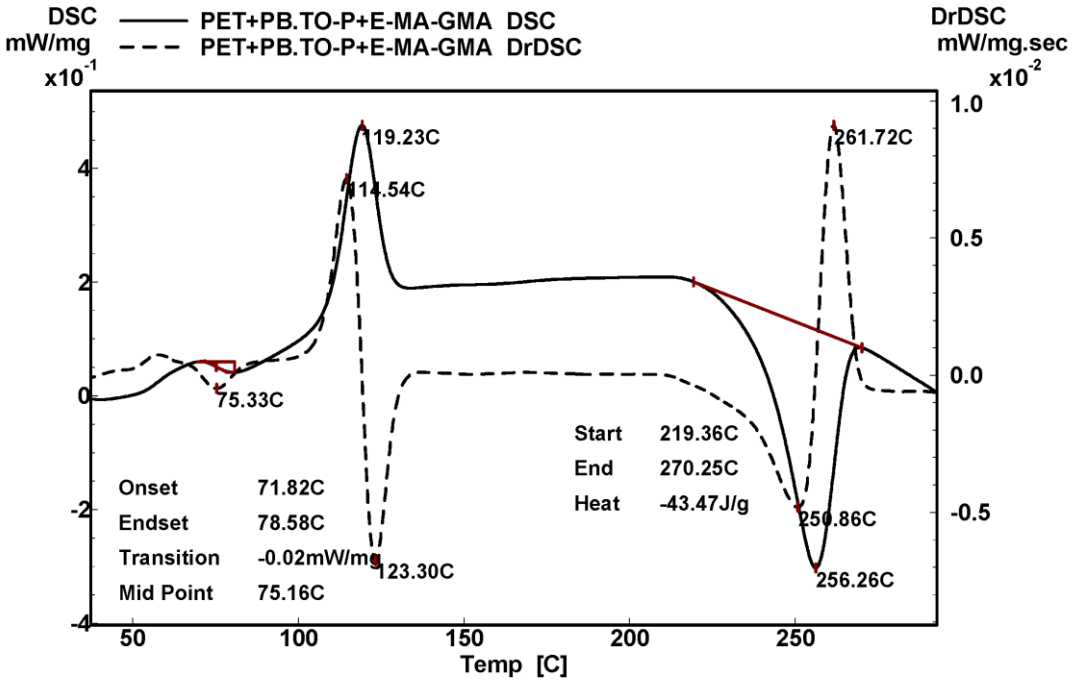

Figure C. 14 DSC thermogram of PET/PB.TO-P/E-MA-GMA

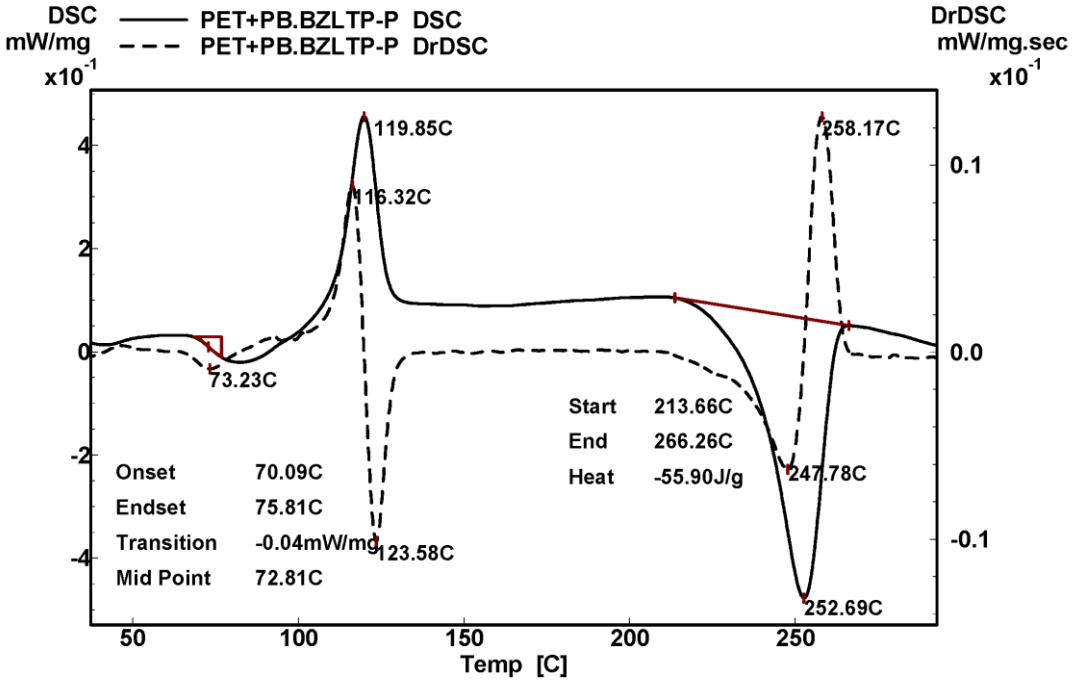

Figure C. 15 DSC thermogram of PET/PB.BZLTP-P

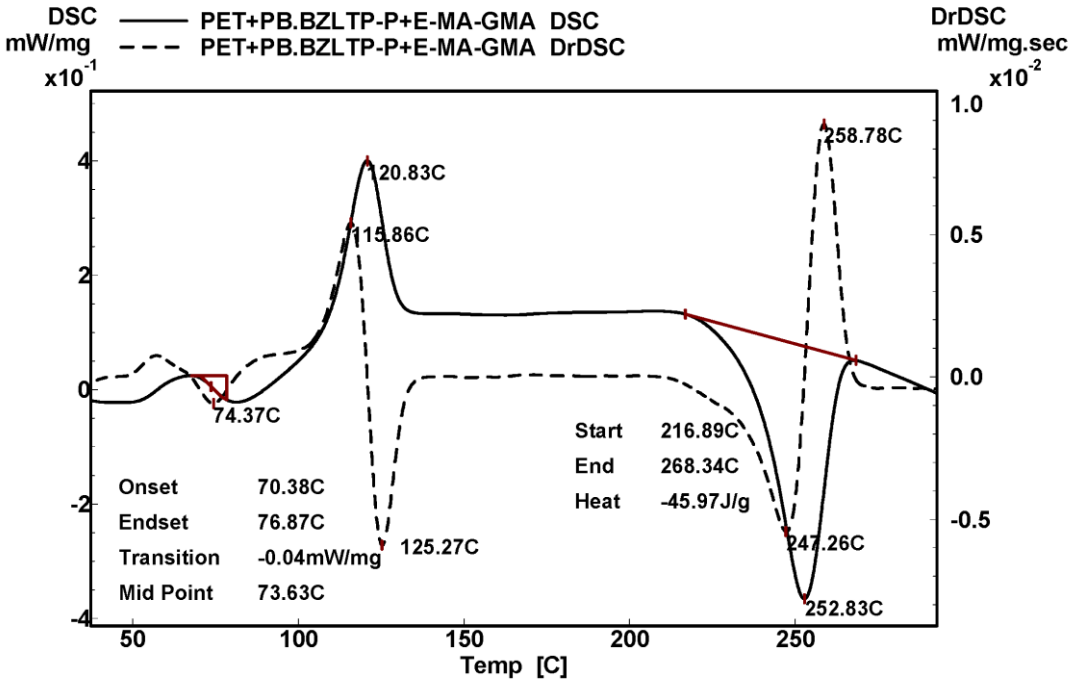

Figure C. 16 DSC thermogram of PET/PB.BZLTP-P/E-MA-GMA

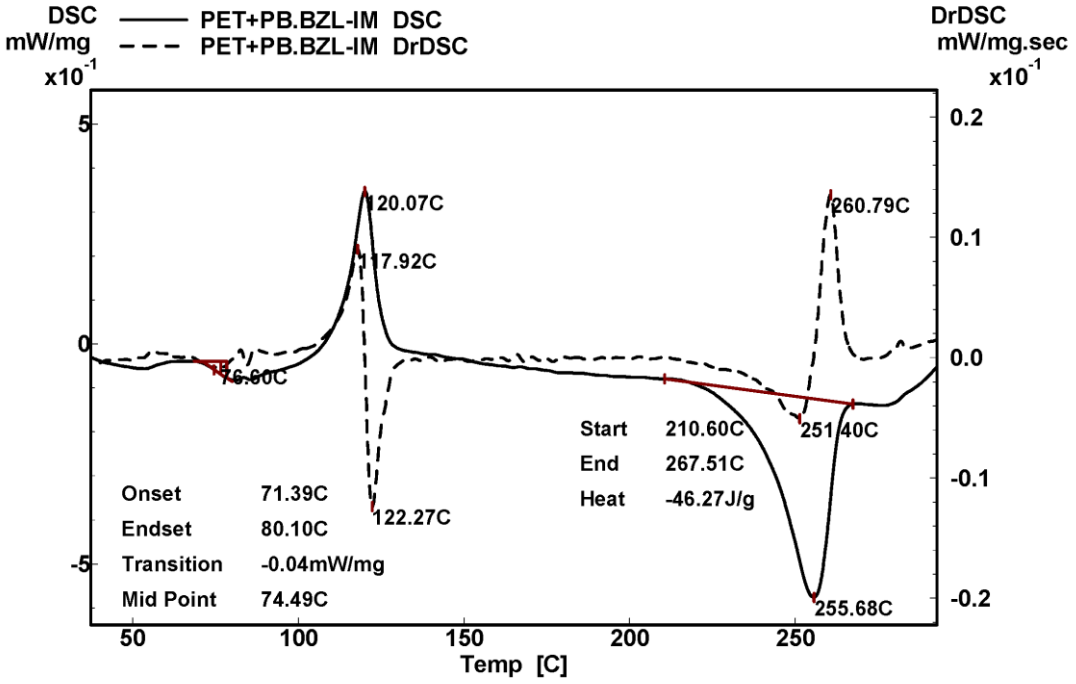

Figure C. 17 DSC thermogram of PET/PB.BZL-IM

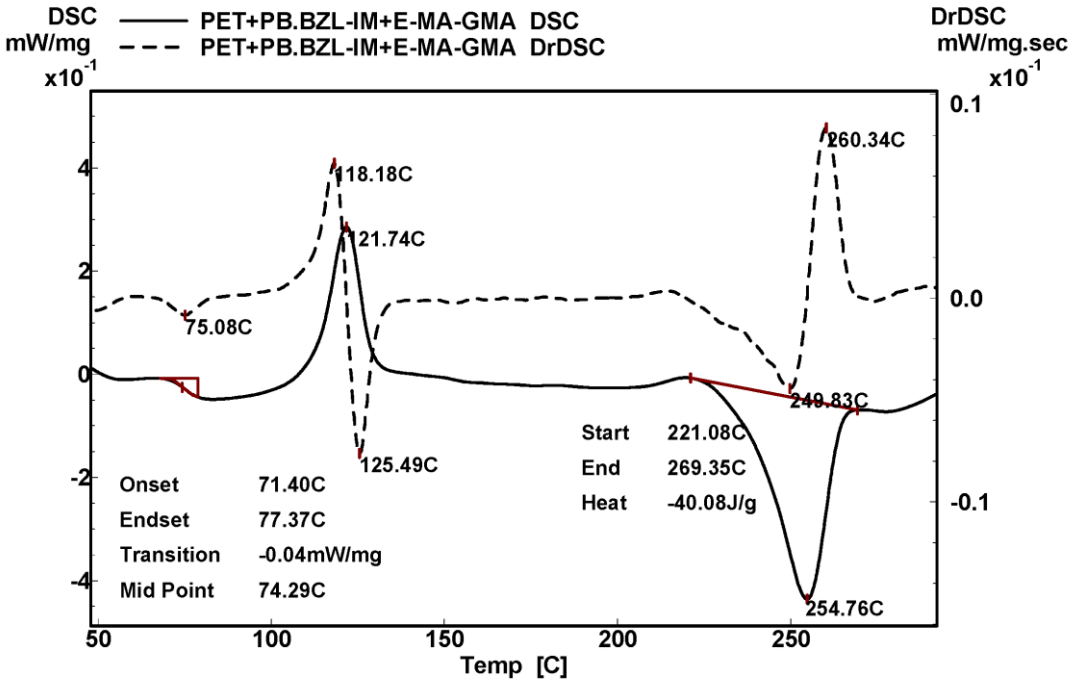

Figure C. 18 DSC thermogram of PET/PB.BZL-IM/E-MA-GMA

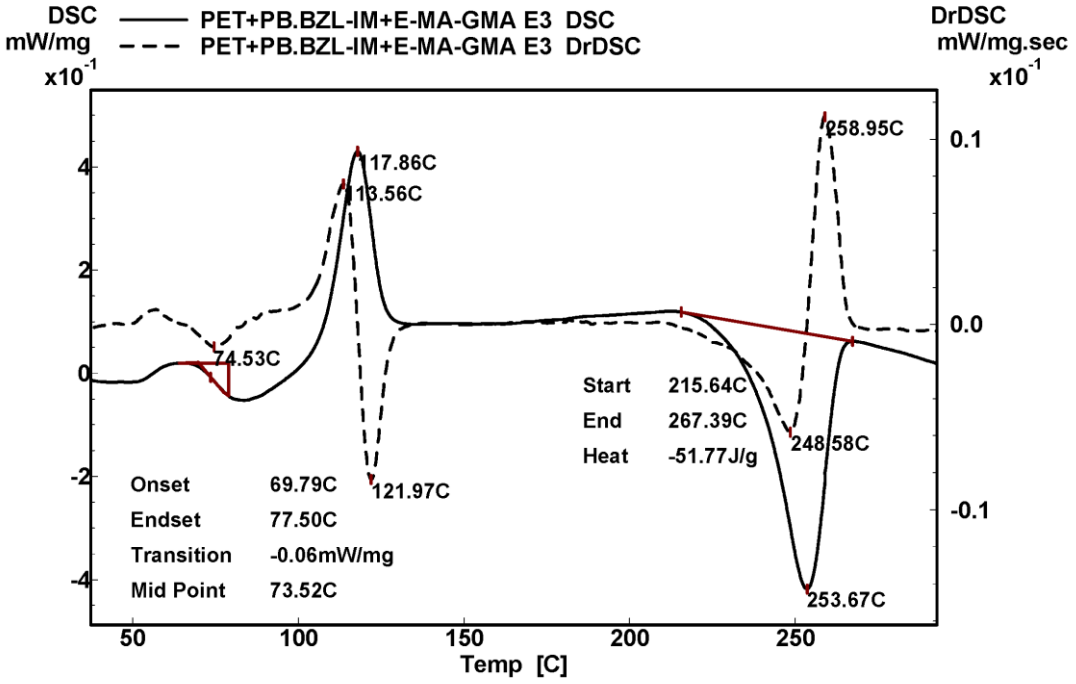

Figure C. 19 DSC thermogram of PET/PB.BZL-IM/E-MA-GMA (E3)

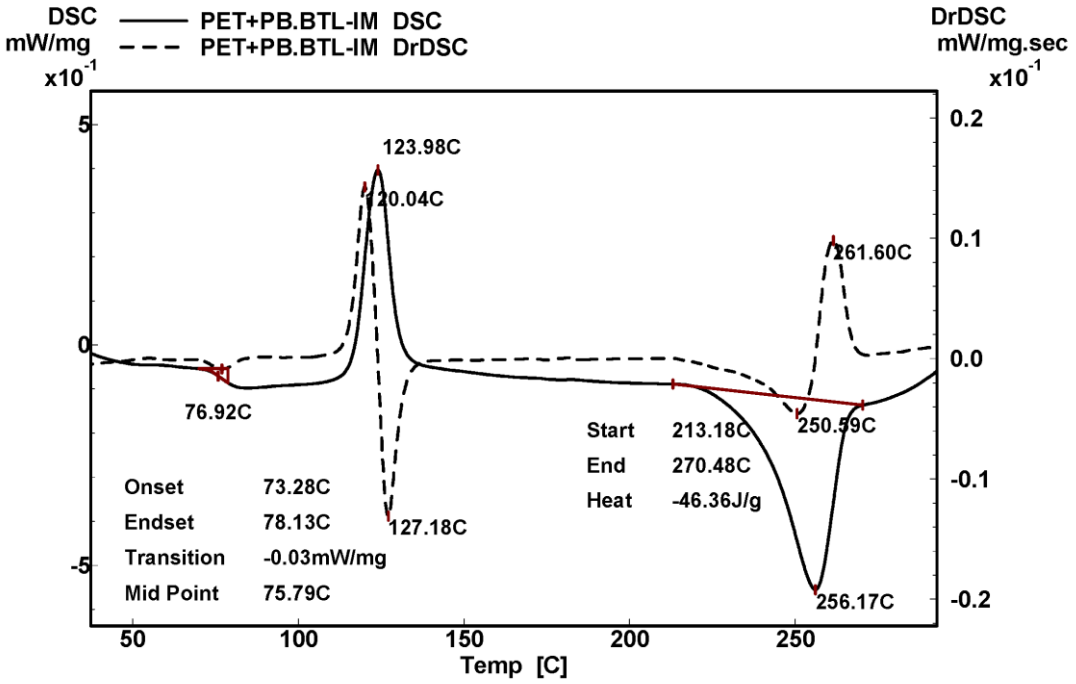

Figure C. 20 DSC thermogram of PET/PB.BTL-IM

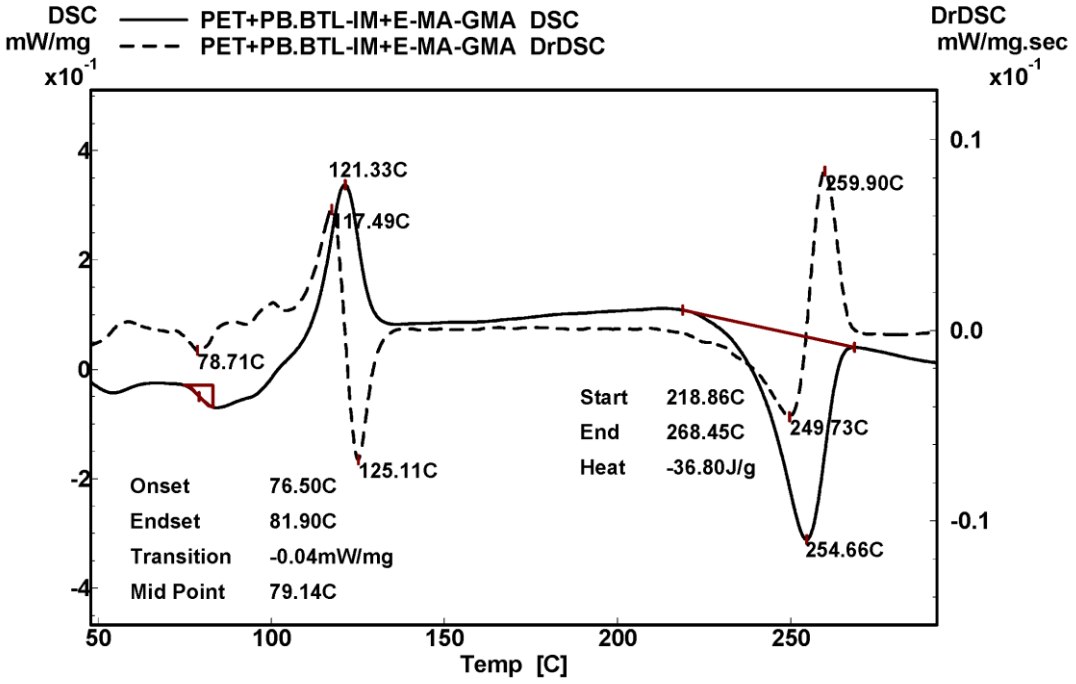

Figure C. 21 DSC thermogram of PET/PB.BTL-IM/E-MA-GMA

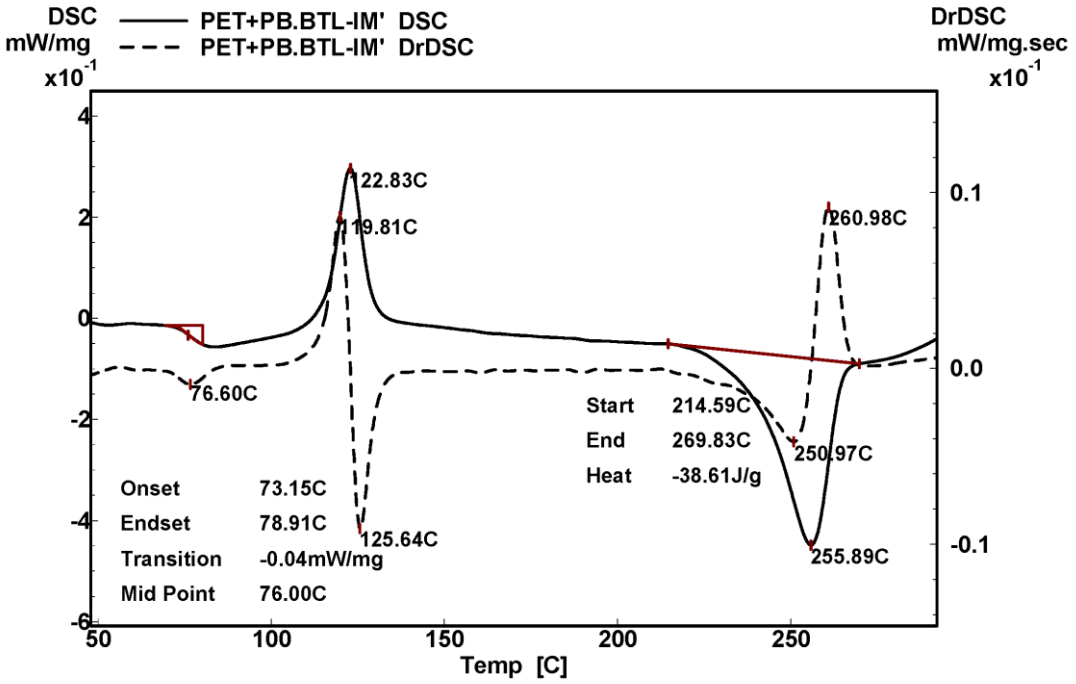

Figure C. 22 DSC thermogram of PET/PB.BTL-IM'

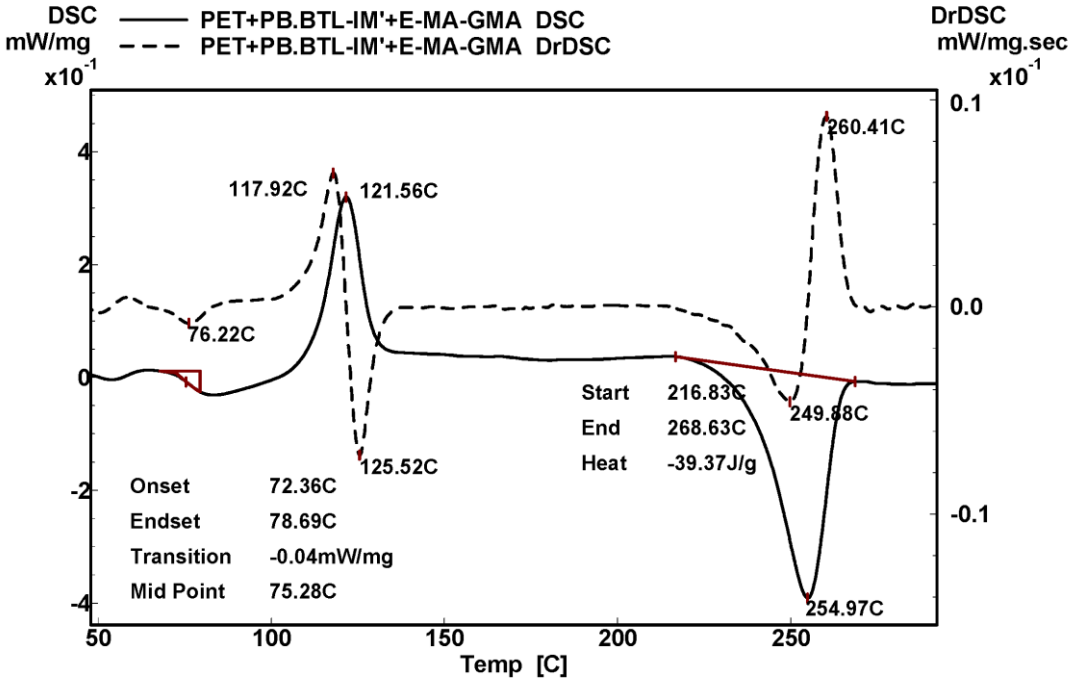

Figure C. 23 DSC thermogram of PET/PB.BTL-IM'/E-MA-GMA

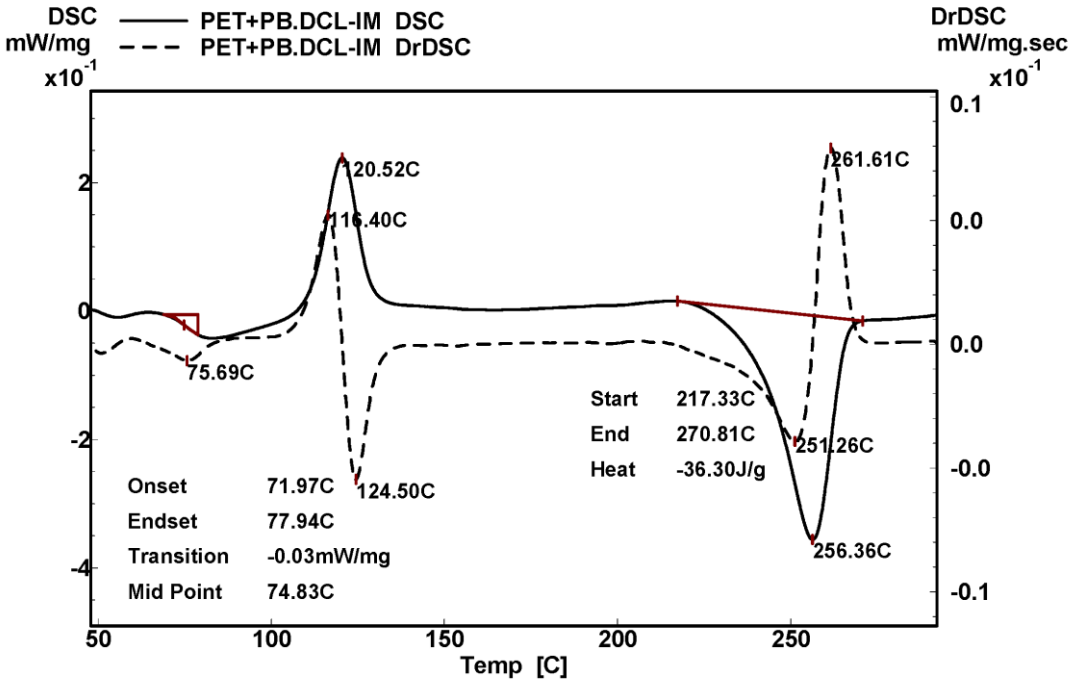

Figure C. 24 DSC thermogram of PET/PB.DCL-IM

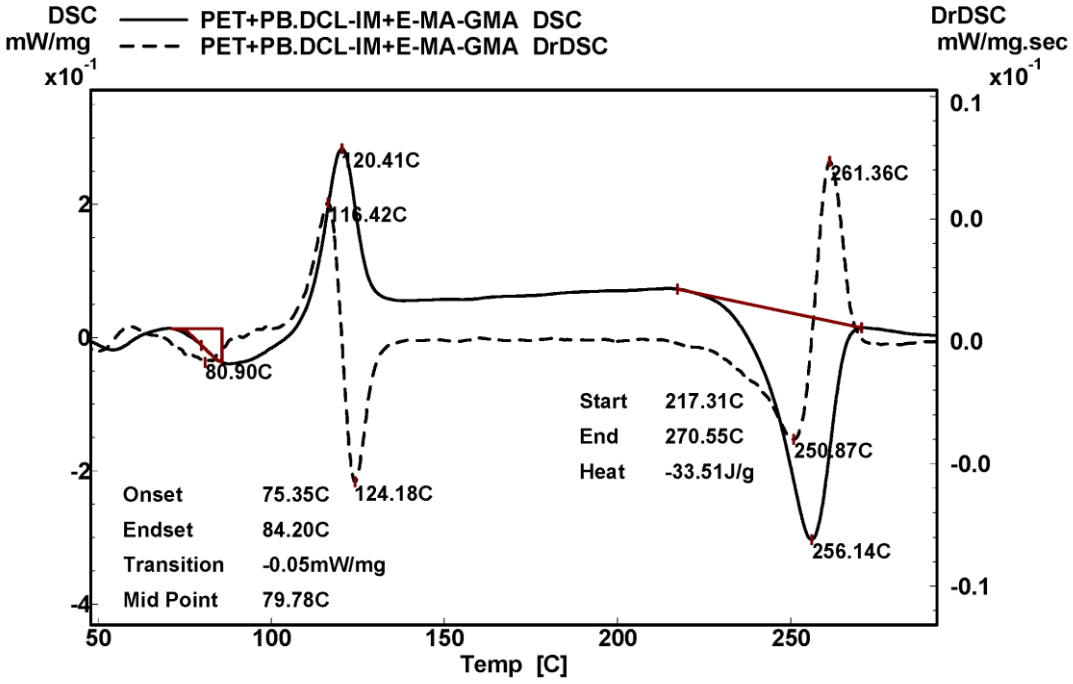

Figure C. 25 DSC thermogram of PET/PB.DCL-IM/E-MA-GMA

VITA

Wissam ABDALLAH

2170 Sherobee Road, 204 MISSISSAUGA, ON L5A 3P8, CANADA

1 (647) 835 3007 w.k.abdallah@hotmail.com

HIGHLIGHTS OF QUALIFICATIONS

- Over 7 years experience in Chemical Engineering (Activated Carbon Production, Clay Purification, Clay Modification, Polymer Extrusion and Injection Molding, Polymer Nanocomposites Production)
- Hold a Master of Science in chemical Engineering with emphasis on Activated Carbon Production and Characterization from the Middle East Technical University in Turkey
- Hold a Doctorate of Philosophy in chemical Engineering with emphasis on Thermally Stable Polymer Nanocomposites Production and Characterization from the Middle East Technical University in Turkey
- Fluent in various languages including but not limited to English, Arabic and Turkish
- Excellent ability in technical analyzing and problem solving in addition to great team spirit and effective communication skills
- Familiar to BET, Helium Pycnometry, Mercury Intrusion Porosimetry, XRD, SEM, TEM, TGA, DSC, DTA, LOI, FT-IR, MFI, Impact Test and Mechanical Machine Tests
- Skilled in Polymath, Fortran, Dendata, MS Office, most common Utility Programs and Internet Applications

PUBLICATIONS

Poster Presentations

Abdallah, W., Yilmazer, U., **Preparation and Characterization of Thermally Stable Layered Silicates for Use in Polymer Based Nanocomposites**, POLYCHAR 18, April 7 - 10, 2010, Siegen, Germany

Abdallah, W., Yilmazer, U., **Isıl Kararlığı Yüksek Fosfonyum ve İmidazolyum Organo-Bentonitlerin Hazırlanması, Karakterizasyonu ve Polimer Bazlı Nanokompozitlerde Kullanılması**, 3. Ulusal Polimer Bilim ve Teknoloji Kongresi ve Sergisi (3. National Polymer Science and Technology Congress), 12-14 May, 2010, Kocaeli, Turkey

Oral Presentations

Abdallah, W., Yilmazer, U., **Preparation and Characterization of Thermally Stable Layered Silicates to be used in Polymer Based Nanocomposites**, SAMPE Europe - 31st. International Technical Conference and Forum, April 12 - 14, 2010, Paris, France

Seminars Attended

Extrusion and Rheology Principles and their Application in Polymer Technology, November 2007, Hacettepe University, Ankara, Turkey

EDUCATION

Middle East Technical University, Ankara, Turkey

Doctorate of Philosophy in Chemical Engineering, 2010
Master of Science in Chemical Engineering, 2004
Bachelor of Science in Chemical Engineering, 2002